

PI-2363

~~UNCLASSIFIED~~

~~Security Information~~

~~RESTRICTED~~

4101-F-1715

Cy #1

Wright Air Development Center

Technical Report No. 52-37

\*

4

March 1952 ✓

WRIGHT-PATTERSON  
TECHNICAL LIBRARY  
WPAPD, O.  
TECHNICAL ASSISTANT  
COMMUNICATION SECTION  
W20573

FILE COPY

# INVESTIGATION OF PRESSURE SURGES IN AIRCRAFT HYDRAULIC SYSTEMS

~~APPROVED FOR PUBLIC RELEASE~~  
~~DISTRIBUTION UNLIMITED~~

E. A. HOUSEL

Classification cancelled in accordance with  
Executive Order 10891 issued 5 November 1953

*J. Biel*  
7/13/54

Document Service Center  
Armed Services Tech. Info Agency

Prepared by

NORTH AMERICAN AVIATION, INCORPORATED

Los Angeles, Calif.

20020104153

Wright Air Development Center

Wright-Patterson Air Force Base, Dayton, Ohio.

~~UNCLASSIFIED~~

NOTICE: This document contains information affecting the national defense of the United States within the meaning of the Espionage Laws, Title 18, U.S.C., Sections 793 and 794, its transmission or the revelation of its contents in any manner to an unauthorized person is prohibited by law.

Reproduced From  
Best Available Copy

~~RESTRICTED~~  
~~UNCLASSIFIED~~

ADA076059

PLEASE RETURN

## NOTICES

When Government drawings, specifications, or other data are used for any purpose other than in connection with a definitely related Government procurement operation, the United States Government thereby incurs no responsibility nor any obligation whatsoever; and the fact that the Government may have formulated, furnished, or in any way supplied the said drawings, specifications, or other data, is not to be regarded by implication or otherwise as in any manner licensing the holder or any other person or corporation, or conveying any rights or permission to manufacture, use, or sell any patented invention that may in any way be related thereto.

The information furnished herewith is made available for study upon the understanding that the Government's proprietary interests in and relating thereto shall not be impaired. It is desired that the Judge Advocate (WCJ), Wright Air Development Center, Wright-Patterson Air Force Base, Ohio, be promptly notified of any apparent conflict between the Government's proprietary interests and those of others.



**UNCLASSIFIED**

WRIGHT AIR DEVELOPMENT CENTER TECHNICAL REPORT NO. 52-37

March 1952

INVESTIGATION OF PRESSURE SURGES  
IN  
AIRCRAFT HYDRAULIC SYSTEMS

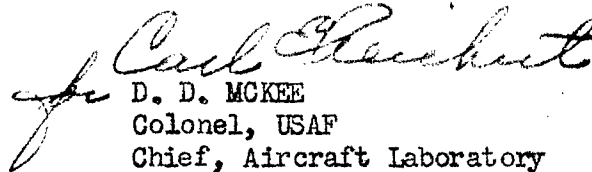
E. A. Housel

Prepared By

North American Aviation, Incorporated  
Los Angeles, Calif.

PUBLICATION REVIEW

This report has been reviewed and is approved.

  
D. D. MCKEE  
Colonel, USAF  
Chief, Aircraft Laboratory  
Directorate of Laboratories

Wright Air Development Center  
Wright-Patterson Air Force Base, Dayton, Ohio

**UNCLASSIFIED**

~~RESTRICTED~~  
**UNCLASSIFIED**

#### FOREWORD

This investigation of pressure surges in aircraft hydraulic systems was undertaken at North American Aviation, Inc., for the Wright Air Development Center as authorized by Contract No. AF33(038)18983, E.O. No. 452-492 SR1g, dated 28 March 1951. The contract was administered under the direction of Capt. H. W. Basham of the Aircraft Laboratory, Aeronautic Division.

This final report includes all of the essential information contained in the three progress reports previously submitted, in addition to the analysis and interpretation of the data presented. The reader, therefore, requires no familiarity with the progress reports in order to utilize the information contained herein.

Chief responsibility for the conduct of this research program was assigned to Mr. E. A. Housel. Included among those who cooperated in the program were Messrs. E. J. Bigelow, J. E. Campbell, and F. A. Grabert. Appreciation is extended to the various aircraft companies and hydraulic system component manufacturers who cooperated in the survey of existing information and data relative to the investigation.

**UNCLASSIFIED**



**UNCLASSIFIED**

ABSTRACT

Theoretical and experimental studies were made to determine the effects of numerous system and component parameters on the magnitude and frequency of pressure surges which occur upon opening or closing a valve in a hydraulic system. It was found necessary to consider the system as a composite unit, due to the complex manner in which the effective resistances, inductances, and capacitances of the system components affected surge characteristics. Electric analogs have been proposed as a convenient means for system analysis, and theoretical approaches for their practical application have been developed.

Analytical studies of existing and experimental data were made to determine the effect of pressure surges on the fatigue characteristics of various hydraulic system components. These studies indicated the magnitude of the surge to be of primary concern, with frequency and rate of pressure rise showing only secondary effects. Secondary high-frequency oscillations were found particularly undesirable because of their excessive peaks, but certain information pertinent to their control has been obtained.

**UNCLASSIFIED**

TABLE OF CONTENTS

	<u>Page No.</u>
FOREWORD. . . . .	ii
ABSTRACT. . . . .	iii
TABLE OF CONTENTS . . . . .	iv
LIST OF ILLUSTRATIONS . . . . .	v
CHAPTER I - INTRODUCTION. . . . .	1
CHAPTER II - SUMMARY OF RESULTS . . . . .	3
<u>2.1</u> The Nature of Pressure Surges . . . . .	3
<u>2.2</u> The Practical Significance of Pressure Surges . . . . .	5
CHAPTER III - THE NATURE OF PRESSURE SURGES . . . . .	7
<u>3.1</u> General . . . . .	7
<u>3.2</u> Closed-end Tube Systems . . . . .	7
<u>3.3</u> Actuating Cylinder Systems. . . . .	53
<u>3.4</u> Accumulators. . . . .	84
<u>3.5</u> Selector Valves . . . . .	93
<u>3.6</u> Pumps . . . . .	97
<u>3.7</u> Energy Dissipating Devices. . . . .	112
CHAPTER IV - THE PRACTICAL SIGNIFICANCE OF PRESSURE SURGES. . . . .	113
<u>4.1</u> General . . . . .	113
<u>4.2</u> Tubing. . . . .	115
<u>4.3</u> Cylinders . . . . .	128
<u>4.4</u> Flow Regulators . . . . .	133
<u>4.5</u> Valves. . . . .	133
<u>4.6</u> Fittings. . . . .	135
<u>4.7</u> Hoses . . . . .	135
<u>4.8</u> Pressure Switches . . . . .	136
BIBLIOGRAPHY. . . . .	137
APPENDIX I - HYDRAULIC SURGE THEORY . . . . .	138

## LIST OF ILLUSTRATIONS

<u>Figure No.</u>		<u>Page No.</u>
1.	Schematic Diagram of Basic Hydraulic System for Investigation of Pressure Surges in Closed-end Tube Systems	9
2.	Test Apparatus for Closed-end Tube System Tests	10
3.	Pertinent Data on Test Valve (Denison Model No. DD063513C)	11
4.	Peak Pressure Ratio vs. Valve Opening Rate - Closed-end Tube System	12
5.	Logarithmic Decrement vs. Valve Opening Rate - Closed-end Tube System	14
6.	Effect of Valve Opening Rate on Pressure Surge Waveform - Closed-end Tube System	15
7.	Amplitude vs. Peak Number for Various Valve Opening Rates - Closed-end Tube System	16
8.	Typical Wavefront Propagation and Resulting Pressure Surges at Various Locations in Closed-end Tube Systems	18
9.	Attenuation of Peak Pressure Ratio at Various Locations - Closed-end Tube System	19
10.	Peak Pressure Ratio vs. Valve Opening Rate at Various System Pressures - Closed-end Tube System	20
11.	Logarithmic Decrement vs. Valve Opening Rate at Various System Pressures - Closed-end Tube System	22
12.	Peak Pressure Ratio vs. Maximum Rate of Pressure Rise at Various System Pressures - Closed-end Tube System	23
13.	Maximum Rate of Pressure Rise vs. Valve Opening Rate at Various System Pressures - Closed-end Tube System	24
14.	Peak Pressure Ratio vs. Pump Discharge Flow Rate for Closed-end Tube Systems With and Without an Accumulator	26
15.	Characteristics of Pressure Surge Waveform Without an Accumulator - Closed-end Tube Systems	27
16.	Peak Pressure Ratio vs. Valve Opening Rate for Various System Lengths - Closed-end Tube Systems	28
17.	Logarithmic Decrement vs. Test Section Length for Rapid Opening Valve - Closed-end Tube Systems	30
18.	Amplitude vs. Peak Number for Various Valve Opening Rates on 48 in. Test Section - Closed-end Tube System	31
19.	Frequency of Fundamental Pressure Wave vs. Valve Opening Rate for Various Test Section Lengths - Closed-end Tube Systems	32
20.	Frequency of Fundamental Pressure Wave vs. Total System Length - Closed-end Tube Systems	33
21.	Pertinent Information on System Configuration for Investigation of Orifices - Closed-end Tube System	34

<u>Figure No.</u>		<u>Page No.</u>
22.	Peak Pressure Ratio vs. Orifice Area for Two Different Orifice Locations - Closed-end Tube System	36
23.	Logarithmic Decrement vs. Orifice Area for Two Different Orifice Locations - Closed-end Tube System	37
24.	Effective Orifice Resistance vs. Orifice Area	38
25.	Peak Pressure Ratio vs. Valve Opening Rate for Various Numbers of Equal Length Branches - Closed-end Tube Systems	40
26.	Logarithmic Decrement vs. Valve Opening Rate for Various Numbers of Equal Length Branches - Closed-end Tube Systems	41
27.	Frequency of Fundamental Pressure Wave vs. Valve Opening Rate for Various Numbers of Equal Length Branches - Closed-end Tube Systems	42
28.	Amplitude vs. Peak Number for Various Valve Opening Rates on a Circuit of Two Equal Length Branches - Closed-end Tube System	43
29.	Typical Pressure Surge Waveforms at Closed Ends of Unequal Length Dual Branches - Closed-end Tube System	44
30.	Peak Pressure Ratio vs. Temperature for Various System Lengths - Closed-end Tube Systems	46
31.	Logarithmic Decrement vs. Temperature - Closed-end Tube System	48
32.	Peak Pressure Ratio vs. Valve Opening Rate at 38 C and -54 C Temperatures - Closed-end Tube System	49
33.	Frequency of Fundamental Pressure Wave vs. Temperature for Various System Lengths - Closed-end Tube Systems	50
34.	Typical Pressure Surge Waveforms Showing Secondary High-Frequency Oscillations Attributed to Entrained Air - Closed-end Tube Systems	52
35.	Schematic Diagram of System Configurations for Investigation of Pressure Surges in Actuating Cylinder Systems	54
36.	Test Apparatus for Loaded Actuating Cylinder Tests	56
37.	Peak Pressure Ratio vs. Valve Opening Rate for Various Volumes in a Bottomed Cylinder - Actuating Cylinder Systems	57
38.	Logarithmic Decrement vs. Valve Opening Rate for Various Volumes in a Bottomed Cylinder - Actuating Cylinder Systems	58
39.	Frequency of Fundamental Pressure Wave vs. System Volume for a Bottomed Cylinder Configuration - Actuating Cylinder Tests	60
40.	Peak Pressure Ratio vs. Valve Opening Rate for Various System Pressures in a Bottomed Cylinder Configuration - Actuating Cylinder Tests	61
41.	Logarithmic Decrement vs. Valve Opening Rate for Various System Pressures in a Bottomed Cylinder Configuration - Actuating Cylinder Tests	62
42.	Typical Pressure Waveforms in a Bottomed Cylinder Configuration - Actuating Cylinder Systems With and Without an Accumulator	64

<u>Figure No.</u>		<u>Page No.</u>
43.	Peak Pressure Ratio vs. Valve Opening Rate for Various Pump Discharge Flow Rates in a Bottomed Cylinder Configuration - Actuating Cylinder System With an Accumulator	65
44.	Logarithmic Decrement vs. Valve Opening Rate for Various Pump Discharge Flow Rates in a Bottomed Cylinder Configuration - Actuating Cylinder System With an Accumulator	66
45.	Typical Pressure Waveforms in a Bottomed Cylinder Configuration, Showing Effect of Volumetric Difference in Pressurized Section of System - Actuating Cylinder System Without an Accumulator	67
46.	Typical Pressure Waveforms in a Mass-Loaded Actuating Cylinder System With an Accumulator	68
47.	Initial Peak Pressure Ratio vs. Valve Opening Rate for Various Weight (Mass) Loads - Actuating Cylinder System With an Accumulator	70
48.	Piston Velocity vs. Applied Weight Load With and Without an Accumulator - Actuating Cylinder Systems	71
49.	Initial Peak Pressure Ratio vs. Valve Opening Rate for Various Weight (Mass) Loads - Actuating Cylinder System Without an Accumulator	72
50.	Typical Pressure Waveforms in a Mass-Loaded Actuating Cylinder System Without an Accumulator	73
51.	Initial Peak Pressure Ratio vs. Applied Air Load for Actuating Cylinder Systems With and Without an Accumulator	74
52.	Initial Peak Pressure Ratio vs. Valve Opening Rate for Various Constant Air Loads - Actuating Cylinder System With an Accumulator	76
53.	Bottoming Pressure Surge vs. Bottoming Piston Velocity - Actuating Cylinder Systems Under Air Load Conditions	77
54.	Initial Peak Pressure Ratio vs. Valve Opening Rate for Increasing Air Loads (Zero Initial Load) - Actuating Cylinder System With an Accumulator	78
55.	Initial Peak Pressure Ratio vs. Valve Opening Rate for Various Degrees of Return Line Restriction - Actuating Cylinder Systems With and Without an Accumulator	80
56.	Initial Peak Pressure Ratio vs. Restrictor Size Showing Relative Effect on an Actuating Cylinder System With and Without an Accumulator	82
57.	Typical Pressure Waveforms Showing Relationship of Pressures on Opposite Sides of Piston - Actuating Cylinder System With a 2 GPM Return Line Restriction	83
58.	Peak Pressure Ratio vs. Valve Opening Rate for Various Types of Accumulators in a Closed-end Tube System	86
59.	Logarithmic Decrement vs. Valve Opening Rate for Various Types of Accumulators in a Closed-end Tube System	87
60.	Frequency of the Fundamental Pressure Wave vs. Valve Opening Rate for Various Types of Accumulators in a Closed-end Tube System	88

<u>Figure No.</u>		<u>Page No.</u>
61.	Peak Pressure Ratio vs. Valve Opening Rate for Various Accumulator Precharge Air Pressures	89
62.	Peak Pressure Ratio vs. Valve Opening Rate for Various Accumulator Piston Weights	90
63.	Logarithmic Decrement vs. Accumulator Piston Weight - Accumulator Tests	91
64.	Modifications in Basic Test Apparatus to Accomodate Tests on Different Types of Selector Valves	92
65.	Pertinent Data on the Characteristics of a Poppet Type Selector Valve (Adel Part No. 18184-2)	94
66.	Pertinent Data on the Characteristics of a Shear Seal Type Selector Valve (Saval Part No. 4840-2)	95
67.	Peak Pressure Ratio vs. Valve Opening Rate for Various Types of Selector Valves in the Same Closed-end Tube System	96
68.	Schematic Diagram of Basic Hydraulic System for Investigation of Pressure Surges in Discharge Line from a Variable Volume (or Displacement) Pump - Rapidly Closing Valve	98
69.	Performance Characteristics of the Variable Volume (or Displacement) Pumps Investigated	99
70.	Typical Pressure Waveforms Resulting from Rapid Valve Closure in the Discharge Lines of Various Types of Variable Volume (or Displacement) Pumps	100
71.	Peak Pressure Ratio vs. Valve Closing Rate for a Variable Displacement Pump (Vickers Model No. AA-32507L2)	102
72.	Peak Pressure Ratio vs. Initial Test Section Pressure for Rapid Closing Valve - Variable Volume (or Displacement) Pump Test	103
73.	Peak Pressure Ratio vs. Pump Discharge Flow Rate for Rapid Closing Valve - Variable Volume (or Displacement) Pump Tests	104
74.	Peak Pressure Ratio vs. Rate of Initial Pressure Rise for Rapid Closing Valve - Variable Volume (or Displacement) Pump Tests	106
75.	Peak Pressure Ratio vs. System Volume (Bottomed Cylinder Configuration) for Rapid Closing Valve - Variable Volume (or Displacement) Pump Tests	107
76.	Pressure Waveforms Showing Unstable Performance of New York Air Brake and Pesco Pumps During Very Slow Valve Closure	108
77.	Pressure Oscillations Resulting from Unstable Performance of New York Air Brake Pump (Part No. 67WA200) Under Constant System Leakage	110
78.	Pressure Oscillations Resulting from Unstable Performance of a Pesco Pump (Part No. S-2324-B) Under Constant System Leakage	111
79.	Schematic Diagram of Basic Hydraulic System for Fatigue Tests of Hydraulic System Components	114
80.	Modified Goodman's Diagram Showing Approximate Method for Adjusting Data From One Stress Ratio to Another Stress Ratio	117

<u>Figure No.</u>		<u>Page No.</u>
81.	Fatigue Data on 61S-T Aluminum Alloy Tubing, With 90 Degree Bends, Subjected to Pressure Impulses (Stress Ratio, R = 0)	118
82.	Fatigue Data on 61S-T Aluminum Alloy Tubing, Without Bends, Subjected to Pressure Impulses (Stress Ratio, R = 0)	120
83.	Fatigue Data on 24S-T Aluminum Alloy Tubing, With and Without Bends, Subjected to Pressure Impulses (Stress Ratio, R = 0)	121
84.	Fatigue Data on Stainless Steel Tubing (Spec. AMS 5566), With 90 Degree Bends, Subjected to Pressure Impulses (Stress Ratio, R = 0)	122
85.	Pressure Surge Characteristics of High-Frequency Fatigue Tests Conducted on Tubing at the Glenn L. Martin Company	124
86.	Fatigue-Strength Curves on 61S-T Aluminum Alloy Tubing, With 90 Degree Bends, at Various Stress Ratios	125
87.	Logarithmic Probability Plots of Fatigue Data Showing the Difference in Life Range Between Single Group Distribution and Combined Group Distribution of Various Data Sources	126
88.	Fatigue Failures of Cylinder Ends Subjected to Pressure Impulses With Surge Peaks	129
89.	Fatigue Failures of Cylinder Barrels Subjected to Pressure Impulses With Surge Peaks	130
90.	Fatigue Failures of Packing Glands in Actuating Cylinder Assemblies Subjected to Pressure Impulses With Surge Peaks	131
91.	Fatigue and Hydrostatic Burst Pressure Failures of Flow Regulators (Waterman No. 196-8-5.89)	132
92.	Fatigue Failure of Restrictor Valve Body Subjected to Pressure Impulses With Surge Peaks (X20 Magnification)	134
93.	Graphical Description of Theoretical, Non-Attenuated Hydraulic Pressure Wave - Closed-end Tube System	143
94.	Graphical Description of Theoretical, Attenuated Hydraulic Pressure Wave - Closed-end Tube System	144
95.	Pressure Wave Distortion - Closed-end Tube System	145

## CHAPTER I

INTRODUCTION1.1 Background

1.1.1 Pressure surges, which often exist in aircraft hydraulic systems, are of importance because of their effect on the fatigue and functional characteristics of the system components. In the past, detrimental pressure surges (and those considered detrimental) have been eliminated or have been controlled by arbitrary design changes based on the practical experience of the hydraulic system and component designers. At present, there is a growing need for criteria which are applicable to improved system design and to the establishment of a general impulse test specification for industry to use in qualifying hydraulic system components.

1.1.2 In order to establish the desired criteria, it is necessary to determine the causes of these pressure surges, the effects of various system parameters on them, and the resulting effect of the surges on the system components. Some basic information on the theory and nature of pressure surges was obtained from an investigation previously performed by the Contractor and described in USAF Technical Report No. 5997 (Ref. 1).

1.1.3 The pressure surges studied in the previous investigation were those accompanying the rapid opening or closing of valves and those existing as oscillations in a pump discharge line during normal pump operation or with pump cavitation. The most significant of these from the standpoint of magnitude were the surges which occurred when a valve was rapidly opened allowing a charged accumulator to discharge into a low-pressure closed-end tube containing fluid free of entrained air (i.e., air not in solution). Results of the research indicated that pressure peaks of approximately twice the nominal system pressure could occur, but this ratio was attenuated by increased system pressure, increased system volume, restriction in the system, lower temperature, and slower valve opening time. Also, it was found that the presence of an entrained air volume of 2 - 3 percent of the system fluid volume could cause surge peaks up to 5 to 6 times the accumulator pressure. However, the scope of the previous investigation was limited in that it considered only a simple closed-end tube system with an accumulator and system pressures up to 1200 psi. The research done was sufficient to establish basic theory, but the need for further work to determine the effects of various other parameters was evident.

1.2 Purpose and Scope

1.2.1 The present research program was designed to investigate the exact nature of the pressure surges which occur in hydraulic systems, to evaluate the practical significance of these surges, and concurrently to establish criteria for use in the design of aircraft hydraulic systems.

1.2.2 In the present investigation, consideration was given to branch systems, actuating cylinder systems with varied load configurations, accumulator parameters, selector valve parameters, systems with and without accumulators, and higher system pressures. Many of the parameters were studied on a closed-end tube system because it facilitated the theoretical analysis. In addition to studies of pressure surges occurring upon opening a valve in a hydraulic system, consideration was given to pressure surges which occur upon closing a valve in a discharge line from a variable volume (or displacement) pump incorporating an unloading device.

1.2.3 Since the practical significance of pressure surges was in their effect on the hydraulic system components, analytical studies of existing information and data pertinent to the problem were made and additional experiments were conducted. Existing information and data were obtained from correspondence with various aircraft companies and hydraulic system component manufacturers, and from published technical reports and literature.



1.2.4 It was originally anticipated that the data obtained from detailed studies of the effects of isolated variables might be integrated into a form of curves, tables, and equations which could be used for design analysis of pressure surges in a hydraulic system. However, combination of data in this manner was not found suitable due to the complex nature of pressure surges. Electric analogs have been proposed as a more adequate means for design analysis. General information and data pertinent to improved design will be found in appropriate sections of this report.

### 1.3 Reports

1.3.1 The present research program extended over a twelve month period and the concurrent status was described by progress reports submitted at intervals as follows:

- (a) First Progress Report dated 21 June 1951
- (b) Second Progress Report dated 24 September 1951
- (c) Third Progress Report dated 26 December 1951

This final report includes all information obtained during the entire investigation.

## CHAPTER II

SUMMARY OF RESULTS2.1 The Nature of Pressure Surges

2.1.1 From the theoretical and experimental investigations conducted in this research program, it was found that analysis to determine the exact nature of pressure surges (i.e., magnitude, frequency, and rate of rise) in a hydraulic system necessitated consideration of the system as a composite unit. This was due to the complex manner in which the effective resistances, inductances, and capacitances of the system components combined. The use of electric analogs (Appendix I) has been proposed as the most convenient means for theoretical analysis of a hydraulic system because:

- (a) They can adequately represent a hydraulic system;
- (b) They provide access to advanced techniques in mathematical calculation procedures;
- (c) Equivalent circuits can be made and operated at lower cost.

The need for further investigation to establish constants for use in the electric analogs and investigation to establish a technique for handling the non-linearity of valve resistance has been evidenced in this investigation.

2.1.2 The data and information presented in Chapter III can be considered as forms of design criteria since they do provide indications of trends. However, the percentage effectiveness shown in the data for a particular parameter should not be used without restraint, because the relative effectiveness is subject to system configuration and operating conditions.

2.1.3 The magnitudes of pressure surges which occurred on opening a valve were found to be affected by system and component parameters in the following general manner:

- (a) Slower valve opening rates (i.e., rate of change of port area), valve interflow prior to actual port opening, and smaller port areas with the valve fully open resulted in lower peak pressure ratios (i.e., the ratio of maximum surge pressure to nominal system pressure). Larger port areas were permissible for a given peak pressure ratio as the valve was located nearer the energy source.
- (b) Variation of accumulator parameters (i.e., geometrical shape and size, precharge air pressure, and piston weight) had little effect on the peak pressure ratio of the system tested. However, large volumetric displacements reduce the system pressure and result in lower peak pressures. Under these conditions, accumulator precharge air pressure becomes significant.
- (c) Lower system flow rates resulted in lower peak pressures, the highest peaks occurring in a system with an accumulator as an energy source. With no accumulator installed in the system, the primary source of energy was the compressed fluid in the pressurized section of the system. Pump discharge flow rate had relatively little effect, except at flow rates above 8 gpm. The magnitude of the pressure surge under these conditions was dependent upon the volumetric ratio between the high-pressure and low-pressure sections of the system.
- (d) Increased system pressure resulted in lower peak pressure ratios.
- (e) Increased system volume resulted in lower peak pressure ratios. Results of tests on various system lengths with the basic valve gave higher peak pressure ratios with increased system volume (i.e., longer test sections), but this was due to manner in which valve resistance affected the damping characteristics during the initial pressure rise.

- (f) Decreased temperatures, especially at low temperatures, resulted in lower peak pressure ratios.
- (g) The presence of entrained air did not appear to affect the magnitude of the fundamental wave, but did result in high-frequency pressure oscillations superimposed upon the fundamental wave. The magnitudes of these secondary oscillations appeared to be dependent upon the quantity of air present. Further investigation of this particular phenomena would be required to establish more exact relationships.
- (h) In actuating cylinder systems, increased opposing loads and increased return line restriction gave higher initial peak pressures and lower bottoming peak pressures. Relatively small mass loads were required to approach a closed-end tube condition. The magnitude of the bottoming pressure surges with an accumulator in the system were considerably higher than those observed in closed-end tubes, except when the opposing load was large. The magnitude of bottoming surges compared favorably with closing valve theory.

2.1.4 The magnitudes of pressure surges which occurred when a valve was closed in the discharge line from a variable volume (or displacement) pump were found to be affected by system parameters in the following general manner:

- (a) Slower valve closing rates resulted in lower peak pressures.
- (b) Decreased flow resulted in lower peak pressures.
- (c) Increased system volume resulted in lower peak pressures.

2.1.5 In the tests on variable volume (or displacement) pumps, unstable pump performance was observed under certain flow conditions and system configurations. This unstable performance was characterized by low-frequency oscillations (30 cps or less), the magnitude of which was a function of the flow conditions in the system. This frequency was attributed to the effect of the pump unloading device on the frequency response characteristics of the system.

2.1.6 The fundamental frequency of the pressure surge which occurred when a valve was opened was relatively independent of valve parameters, accumulator parameters, system pressure, and system flow rate, but increased slightly when the temperature was lowered, due to the effect of temperature on the velocity of wave propagation. The fundamental frequency of the pressure surge was affected by system configuration in the following general manner:

- (a) Increased system length resulted in lower frequencies. The frequency of a single line circuit was inversely proportional to the system length between the accumulator to the closed end of the tube.
- (b) The addition of equal length branch circuits resulted in lower frequencies.
- (c) Dual branches of unequal length gave complex frequency characteristics which appeared to include the fundamental frequencies of the individual branches and certain phase relationships.
- (d) Bottomed cylinders at the closed end of a single line circuit resulted in lower frequencies. Increased volume in the cylinder resulted in further lowering of the frequency. The frequency was inversely proportional to the square root of the product of system inductance and capacitance (Appendix I).
- (e) The fundamental frequency of the pressure surge did not appear to be affected by entrained air, but the presence of air resulted in secondary oscillations of high frequency, 1000 - 2000 cps.

- (f) In actuating cylinder systems, it was theorized that the frequency of the initial pressure surge would increase as the mass load was increased, due to the effect on system inductance. The trend was indicated by experimental data, but complete analysis of the data collected was not accomplished. The frequency of the bottoming surge would be described by the same factors as in (d) above.

2.1.7 Theoretical studies of the initial pressure rise characteristics indicated that the maximum rate of rise could approach infinity if an essentially step input function was propagated down the line. In tests conducted on a valve with low interflow characteristics and fast valve opening rates, it was found that the shape of the wavefront propagated down the tube approximated a step function (Appendix I).

## 2.2 The Practical Significance of Pressure Surges

2.2.1 From analysis of existing and experimentally determined information and data on the fatigue characteristics of hydraulic system components subjected to pressure surges, it was found that the practical significance of pressure surges was primarily in the magnitude of the maximum peak which occurred and the maximum range of pressure variation. Comparison of fatigue data on tubing subjected to pressure impulses without surges to fatigue data on the same type of tubing subjected to pressure impulses with surge peaks indicated no significant difference in the life of the tubing for a given pressure ratio. Studies of available records of pressure surge waveforms indicated that the range of fundamental frequencies represented in the data was 30 - 130 cps. There was no apparent effect on the fatigue life of the tubing due to this variation in the fundamental frequency. The range of impulse cycling rates represented in the data was 30 - 120 cpm. Here, also, no effect on fatigue life was ascertained. Analysis of data obtained on fatigue tests of 61S-T tubing subjected to high-frequency oscillations (approximately 1400 cps) between 2100 and 4800 psi gave some indication that even this frequency did not appreciably affect the fatigue-strength values of the material.

2.2.2 The range of fatigue life observed at a particular stress level was found to be quite wide, even under closely controlled tests on selected samples. In Ref. 4, Freudenthal has proposed that the distribution characteristics of fatigue data can be represented by logarithmic-normal distribution. Relatively good correlation to this distribution was observed in the fatigue data obtained on tubing. However, as was pointed out by Freudenthal, the establishment of the lower limit for design requires that at least 20 or more samples be tested at a particular stress level. The establishment of the modal point of the distribution, which can be used for correlation purposes, requires that at least six samples be tested. Consequently, to establish significant correlation as to the effect of variations in the pressure surge waveform (i.e., frequency and cumulative damage due to underdamped fundamental, secondary oscillations, etc.) would have required considerably more experimental investigation than time permitted in this research program.

2.2.3 Detailed studies of the data collected on 61S-T tubing subjected to pressure impulses indicated the presence of certain parameters which effected the fatigue life of individual samples. Results of these studies were as follows:

- (a) Tubing bends reduced the fatigue life. This was definitely established by fatigue data on straight tubing and tubing with 90 deg bends. All data were for tubing having one end fixed and one end free.
- (b) Double-flared tubing seemed to possess greater susceptibility to fatigue failure in the flare than single-flared tubing. This was attributed to stress concentration which might have been accentuated by the torques used to tighten the nut.
- (c) There was some indication that proof-testing tubing with 90 deg bends prior to fatigue testing increased the fatigue life.

2.2.4 From an investigation by Marin and Shelson (Ref. 2) on 24S-T aluminum alloy tubing, it was found that uniaxial fatigue-strength values, determined by standard fatigue test methods, could not be used to predict fatigue strength under biaxial stress conditions. Results obtained in this investigation indicated good agreement with Marin and Shelson.

2.2.5 Results of fatigue tests on various system components, other than tubing, indicated the importance of stress concentrations in the component design. Due to limited data, no attempt to establish stress concentration factors was made. Since there was no established relationship between uniaxial fatigue-strength values and biaxial fatigue-strength values, similar discrepancies might be found in stress concentration factors under biaxial stress conditions. Fatigue data on restrictor valves indicated that torques used to tighten fittings into valve ports could reduce the fatigue life of the component. Failures observed in these tests occurred in the threaded section of the port. Results of tests on cylinder assemblies indicated that initial cylinder failure occurs in the packing installations. Establishment of data on the life expectancy of packing installations was considered a field for future investigation. Teflon back-up rings have exhibited characteristics which might increase the fatigue life of packing glands over the conventional leather back-up rings being presently used.

2.2.6 Since it has been indicated from analysis of fatigue data that the stress range between the maximum and minimum pressures observed during a complete cycle is the primary consideration for design, the importance of high frequency secondary oscillations in a hydraulic system becomes apparent. The frequency of this secondary oscillation was found to be generally between 1000 - 2000 cps. Consequently, experimental survey of the pressure surge characteristics in an actual aircraft hydraulic system demands instrumentation which responds accurately at these high frequencies. In several instances during the research program, the introduction of a low-pressure relief valve (modified check valve) in the system return was found an effective means of reducing the magnitude of the secondary oscillation to an essentially negligible value. The significance of this was that as long as air remained in solution with the fluid and vapor-filled bubbles (cavities) were not formed, the occurrence of secondary high-frequency oscillations was minimized.

## CHAPTER III

THE NATURE OF PRESSURE SURGES3.1 General

3.1.1 When the kinetic energy of fluid in motion in a hydraulic system is suddenly converted into potential (pressure) energy, the result is a surge of pressure to an excessive or abnormal value followed by an underdamped pressure oscillation. A surge of a similar nature might also be created in an actuating cylinder dashpot or some other type of energy dissipating device if the kinetic energy of external dynamic forces is suddenly converted into pressure energy within the component. The purpose of this section of the investigation was to conduct theoretical and experimental studies to determine the effects of various parameters on the magnitude, frequency, and rate of rise of these surges.

3.1.2 The investigation of pressure surges induced by energy within the hydraulic system itself was divided into five parts as follows:

- (a) Closed-end Tube Systems. These configurations offered a simple means of studying the effects of various system parameters.
- (b) Actuating Cylinder Systems. These configurations were used to study the effects of parameters common to actuating cylinder systems only.
- (c) Accumulators. Since an accumulator is the primary source of energy for pressure surges arising in a hydraulic system when a valve is opened rapidly, studies were made to determine the effects of parameters related to accumulators.
- (d) Selector Valves. Since rapid operation of a selector valve is almost essential in producing pressure surges when the source of energy is within the system itself, studies were made to determine the effect of valve geometry and rate of valve opening.
- (e) Pumps. Since it is possible that a variable volume pump discharging through a valve might cause pressure surges when the valve is rapidly closed, studies were made to determine the nature of these surges and the effects of various system parameters on them.

3.1.3 Pressure surges induced in hydraulic systems by energy derived from external dynamic forces were given limited consideration.

3.1.4 The hydraulic fluid used in the investigation conformed to Spec. MIL-O-5606. All tubing used in the test configurations, except return lines, conformed to Spec. AMS 5566 for stainless steel tubing.

3.2 Closed-end Tube Systems3.2.1 General Notes

3.2.1.1 The pressure surges studied in this part of the investigation were those which occurred when a valve was rapidly opened allowing a pressurized system to discharge into a low-pressure closed-end tube configuration. The basic hydraulic system used for these tests is shown schematically in Fig. 1 and physically in Fig. 2. The Denison valve (Model No. DDO63513C) chosen for the experimental test work was selected primarily because it was designed for pressures up to 5000 psi and because the valve spool could be easily adapted to external actuation with controlled velocity. Variation of spool velocity was obtained by controlling the flow characteristics in the pilot system.

3.2.1.2 From dimensional measurements of the valve spool and valve body, the annulus area vs. spool displacement (Fig. 3) was calculated and the spool position at which the valve porting started to open was determined. The relationship between annulus area and spool displacement is described by the equation,

$$A = 1.57X_v - 0.68X_v^2 \approx 1.57X_v \quad (3-1)$$

where

A = annulus area, in<sup>2</sup>

X<sub>v</sub> = spool displacement measured from initial opening position, in.

This relationship was valid for annulus areas up to 0.145 sq in., which was equivalent to the internal cross-sectional area of the test section, 1/2 in. OD x 0.035 in. wall tubing. Due to clearance between the spool and valve body the minimum area at initial opening of the valve porting was  $7.86 \times 10^{-4}$  in<sup>2</sup>. Further description of the valve is shown by the pressure drop-flow-displacement ( $\Delta P$ -Q-X) relationships in Fig. 3. The relationships were experimentally determined for steady-state flow conditions.

3.2.1.3 Simultaneous records of the pressure characteristics in the closed-end tube system and of the Denison valve spool position were taken by photographing the screens of two Aeroquip Hydrauliscopes (Model No. 10000A). One Hydrauliscopes received its signal from an Aeroquip pressure transducer (Part No. 10050) at the closed end of the test section while the other Hydrauliscopes received its signal from a cantilever beam type position transducer attached to the valve spool. The principle of this type of position transducer is the measurement of the strain in a deflected beam by means of electric resistance strain gages and, since the strain is proportional to deflection up to the proportional limit of the beam material, the calibration of the signal in terms of deflection. Simultaneous recording was accomplished by triggering the beams of both Hydrauliscopes from one common switch which was actuated by a lever attached to the pilot cylinder piston rod (Fig. 2). Synchronization of the two recorded traces was established by momentarily interrupting the signals of both Hydrauliscopes by the discharge of a condenser and by introducing reference timing traces from a common oscillator source.

3.2.1.4 The general procedure followed for a specific test run was as follows:

- (a) The test section was bled of entrapped air and the Denison valve between the test section and the energy source (accumulator and/or system pump) was closed.
- (b) The main system was charged to the desired pressure and the pilot system was adjusted to give the desired Denison valve spool velocity.
- (c) The pilot system selector valve was operated at a uniform rapid rate and simultaneous records of pressure and spool position were taken as the Denison valve opened.
- (d) Records were made of the necessary reference traces.

3.2.1.5 Data reduction procedures used to convert experimental data into the desired form for presentation were as follows:

- (a) Valve opening rate ( $dA/dt$  or  $\dot{A}$ ) was obtained by substitution of valve spool velocity ( $dx/dt$ ) in Eq. 3-1. The second term in the exact equation was small and could be neglected. Valve spool velocity was determined from the slope of the position vs. time record.
- (b) The peak pressure ratio ( $P_m/P_o$ ), herein identified as the ratio of the maximum pressure of the initial surge to the nominal system pressure, was based on the system pressure as determined from the mean between the envelope curves of the underdamped oscillatory pressure wave.

Figure 1

SCHEMATIC DIAGRAM OF BASIC HYDRAULIC SYSTEM FOR INVESTIGATION OF PRESSURE SURGES IN CLOSED-END TUBE SYSTEMS

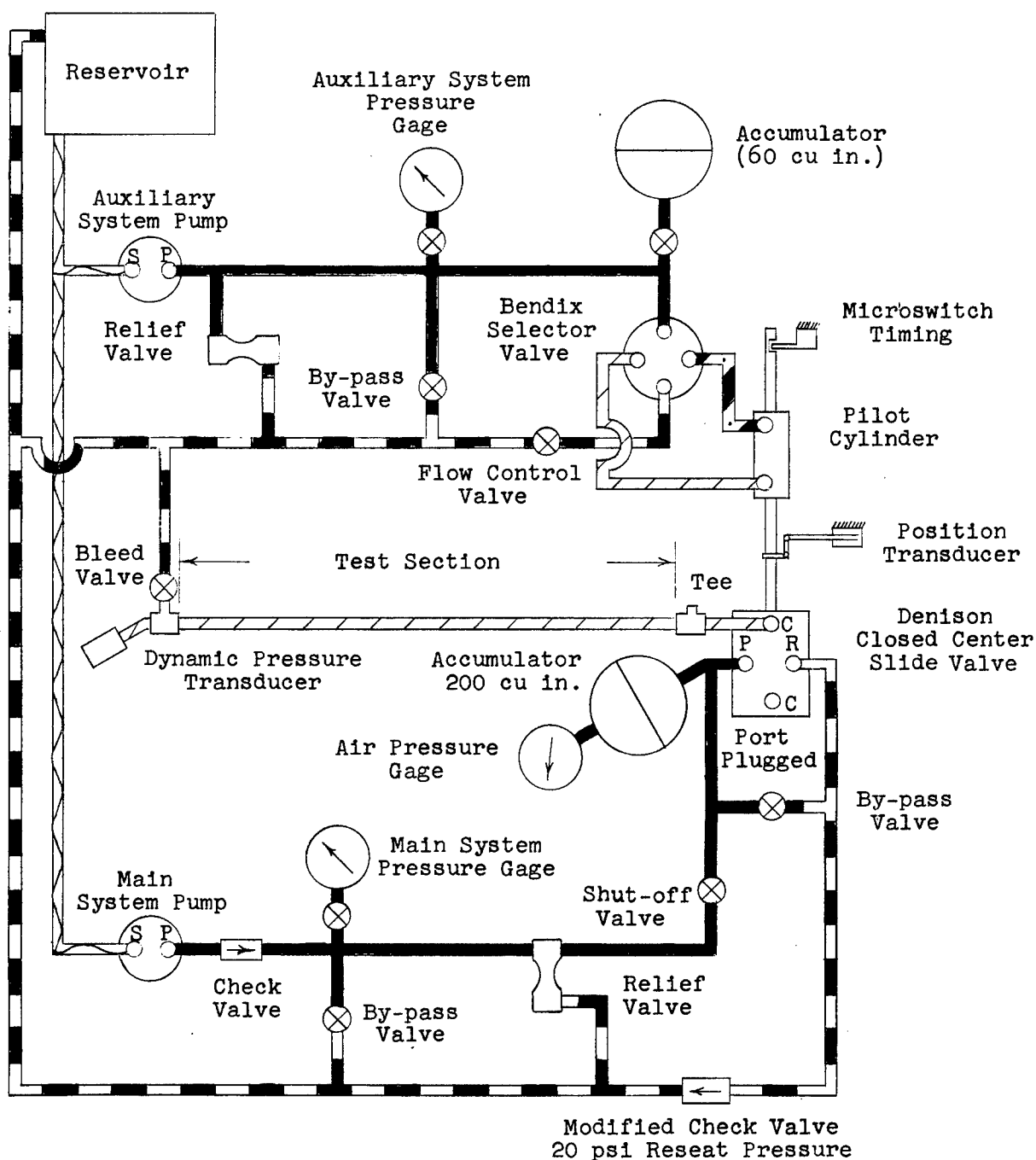




Figure 2

TEST APPARATUS FOR CLOSED-END TUBE SYSTEM TESTS

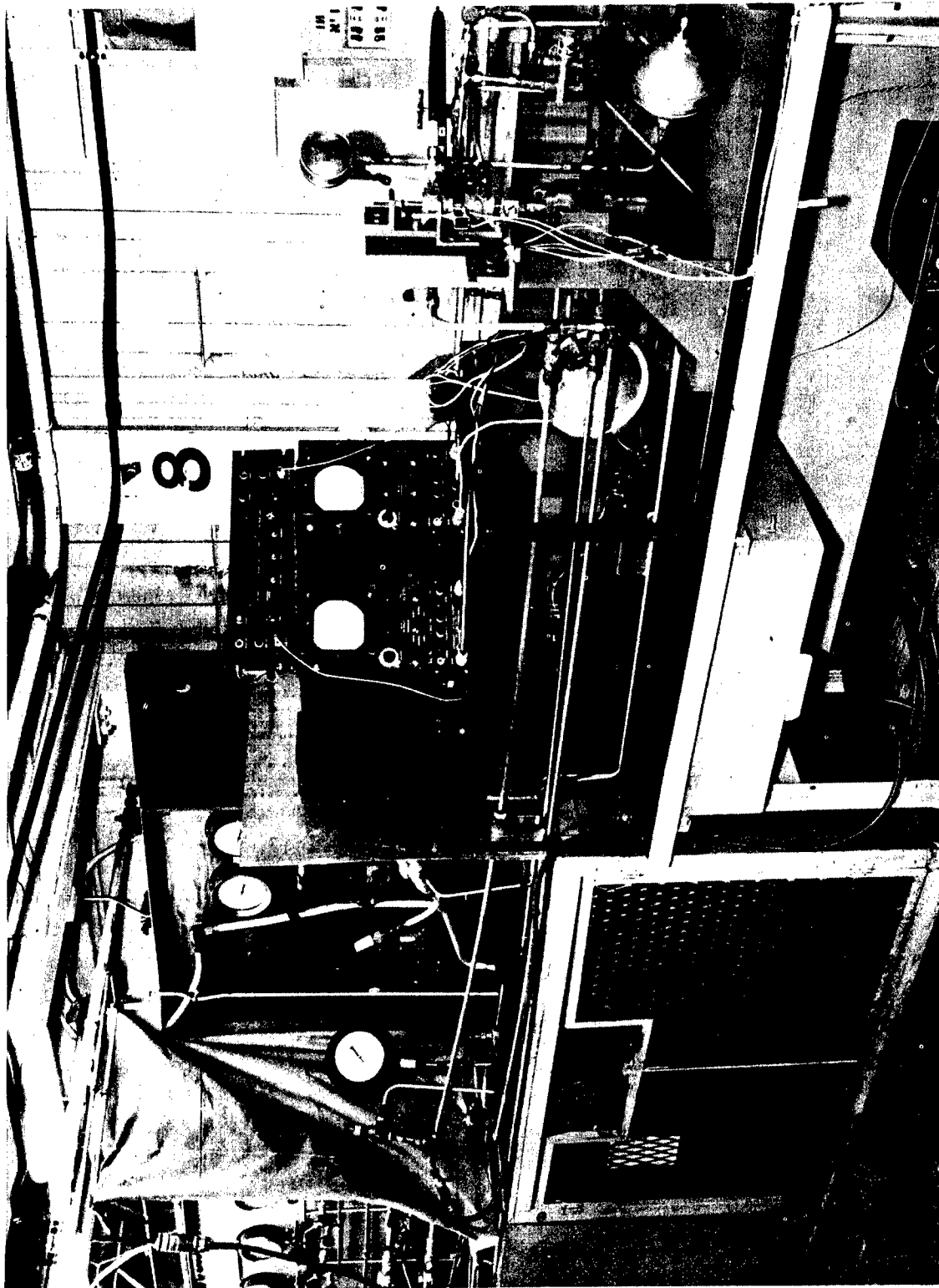


Figure 3

PERTINENT DATA ON TEST VALVE (DENISON MODEL NO. DD063513C)

Note: Negative valve displacement represents overlap between valve spool and sleeve (i.e. housing).

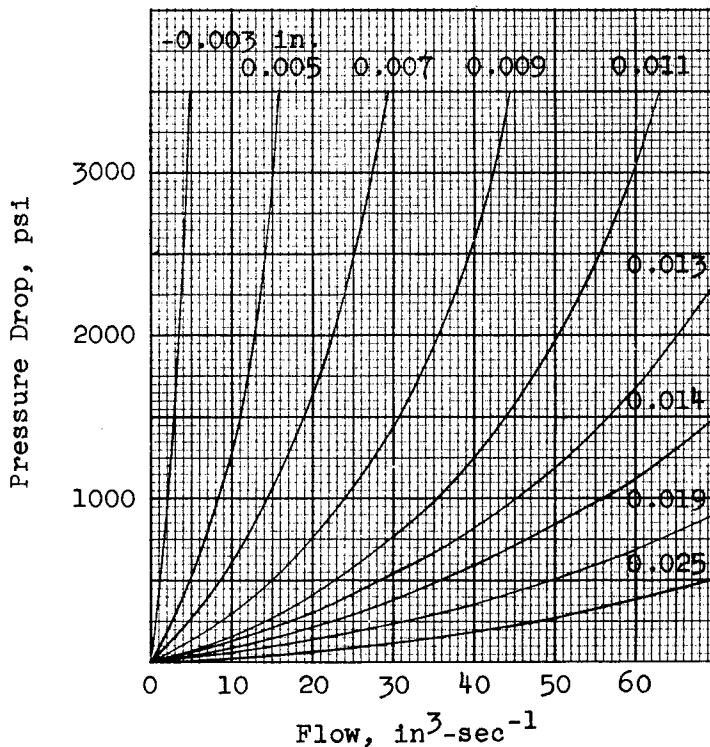
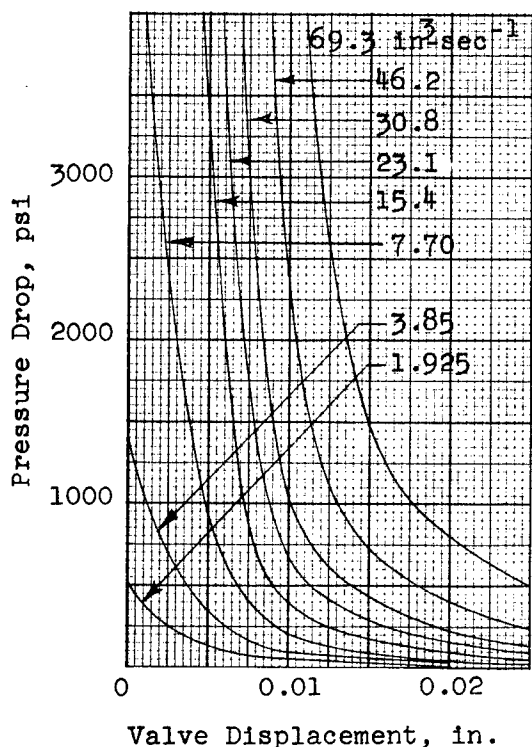
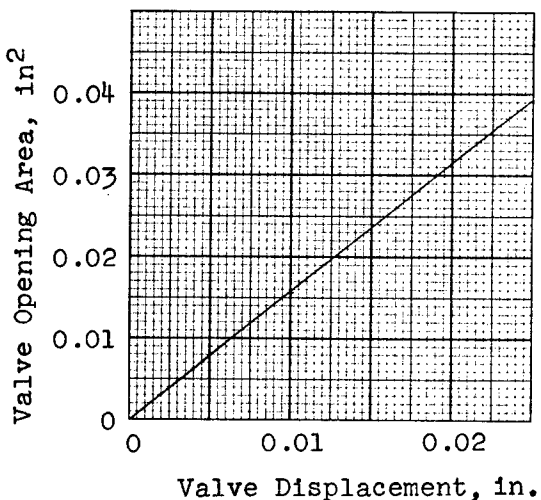
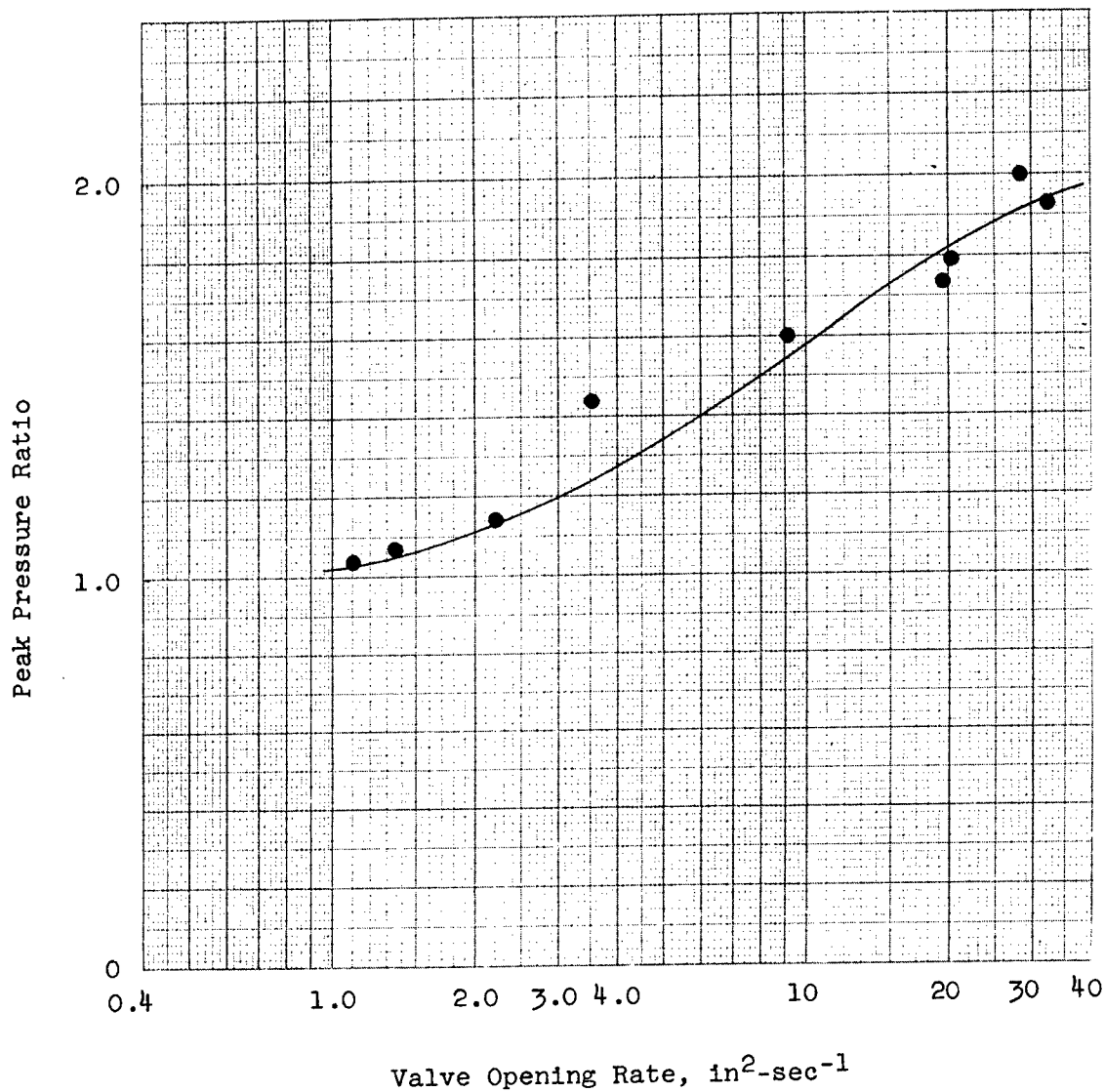


Figure 4

PEAK PRESSURE VS. VALVE OPENING RATE  
CLOSED-END TUBE SYSTEM



Note: 96 in. test section length.

- (c) The logarithmic decrement ( $\delta$ ) of the underdamped oscillatory pressure wave was obtained by plotting the total amplitude between the envelope curves against peak number on semi-logarithmic graph paper and then determining the logarithmic decrement from the slope of this curve by means of the mathematical expression

$$\delta = \frac{1}{m - n} \ln \frac{X_n}{X_m} \quad (3-2)$$

where

$\delta$  = logarithmic decrement  
 $X_n$  = total amplitude between envelope curves at  $n$ th peak, record in.  
 $X_m$  = total amplitude between envelope curves at  $m$ th peak, record in.

The logarithmic decrement was of significance because it indicated the amount of damping in the system.

- (d) The rate of pressure rise ( $\dot{p}$ ) was determined graphically from the slope of the pressure vs. time record.
- (e) The frequency ( $f$ ) of the underdamped oscillatory pressure wave was determined from the peaks and reference timing trace on the pressure vs. time record.

### 3.2.2 Valve Opening Rate

3.2.2.1 The effect of valve opening rate was investigated by varying the Denison valve spool velocity and studying the resulting pressure surges in a closed-end tube. Specific test conditions were as follows:

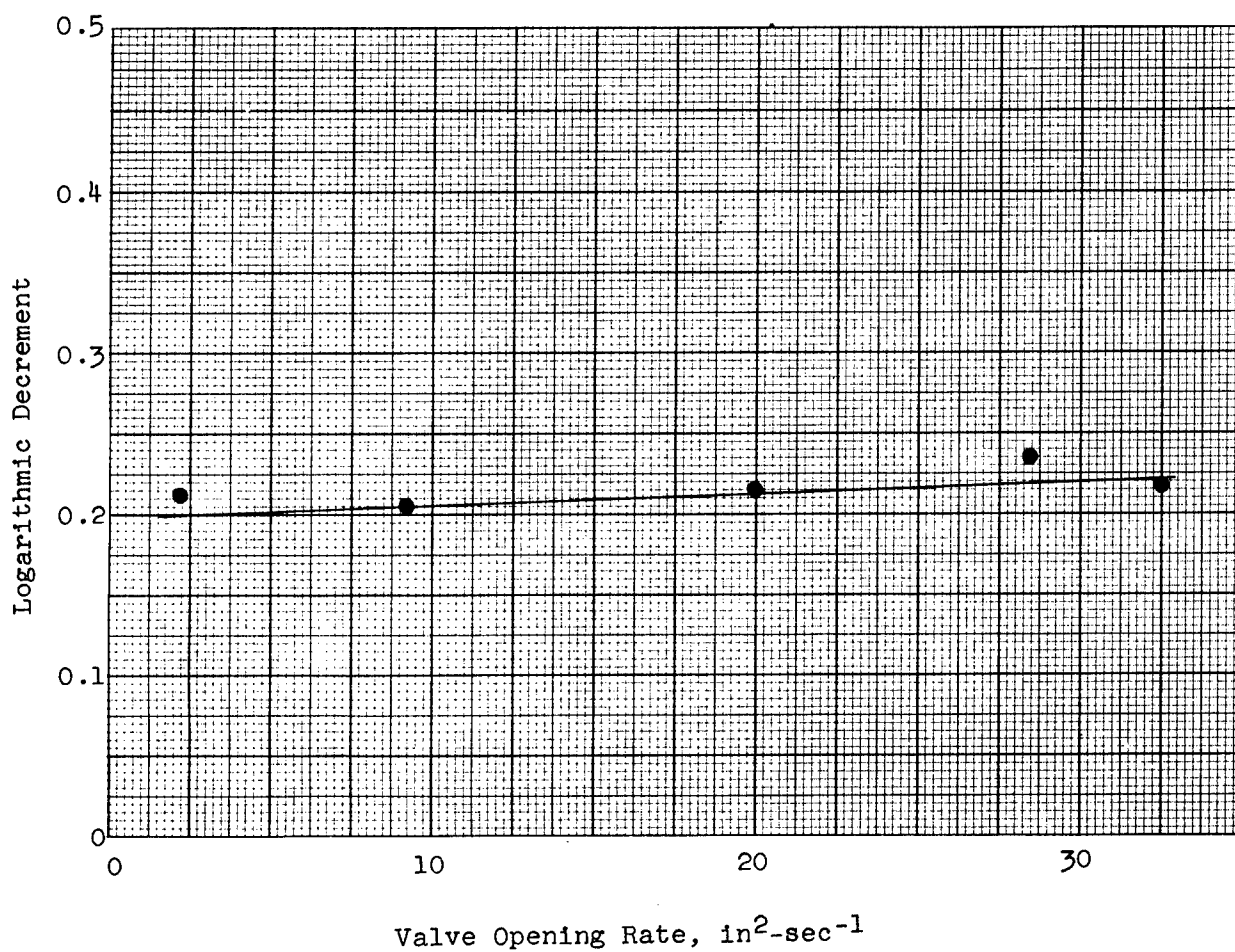
- (a) System pressure, 3000 psi.
- (b) Accumulator precharge air pressure, 1000 psi.
- (c) Pump discharge flow rate, 2 gpm.
- (d) Fluid temperature,  $38 \pm 5$  C ( $100 \pm 9$  F).
- (e) Test section length, 96 in.
- (f) Valve opening rate, 1 - 30 in<sup>2</sup>-sec<sup>-1</sup>.

3.2.2.2 Results of the tests indicated that the magnitude of the pressure surge decreased rapidly as the valve opening rate was decreased (Fig. 4), while the logarithmic decrement of the underdamped oscillatory wave remained relatively constant (Fig. 5). According to theory (Appendix I), if the logarithmic decrement is small, the magnitude of the initial surge peak should be approximately equal to two times the system pressure. From this it was evident that the damping effective during the initial pressure rise at slower valve opening rates was considerably higher than that which was indicated by the logarithmic decrement shown in Fig. 5.

3.2.2.3 A study of the pressure waveforms at various valve opening rates (Fig. 6) shows that the intersection point between the lower envelope of the underdamped oscillatory pressure wave and the initial pressure rise occurs at a higher pressure when the valve is opened more slowly. This intersection point was theorized to be a fair approximation of the initial pressure at the start of the underdamped oscillatory pressure wave. When the initial pressure ( $P_i$ ) at the start of the underdamped oscillatory wave was considered, the modified peak pressure ratio ( $P_m - P_i / P_o - P_i$ ) was approximately equal to two, which was in agreement with theory. The characteristics of the pressure wave below the described intersection point were those of an overdamped system. The portion of the pressure rise curve between the described intersection point and the point at which maximum rate of change in pressure rise occurs was considered indicative of the effect of valve resistance just after the valve started to open. It can be observed in Fig. 6 that the difference between these points increases as the valve opening rate decreases. The remaining portion of the pressure rise curve was considered to represent the highly overdamped condition prevalent during the lapped leakage range of valve travel.

Figure 5

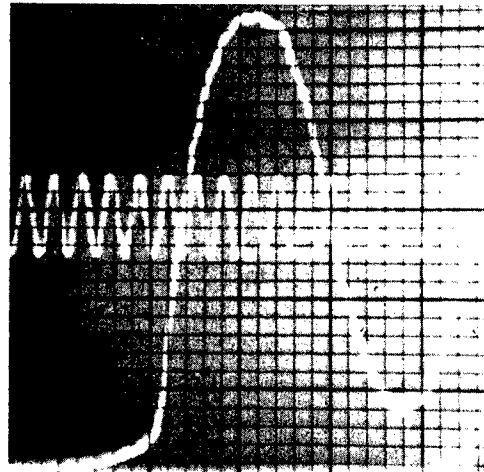
LOGARITHMIC DECREMENT VS. VALVE OPENING RATE  
CLOSED-END TUBE SYSTEM



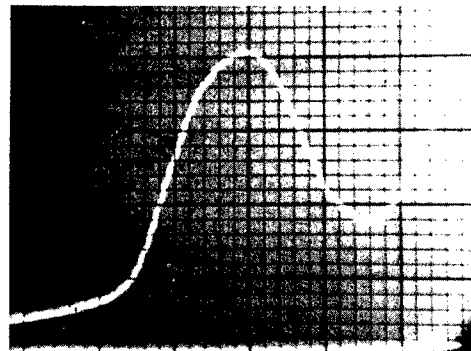
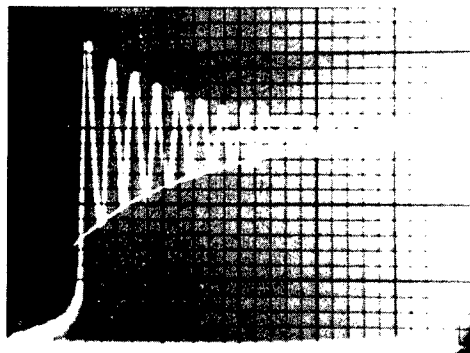
Notes: 96 in. test section length.  
Logarithmic decrement, based on first two peaks of pressure oscillation.

Figure 6

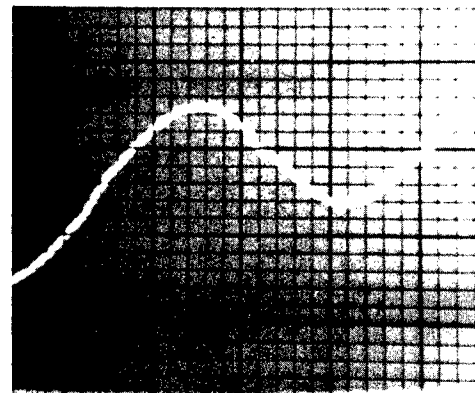
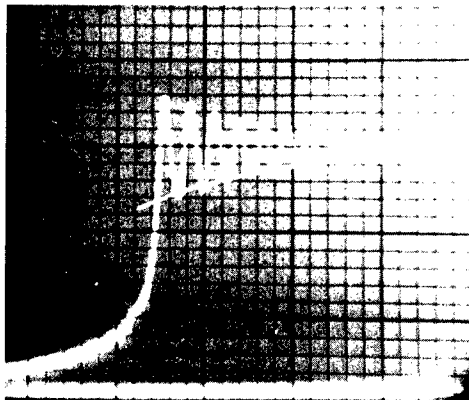
EFFECT OF VALVE OPENING RATE ON PRESSURE SURGE WAVEFORM  
CLOSED-END TUBE SYSTEM



21.  $\text{in}^2\text{-sec}^{-1}$  Valve Opening Rate



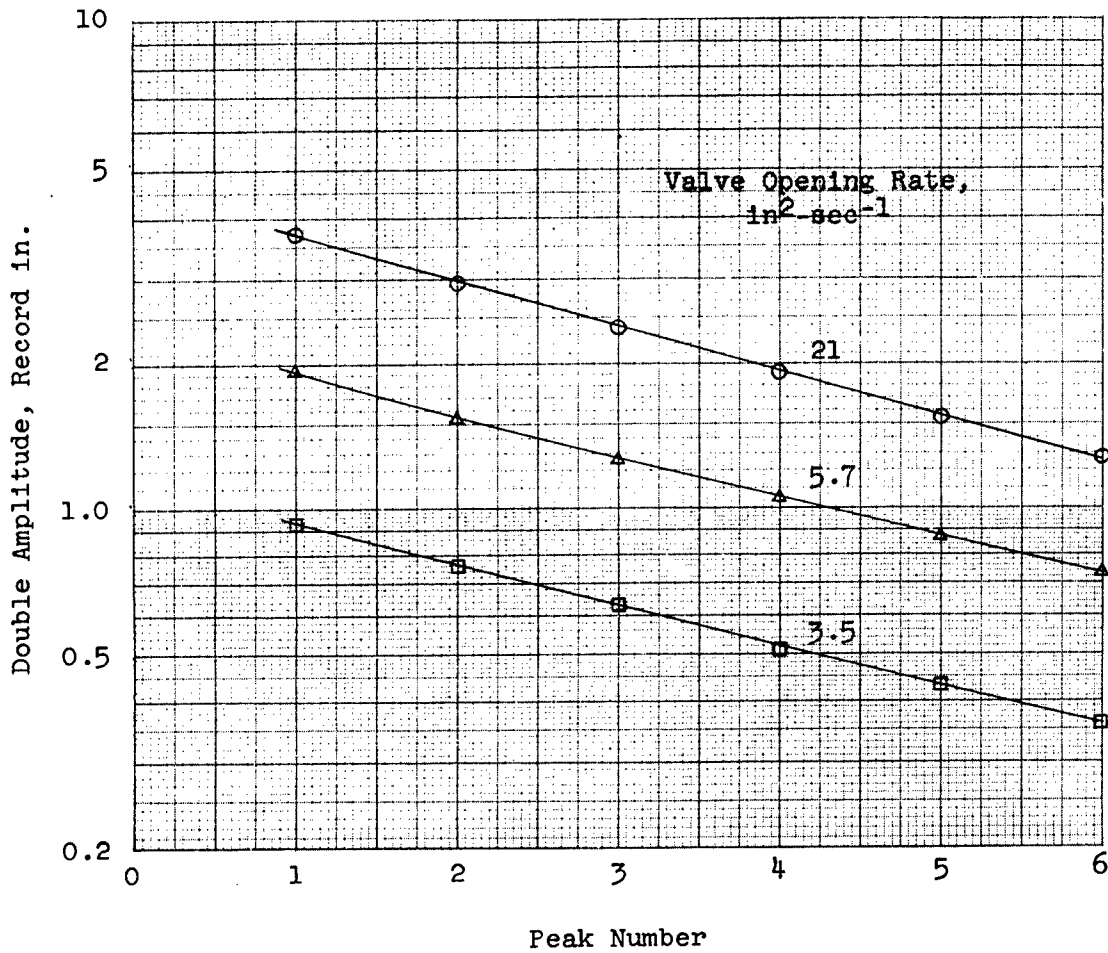
5.7  $\text{in}^2\text{-sec}^{-1}$  Valve Opening Rate



3.5  $\text{in}^2\text{-sec}^{-1}$  Valve Opening Rate

Figure 7

AMPLITUDE VS. PEAK NUMBER FOR VARIOUS VALVE OPENING RATES  
CLOSED END TUBE SYSTEM



Note: 96 in. test section length.

3.2.2.4 Semi-logarithmic plots of amplitude vs. peak number for the records shown in Fig. 6 indicated that the logarithmic decrement (slope of the plotted curve) varied slightly with peak number as well as valve opening rate (Fig. 7). This was attributed to the effect of turbulent damping and to the variation in effective valve resistance with spool position.

3.2.2.5 In order to establish the relationship between valve spool position and the pressure characteristics in the hydraulic system, pressure transducers (Statham Model No. P74-10MG-350) were located at various points in the system and simultaneous records of the pressure characteristics were made by photographing the traces on the screen of a dual-beam oscilloscope (Dumont Model No. 279). By use of this instrument synchronous traces were obtained and the relationship between the pressures was evaluated from a reference timing trace. Typical photographs of the pressure characteristics at various locations in the system are shown in Fig. 8. The test section length used in these tests was 192 in.

3.2.2.6 From data obtained by the method described in Par. 3.2.2.5, the following information was obtained:

- (a) When the Denison valve was opened, a pressure wave was sent down the tube and the shape of the wavefront was determined by the valve opening rate.
- (b) The time required for this wavefront to reach the closed end of the tube was determined by the velocity of wave propagation and the length of the system.
- (c) The magnitude of the pressure surge varied with location in the system, approximately as shown in Fig. 9.
- (d) On the basis of time intervals between wave fronts and the system length between pressure transducers, the velocity of wave propagation was found to be approximately  $50 \times 10^3$  in. sec<sup>-1</sup>.
- (e) Although the exact relationship between spool position and the pressure characteristics in the system was not definitely ascertained, a study of the data seemed to substantiate the assumption that initial opening of the valve porting was coincident with the maximum rate of change in the pressure rise curve adjacent to the valve.

3.2.2.7 From Ref. 1, p. 170, the fundamental frequency of an underdamped pressure oscillation in a closed-end tube system was found to be theoretically represented, if the damping is low, by

$$f = \frac{\mu_p}{4l} = \frac{1}{4l} \sqrt{\frac{1}{\beta_e \rho}} \quad (3-3)$$

where

- $f$  = fundamental frequency, cps  
 $l$  = total system length between accumulator and closed end of tube, in.  
 $\mu_p$  = velocity of wave propagation in oil filled tube, in. sec<sup>-1</sup>  
 $\beta_e$  = effective compressibility of oil filled tube, psi<sup>-1</sup>  
 $\rho$  = fluid mass density, lb-sec<sup>2</sup>-in<sup>-4</sup>

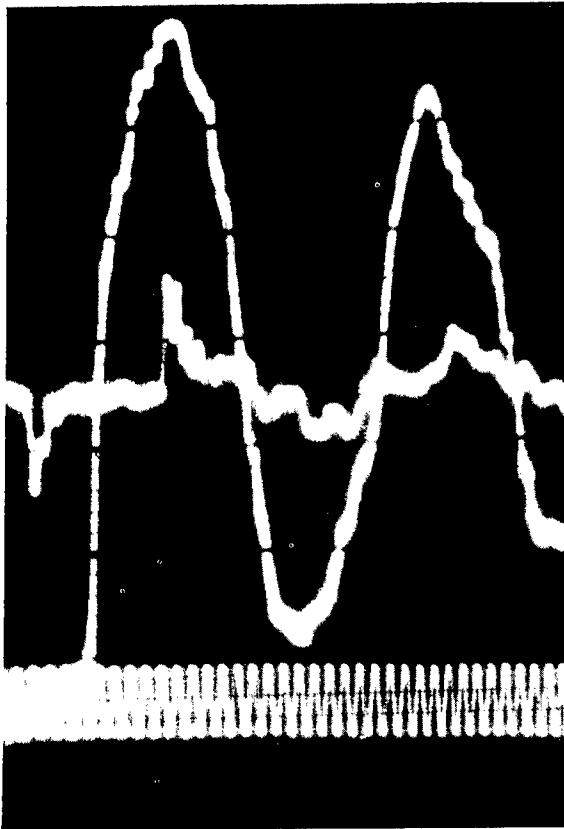
Using the isothermal compressibility of the test configuration, which was determined experimentally, the fluid mass density [at 38 C (100 F) temperature and 3000 psi pressure], and the total system length between the accumulator and the closed end of the tube, the fundamental frequency was calculated to be

$$f = \frac{1}{4 \times 132.5} \sqrt{\frac{1}{(4.7 \times 10^{-6})(79.4 \times 10^{-6})}} = \frac{51.8 \times 10^3}{530} = 98 \text{ cps}$$

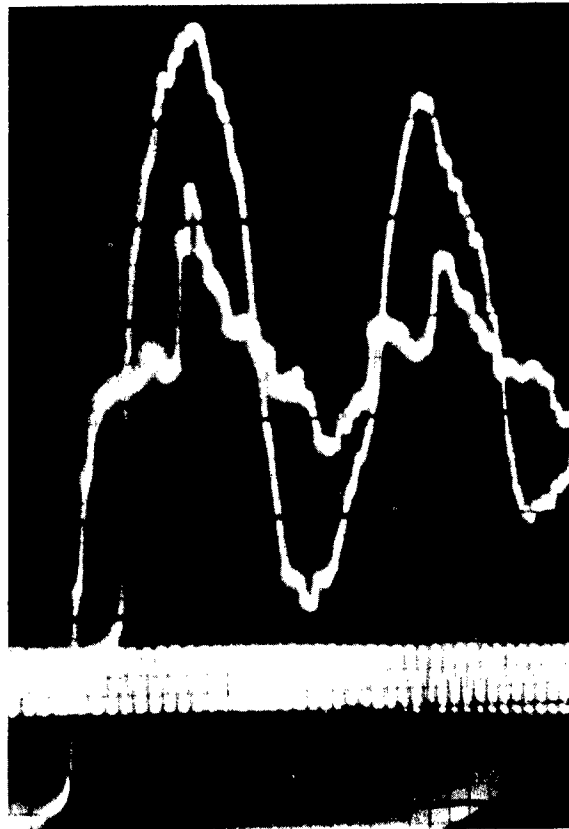


Figure 8

TYPICAL WAVEFRONT PROPAGATION AND RESULTING PRESSURE SURGES  
AT VARIOUS LOCATIONS IN CLOSED-END TUBE SYSTEMS



Before Denison Test Valve  
and at Closed-end  
of Test Section



After Denison Test Valve  
and at Closed-end  
of Test Section

Figure 9

ATTENUATION OF PEAK PRESSURE RATIO AT VARIOUS LOCATIONS  
CLOSED-END TUBE SYSTEM

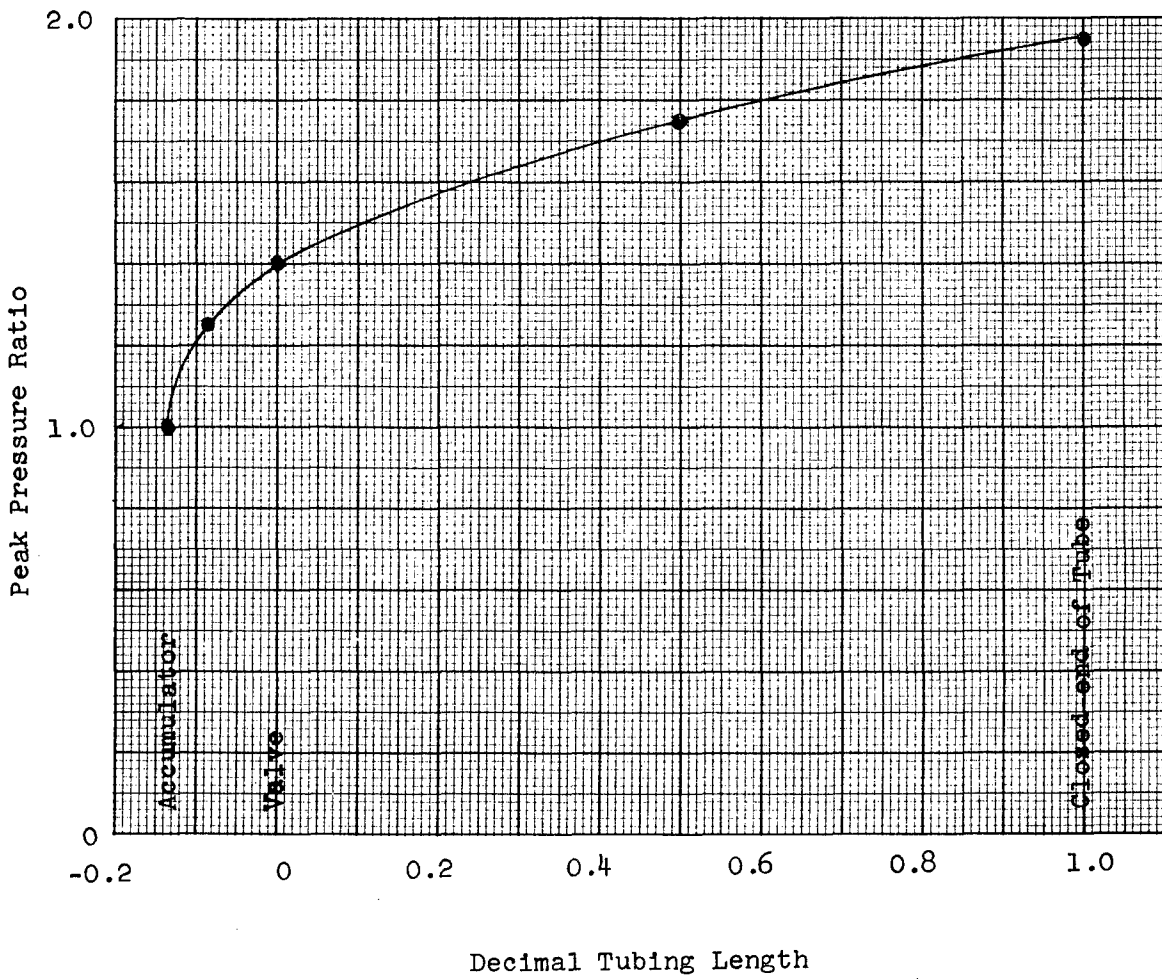
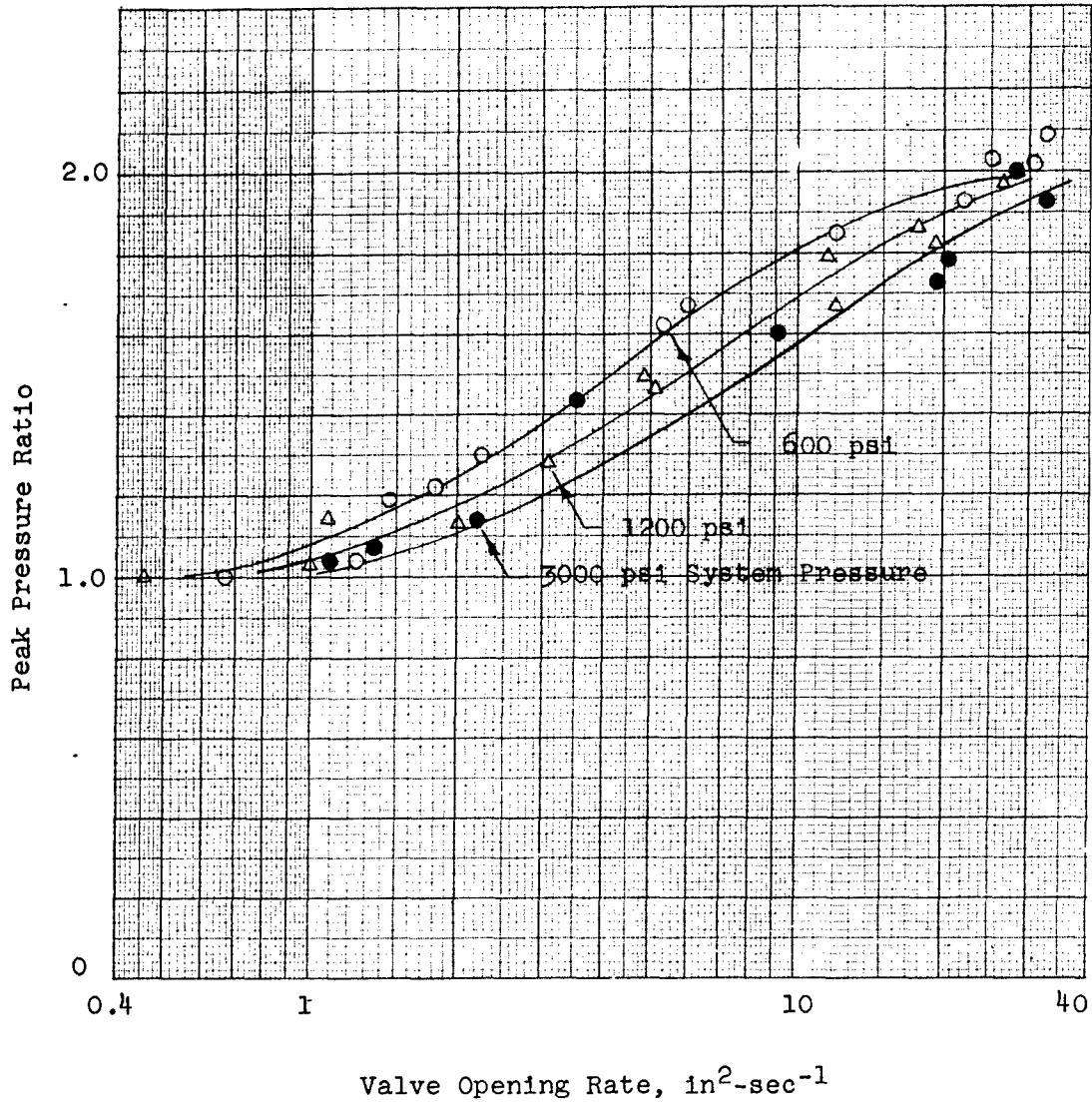


Figure 10

PEAK PRESSURE RATIO VS. VALVE OPENING RATE  
 AT VARIOUS SYSTEM PRESSURES  
 CLOSED-END TUBE SYSTEM



Note: 96 in. test section length

The total system length included the length of the flow path through the valve body as well as all fittings and tubing between the accumulator port and the closed end of the pressure transducer. By using experimentally determined values of isothermal compressibility, the elasticities of system elements such as the pressure transducer were accounted for more readily and the relationship between the effective (or adiabatic) and isothermal compressibilities could be correlated more accurately.

3.2.2.8 The average fundamental frequency measured from test records was 94.5 cps. Variations of  $\pm 2$  cps were observed, but these were considered within the limits of data reduction accuracy. Using the average frequency from the records, the effective compressibility of the system was calculated to be  $5.0 \times 10^{-6}$  psi<sup>-1</sup>. Results of the tests do not verify the difference between effective (adiabatic) compressibility and isothermal compressibility which was obtained in a previous investigation (Ref. 1, Fig. 120). This is more conclusively shown in the subsequent tests on closed-end tubes of varied lengths (Par. 3.2.4). Further substantiation that the difference between the effective and isothermal compressibilities was small is shown by comparison of the velocity of wave propagation experimentally determined (Par. 3.2.2.6) to that which was calculated in Par. 3.2.2.7.

### 3.2.3 System Pressure

3.2.3.1 To study the effect of system pressure on pressure surges, tests were conducted on a closed-end tube system under the following conditions:

- (a) System pressure, 600, 1200, 1800, 2400, and 3000 psi (Par. 3.2.2).
- (b) Accumulator precharge air pressure, 1/3 of system pressure.
- (c) Pump discharge flow rate, 2 gpm.
- (d) Fluid temperature,  $38 \pm 5$  C ( $100 \pm 9$  F).
- (e) Test section length, 96 in.
- (f) Valve opening rate, 1 - 30 in<sup>2</sup>-sec<sup>-1</sup>.

By using accumulator precharge air pressures of 1/3 system pressure, the performance characteristics of the accumulator were essentially the same for the various tests.

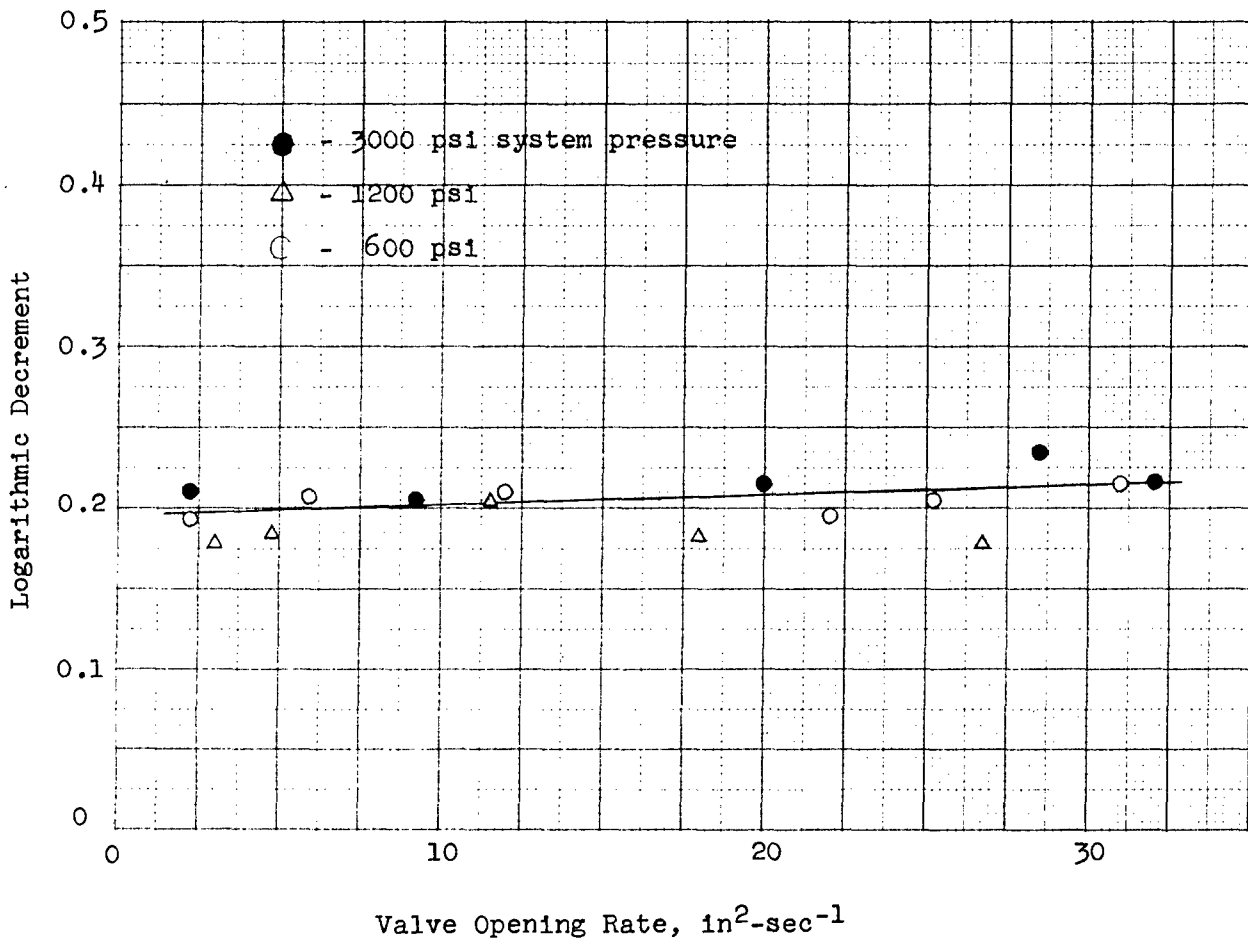
3.2.3.2 Comparison of the peak pressure ratio vs. valve opening rate curves at different system pressures indicated that for a given valve opening rate higher peak pressure ratios occurred at the lower system pressures (Fig. 10). A study of the logarithmic decrements of the underdamped oscillatory pressure waves (Fig. 11) revealed no significant variation which would account for the fore-mentioned differences in peak pressure ratios. This indicated that the damping effective during the initial pressure rise at a given valve opening rate increased with system pressure. Since damping is a function of resistance and since resistance is defined by the ratio of the pressure differential to flow rate (Appendix I, Eq. 20), a study of the curves in Fig. 3 will show that higher peak pressure ratios were to be expected due to lower valve resistances at the lower pressure differentials. For actual system analysis, however, the  $\Delta p$ -Q-X relationships for dynamic flow conditions should be considered.

3.2.3.3 The relationship between the peak pressure ratio and the maximum rate of pressure rise indicated that for a given peak pressure ratio the maximum rate of pressure rise increased with system pressure (Fig. 12). By cross-plotting the data from Fig. 10 and 12 on logarithmic graph paper (Fig. 13) it was found that the relationship between the maximum rate of pressure rise and valve opening rate at a given system pressure conformed reasonably well with the general law of the form  $x = cy^n$ , in which n was approximately equal to 1. This indicates the effective damping during the initial pressure rise to be primarily due to valve resistance.

3.2.3.4 The fundamental frequency of the underdamped oscillatory pressure wave was found to increase slightly with system pressure in the following manner:

Figure 11

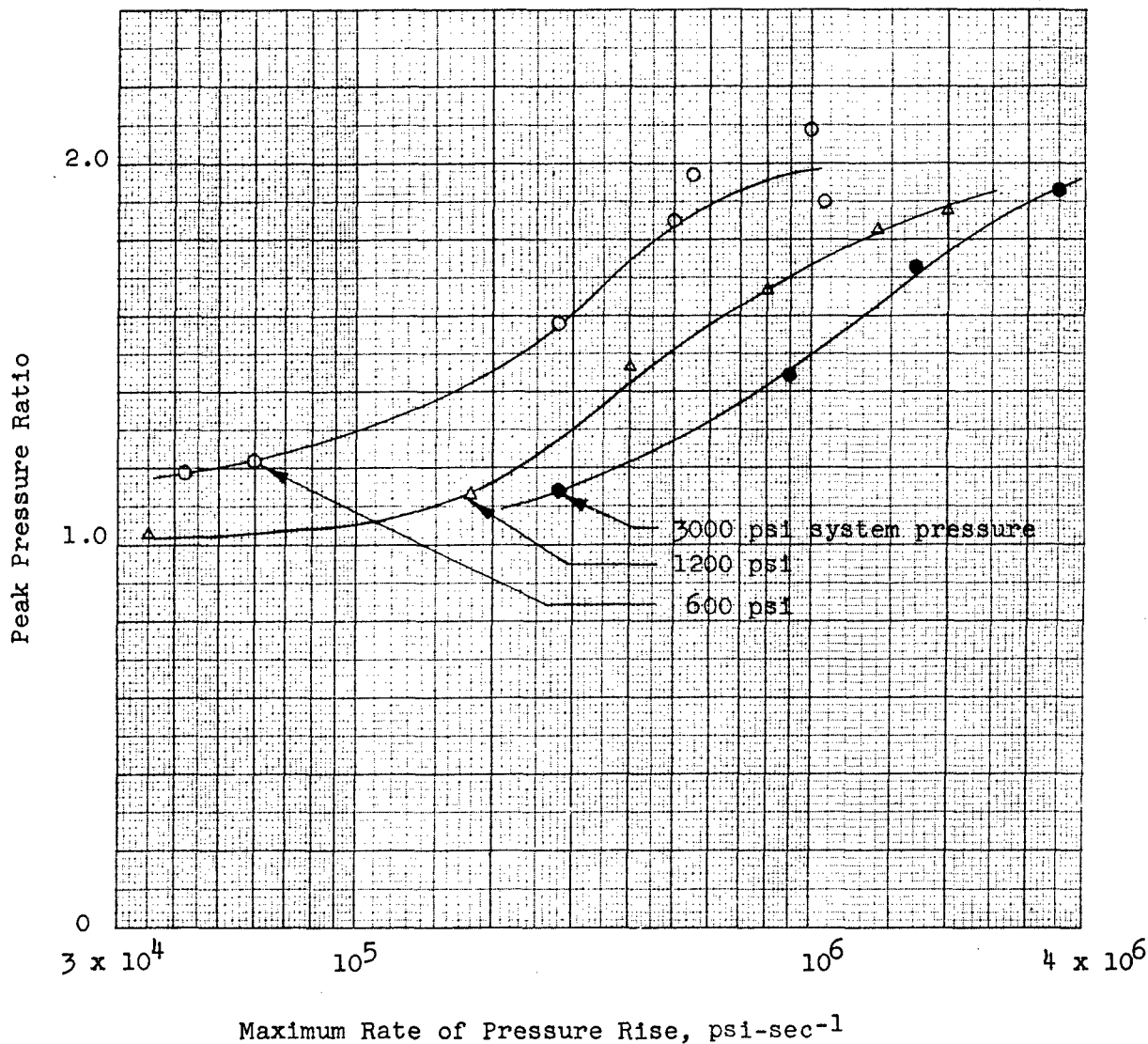
LOGARITHMIC DECREMENT VS. VALVE OPENING RATE  
 AT VARIOUS SYSTEM PRESSURES  
 CLOSED-END TUBE SYSTEM



Notes: 96 in. test section length.  
 Logarithmic decrement based on first two peaks of pressure oscillation.

Figure 12

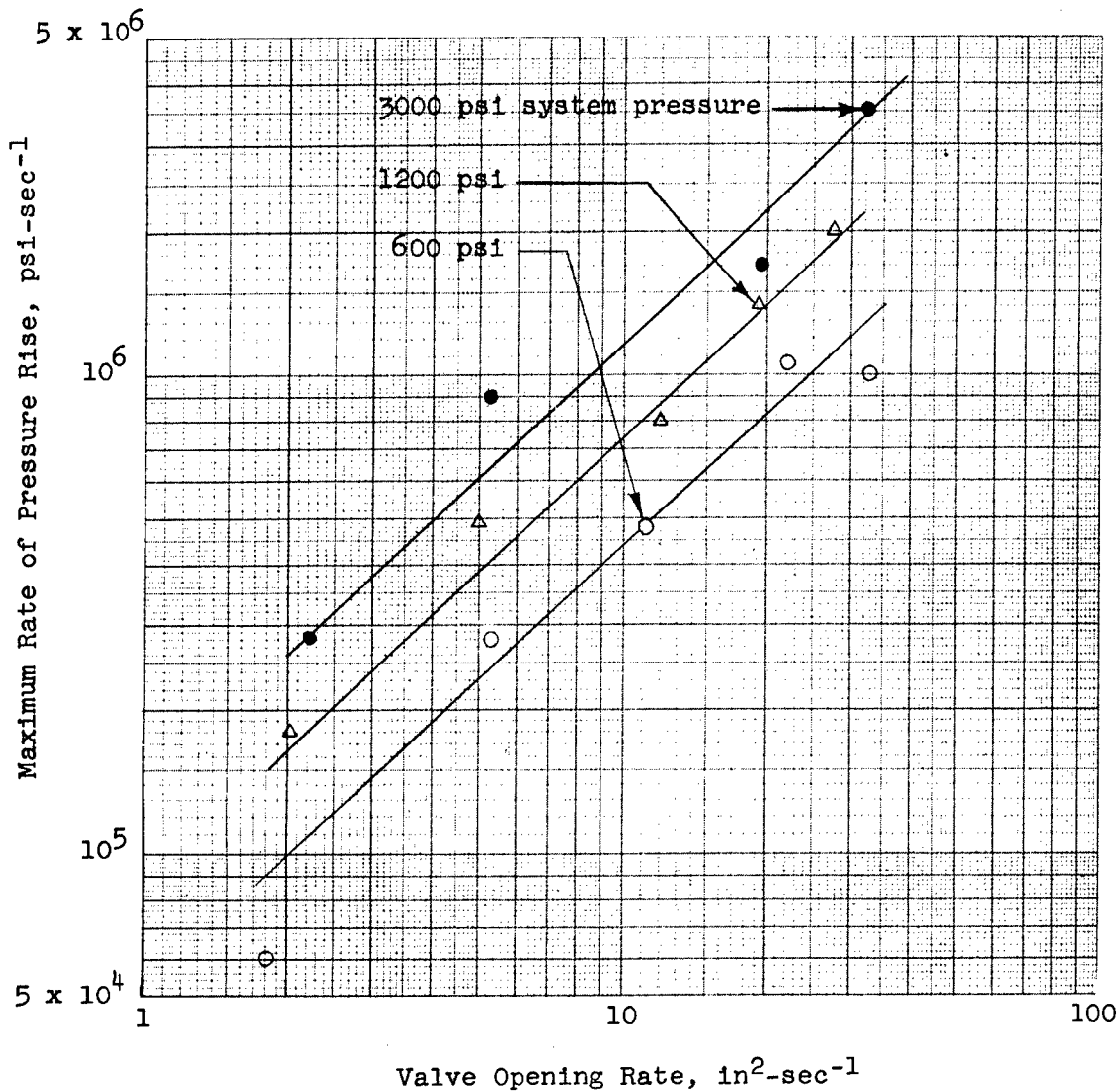
PEAK PRESSURE RATIO VS. MAXIMUM RATE OF PRESSURE RISE  
 AT VARIOUS SYSTEM PRESSURES  
 CLOSED-END TUBE SYSTEM



Note: 96 in. test section length.

Figure 13

MAXIMUM RATE OF PRESSURE RISE VS. VALVE OPENING RATE  
 AT VARIOUS SYSTEM PRESSURES  
 CLOSED-END TUBE SYSTEM



Note: 96 in. test section length

<u>System Pressure, psi</u>	<u>Frequency of Fundamental Wave, cps</u>
600	89.5
1200	92.2
1800	92.4
2400	93.3
3000	94.5

The values shown are average for the test runs made at the specific system pressures. The variation of frequency with pressure was attributed to the effect of pressure on the compressibility and mass density of the hydraulic fluid, the factors used to determine the velocity of wave propagation.

### 3.2.4 System Flow Rate

3.2.4.1 The effect of system flow rate was investigated by studying the pressure surges in a closed-end tube at various pump discharge flow rates both with and without a system accumulator. Specific test conditions were as follows:

- (a) System pressure, 3000 psi.
- (b) Accumulator precharge air pressure, 1000 psi.
- (c) Pump discharge flow rate, 2, 4, 8, and 16 gpm.
- (d) Fluid temperature,  $38 \pm 5$  C ( $100 \pm 9$  F).
- (e) Test section length, 96 in.
- (f) Valve opening rate,  $28 \pm 2$  in<sup>2</sup>-sec<sup>-1</sup>.

Pump discharge flow rates up to 8 gpm were obtained by controlling the speed of the constant displacement pump (Vickers Model No. PF-3911-25ZE) used in the basic hydraulic system (Fig. 1). Pump discharge flow rates above 8 gpm were obtained by use of the Laboratory test stand which had a manually controlled variable displacement pump (Denison Model No. PA-172-570-B). All flows were adjusted to the desired value at 3000 psi pump discharge pressure.

3.2.4.2 Tests conducted with the accumulator installed in the system indicated that the pump discharge flow rate had no appreciable effect on the magnitude of the pressure surge (Fig. 14). In tests performed with no accumulator in the system, the magnitude of the initial surge peak was low and was affected only slightly by the pump discharge flow rate (Fig. 14). The significance of the difference between the curves for the two different system pumps without the system accumulator was in the volumetric difference in the pressurized systems. A study of the characteristic form of the pressure wave which resulted when there was no accumulator installed was that of an underdamped oscillatory pressure wave superimposed upon a mean rate of pressure rise which varied with pump discharge flow rate. Typical photographs of the characteristic waveform for the systems using the two different pumps are shown in Fig. 15. For a clearer understanding of the characteristics of these waveforms, it is necessary to visualize the pressure waveform which would result in the closed-end tube if no system pump had been present at the time the valve was opened. In this case, the pressure surge would have oscillated about a mean system pressure which was a function of the initial pressures and volumes of the pressurized and unpressurized regions of the system. It was noted from the test records that the intercept point between the mean pressure curve, determined from the envelopes of the underdamped oscillation, and the initial pressure rise were not appreciably affected by the pump discharge flow rate.

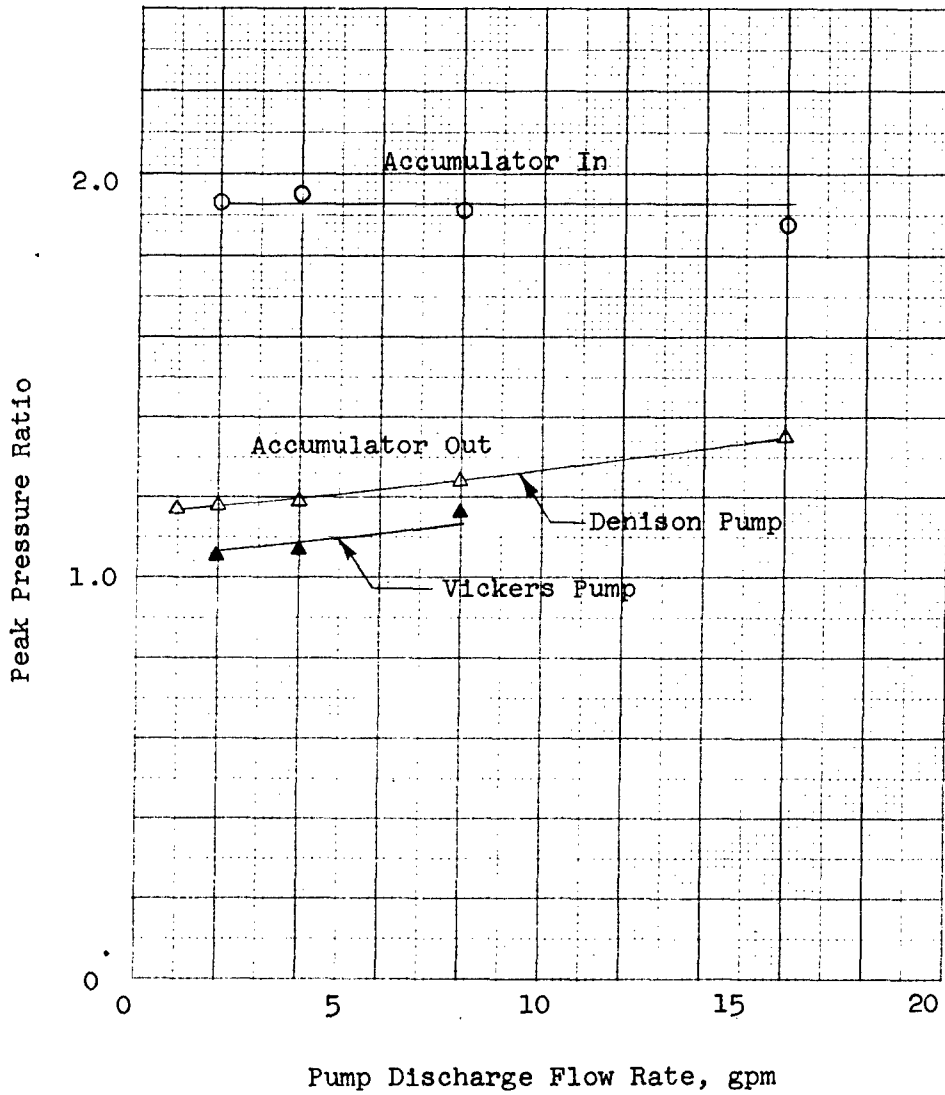
3.2.4.3 The effect of pump discharge flow rate on the logarithmic decrement of the underdamped pressure oscillation which occurred with an accumulator installed in the system was negligible. The logarithmic decrement varied with valve opening rate approximately as shown in Fig. 5. The determination of logarithmic decrements from the underdamped pressure oscillations which occurred with no accumulator installed in the system was rendered impractical due to the characteristics of the waveform (Fig. 15).

3.2.4.4 With the accumulator installed in the system, the frequency of the fundamental pressure wave was not affected by the pump discharge flow rate. The average frequency observed was essentially the same as in Par. 3.2.2.8. With



Figure 14

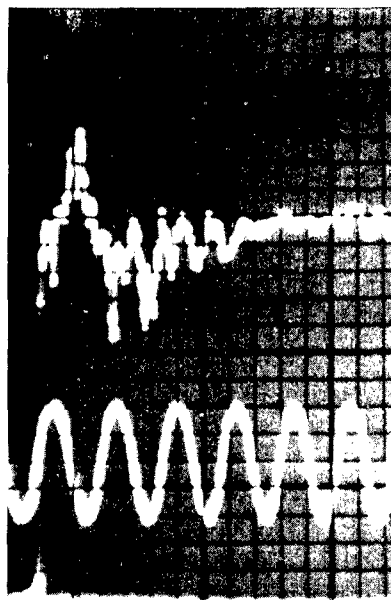
PEAK PRESSURE RATIO VS. PUMP DISCHARGE FLOW RATE  
 FOR CLOSED END TUBE SYSTEMS  
 WITH AND WITHOUT AN ACCUMULATOR



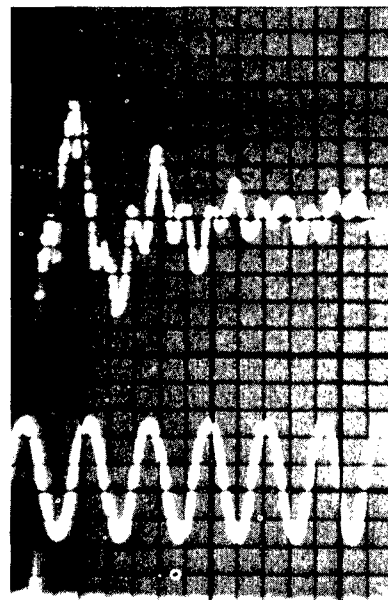
Note: 96 in. test section length.

Figure 15

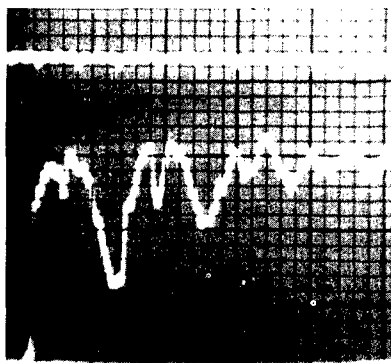
CHARACTERISTICS OF PRESSURE SURGE WAVEFORM WITHOUT AN ACCUMULATOR  
CLOSED-END TUBE SYSTEMS



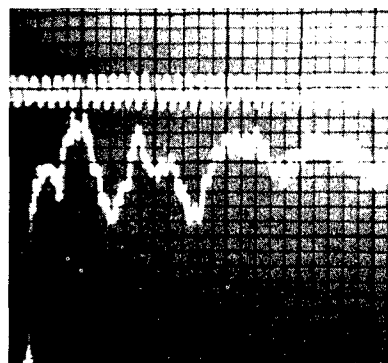
Denison Pump - 2 gpm



Denison Pump - 8 gpm



Vickers Pump - 2 gpm

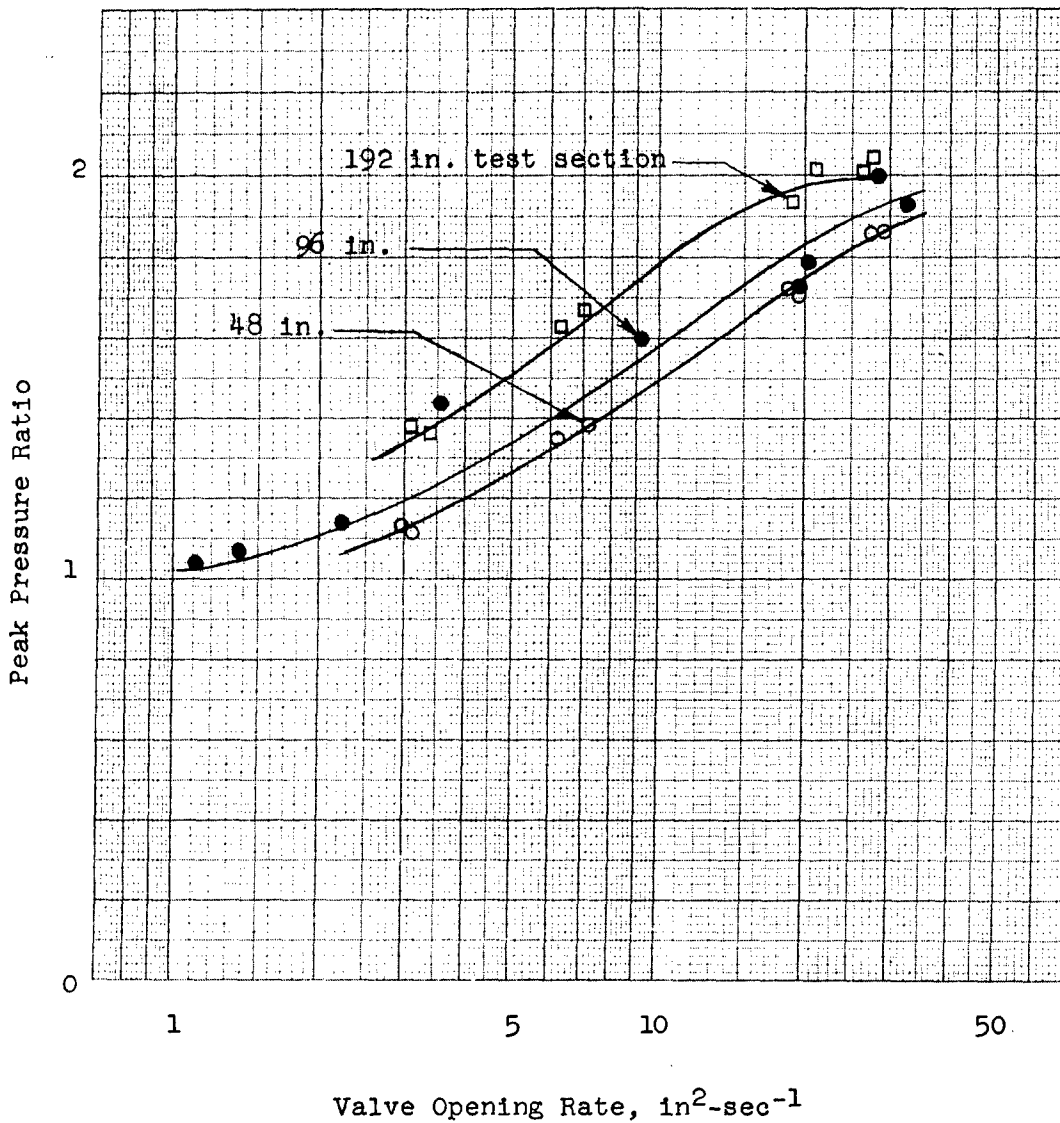


Vickers Pump - 8 gpm

Notes: Higher frequencies on waveform of Vickers pump were due to pump ripple  
96 in. test section length.

Figure 16

PEAK PRESSURE RATIO VS. VALVE OPENING RATE  
 FOR VARIOUS SYSTEM LENGTHS  
 CLOSED-END TUBE SYSTEMS



no accumulator installed in the system, there were two or more frequencies present (Fig. 15). The lower frequency, considered to be the fundamental, appeared to be a function of system configuration, but did increase somewhat with pump discharge flow rate. The higher frequencies appeared to be characteristic of the frequencies present in pump ripple. Data obtained from the records on the two system configurations (Vickers pump and Denison pump) were as follows:

<u>Pump Identification</u>	<u>Discharge Flow Rate, gpm</u>	<u>Frequency of Fundamental, cps</u>	<u>Frequency of Pump Ripple, cps</u>
Vickers	2	66	162
Vickers	4	68	299
Vickers	8	70	608
Denison	1	30	259
Denison	2	31	259
Denison	4	41	259
Denison	8	44	259
Denison	16	40	259

### 3.2.5 System Length

3.2.5.1 Studies were made of the pressure surges which occurred in closed-end tubes of various lengths under the following test conditions:

- (a) System pressure, 3000 psi.
- (b) Accumulator precharge air pressure, 1000 psi.
- (c) Pump discharge flow rate, 2 gpm.
- (d) Fluid temperature,  $38 \pm 5$  C ( $100 \pm 9$  F).
- (e) Test section length, 24, 48, 96 (Par. 3.2.2), 144, and 192 in.
- (f) Valve opening rate, 1 - 30 in<sup>2</sup>-sec<sup>-1</sup>.

For use in theoretical analysis, measurements were made of the system length, system volume, and isothermal compressibility of that portion of the system between the accumulator and closed end of the tube. Pertinent data were as follows:

<u>Test Section Length, in.</u>	<u>Total System Length, in.</u>	<u>Total System Volume, in<sup>3</sup></u>	<u>Isothermal Compressibility, psi</u>
24	60.5	7.4	$5.0 \times 10^{-6}$
48	84.5	10.7	$4.9 \times 10^{-6}$
96	132.5	17.5	$4.7 \times 10^{-6}$
144	180.5	23.9	$4.65 \times 10^{-6}$
192	228.5	30.3	$4.6 \times 10^{-6}$

Isothermal compressibility measurements did not include the valve, but the error was considered small.

3.2.5.2 The results of the tests indicated that the magnitude of the pressure surge increased with system length, the increase being greatest at the intermediate valve opening rates (Fig. 16). Although lower surge peaks might have been expected due to the increased damping associated with longer lines, it was evident from the test results that the relative effect of valve resistance on the total system damping during the initial pressure rise was less on the longer systems. Another way of visualizing this effect is to consider that for a given valve opening rate the leakage through the valve prior to actual opening is essentially constant. Consequently, the pressure buildup in the test section prior to actual opening of the valve will be a function of the volume.

3.2.5.3 Studies of the logarithmic decrements of the underdamped oscillatory pressure waves indicated the influence of the valve resistance on the total system damping (Fig. 17). Semi-logarithmic plots of amplitude vs. peak number at various valve opening rates on the 48 in. test section (Fig. 18) show how influential the valve resistance became on the total system damping (indicated by slope of curve) when the frequency of the fundamental pressure wave was high. From the work accomplished thus far, it could be seen that one of the major problems in theoretical analysis of a hydraulic system was that of adequately accounting for the effect of non-linear valve resistance on the total system damping.

Figure 17

LOGARITHMIC DECREMENT VS. TEST SECTION LENGTH  
FOR RAPID OPENING VALVE  
CLOSED-END TUBE SYSTEMS

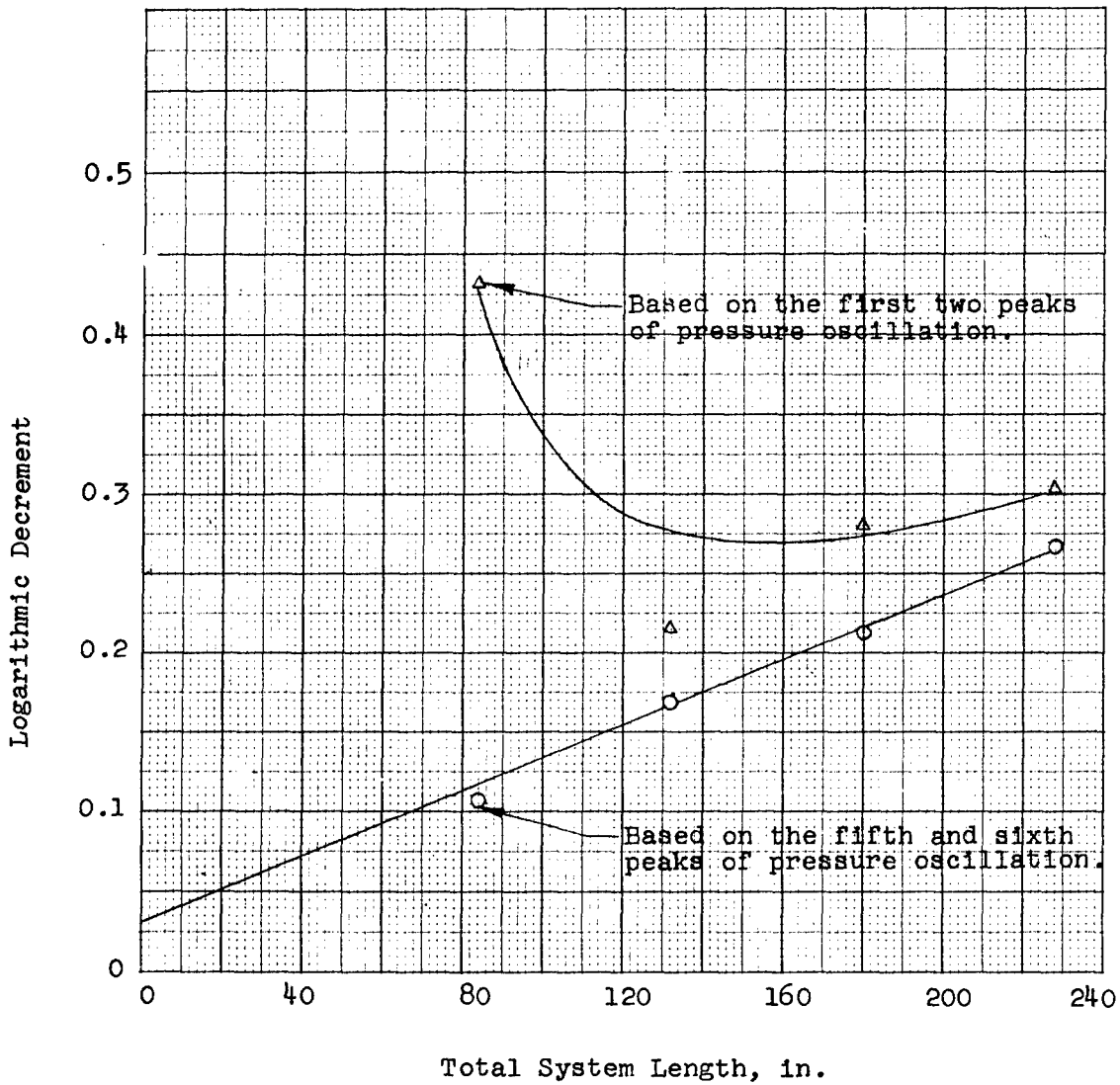
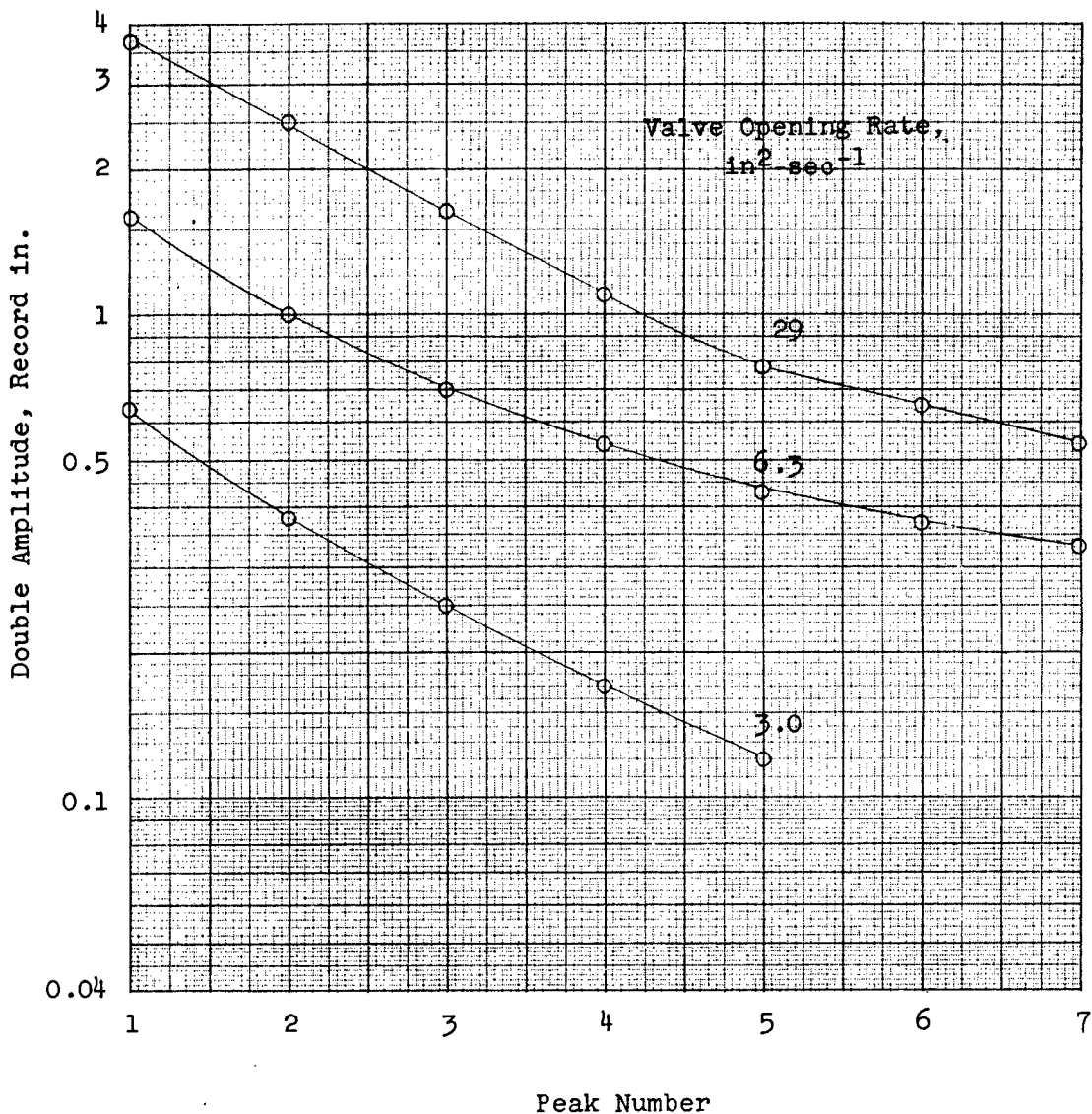


Figure 18

AMPLITUDE VS. PEAK NUMBER FOR VARIOUS VALVE OPENING RATES  
ON 48 IN. TEST SECTION  
CLOSED-END TUBE SYSTEM



Note: 48 in. test section length.

Figure 19

FREQUENCY OF FUNDAMENTAL PRESSURE WAVE VS. VALVE OPENING RATE  
 FOR VARIOUS TEST SECTION LENGTHS  
 CLOSED-END TUBE SYSTEMS

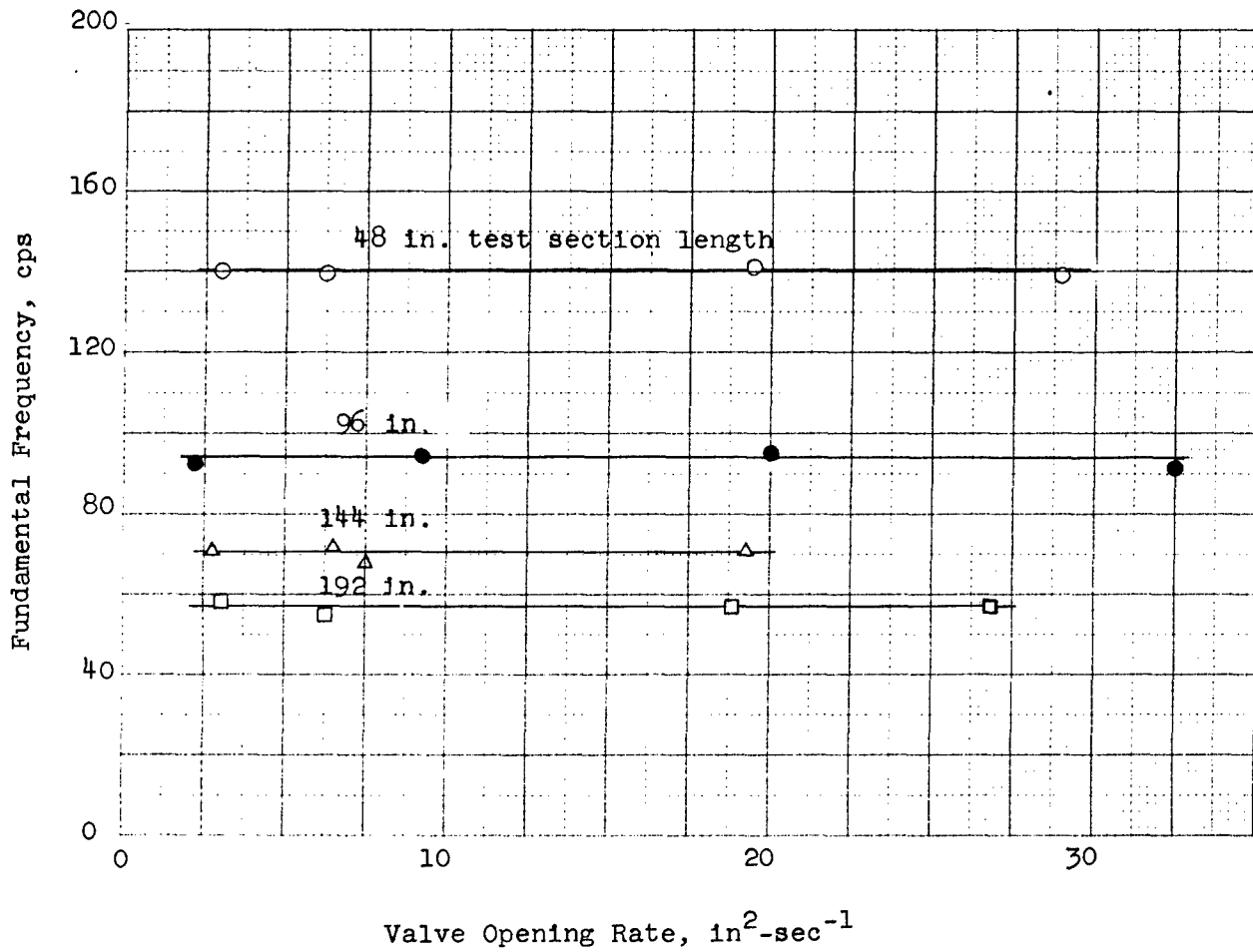
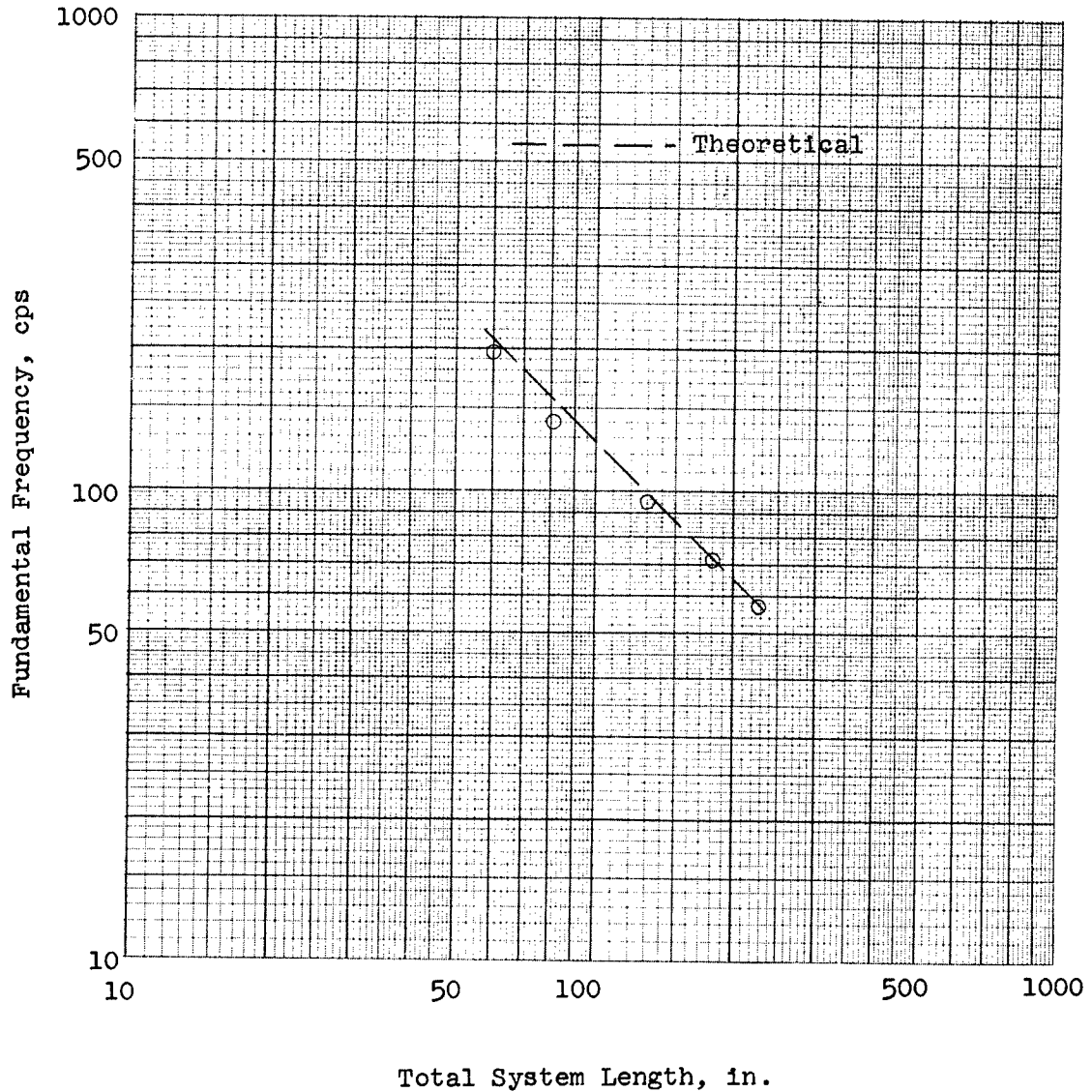


Figure 20

FREQUENCY OF FUNDAMENTAL PRESSURE WAVE VS. TOTAL SYSTEM LENGTH  
CLOSED-END TUBE SYSTEMS

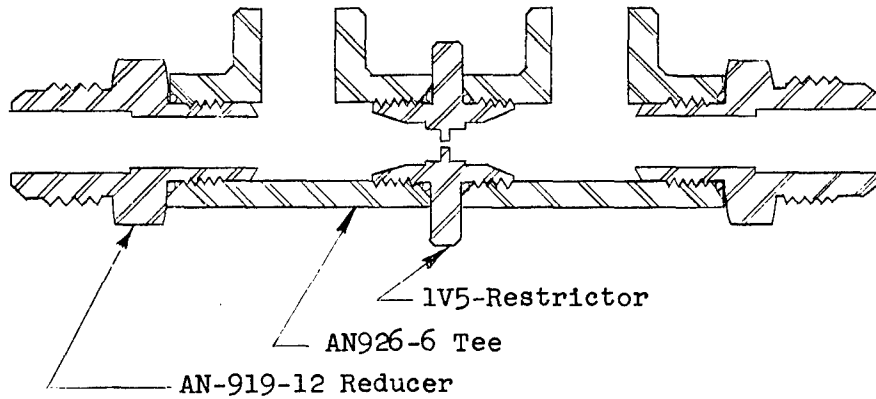


Note: Theoretical curve based on Eq. 3-3 and data in Par. 3.2.5.1.



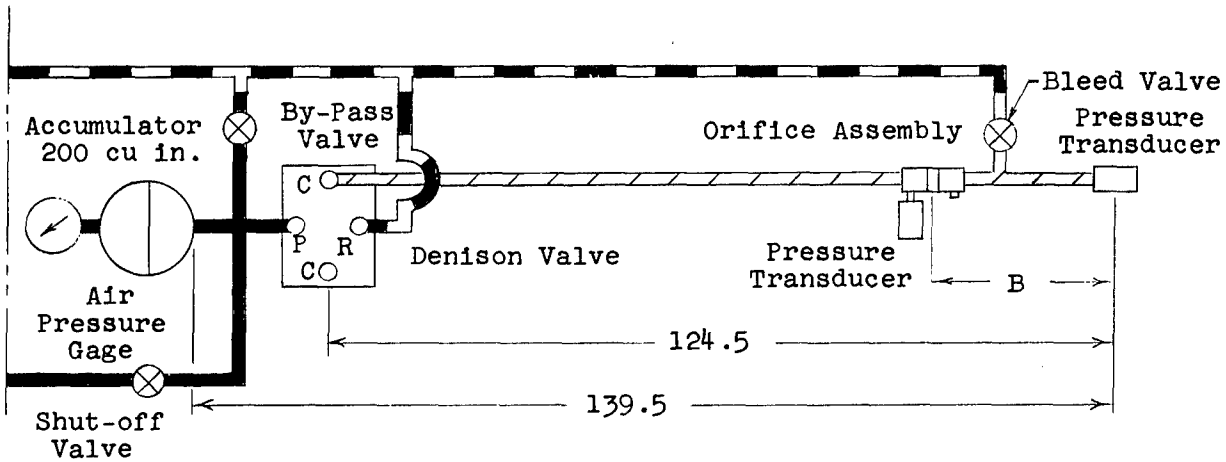
Figure 21

PERTINENT INFORMATION ON SYSTEM CONFIGURATION  
FOR INVESTIGATION OF ORIFICES, CLOSED-END TUBE SYSTEM



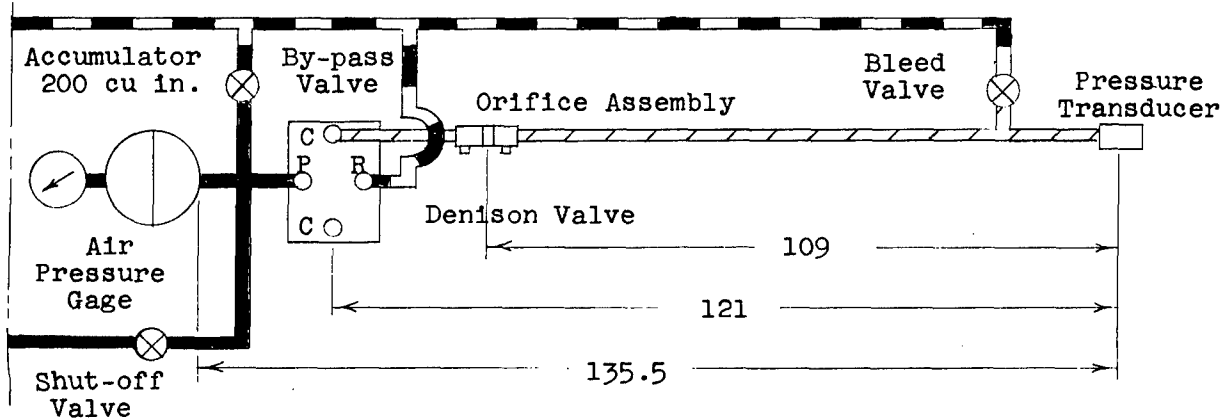
Basic Orifice Assembly

For Line Continuation  
See Fig. 1



Configuration A

For Line Continuation  
See Fig. 1



Configuration B

3.2.5.4 The frequency of the fundamental pressure wave, measured from the test records, was found to be relatively independent of valve opening rate (Fig. 19), but varied with total system length as shown in Fig. 20. Comparison of theoretical values of frequency, calculated from Eq. 3-3 and the data presented in Par. 3.2.5.1, to the experimental values (Fig. 20) did not show any appreciable difference. This seemed to indicate that the effective compressibility of the system under dynamic conditions was approximately the same as the compressibility of the system under isothermal conditions.

### 3.2.6 Orifices

3.2.6.1 The effect of orifices was investigated by locating orifices of various sizes at different points in the system and studying the resulting pressure surges in the closed-end tube. Specific test conditions were as follows:

- (a) System pressure, 3000 psi.
- (b) Accumulator precharge air pressure, 1000 psi.
- (c) Pump discharge flow rate, 2 gpm.
- (d) Fluid temperature,  $38 \pm 5$  C ( $100 \pm 9$  F).
- (e) Valve opening rate,  $28 \pm 2$  in<sup>2</sup>-sec<sup>-1</sup>.
- (f) Orifice diameter, 0.50 - 0.20 in.
- (g) Orifice location, configuration A and configuration B (Fig. 21).

Details of the basic orifice assembly and of the system configurations tested are shown in Fig. 21. For these tests the two Hydrauliscopes (Par. 3.2.1.3) were used to simultaneously record the pressures at two points in the system. Valve opening rates within the described tolerance was established by the controlled flow conditions in the pilot system.

3.2.6.2 Results of the tests indicated that orifice size (area) was very effective in attenuating the magnitude of the surge peak at the closed end of the tube (Fig. 22), especially when the orifice was located near the energy source. This was due to the effect of orifice size and location on the total system damping, indicated by the logarithmic decrement vs. orifice area plots shown in Fig. 23.

3.2.6.3 Using the experimental data on logarithmic decrements and the method presented in Appendix I (Par. 7.1.3), the effective resistances of the various orifices were evaluated. From basic equations, resistance is described by the equation

$$R = \frac{\Delta p}{Q} \quad (3-4)$$

where

$$\begin{aligned} R &= \text{resistance, lb-sec-in}^{-5} \\ \Delta p &= \text{pressure differential, lb-in}^{-2} \\ Q &= \text{flow rate, in}^3\text{-sec}^{-1} \end{aligned}$$

The equation for flow through a sharp-edged orifice is

$$Q = cA_o \sqrt{\frac{2\Delta p}{\rho}} \quad (3-5)$$

where

$$\begin{aligned} Q &= \text{flow rate, in}^3\text{-sec}^{-1} \\ A_o &= \text{orifice area, in}^2 \\ \Delta p &= \text{pressure differential across orifice, lb-in}^{-2} \\ \rho &= \text{mass density of fluid, lb-sec}^2\text{-in}^{-4} \\ c &= \text{discharge coefficient (including contraction and velocity coefficients)} \end{aligned}$$

Figure 22

PEAK PRESSURE RATIO VS. ORIFICE AREA  
FOR TWO DIFFERENT ORIFICE LOCATIONS  
CLOSED-END TUBE SYSTEM

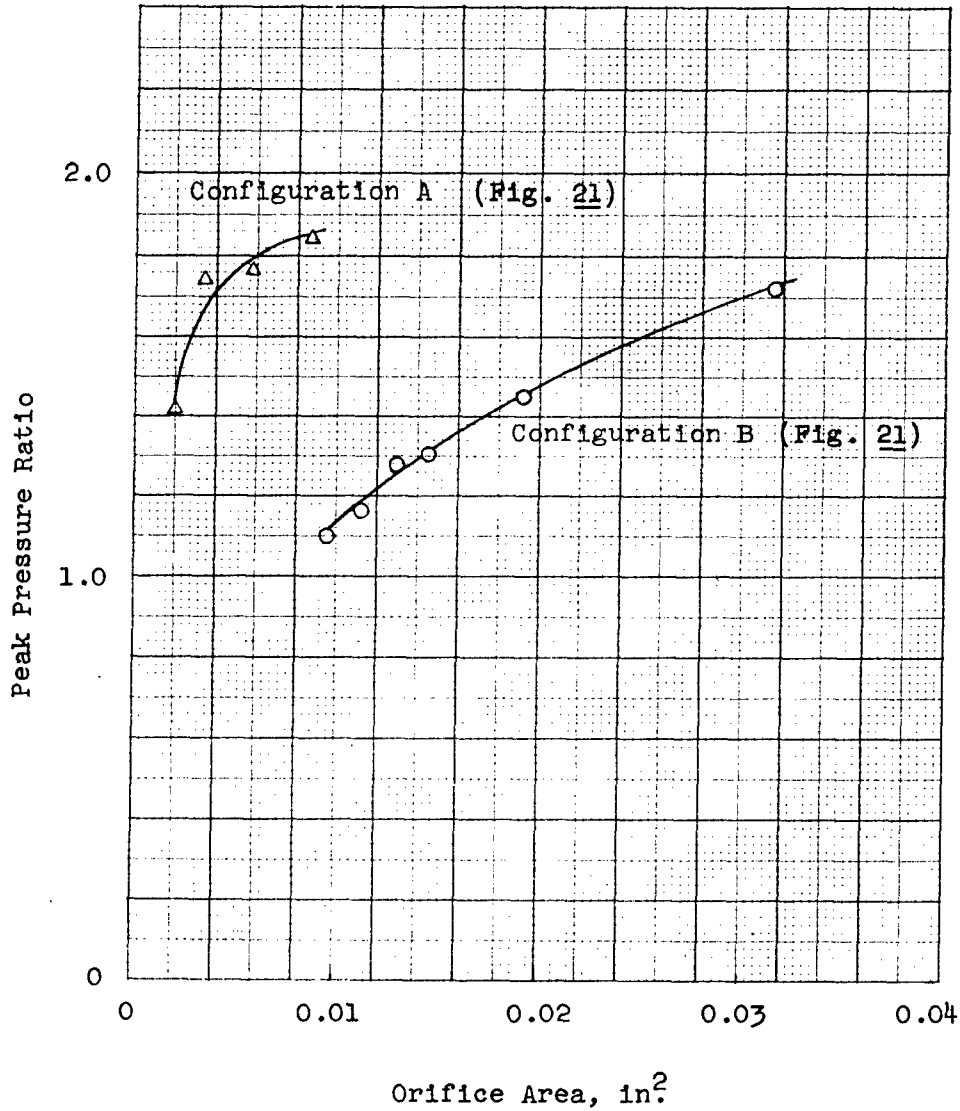


Figure 23

LOGARITHMIC DECREMENT VS. ORIFICE AREA  
 FOR TWO DIFFERENT ORIFICE LOCATIONS  
 CLOSED-END TUBE SYSTEM

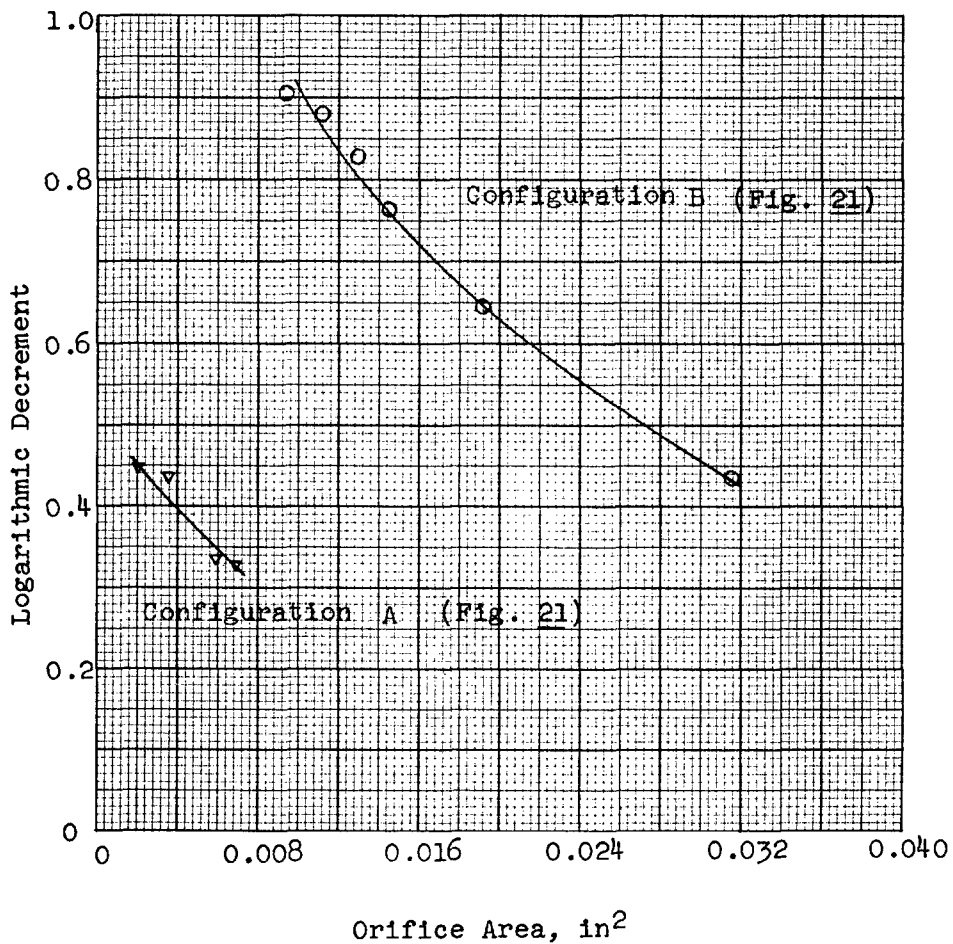
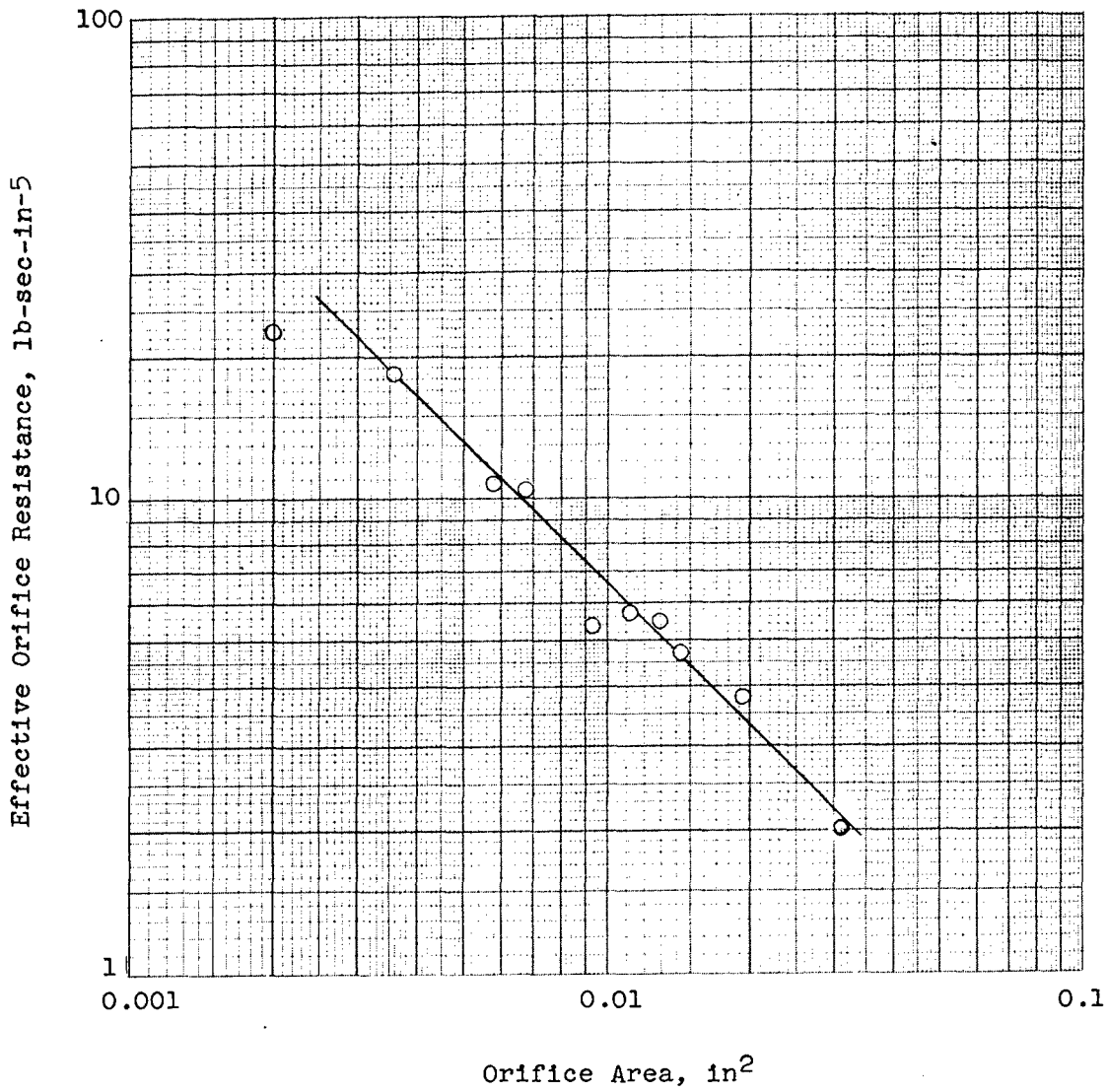


Figure 24

EFFECTIVE ORIFICE RESISTANCE VS. ORIFICE AREA



Assuming that the average pressure differential across the orifices, the discharge coefficient, and the mass density of the fluid were nearly constant for the tests conducted, Eq. 3-5 can be reduced to the general form of  $Q = KA^{-1}$ , which should give a straight line with a slope of -1 on logarithmic graph paper. Plotting the effective resistance values obtained from experimental data vs. orifice area on logarithmic graph paper (Fig. 24) indicated that the assumption made were reasonable. The developed relationships also show that the effective resistance of a given orifice varies as the square root of the pressure differential across the orifice.

3.2.6.4 The frequency of the fundamental pressure wave was found to be relatively constant even though the attenuation factor ( $\alpha$ ) of the system was increased appreciably. The average frequency observed was approximately the same as in Par. 3.2.2.8.

### 3.2.7 Branch Circuits

3.2.7.1 The effect of branch circuits on the pressure surges in closed-end tube systems was investigated by conducting tests under the following conditions:

- (a) System pressure, 3000 psi.
- (b) Accumulator precharge air pressure, 1000 psi.
- (c) Pump discharge flow rate, 2 gpm.
- (d) Fluid temperature,  $38 \pm 5$  C ( $100 \pm 9$  F).
- (e) Valve opening rate, 3-30 in<sup>2</sup>-sec<sup>-1</sup>.
- (f) Branch circuit configurations, variable numbers of 1, 2, 3, and 4 branches of equal length (96 in. test sections), variable lengths on dual branch circuits of 48 and 96 in., 96 and 144 in., 96 and 192 in., and 48 and 192 in. test sections.

For these tests a symmetrical manifold, with four ports located at 90 deg intervals normal to the inlet port, was installed at the tee adjacent to the Denison valve (Fig. 1). The test sections were connected to bulkhead elbows in these ports, such that the tubing was parallel, and bleed valves were located at the closed end of each test section. With this configuration, the fluid followed symmetrical flow paths to each test section.

3.2.7.2 Results of the tests on branch circuits of varying numbers of equal length test sections gave the following relationships:

- (a) The magnitude of the surge peak decreased as the number of branches was increased and as the valve opening rate was decreased (Fig. 25).
- (b) The logarithmic decrement increased with the number of branches and varied considerably with valve opening rate (Fig. 26).
- (c) The frequency of the fundamental pressure wave decreased as the number of branches was increased, but remained relatively constant for variations of valve opening rate (Fig. 27).

3.2.7.3 The addition of two 90 deg bends in the flow path increased the logarithmic decrement of the single branch circuit (Fig. 26), but this increase did not appreciably effect the magnitude of the surge peak. This can be seen by comparing the data in Fig. 4 and 25. The logarithmic decrement was found to vary considerably with the peak number (Fig. 28) as well as with valve opening rate. Due to limited time, a complete analysis of the factors which influenced the characteristics shown was not possible. Consideration of the equivalent electrical analog of these parallel circuits will show the complexity of the problem.

3.2.7.4 A method was developed in Appendix I, Par. 3.4, which provided a means for predicting the approximate frequency of the fundamental wave for varying numbers of equal length branches. A comparison of actual test results to values calculated by the developed relationships is given in the following table:

Figure 25

PEAK PRESSURE RATIO VS. VALVE OPENING RATE  
FOR VARIOUS NUMBERS OF EQUAL LENGTH BRANCHES  
CLOSED-END TUBE SYSTEMS

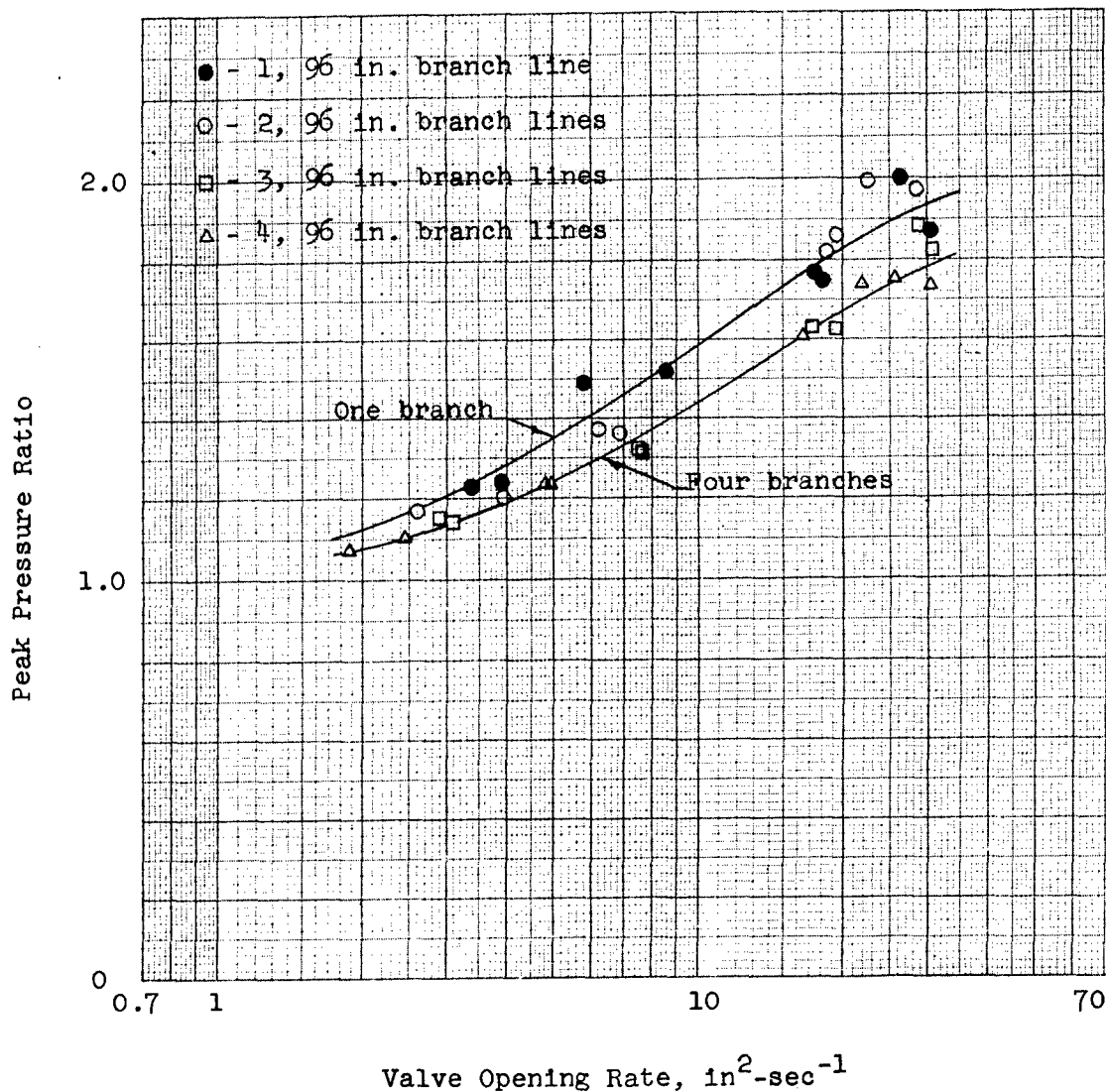
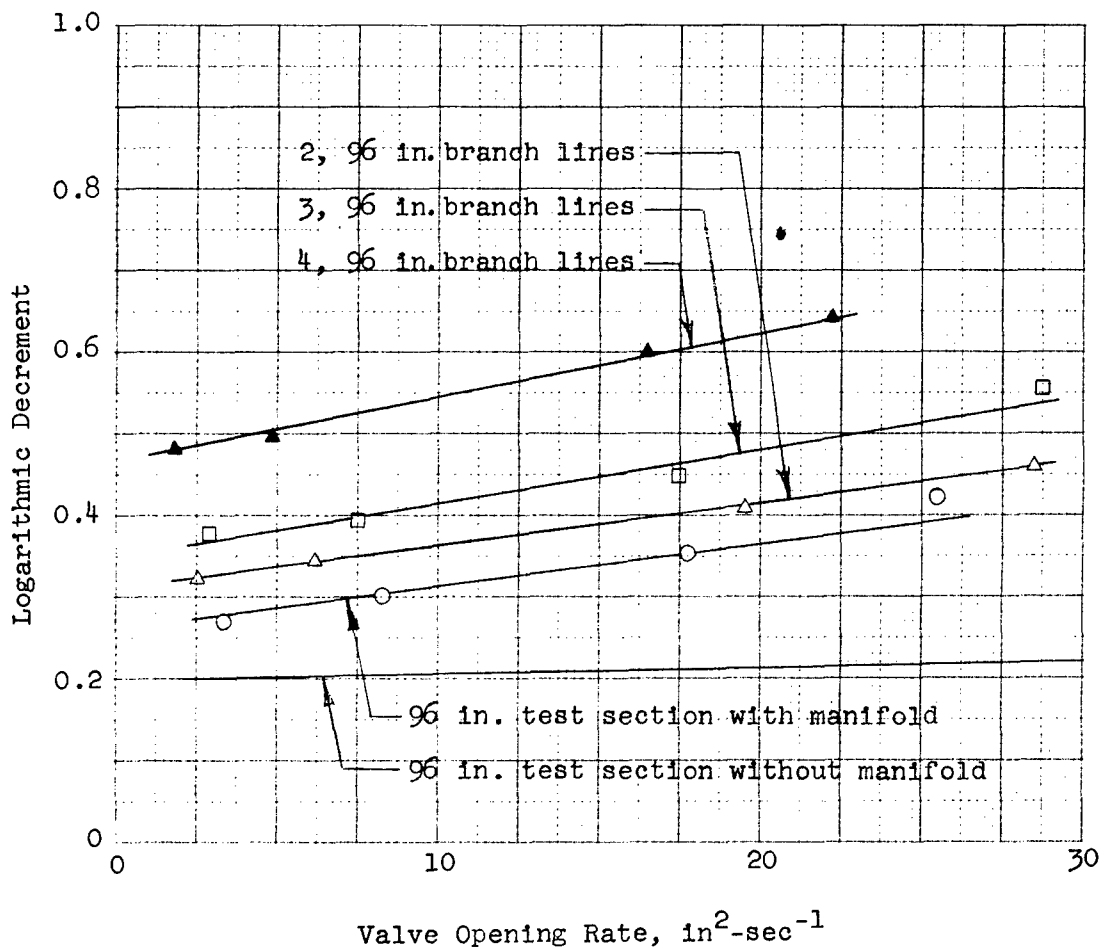


Figure 26

LOGARITHMIC DECREMENT VS. VALVE OPENING RATE  
FOR VARIOUS NUMBERS OF EQUAL LENGTH BRANCHES  
CLOSED-END TUBE SYSTEMS



Note: Logarithmic decrement based on first two peaks of pressure oscillation.



Figure 27

FREQUENCY OF FUNDAMENTAL PRESSURE WAVE VS. VALVE OPENING RATE  
 FOR VARIOUS NUMBERS OF EQUAL LENGTH BRANCHES  
 CLOSED-END TUBE SYSTEMS

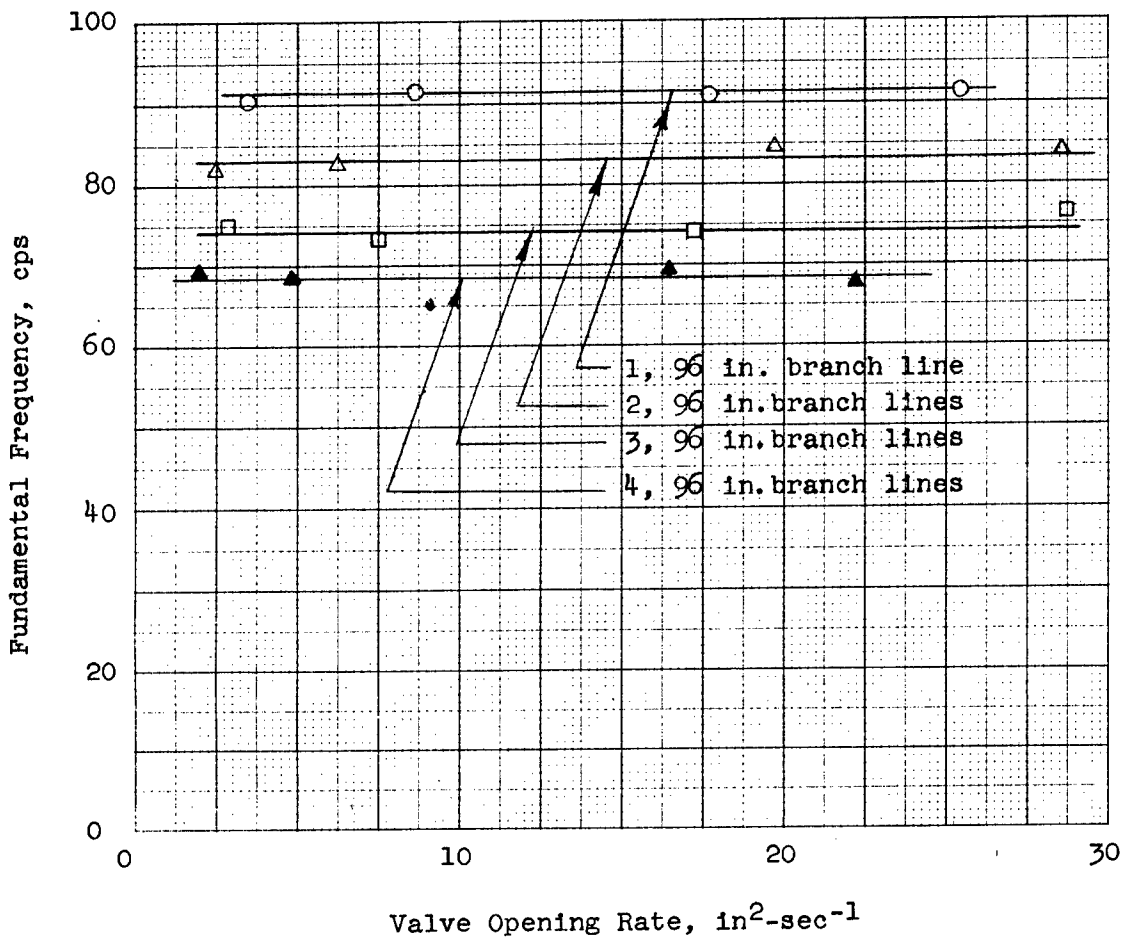
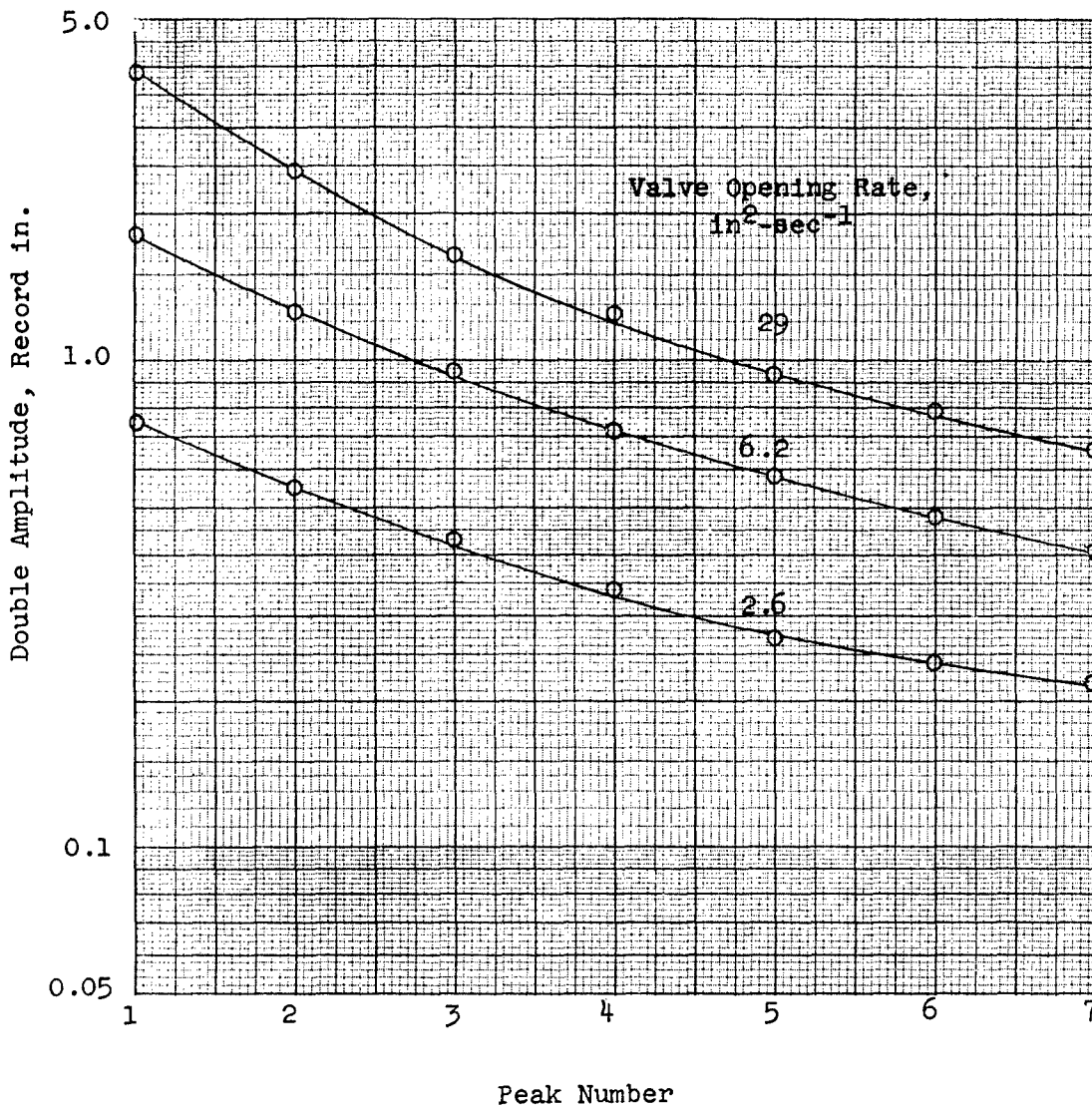


Figure 28

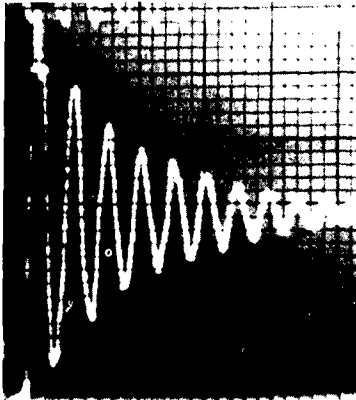
AMPLITUDE VS. PEAK NUMBER FOR VARIOUS VALVE OPENING RATES  
ON A BRANCH CIRCUIT OF TWO EQUAL LENGTH BRANCHES  
CLOSED-END TUBE SYSTEM



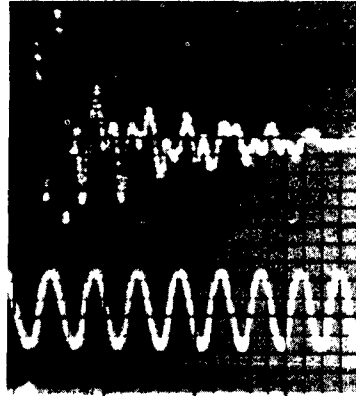
Note: 96 in. test section lengths.

Figure 29

TYPICAL PRESSURE SURGE WAVEFORMS AT CLOSED ENDS  
OF UNEQUAL LENGTH DUAL BRANCHES - CLOSED-END TUBE SYSTEM

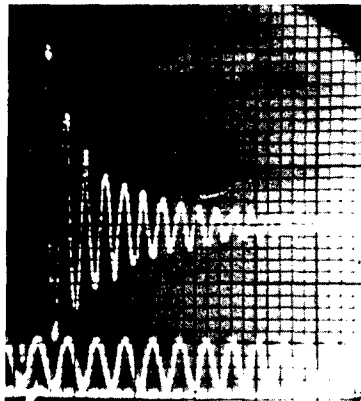


192 in. Branch

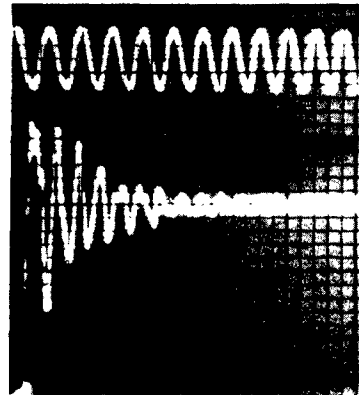


48 in. Branch

48 in. and 192 in. Dual Branch Lines

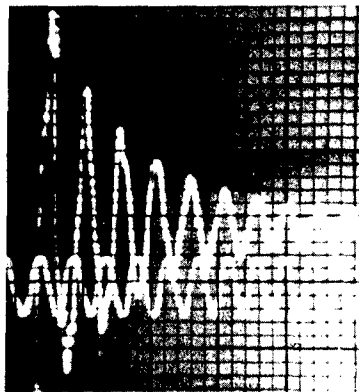


96 in. Branch

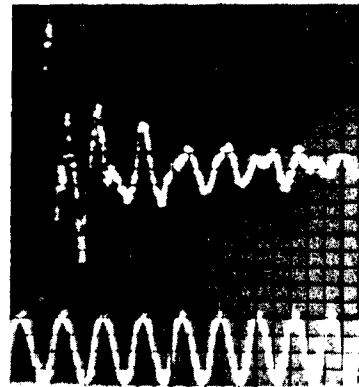


48 in. Branch

48 in. and 96 in. Dual Branch Lines



192 in. Branch



96 in. Branch

96 in. and 192 in. Dual Branch Lines

<u>Number of Branches</u>	<u>Actual Frequency, cps</u>	<u>Calculated Frequency, cps</u>
1	92	92
2	83	89
3	74	82
4	69	73

3.2.7.5 In the tests on a closed-end tube system with two unequal length branches, the following significant data were obtained:

- (a) The shape of the waveform recorded at the closed end of the longer branch was very similar to the waveform of a single branch of the same length. The shape of the waveform at the closed end of the shorter line was distorted and appeared to be a combination of the wave forms produced in each of the individual lines when not in a parallel circuit. Typical photographs of the observed waveforms are shown in Fig. 29. The shape of the waveform recorded at the manifold was very similar to the distorted waveform observed at the closed end of the shorter branch.
- (b) The magnitude of the pressure surge at the closed end of the longer branch was greater for all configurations tested. The maximum peak of the pressure surge in the shorter line did not necessarily occur on the initial rise (Fig. 29). A comparison of the peak pressure ratios at the closed ends of the branches are shown for two different valve opening rates in the following table:

Test Section Lengths on Dual Branches, in.	Valve Opening Rate, $\text{in}^2\text{-sec}^{-1}$ ( $\pm 10$ percent)	Peak Pressure Ratio (Based on Maximum Peak)	
		Short Branch	Long Branch
48 and 96	28	1.44	2.11
	21	1.30	1.96
96 and 144	28	1.64	2.07
	21	1.53	2.00
96 and 192	28	1.61	2.09
	21	1.43	1.96
48 and 192	28	1.49	1.98
	21	1.43	1.93

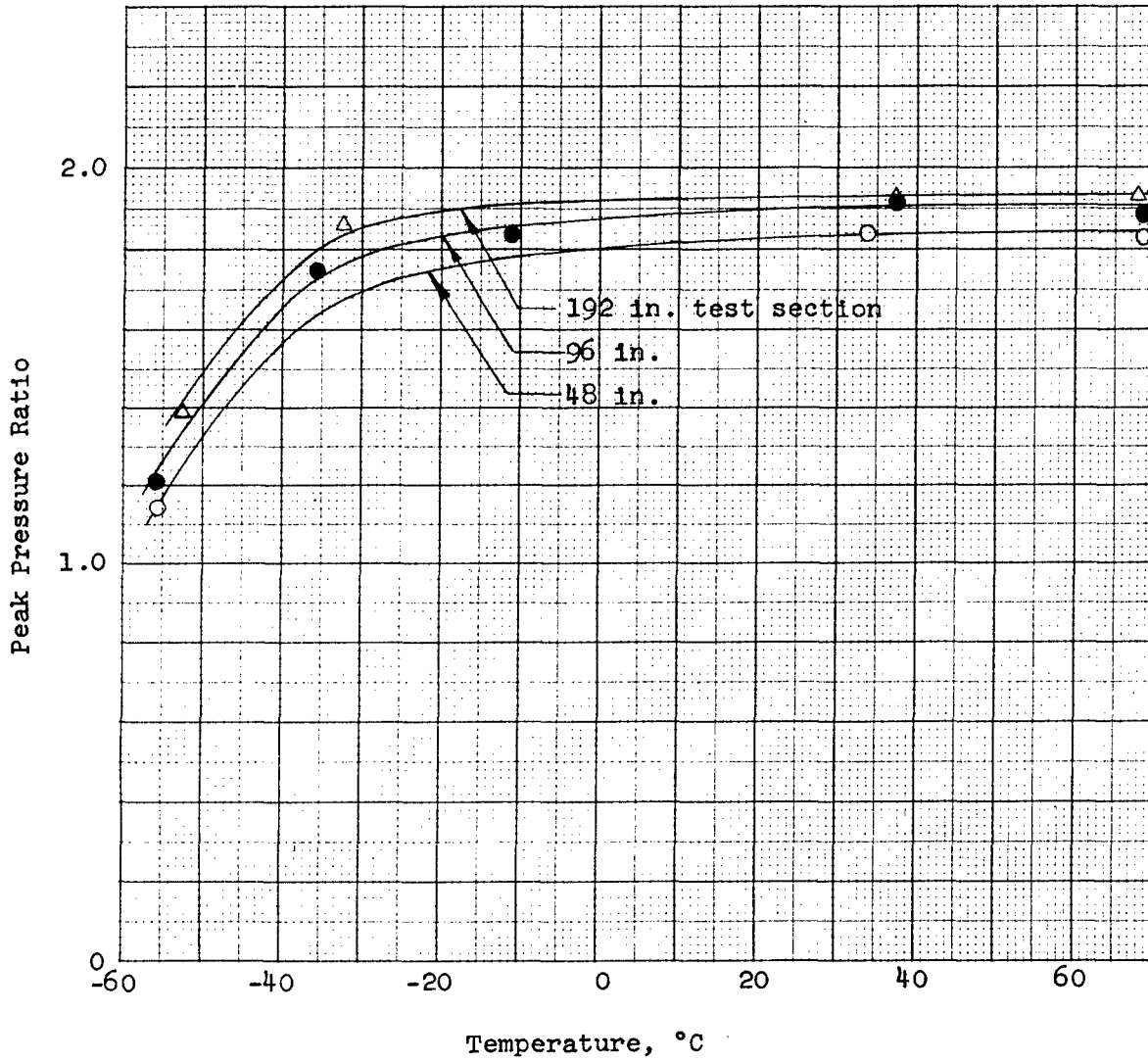
### 3.2.8 Temperature

3.2.8.1 The effect of temperature on pressure surges in a closed-end tube was investigated by studying the resulting pressure waveforms under the following conditions:

- (a) System pressure, 3000 psi.  
 (b) Accumulator precharge air pressure, 1000 psi.  
 (c) Pump discharge flow rate, 2 gpm.  
 (d) Fluid temperature, 71 C to -54 C (160 F to -65 F).  
 (e) Test section length, 48, 96, and 144 in.  
 (f) Valve opening rate, 4-30  $\text{in}^2\text{-sec}^{-1}$ .

Figure 30

PEAK PRESSURE RATIO VS. TEMPERATURE  
 FOR VARIOUS SYSTEM LENGTHS  
 CLOSED-END TUBE SYSTEMS



For these tests, the basic hydraulic system (Fig. 1), except the pilot system, was set up in an insulated room with controlled temperature regulation. To facilitate control from outside the room, the bleed valve at the closed end of the test section and system by-pass valves (as required) were replaced by solenoid operated shutoff valves. Temperatures of the fluid in the test section and at other locations in the system were determined by thermocouples and a direct-reading temperature recorder. To ensure uniformity of temperature in the test system during a specific test run, the general procedure described in Par. 3.2.1.4 was modified to the following:

- (a) With the pumps off, the system was stabilized at a temperature somewhat below the desired temperature.
- (b) With the Denison valve, the main system by-pass valve, and the bleed valve at the closed end of the test section open, fluid was circulated through the system until the desired temperature was approximately obtained. During this period the pilot system was adjusted to give the desired Denison valve spool velocity.
- (c) The valves were then closed and the main system was charged to the desired pressure.
- (d) The pilot system selector valve was operated at a uniform rapid rate and simultaneous records of pressure and spool position were taken as the Denison valve opened. Temperatures were automatically recorded as the test run was made.
- (e) Records of the necessary reference traces were made on the Hydrauliscope photographs.
- (f) The test run was made as rapidly as possible to minimize fluid temperature increases.

3.2.8.2 Results of the tests indicated that the magnitude of the pressure surge in a given system remained relatively constant for temperatures above 0°C (32 F), but decreased at an increasing rate as the temperature was lowered (Fig. 30). Increases in system length resulted in higher peak pressure ratios at all temperatures, as shown in Fig. 30. The total system damping increased rapidly at low temperatures as is indicated by the logarithmic decrement vs. temperature plot shown in Fig. 31. Analysis of the data gave some indication that the total system damping increased linearly with the kinematic viscosity of the fluid, but further investigation would be required to establish an exact relationship.

3.2.8.3 It was originally anticipated that logarithmic decrement vs. total system length plots of data obtained at various temperatures would result in straight-line relationships, the slope of which could be used to determine tubing resistance values. This did not prove to be the case due to the relative manner in which valve resistance and tubing resistance combined. Attempts to separate these resistances gave unsatisfactory values and indicated the need for further investigation.

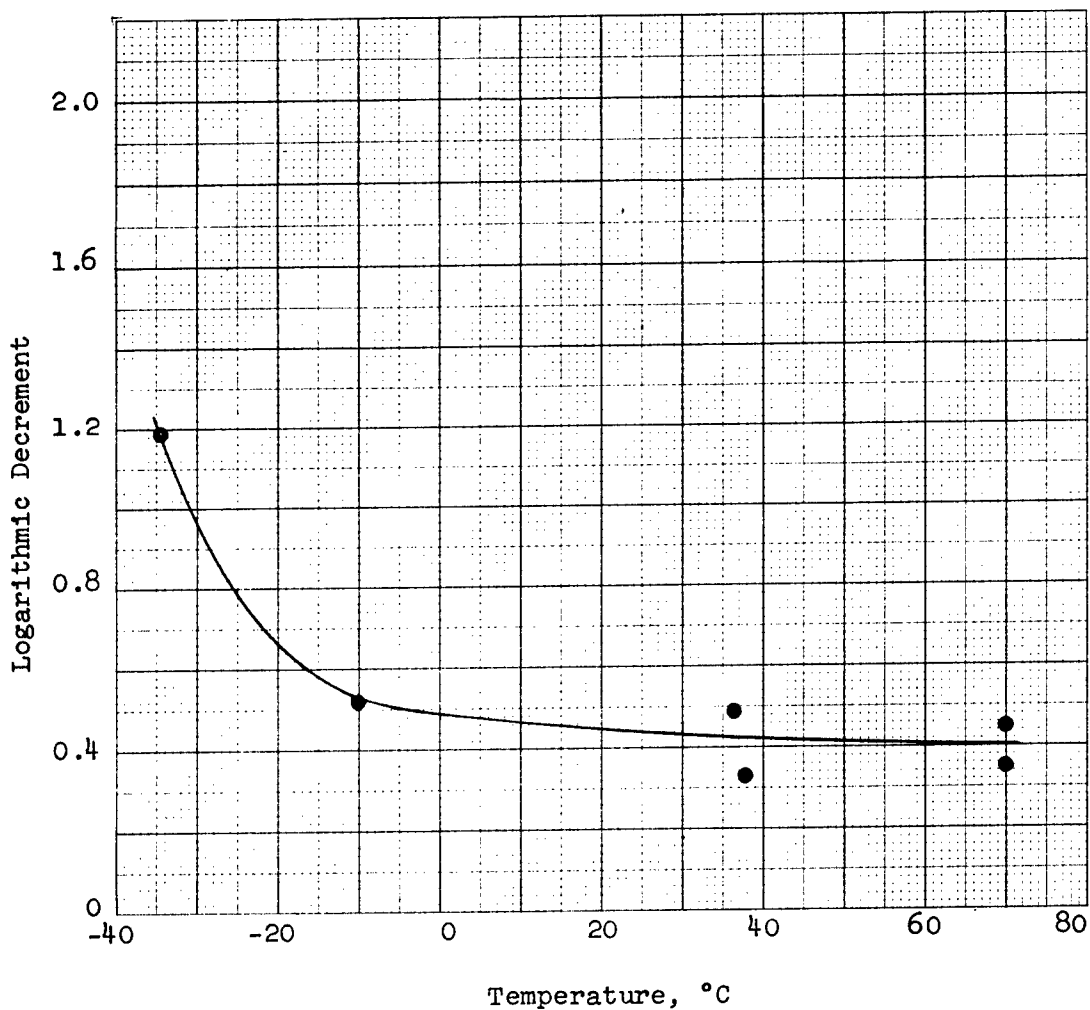
3.2.8.4 A comparison of the peak pressure ratio vs. valve opening rate relationships on the 96 in. test section at 38 C (100 F) and -54 C (-65 F) indicated that changes in valve opening rate became less effective at lower temperatures (Fig. 32).

3.2.8.5 The frequency of the fundamental pressure wave increased as the temperature was decreased (Fig. 33), but correlation between theoretical and experimental values was not as good as had been expected. The theoretical curves were calculated using Eq. 3-3 and data as follows:

- (a) The effective compressibility factors for each system length at 38 C (100 F) temperature was determined from the experimental curve in Fig. 20. These factors were assumed to be more exact than the isothermal compressibility factors presented in Par. 3.2.5.1. Temperature corrections were made using information shown in Ref. 1, Fig. 45.

Figure 31

LOGARITHMIC DECREMENT VS. TEMPERATURE  
CLOSED-END TUBE SYSTEM



Note: Logarithmic decrement based on first two peaks of pressure oscillation.

Figure 32

PEAK PRESSURE RATIO VS. VALVE OPENING RATE  
 AT 38 C AND -54 C TEMPERATURES  
 CLOSED-END TUBE SYSTEM

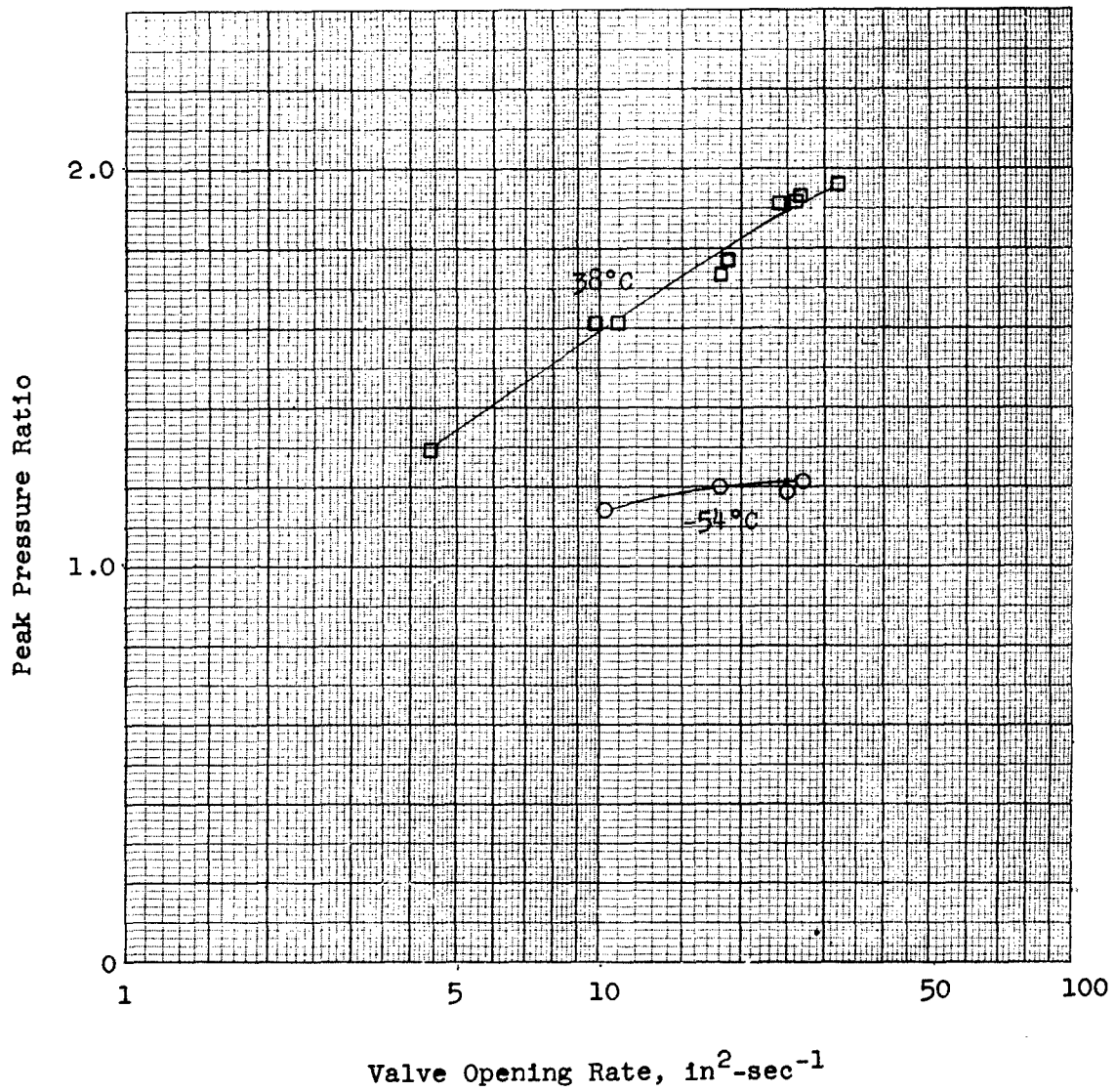
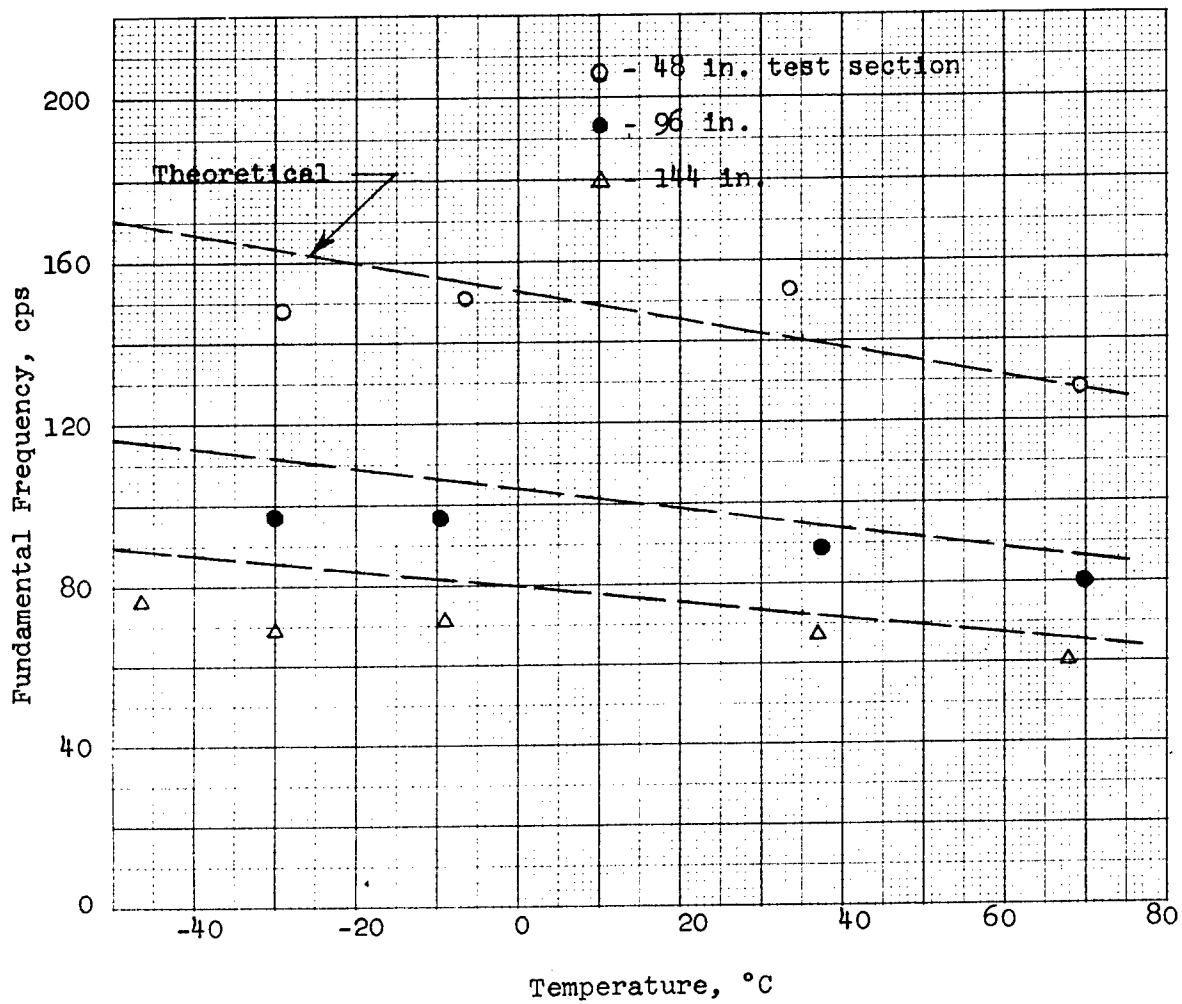




Figure 33

FREQUENCY OF FUNDAMENTAL PRESSURE WAVE VS. TEMPERATURE  
 FOR VARIOUS SYSTEM LENGTHS  
 CLOSED-END TUBE SYSTEMS



Note: Theoretical curves calculated as described in Par. 3.2.8.5.

- (b) The fluid mass density at various temperatures was obtained from Ref. 1, Fig. 3.
- (c) Total system lengths were the same as presented in Par. 3.2.5.1.

Comparison of the actual system configuration used in these tests with that used in experimental work in Par. 3.2.5 indicated that the system configurations between the accumulator and pump were not identical. The significance of this was not definitely ascertained, but it seemed possible that a branch effect on the pressurized side of the valve might have caused the frequency variations shown in Fig. 33.

3.2.8.6 Failure of the Vickers accumulator diaphragm occurred during the -54 C (-65 F) temperature tests, but most of the scheduled test runs had been made. Supplementary data available from the tests conducted with a piston type accumulator installed in the system (Par. 3.4.5) indicated no significant difference in test results for the runs made prior to failure of the diaphragm.

### 3.2.9 Entrained Air

3.2.9.1 Although no specific tests were conducted to determine the effect of entrained air on pressure surges in hydraulic systems, certain significant information and data relevant to the parameter were obtained during the course of the research program.

3.2.9.2 At the start of the experimental work on closed-end tube systems, secondary high-frequency oscillations were observed on the fundamental pressure surge waveform (Fig. 34) when the Denison valve was actuated rapidly. These were attributed to the collapse of aerated oil present in the valve body, as system pressure was applied to the test section. Although it is difficult to distinguish between cavitation and the collapse of entrained air, an examination of the oil contained in the valve body revealed a high content of air, especially after several rapid valve cycles. The installation of a check valve in the system return line (Fig. 1), which maintained a positive 20 psi static head on the Denison valve and test section, reduced the magnitude of the oscillation and made possible good reproducibility of a smooth fundamental waveform.

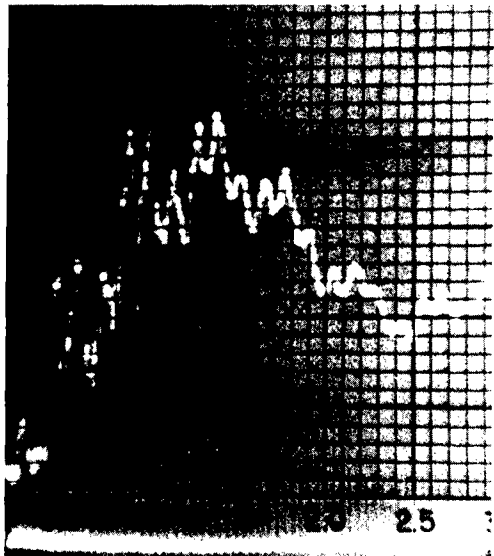
3.2.9.3 While a method was established to reduce the magnitude of, or essentially eliminate, the secondary oscillation, a search was undertaken to determine if the frequency of this oscillation was effected by variations in the basic system configuration. Observations and/or records were made for each of the following system changes:

- (a) Test section lengths, 48, 96, and 192 in.
- (b) Branch line lengths to bleed valve at closed-end of test section, capped, 4 in., and 16 in.
- (c) Pressure transducer attachment configuration, straight into test section, 45 deg to test section, 90 deg to test section.
- (d) Pressure transducer, Aeroquip No. 10050 (two transducers), Aeroquip No. 10030, Statham Model P74-5MG-350.
- (e) System pressure, 600 and 1200 psi (with 200 psi accumulator precharge air pressure in both cases).
- (f) System flow rate, accumulator only (shutoff valve, Fig. 1, closed) and accumulator and system pump.
- (g) Line length from Denison valve to accumulator, 12 in. and 36 in.
- (h) Accumulator, Vickers (Model No. AA-14307A) diaphragm type and Bendix (Part No. 409201) piston type.
- (i) Selector valve, Denison slide valve and Bendix (Part No. 405883) poppet valve. Both valves were 4-way, closed center, type.

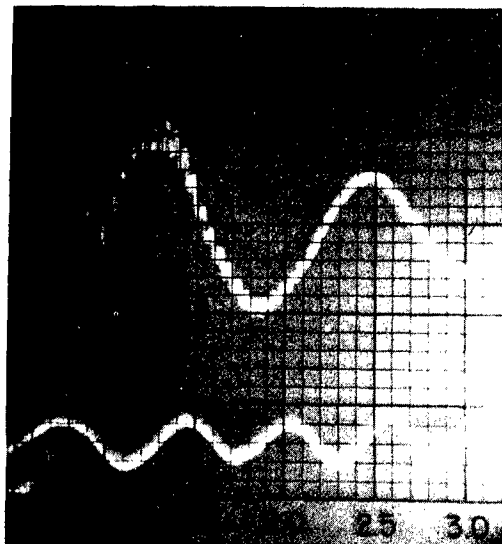
Figure 34

TYPICAL PRESSURE SURGE WAVEFORMS SHOWING SECONDARY HIGH-FREQUENCY OSCILLATIONS ATTRIBUTED TO ENTRAINED AIR CLOSED-END TUBE SYSTEMS

Secondary High-Frequency Oscillations Observed During Initial Experimental Work on Closed-end Tube Systems



Secondary High-frequency Oscillations Observed During Fatigue Test Work on Tubing



Secondary High-Frequency Oscillations Observed During Fatigue Test Work on Cylinder Assemblies

- (j) Test section location, cylinder port A and cylinder port B on Denison valve.
- (k) Hose installed between 96 in. test section and pressure transducer. Hose was approximately 12 in. long.

The secondary frequencies observed and/or recorded ranged between 1000 and 1800 cps, but no definite correlation with any system configuration could be established because this scatter also occurred with a given system configuration.

3.2.9.4 During the course of experimental fatigue tests on hydraulic system components (Chapter IV), secondary frequencies of the described nature were observed even though the system configuration was greatly different. Two typical waveforms observed during the course of this fatigue test work are also shown in Fig. 34. The secondary frequency observed on the tubing test configuration was 1215 cps and the magnitude was essentially eliminated by the same technique as was described in Par. 3.2.9.2. The secondary frequency observed on the cylinder test configuration was 1200 cps and appeared to be an under-damped high-frequency oscillation superimposed on the fundamental pressure wave. The secondary frequency on the cylinder test configuration existed even though the check valve was installed in the system return. It is possible that a higher positive return line pressure might have reduced the magnitude, but no investigation was made.

3.2.9.5 Studies of the pump ripple characteristics of a Vickers constant displacement pump under cavitation conditions (Fig. 85), used by the Glenn L. Martin Company in fatigue test work on tubing, indicated the presence of a secondary frequency of 1400 - 1500 cps. With an inlet pressure of one atmosphere, the ripple characteristics of the same pump, in a typical aircraft hydraulic system, were observed to contain a secondary frequency of 1400 cps, but the total amplitude of the oscillation was reduced to approximately one-fifth of that shown in Fig. 85.

3.2.9.6 From these data and information it appeared that the following significant facts could be established:

- (a) The presence of air in a hydraulic system usually resulted in a secondary frequency in the 1000 - 2000 cps range.
- (b) The magnitude of this secondary oscillation was a function of the quantity of air present.
- (c) Sub-atmospheric pressures were usually associated with the greater magnitudes of the secondary oscillation. This was probably due to the formation of air bubbles at pressures below one atmosphere when the fluid was considered 100 percent air saturated at one atmosphere and/or the formation of vapor-filled bubbles (cavities) at the fluid's vapor pressure, and the subsequent collapse of either upon passing into a high-pressure zone.
- (d) Variations in the frequency of the secondary oscillation were practically independent of system configuration. These variations might have been due to the effect of quantity or size of air bubbles present.

### 3.3 Actuating Cylinder Systems

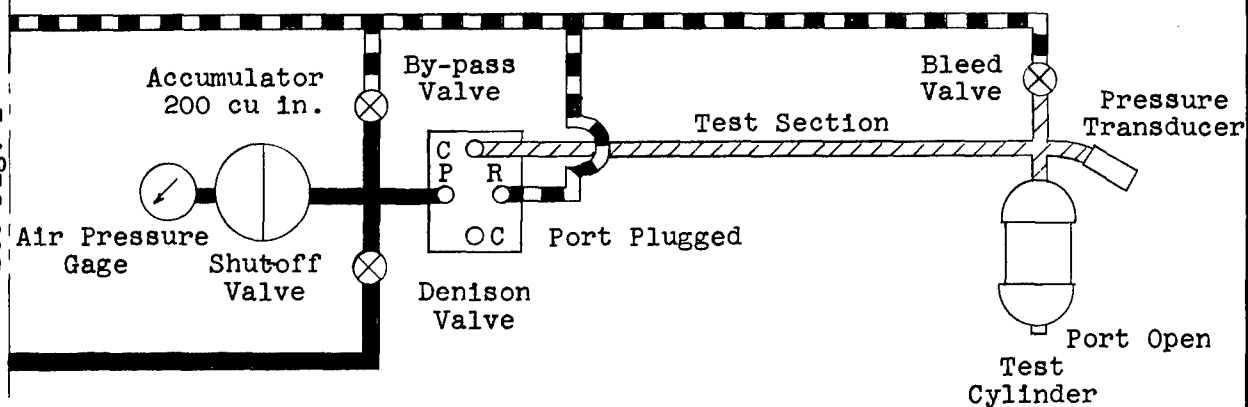
#### 3.3.1 General Notes

3.3.1.1 The pressure surges studied in this part of the investigation were those which occurred in an actuating cylinder when a valve was rapidly opened allowing a pressurized system to actuate the piston. To facilitate the theoretical investigation, parameters such as cylinder volume, system pressure, and system flow rate were studied on a bottomed cylinder configuration. The effect of opposing external loads (mass loads and simulated air loads) and of return line restriction were studied on a simple actuating cylinder system.

Figure 35

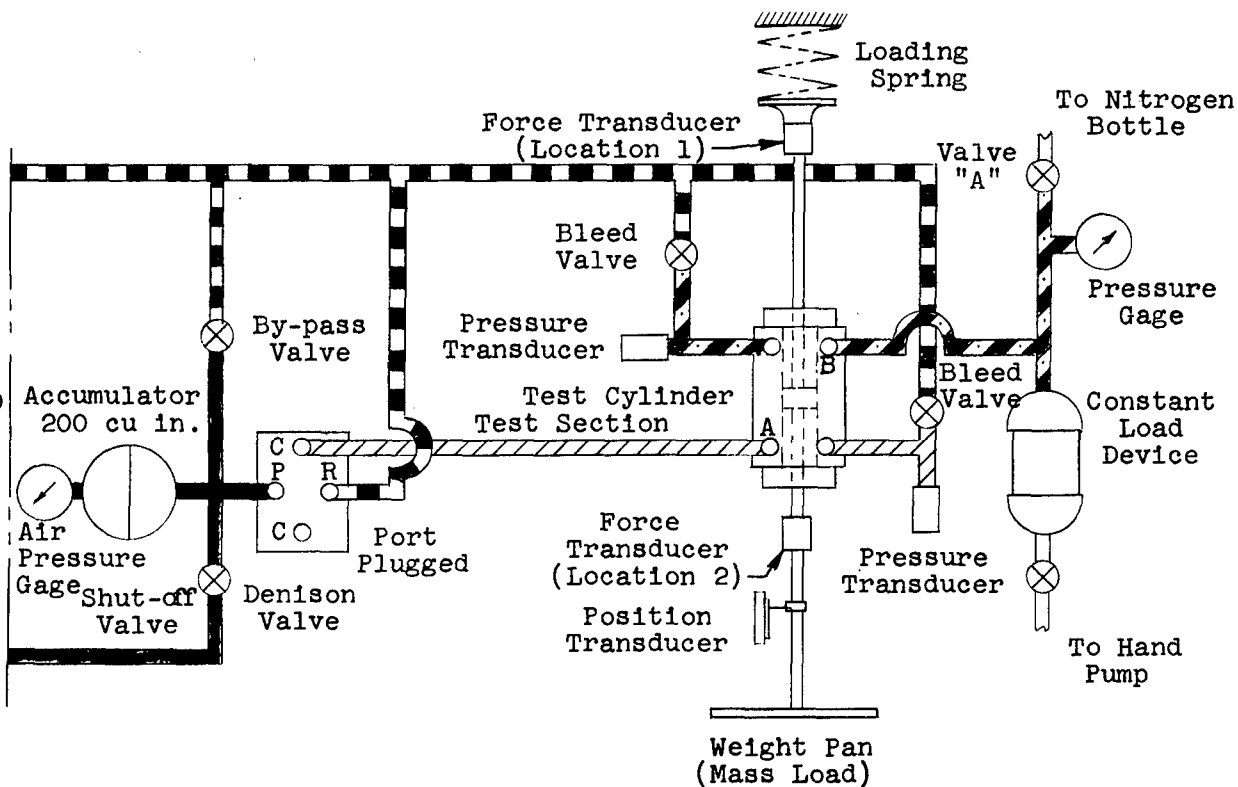
SCHEMATIC DIAGRAM OF SYSTEM CONFIGURATIONS  
FOR INVESTIGATION OF PRESSURE SURGES  
IN ACTUATING CYLINDER SYSTEMS

For Line Continuation  
See Fig. 1



Bottomed Cylinder Configuration

For Line Continuation  
See Fig. 1



Loaded Cylinder Configuration

3.3.1.2 The apparatus and general procedure used for the tests conducted on the bottomed cylinder configurations were the same as described in Par. 3.2.1, except that a bottomed cylinder was installed at the end of a 96 in. test section (Fig. 35). The bottomed cylinder was simulated by a piston type accumulator (Contractor part No. 161-58095) with the air valve removed and with internal spacers to provide the desired cylinder capacity. The use of this accumulator, designed for a 12,000 psi burst pressure, eliminated the necessity for designing a special cylinder and provided an adequate safety factor on the expected surge peaks.

3.3.1.3 The basic hydraulic system used for the loaded cylinder configuration was the same as shown in Fig. 1, except that a specially designed balanced cylinder with a net area of approximately one square inch and a stroke of 1-1/2 in. was installed at the end of a 96 in. test section. This actuating cylinder and the basic loading devices are shown physically in Fig. 36 and schematically in Fig. 35. Instrumentation for these tests consisted of the following:

- (a) Pressure transducers, Statham Model No. P74-10MG-350 and No. P74-5MG-350, for measuring the pressure on each side of the piston.
- (b) Position transducers, one on the selector valve spool (cantilever beam type) and one on the test cylinder piston rod (slide wire type).
- (c) A force transducer, strain gage type, for measuring external forces.
- (d) Oscillograph recorder, galvanometer type with six or more channels, for recording data.
- (e) An Aeroquip Hydrauliscope (Model No. 10000A) and associated pressure transducer (Model No. 10050) for observing high frequency characteristics in the pressure waveform.

3.3.1.4 The general test procedure followed for a specific test run on the loaded cylinder configuration was as follows:

- (a) The desired load configuration was applied to the cylinder.
- (b) The hydraulic system and test cylinder were bled of entrapped air, and the Denison valve between the energy source (accumulator and/or system pump) and the cylinder was closed.
- (c) The main system was charged to the desired pressure and the pilot system was adjusted to give the desired Denison valve spool velocity.
- (d) The pilot system selector valve was operated at a uniform rapid rate and oscillograph records of pertinent data were taken as the Denison valve opened.
- (e) Records were made of the necessary reference and calibration traces.

3.3.1.5 All tests in this part of the investigation were conducted with fluid at a temperature of  $38 \pm 5$  C ( $100 \pm 9$  F).

### 3.3.2 Cylinder Volume

3.3.2.1 To study the effect of cylinder volume on pressure surges in an actuating cylinder, tests were conducted on a bottomed cylinder configuration under the following conditions:

- (a) System pressure, 3000 psi.
- (b) Accumulator precharge air pressure, 1000 psi.
- (c) Pump discharge flow rate, 2 gpm.
- (d) Nominal cylinder volume, 0, 45, 90, 135, 180 in<sup>3</sup>.
- (e) Valve opening rate, 2 - 30 in<sup>2</sup>-sec<sup>-1</sup>.

Figure 36  
TEST APPARATUS FOR LOADED ACTUATING CYLINDER TESTS

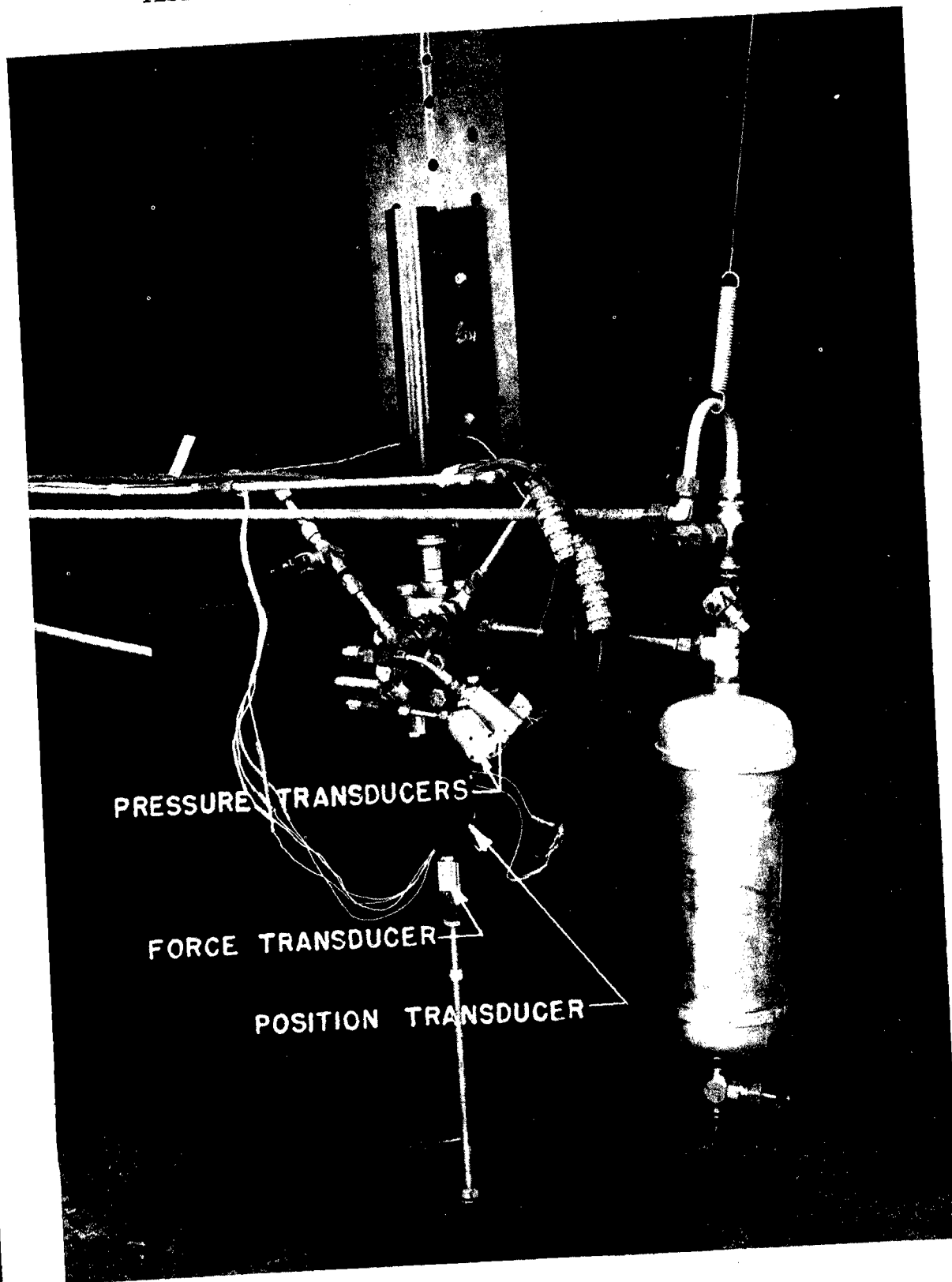
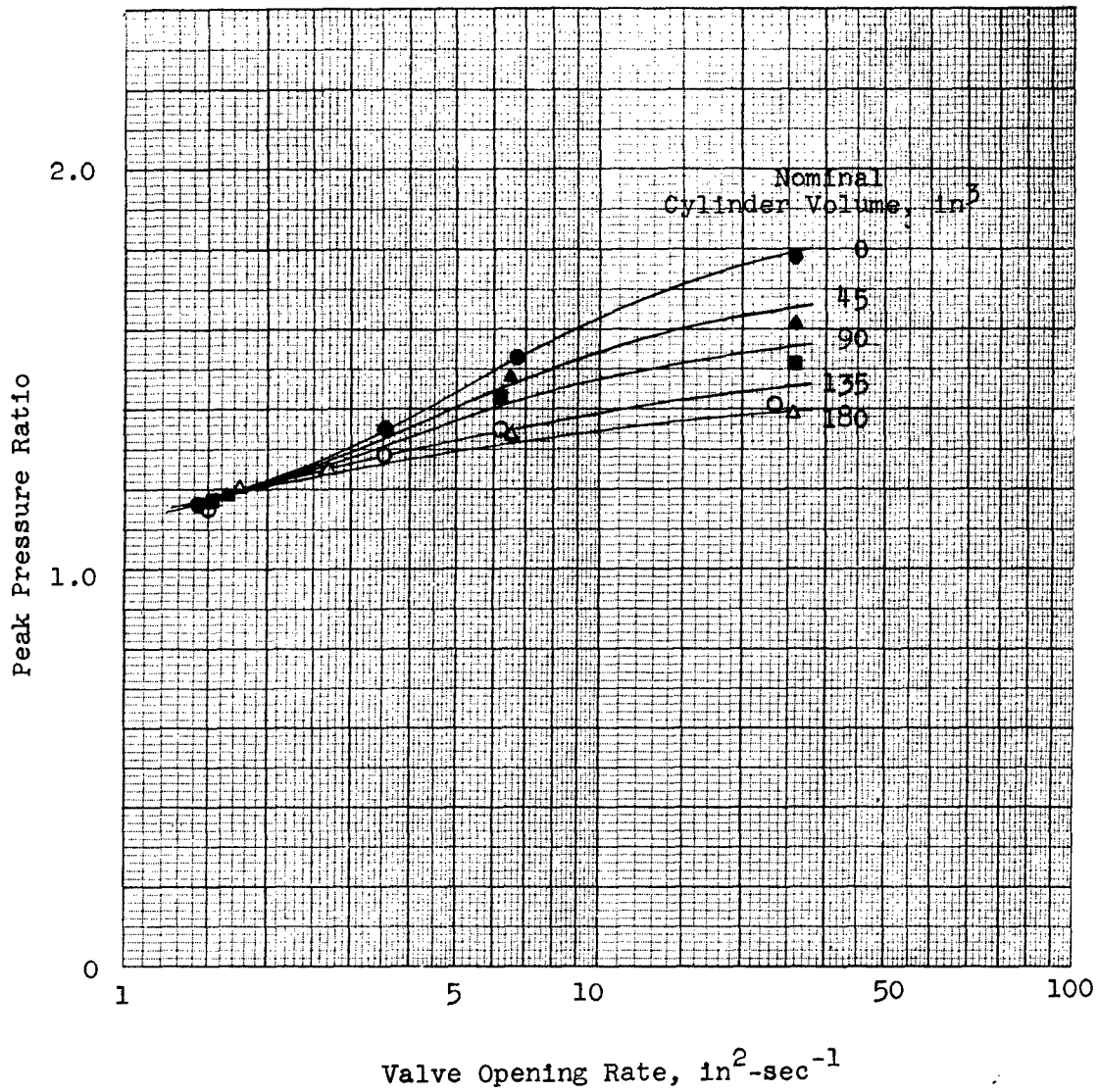


Figure 37

PEAK PRESSURE RATIO VS. VALVE OPENING RATE  
 FOR VARIOUS VOLUMES IN A BOTTOMED CYLINDER  
 ACTUATING CYLINDER SYSTEMS

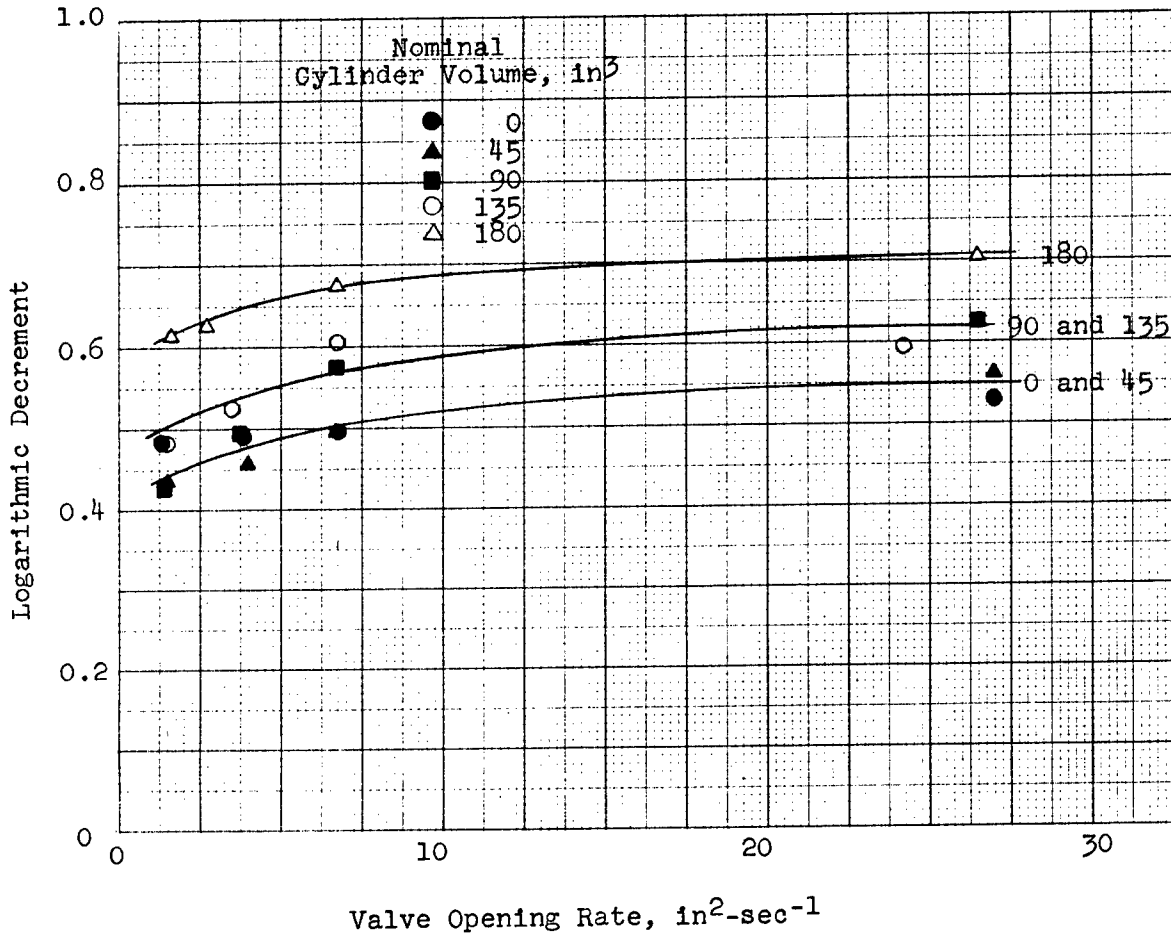


Note: 96 in. test section length



Figure 38

LOGARITHMIC DECREMENT VS. VALVE OPENING RATE  
FOR VARIOUS VOLUMES IN A BOTTOMED CYLINDER  
ACTUATING CYLINDER SYSTEMS



Notes: 96 in. test section length.  
Logarithmic decrement based on first two peaks of pressure oscillation.

Measurements of system length, system volume, and isothermal compressibility of that portion of the system between the accumulator and the closed end of the pressure transducer gave the following:

<u>Nominal Cylinder Volume, in<sup>3</sup></u>	<u>Total System Volume, in<sup>3</sup></u>	<u>Total System Length, in.</u>	<u>Isothermal Compressibility, psi<sup>-1</sup></u>
0	20	132.5	12.2 x 10 <sup>-6</sup>
45	63	132.5	6.4 x 10 <sup>-6</sup>
90	106	132.5	5.9 x 10 <sup>-6</sup>
135	150	132.5	5.3 x 10 <sup>-6</sup>
180	195	132.5	4.9 x 10 <sup>-6</sup>

3.3.2.2 The effect of cylinder volume at the end of a closed-end system was to reduce the magnitude of the pressure surge, the effective reduction becoming less as the valve opening rate was decreased (Fig. 37). As was observed in experimental work on closed-end tube systems, the effect of the valve resistance on the system damping during the initial pressure rise became of importance at the slower valve opening rates.

3.3.2.3 Studies of the logarithmic decrement of the underdamped oscillatory pressure waves indicated a decrease of the logarithmic decrement at slower valve opening rates, but indicated an overall increase in the logarithmic decrement as the cylinder volume was increased (Fig. 38). Semi-logarithmic plots of amplitude vs. peak number gave essentially straight lines for all valve opening rates and cylinder volumes tested.

3.3.2.4 The frequency of the fundamental pressure wave was found to be independent of valve opening rate, but decreased with system volume as shown in Fig. 39. Using the data presented in Par. 3.3.2.1 and the theoretical equation (Eq. 59) developed in Appendix I, calculations of the theoretical frequency were made. These calculations compared favorably with the experimental values (Fig. 39).

### 3.3.3 System Pressure

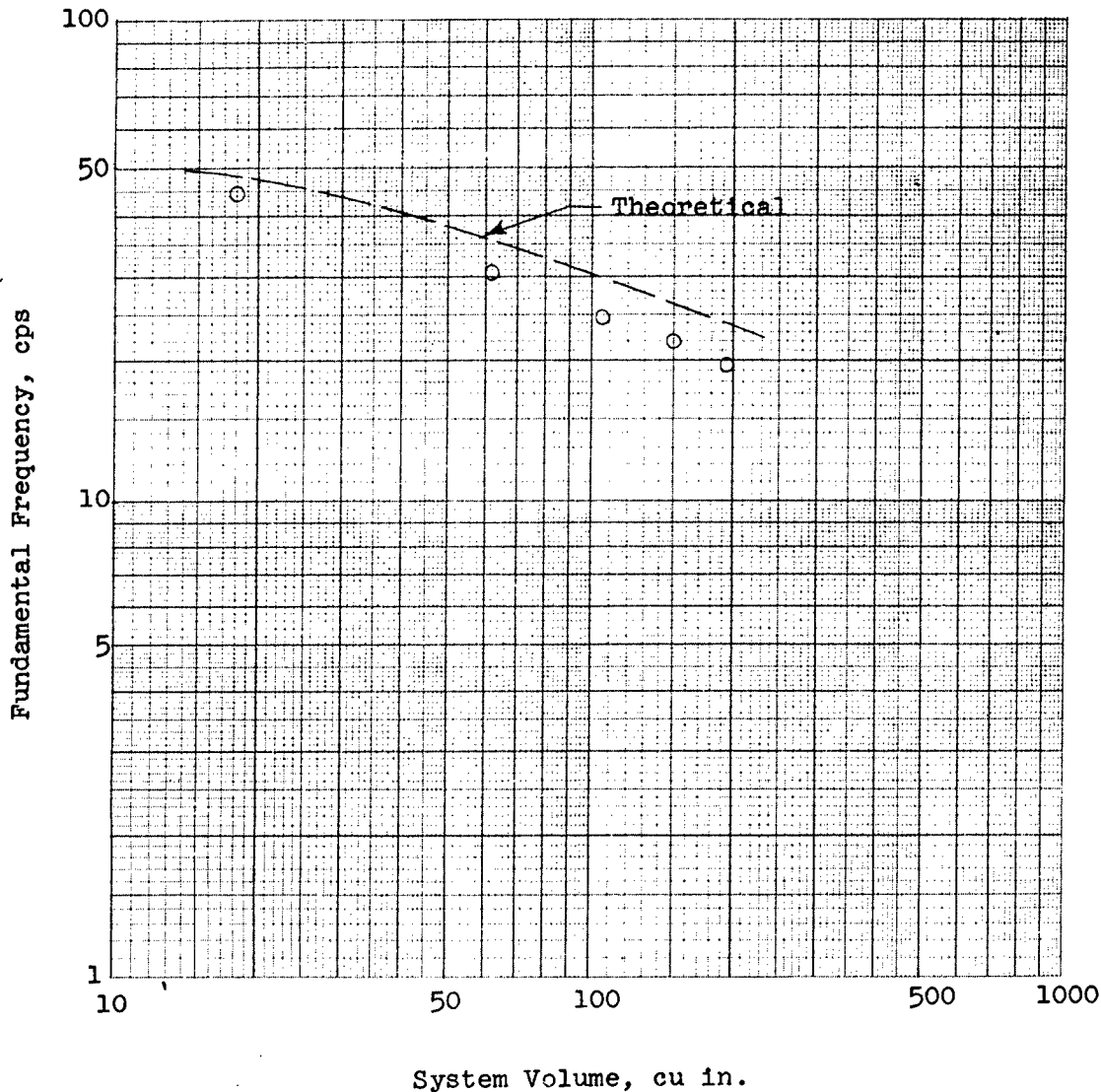
3.3.3.1 The effect of system pressure on the pressure surges in a bottomed cylinder configuration were studied under the following conditions:

- (a) System pressure, 600, 1200, 1800, 2400, and 3000 psi (Par. 3.3.2).
- (b) Accumulator precharge air pressure, 1/3 of system pressure.
- (c) Pump discharge flow rate, 2 gpm.
- (d) Nominal cylinder volume, 180 in<sup>3</sup>.
- (e) Valve opening rate, 2-30 in<sup>2</sup>-sec<sup>-1</sup>.

3.3.3.2 The peak pressure ratio vs. valve opening rate relationships at various system pressures indicated that lower peak pressure ratios were obtained at the higher system pressures (Fig. 40). The variation of the peak pressure ratio with valve opening rate was less than had been observed in the tests on a closed-end tube (Par. 3.2.3). This was attributed to a more constant relative effect of valve resistance on the total system damping in the bottomed cylinder configuration.

Figure 39

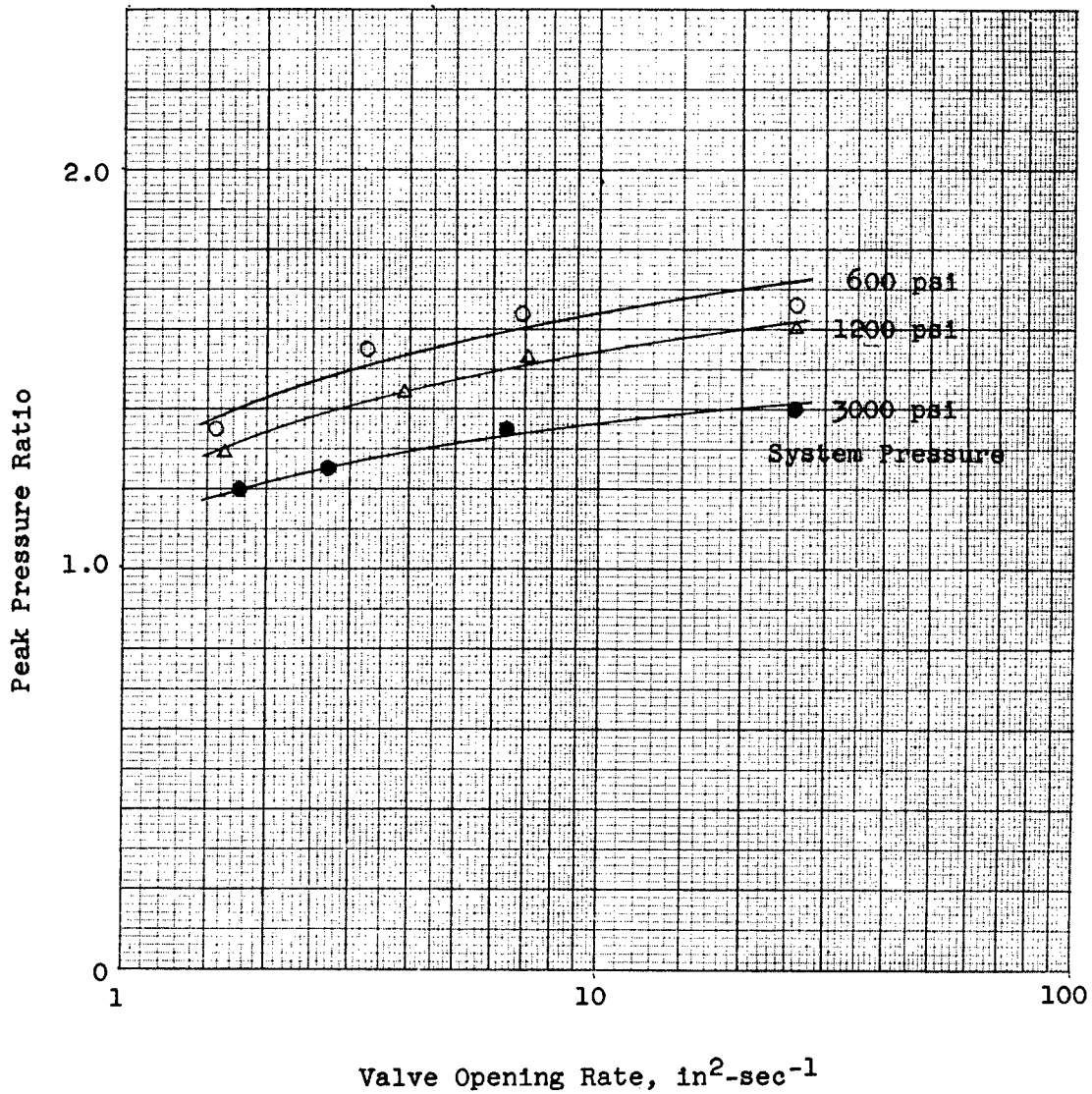
FREQUENCY OF FUNDAMENTAL PRESSURE WAVE VS. SYSTEM VOLUME  
 FOR A BOTTOMED CYLINDER CONFIGURATION  
 ACTUATING CYLINDER TESTS



Note: Theoretical curve based on Eq. 59, Appendix I, and data in Par. 3.3.2.1.

Figure 40

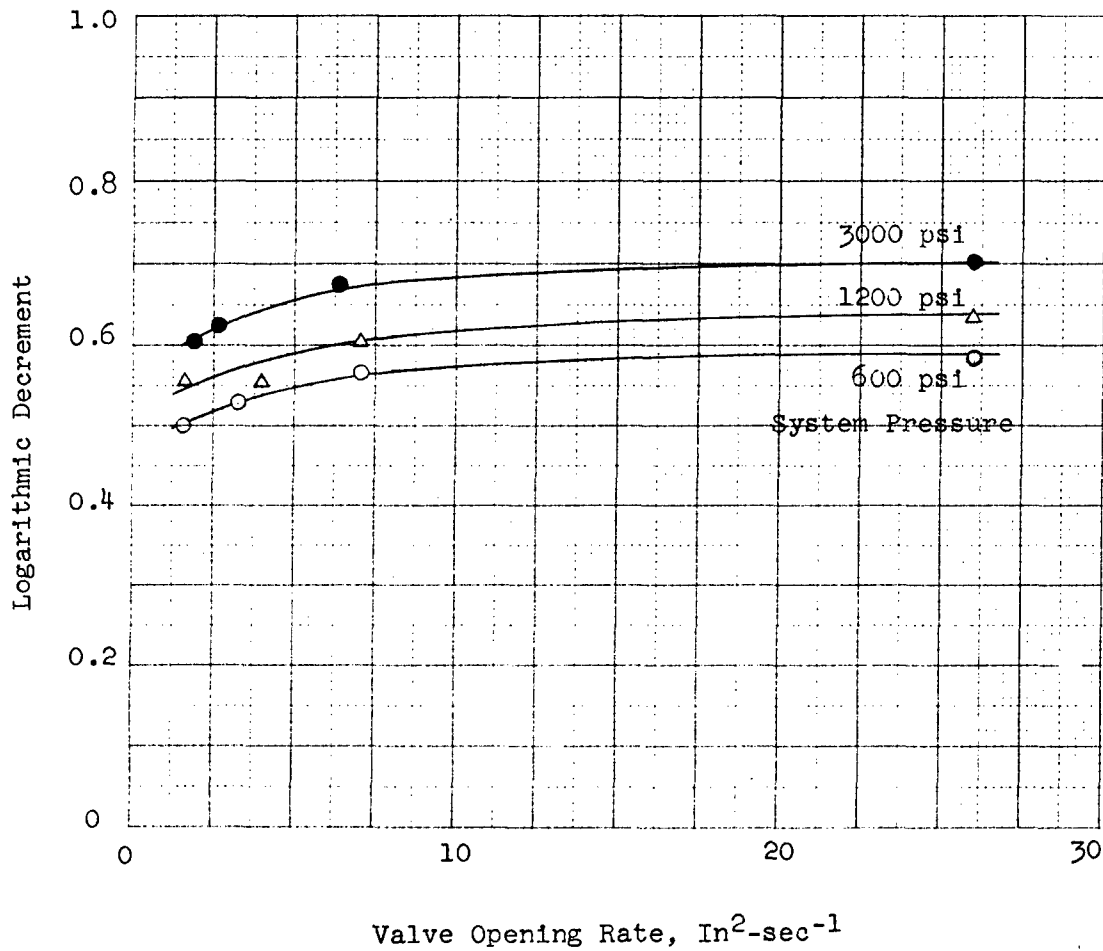
PEAK PRESSURE RATIO VS. VALVE OPENING RATE  
 FOR VARIOUS SYSTEM PRESSURES  
 IN A BOTTOMED CYLINDER CONFIGURATION  
 ACTUATING CYLINDER TESTS



Note: 96 in. test section length.

Figure 41

LOGARITHMIC DECREMENT VS. VALVE OPENING RATE  
 FOR VARIOUS SYSTEM PRESSURES  
 IN A BOTTOMED CYLINDER CONFIGURATION  
 ACTUATING CYLINDER TESTS



Notes: 96 in. test section length.  
 Logarithmic decrement based on first two peaks of pressure oscillation.

3.3.3.3 Studies of the logarithmic decrements of the underdamped oscillatory pressure waves indicated that the logarithmic decrement increased with higher system pressure and decreased with slower valve opening rate (Fig. 41). Semi-logarithmic plots of amplitude vs. peak number gave essentially straight lines for all system pressures and valve opening rates tested.

3.3.3.4 The frequency of the fundamental pressure wave increased from an average of 18.4 cps at 600 psi system pressure to an average of 19.5 cps at 3000 psi. Although this variation was small, the trend was definitely observed. This slight variation was attributed primarily to the effect of system pressure on the effective compressibility of the system.

3.3.3.5 Additional tests were conducted with the accumulator removed from the system. Under these conditions, the waveform of pressure rise was characterized by a rapid rise to an initial step pressure, followed by a slow pressure rise to system pressure (Fig. 42). The initial step pressure was a function of the initial pressures and volumes of the pressurized and unpressurized sections of the system. As was pointed out in Par. 3.2.4.2, the effect of the system pump must be added to the pressure wave form which would occur if the pump were not present. The time delay at the step was attributed to the response characteristics of the system pump and pressure relief valve. The slope of the pressure rise following the initial step was a function of the pump discharge flow rate and the system capacitance ( $\beta_e V$ , in which  $\beta_e$  is the effective compressibility of the system and  $V$  is the total system volume).

### 3.3.4 System Flow Rate

3.3.4.1 The effects of system flow rate on the pressure surges in a bottomed cylinder configuration were studied by tests conducted at various pump discharge flow rates both with and without a system accumulator. Specific test conditions were as follows:

- (a) System pressure, 3000 psi.
- (b) Accumulator precharge air pressure, 1000 psi.
- (c) Pump discharge flow rate, 2, 4, 8, and 16 gpm.
- (d) Nominal cylinder volume, 180 in<sup>3</sup>.
- (e) Valve opening rate, 2-30 in<sup>2</sup>-sec<sup>-1</sup>.

The desired flow rates were obtained as described in Par. 3.2.4.1.

3.3.4.2 With an accumulator installed in the system, the effect of pump discharge flow rate on the magnitude of the peak pressure was negligible (Fig. 43). Studies of the logarithmic decrements of the underdamped oscillatory pressure waves indicated no significant differences attributable to the pump discharge flow rate (Fig. 44). The frequency of the fundamental wave remained at  $19.5 \pm 0.2$  cps over the range of pump discharge flow rates tested.

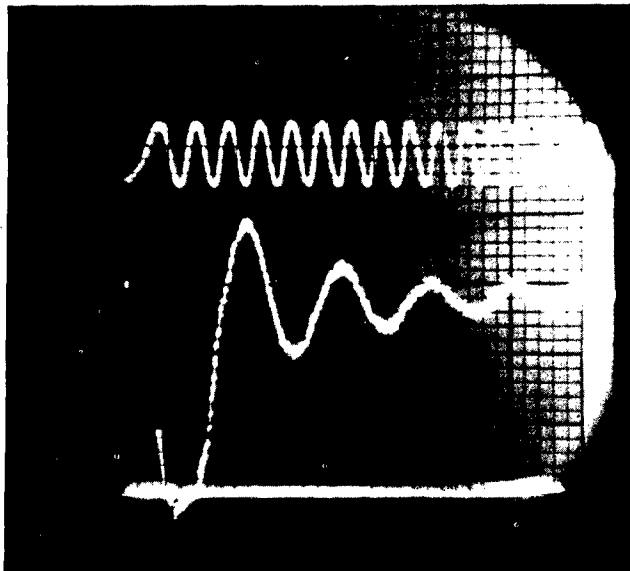
3.3.4.3 With the accumulator removed from the system, the characteristics of the pressure rise waveform were similar to those shown in Fig. 42. The rapid rise to the initial step pressure and the magnitude of the initial step pressure remained approximately the same for all pump discharge flow rates using the Vickers pump. The slope of the pressure rise following the initial step increased directly with the pump discharge flow rate. For equivalent flow rates on the Denison pump, the slope of the pressure rise following the initial step was essentially the same as for the Vickers pump, but the magnitude of the initial step pressure was greater. This was attributed to the volumetric difference in the pressurized sections of the two different systems. Typical photographs of the pressure rise characteristics using the Vickers and Denison pump systems are shown in Fig. 45 for comparison.

### 3.3.5 Mass Load

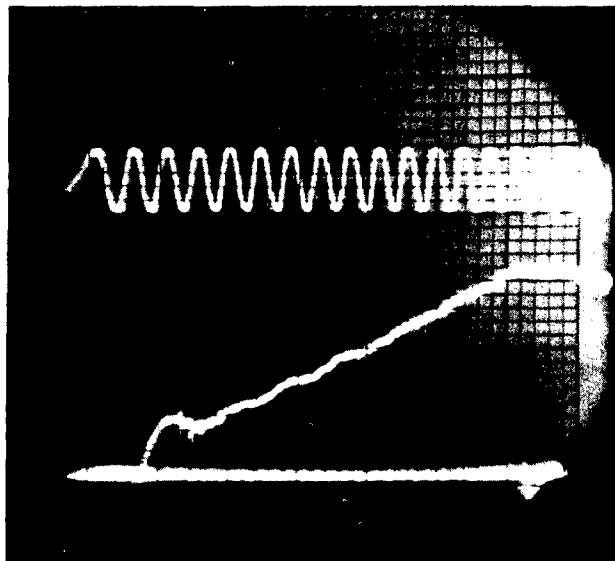
3.3.5.1 The effect of mass load on the pressure surges in an actuating cylinder was investigated by studying the resulting pressure waveforms under the following test conditions:

Figure 42

TYPICAL PRESSURE WAVEFORMS ON A BOTTOMED CYLINDER CONFIGURATION  
- ACTUATING CYLINDER SYSTEMS WITH AND WITHOUT AN ACCUMULATOR



System With Accumulator

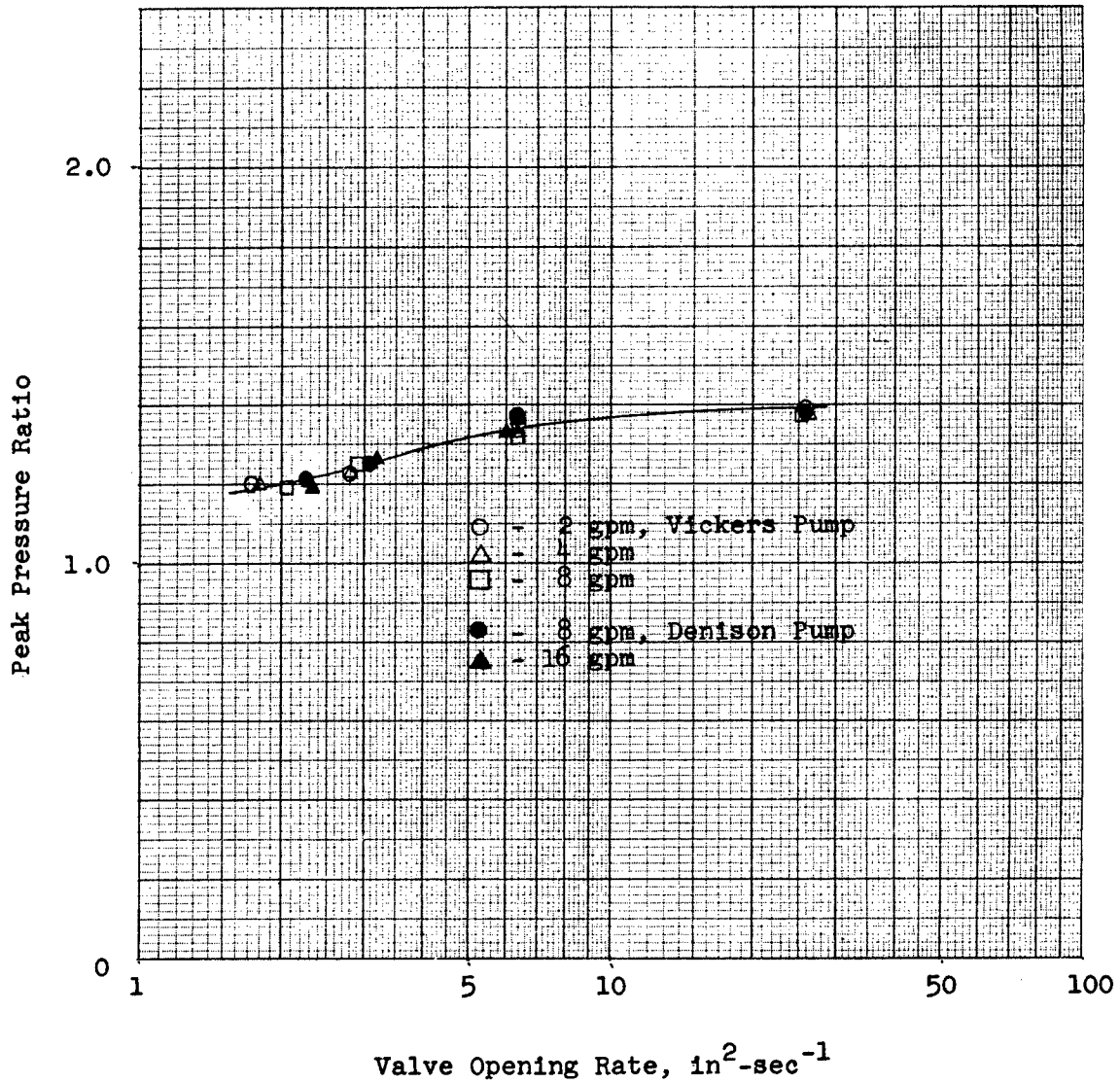


System Without Accumulator

Note: Pressure characteristics at inlet port of bottomed cylinder.  
Test section length between valve and cylinder, 96 in.

Figure 43

PEAK PRESSURE RATIO VS. VALVE OPENING RATE  
 FOR VARIOUS PUMP DISCHARGE FLOW RATES  
 IN A BOTTOMED CYLINDER CONFIGURATION  
 ACTUATING CYLINDER SYSTEM WITH AN ACCUMULATOR

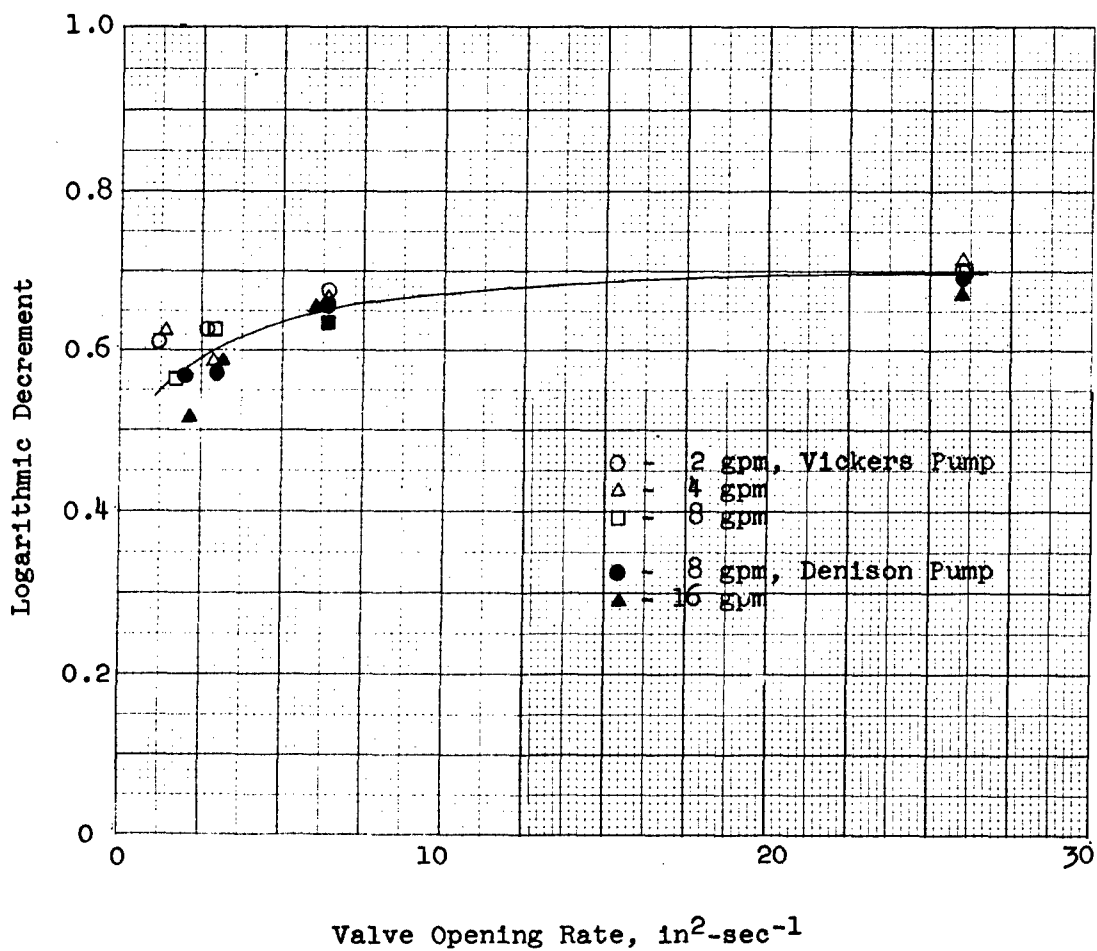


Note: 96 in. test section length.



Figure 44

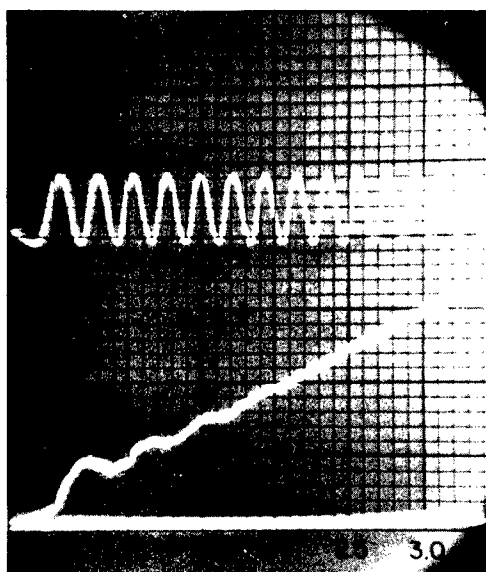
LOGARITHMIC DECREMENT VS. VALVE OPENING RATE  
 FOR VARIOUS PUMP DISCHARGE FLOW RATES  
 IN A BOTTOMED CYLINDER CONFIGURATION  
 ACTUATING CYLINDER SYSTEM WITH AN ACCUMULATOR



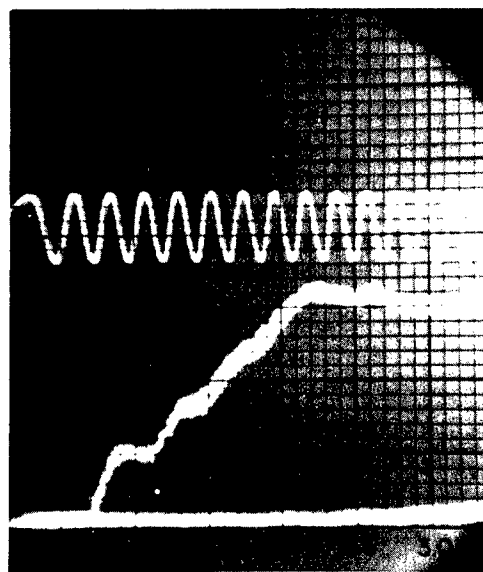
Notes: 96 in. test section length.  
 Logarithmic decrement based on first two peaks of pressure oscillation.

Figure 45

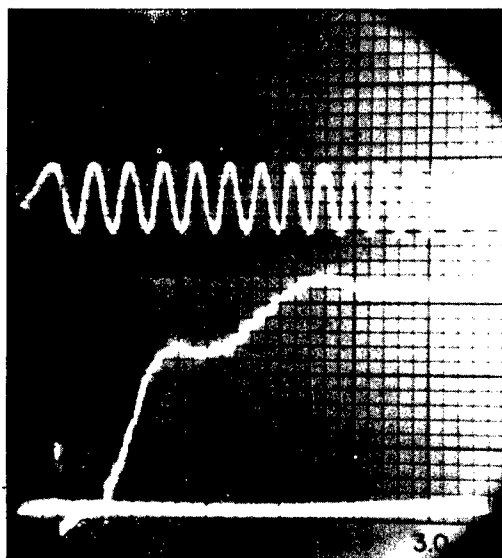
TYPICAL PRESSURE WAVEFORMS IN A BOTTOMED CYLINDER CONFIGURATION,  
SHOWING EFFECT OF VOLUMETRIC DIFFERENCE IN PRESSURIZED SECTION OF SYSTEM  
ACTUATING CYLINDER SYSTEM WITHOUT AN ACCUMULATOR



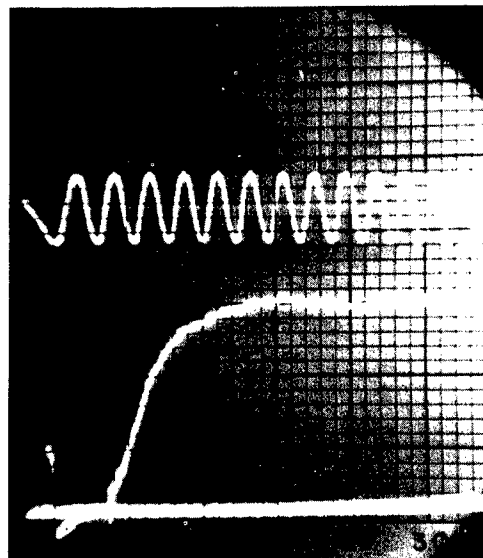
4 gpm, Vickers Pump



8 gpm, Vickers Pump



8 gpm, Denison Pump

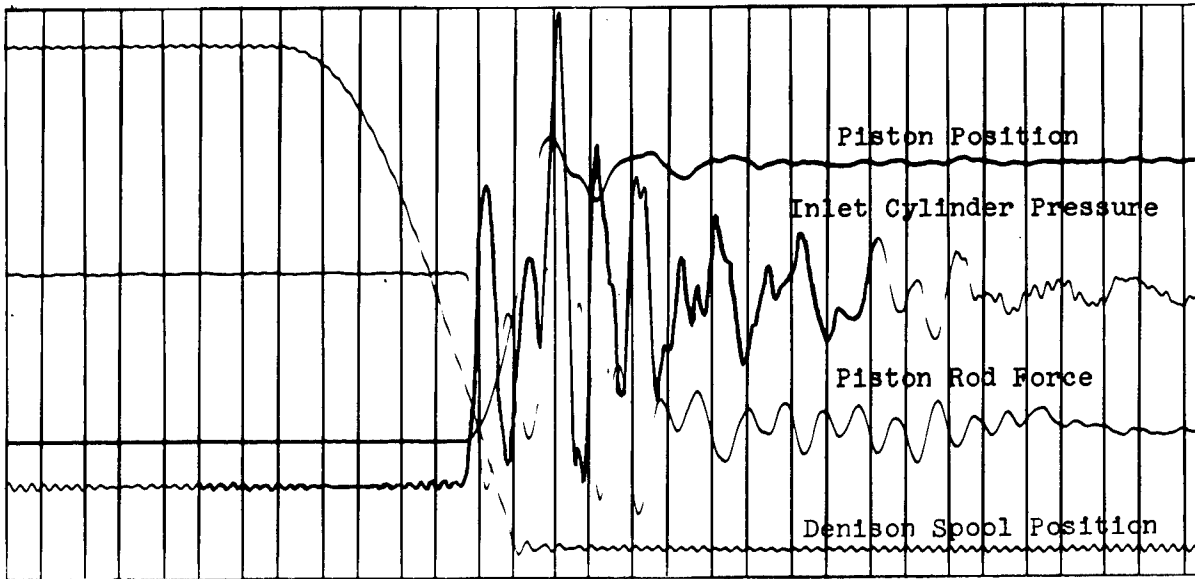


16 gpm, Denison Pump

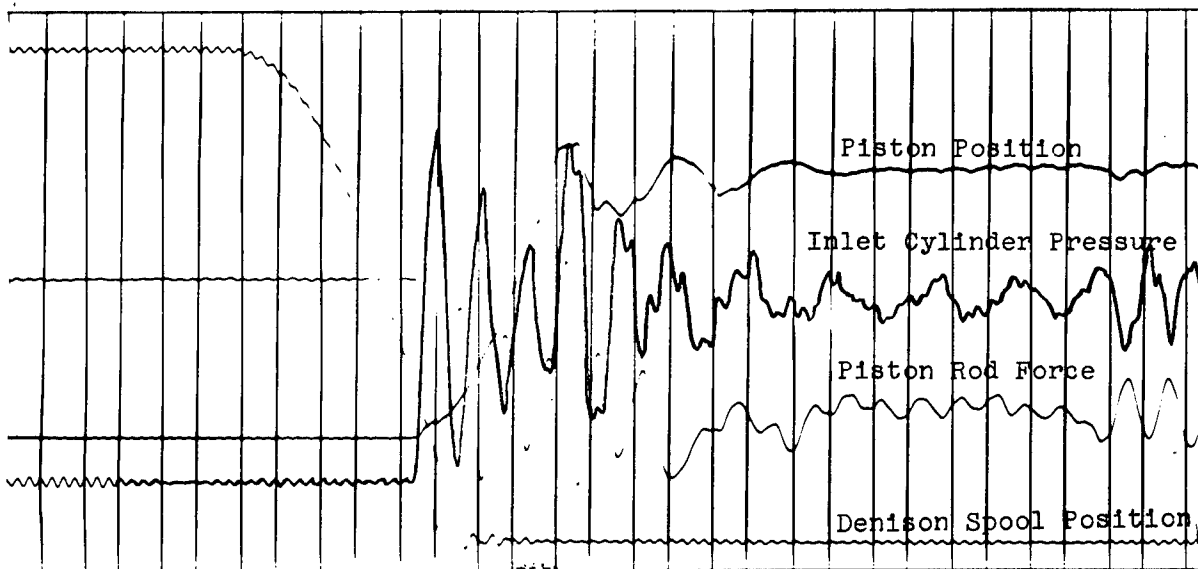
Notes: 96 in. test section length.  
Valve opening rate,  $27 \pm 1 \text{ in}^2\text{-sec}^{-1}$   
Sweep speed of the signal trace was the same in all photographs.

Figure 46

TYPICAL PRESSURE WAVEFORMS IN A MASS-LOADED  
ACTUATING CYLINDER SYSTEM WITH AN ACCUMULATOR



Applied Weight Load, 114 lb Per Unit Piston Area



Applied Weight Load, 425 lb Per Unit Piston Area

- (a) System pressure, 3000 psi.
- (b) Accumulator precharge air pressure, 1000 psi.
- (c) System flow conditions, accumulator in (pump discharge flow rate, 2 gpm), pump discharge flow rates (accumulator out) of 2, 4, 8, and 16 gpm.
- (d) Valve opening rate, 3-30 in<sup>2</sup>-sec<sup>-1</sup>.
- (e) Mass load conditions, "dead weight" loads from 60 to 420 lb.

Opposing loads were applied to the cylinder by means of dead weight on a weight pan connected to the lower end of the piston rod (Fig. 36). Suitable stops were installed such that the sudden deceleration of the weight was prevented from damaging the test cylinder or instrumentation. For these tests, the force transducer was placed at Location 2, Fig. 35. Tare weight of the moving parts of the test cylinder configuration (i.e., piston and rod, weight pan, fittings, etc.) was 10 lb.

3.3.5.2 In preliminary test runs with the return port of the test cylinder connected to the Denison valve, it was found that the resistance of the system return line had an appreciable effect on the test results. To facilitate theoretical analysis, it was deemed advisable to minimize this effect, and the return port of the test cylinder was left open to atmosphere.

3.3.5.3 With the accumulator installed in the system, the pressure waveform in the cylinder was characterized by two pressure surges, one when the mass load was accelerated and another when the piston reached the end of its stroke. Typical oscillograph records of the waveform are shown in Fig. 46. Results of the tests indicated that the effect of mass load on the magnitude of the initial pressure surge was very great, especially at fast valve opening rates (Fig. 47). The data shown in Fig. 47 were determined from cross-plots of original data taken from oscillograph records. This was done to obtain more presentable data at constant values of unit loading (i.e., "dead-weight" load per unit of piston area). The peak pressure ratios were determined from the maximum pressure of the initial surge and from the system pressure at the end of the test run.

3.3.5.4 Studies of the oscillograph records for fast valve opening rates indicated that the mass was suddenly accelerated by the energy of the pressure wavefront and then accelerated again as the fluid flow from the accumulator became effective. This was shown on the position vs. time trace of the position transducer on the piston of the test cylinder (Fig. 46). The magnitude of the pressure surge which occurred when the piston bottomed was a function of the fluid velocity in the cylinder and system as will be shown in Par. 3.3.6.3. The effect of mass load on piston velocity was to reduce the velocity as the mass load was increased (Fig. 48). With the accumulator removed from the system, the magnitude of the initial pressure surge was found to increase rapidly with increases in mass loading (Fig. 49). The magnitude of the pressure surge was found to increase with pump discharge flow rate in about the same proportion as was observed in similar investigation on closed-end tubes (Par. 3.2.4 and Fig. 14). This indicated that the magnitude of the initial pressure surge was dependent upon the energy of the compressed fluid in the pressurized system and not upon the energy derived from the pump output. By studying the typical oscillograph records shown in Fig. 50, it will be noted that the mean pressure of the underdamped oscillatory wave drops rapidly with piston displacement, which was indicative that the pressurized system was discharging.

3.3.5.5 A complete analysis of the effect of mass load on the frequency of the initial pressure surge was not made, but it was noted that lower frequencies were associated with the lower mass loads. This was in agreement with the theory developed in Appendix I, Par. 3.5. The frequency of the bottoming surge with the accumulator installed was essentially the same as for a 96 in. test section in the closed-end tube system (Par. 3.2.2.8).

Figure 47

INITIAL PEAK PRESSURE RATIO VS. VALVE OPENING RATE FOR VARIOUS WEIGHT (MASS) LOADS ACTUATING CYLINDER SYSTEM WITH AN ACCUMULATOR

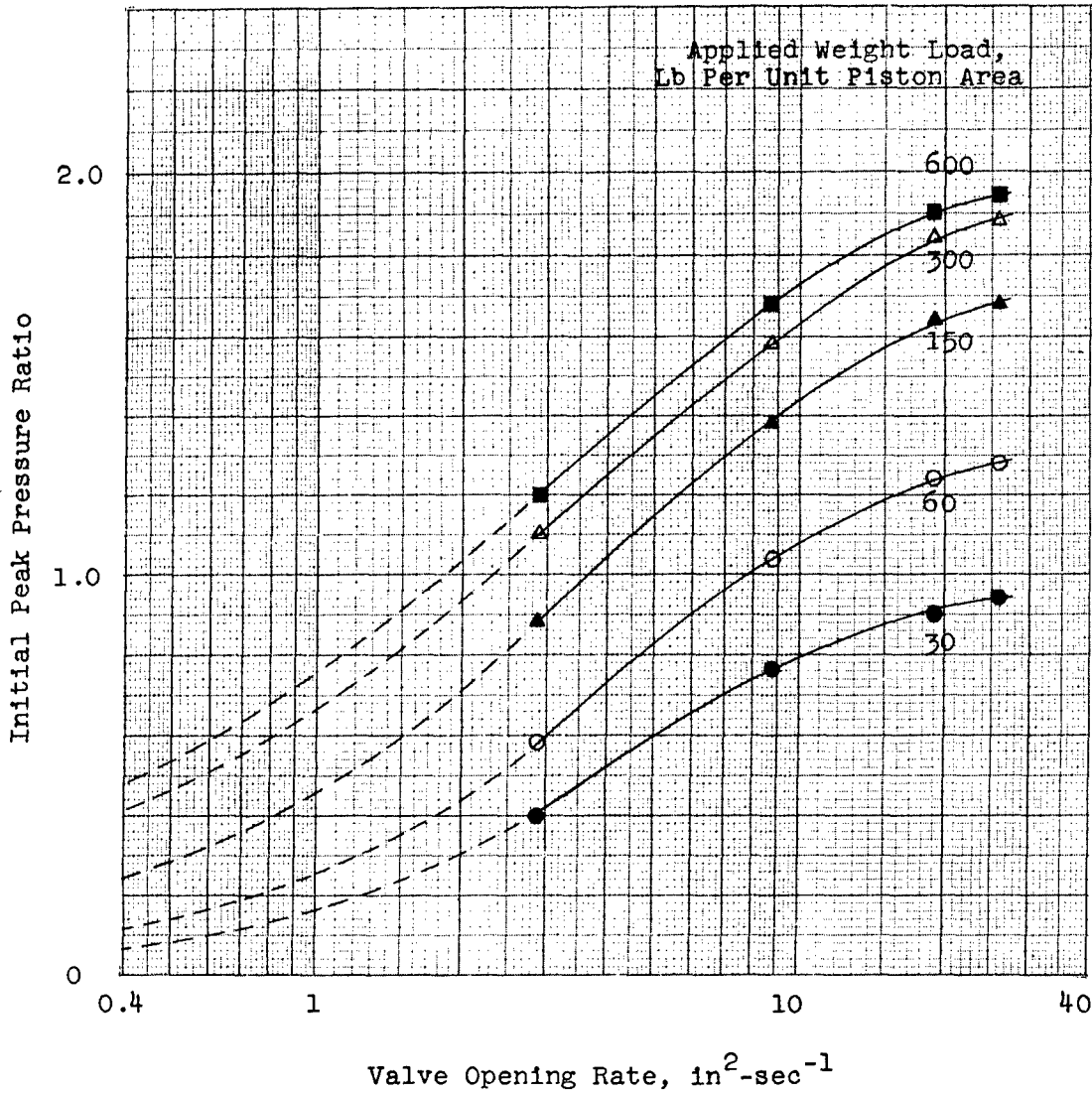
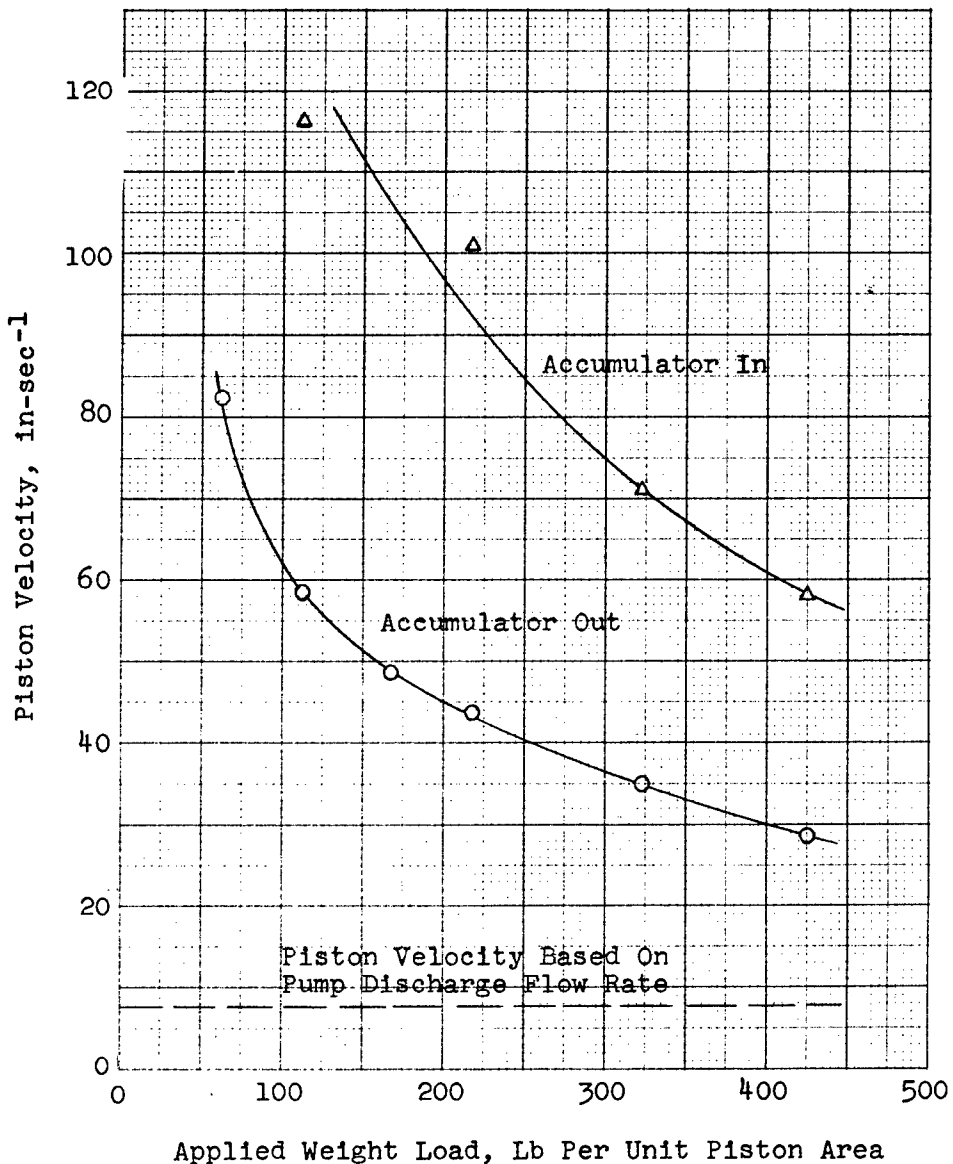


Figure 48

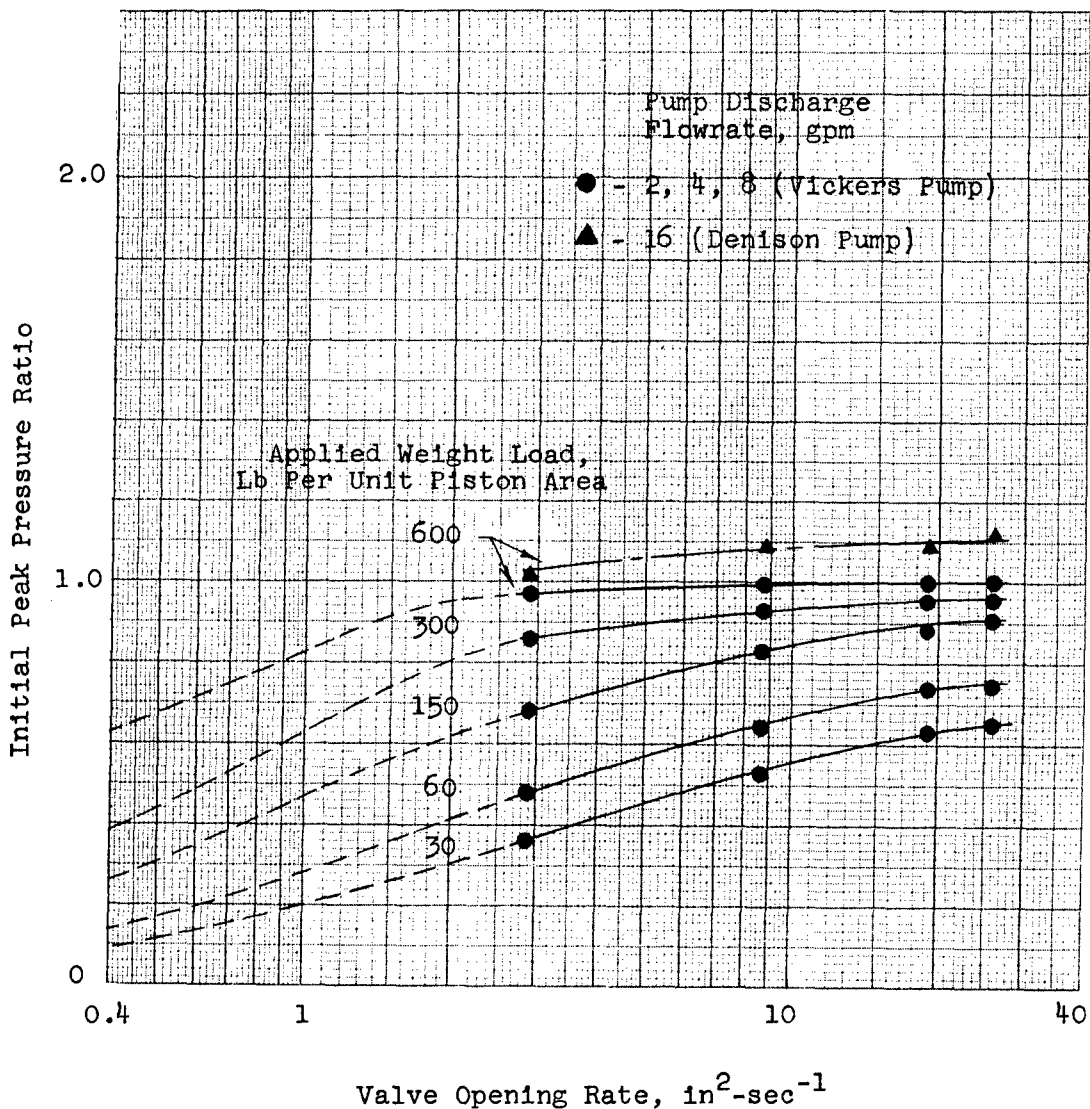
PISTON VELOCITY VS. APPLIED WEIGHT LOAD  
WITH AND WITHOUT AN ACCUMULATOR  
ACTUATING CYLINDER SYSTEMS



Notes: Valve opening rate,  $28 \pm 2 \text{ in}^2\text{-sec}^{-1}$ .  
Pump discharge flow rate, 2 gpm.

Figure 49

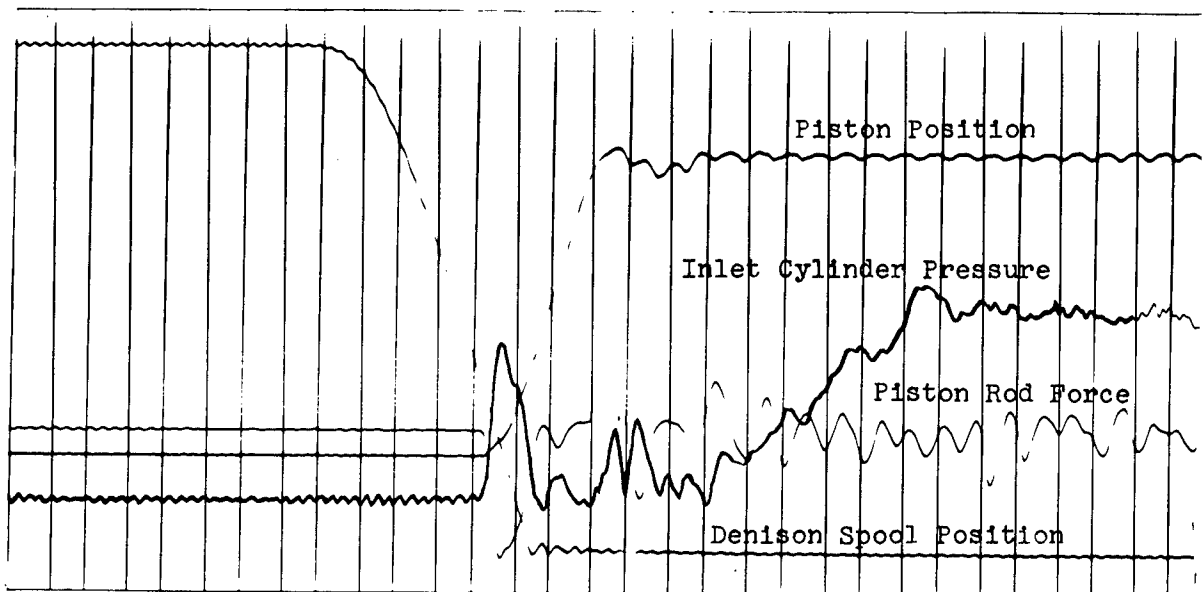
INITIAL PEAK PRESSURE RATIO VS. VALVE OPENING RATE FOR VARIOUS WEIGHT (MASS) LOADS ACTUATING CYLINDER SYSTEM WITHOUT AN ACCUMULATOR



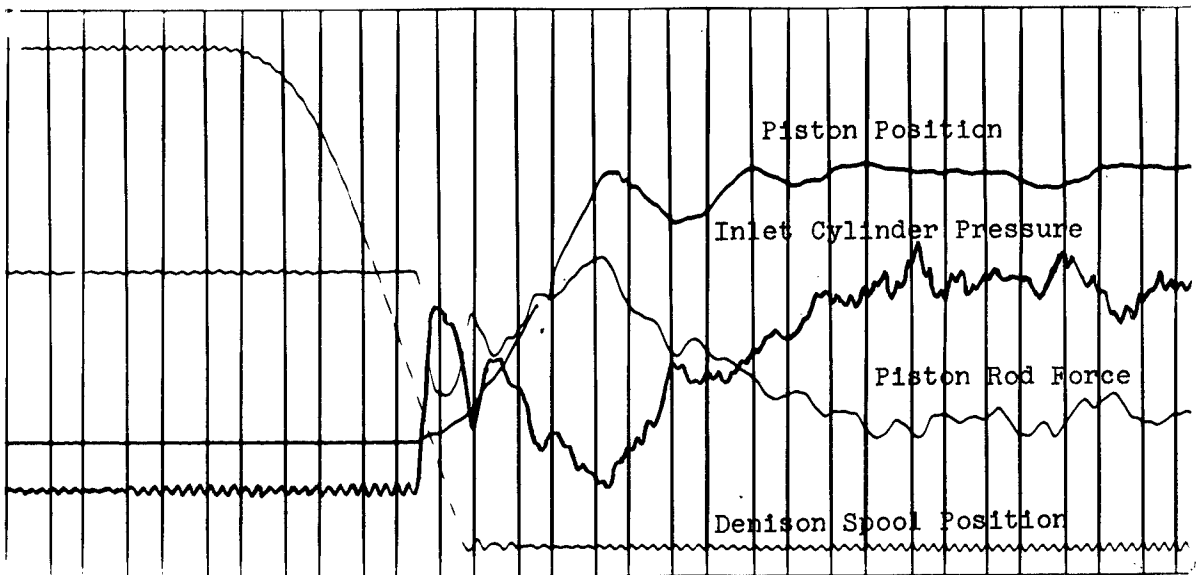
Note: Difference in curves at 600 lb unit weight load was due primarily to volumetric difference in pressurized section of test system (Par. 3.2.4.2).

Figure 50

TYPICAL PRESSURE WAVEFORMS IN A MASS-LOADED  
ACTUATING CYLINDER SYSTEM WITHOUT AN ACCUMULATOR



Applied Weight Load, 114 Lb Per Unit Piston Area

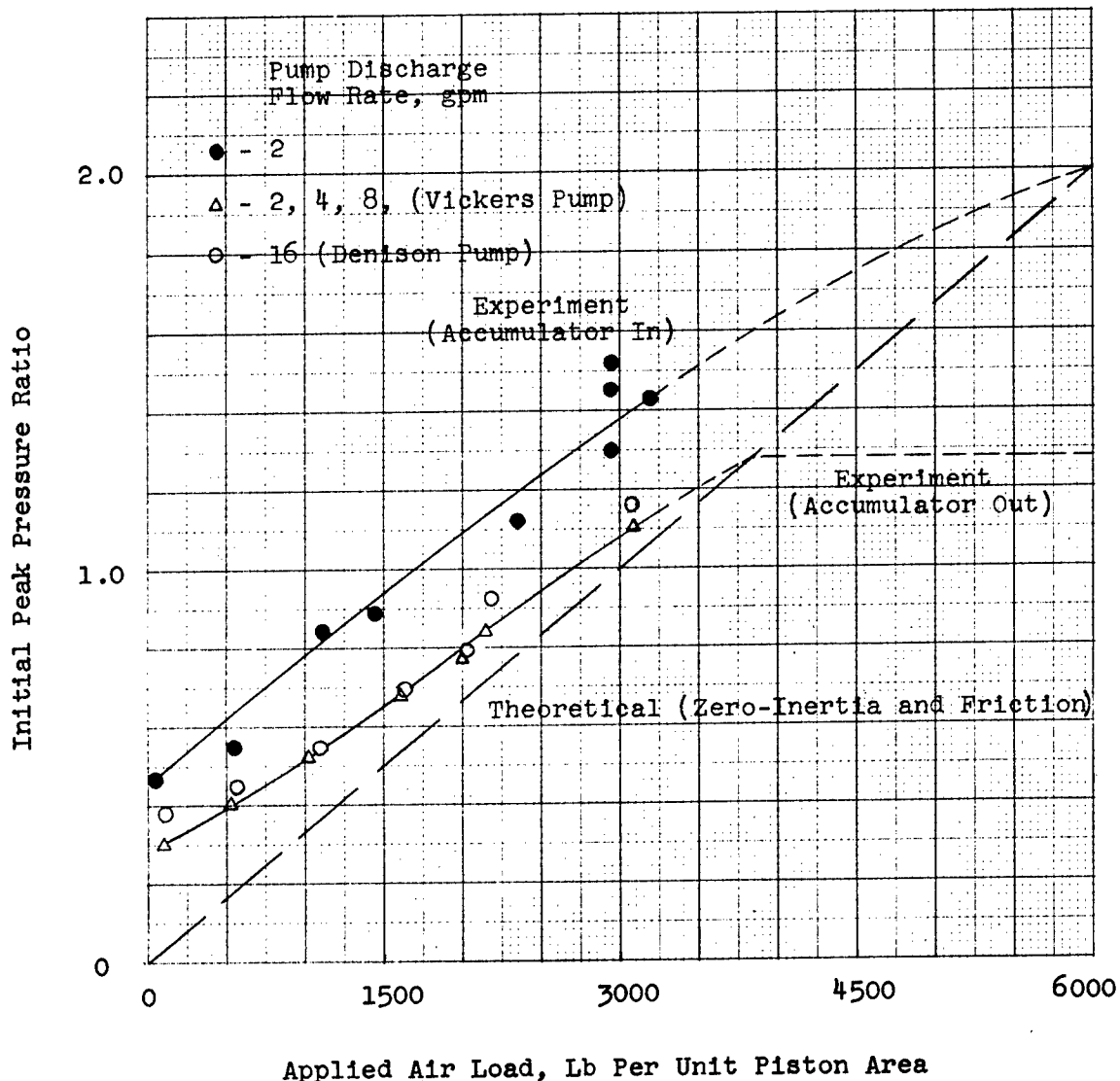


Applied Weight Load, 425 Lb Per Unit Piston Area



Figure 51

INITIAL PEAK PRESSURE RATIO VS.  
 APPLIED AIR LOAD FOR ACTUATING CYLINDER  
 SYSTEMS WITH AND WITHOUT AN ACCUMULATOR



Notes: Valve opening rate,  $28 \pm 2 \text{ in}^2 \text{-sec}^{-1}$ .  
 Tare weight, 9.0 lb per unit piston area.  
 Difference in initial peak pressure ratios at 16 gpm pump discharge flow rate was due primarily to volumetric difference in pressurized section of test system (Par. 3.2.4.2).

3.3.6 Air Load

3.3.6.1 The effect of air load on the pressure surges in an actuating cylinder was investigated by studying the resulting pressure waveforms under the following conditions:

- (a) System pressure, 3000 psi.
- (b) Accumulator precharge air pressure, 1000 psi.
- (c) System flow conditions, accumulator in (pump discharge flow rate, 2 gpm), pump discharge flow rates (accumulator out) of 2, 4, 8, and 16 gpm.
- (d) Valve opening rate, 3-30 in<sup>2</sup>-sec<sup>-1</sup>.
- (e) Simulated air load conditions, constant loads from 50 to 3000 psi (air pressure on opposing side of piston), and increasing loads at spring rates of 170 to 1000 lb/in. of piston travel.

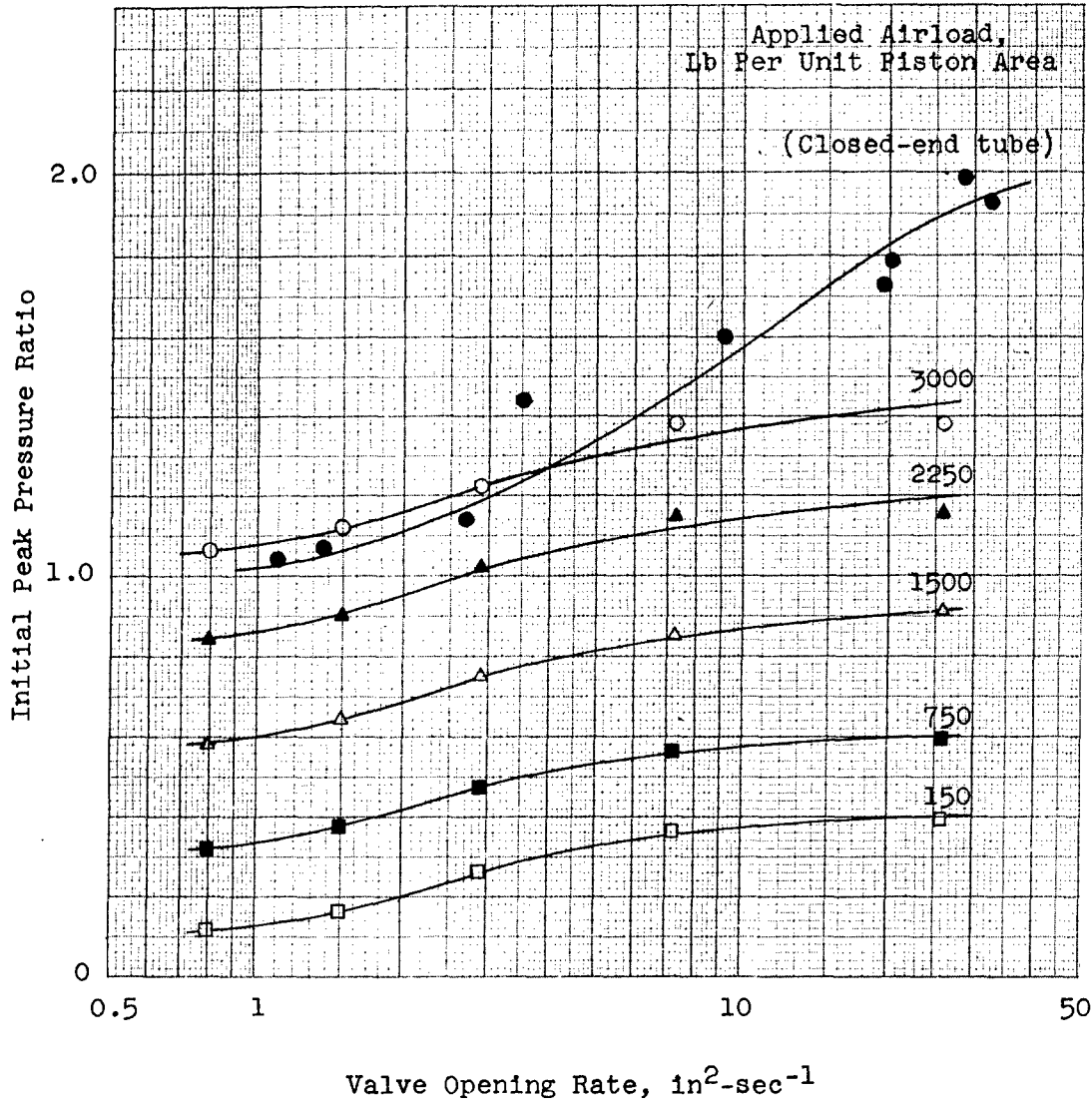
Constant air loads were applied to the cylinder by means of an air chamber connected to the opposing side of the piston (Fig. 35) and charged to the desired pressure with nitrogen. The air chamber used was a 200 cu in., piston type, accumulator (Contractor part No. 161-58095) with the piston removed and the air port capped. With this volume available, the volumetric change due to piston displacement had essentially no effect on the pressure in the chamber. Increasing air loads were simulated by helical compression springs, of various spring rates, which applied load to a platform on the upper end of the piston rod (Fig. 35). Buckling of the springs was prevented by a tubular guide. Adjustment was provided at the fixed end support so that the initial load on the platform could be controlled. The force transducer was placed at Location 1, Fig. 35. The mass load present in these tests was primarily the tare weight (10 lb) of the movable parts of the cylinder. In the increasing air load tests, there was a small increase due to the effective spring mass.

3.3.6.2 Under constant load conditions, the initial peak pressure ratio was found to increase almost proportionally with the magnitude of the applied air load (Fig. 51). In the equivalent electric analog, (Appendix I, Par. 3.6) a constant air load is represented by an infinite capacitor (battery) in opposition to the accumulator capacitor charge ( $P_0$ ), which has the primary effect of decreasing the potential difference, thereby decreasing the current flow in the circuit. From this, it was concluded that the magnitude of the initial pressure rise under constant air load conditions with no mass or friction present in the cylinder should be approximately proportional to the applied air load (Fig. 51). The difference between the peak pressure ratios of the theoretical (zero inertia and friction) and experimental curves was attributed to the effect of the pressure wavefront on the mass and friction forces present in the cylinder. It can be seen from the curves that the inertia effect decreased as the magnitude of the applied air load increased, which was indicative of the reduction of available energy for acceleration of the mass. The intercept points on the curves (Fig. 51) are the peak pressure ratios of a closed-end tube. As was observed in the mass load tests (Par. 3.3.5) with no accumulator in the system, the magnitude of the initial pressure surge was not appreciably effected by pump discharge flow rate. The effect of slower valve opening rate was to decrease the initial peak pressure ratio in a similar manner as was observed in the mass load tests. Initial peak pressure ratios vs. valve opening rates for various applied air loads with the accumulator installed in the system are shown in Fig. 52. The data shown in Fig. 52 were determined from cross-plots of original data obtained from the oscillograph records.

3.3.6.3 Studies of the pressure surges which occurred when the piston bottomed indicated that the magnitude was approximately proportional to the piston velocity. Good correlation was obtained between experimental values and theoretical values based on instantaneous closing valve theory (Ref. 1, Appendix X),

Figure 52

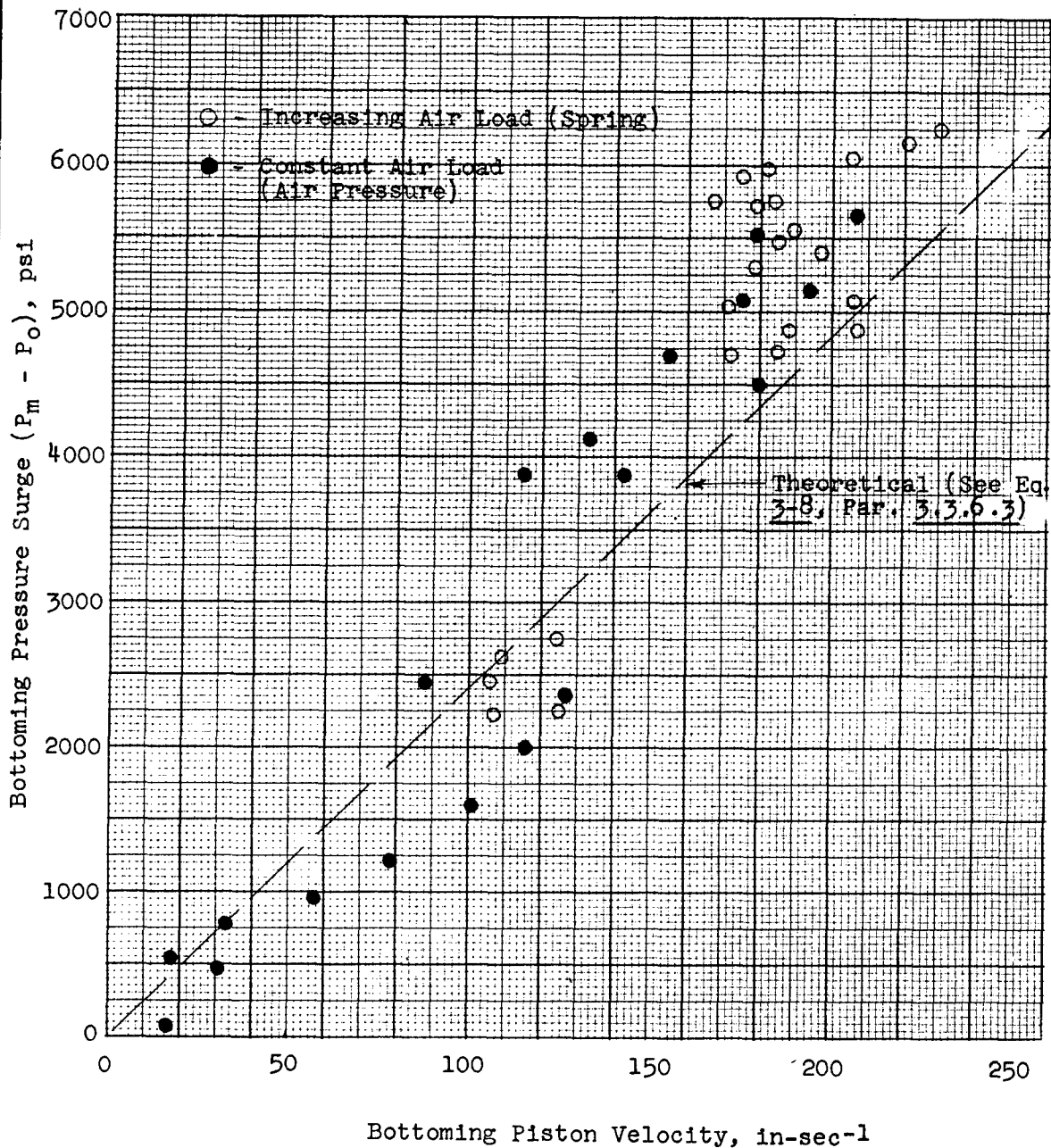
INITIAL PEAK PRESSURE RATIO VS. VALVE OPENING RATE FOR VARIOUS CONSTANT AIR LOADS ACTUATING CYLINDER SYSTEM WITH AN ACCUMULATOR



Note: Tare weight, 9.0 lb per unit piston area.

Figure 53

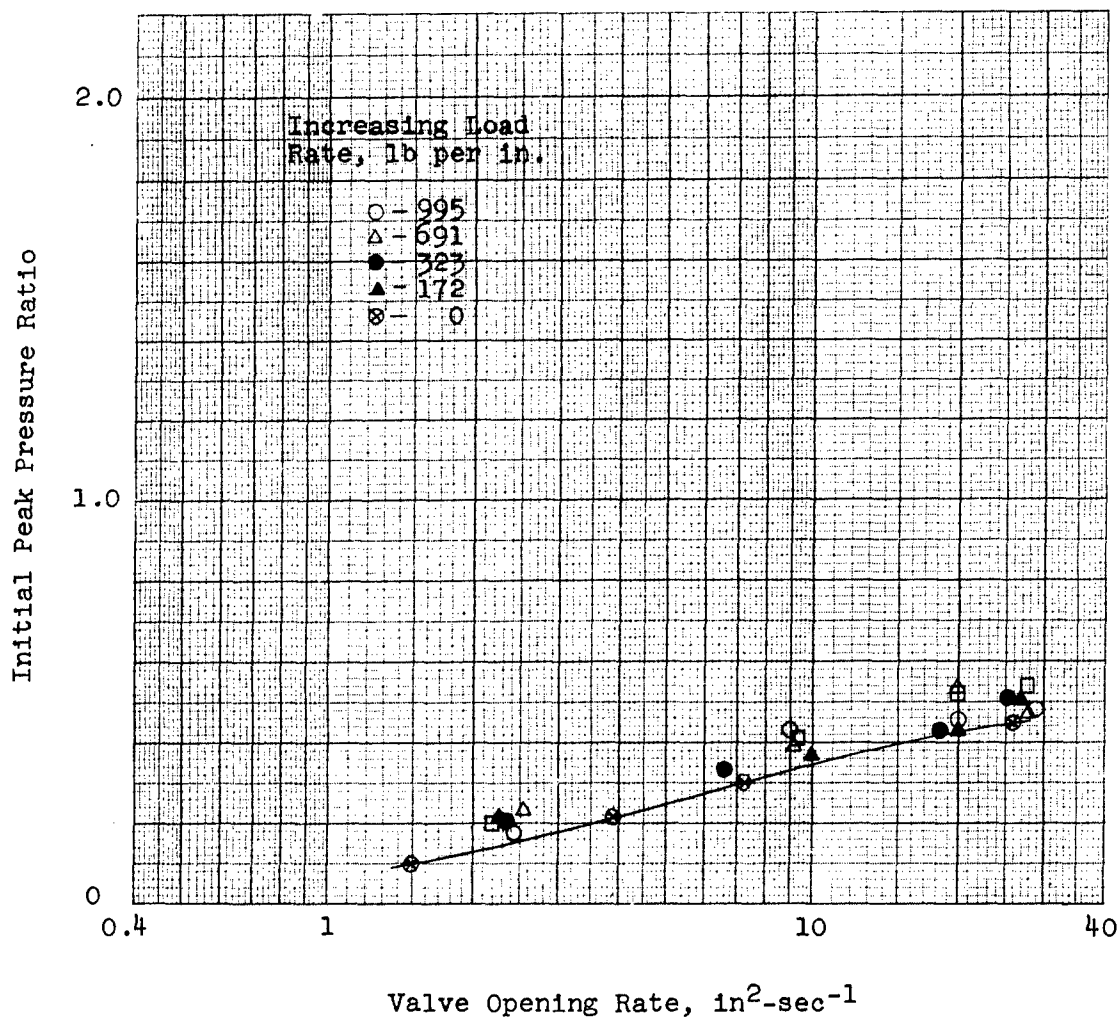
BOTTOMING PRESSURE SURGE VS. BOTTOMING PISTON VELOCITY - ACTUATING CYLINDER SYSTEMS UNDER AIR LOAD CONDITIONS



Note: P<sub>m</sub> = maximum pressure of bottoming surge, psi.  
P<sub>o</sub> = system pressure (3000 psi).

Figure 54

INITIAL PEAK PRESSURE RATIO VS. VALVE  
 OPENING RATE FOR INCREASING AIR LOADS (ZERO INITIAL LOAD)  
 ACTUATING CYLINDER SYSTEM WITH AN ACCUMULATOR



Note: Tare weight, 9.0 lb per unit piston area.

$$P_m - P_o = \sqrt{\frac{\rho}{\beta_e}} U_o \quad (3-6)$$

where

$P_m$  = maximum pressure of surge, psi.  
 $P_o$  = accumulator pressure, psi.  
 $\rho$  = fluid mass density, lb-sec<sup>2</sup>-in<sup>-4</sup>  
 $\beta_e$  = effective system compressibility, psi<sup>-1</sup>  
 $U_o$  = average fluid velocity, in-sec<sup>-1</sup>

For specific application of the theory to actuating cylinder systems, consideration has to be given the fact that energy is derived from two different volumes of fluid moving at different average velocities. To take this into account, Eq. 3-6 was modified as follows:

$$P_m - P_o = \sqrt{\frac{\rho}{\beta_e}} \left[ U_c \frac{V_c}{V_T} + U_L \frac{V_L}{V_T} \right] \quad (3-7)$$

where

$U_c$  = average fluid velocity in cylinder, in-sec<sup>-1</sup>  
 $U_L$  = average fluid velocity in tubing, in-sec<sup>-1</sup>  
 $V_c$  = volume of fluid in cylinder (at end of piston stroke), in<sup>3</sup>  
 $V_L$  = volume of fluid in tubing (from accumulator to cylinder port), in<sup>3</sup>  
 $V_T = V_c + V_L$  = total volume of fluid in motion, in<sup>3</sup>

Since  $U_L \approx U_c \frac{A_c}{A_L}$

where

$A_c$  = net area of piston, in<sup>2</sup>  
 $A_L$  = internal cross-sectional area of tube, in<sup>2</sup>

Eq. 3-7 can be written

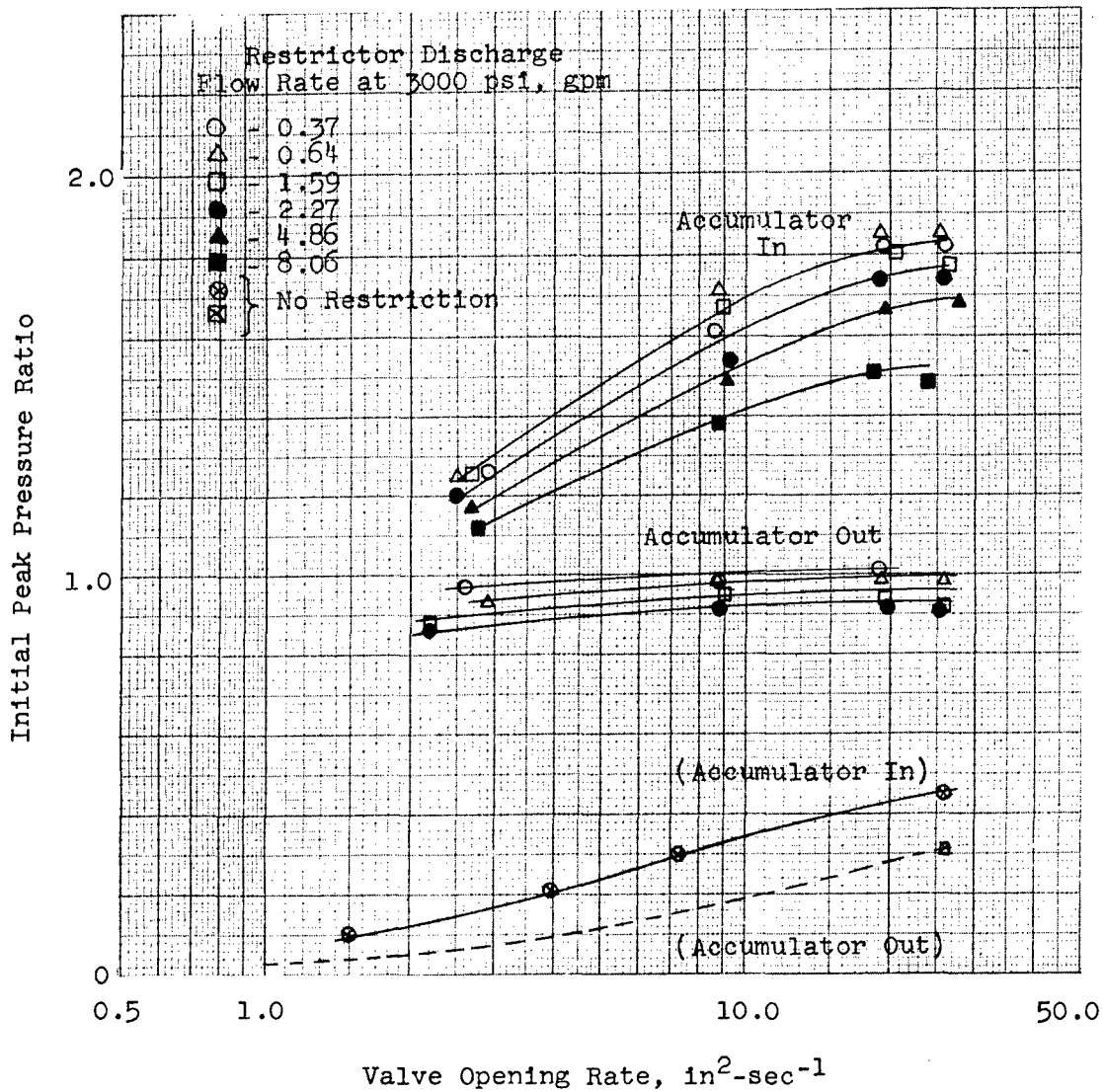
$$P_m - P_o = \sqrt{\frac{\rho}{\beta_e}} U_c \left[ \frac{V_c}{V_T} + \left( \frac{A_c}{A_L} \right) \left( \frac{V_L}{V_T} \right) \right] \quad (3-8)$$

From experimental data, the piston velocity was found to decrease as the applied air load was increased. As can be seen from the electric analog, the current flow in the circuit will be a function of the potential difference between the accumulator charge and the air load battery in the system, which decreases as the battery potential increases. A comparison of experimental values of  $P_m - P_o$  with theoretical values calculated from Eq. 3-8 is given in Fig. 53. Although the theoretical formula (Eq. 3-8) is considered valid, further investigation is recommended to determine the effect of different area and volume ratios.

3.3.6.4 Results of the tests under increasing load conditions indicated that the magnitude of the initial pressure surge was essentially independent of spring rate (Fig. 54). For these tests, the initial air load on the cylinder was approximately zero. The peak pressure ratios for increasing load conditions were slightly higher than were obtained on the basic cylinder with no external forces other than the tare weight of movable parts (Fig. 54). This was attributed primarily to the small increase in mass load resulting from the spring inertia. In the equivalent electric analog (Appendix I, Par. 3.6) an increasing air load is represented by a capacitor of finite value. As the charge on this capacitor is increased by increasing air loads and by transfer from the accumulator capacitor, the potential difference, and the consequent current flow, in the system is reduced more rapidly than in the constant air load case. From this, it was concluded that the primary effect

Figure 55

INITIAL PEAK PRESSURE RATIO VS. VALVE OPENING RATE  
 FOR VARIOUS DEGREES OF RETURN LINE RESTRICTION  
 ACTUATING CYLINDER SYSTEMS WITH AND WITHOUT AN ACCUMULATOR



Notes: Pump discharge flow rate at 3000 psi, 2 gpm.  
 Tare weight, 10.2 lb per unit piston area.

of an increasing load would be to reduce the bottoming surge. Studies of the piston velocity under various spring rates substantiated this. Experimental data on the magnitude of the bottoming pressure surge as a function of piston velocity are shown in Fig. 53. Although no tests were conducted with an initial load which increased with piston stroke, it is anticipated that the magnitude of the initial pressure surge under a given set of conditions would be comparable to the value obtained under constant load conditions, while the bottoming pressure surge would be decreased.

3.3.6.5 The effect of an air load which decreases with piston travel can be visualized by considering the equivalent electric analog. In the analog (Appendix I, Par. 3.6), the decreasing air load is represented by a capacitor of finite negative value, which has the effect of increasing the potential difference in the system as the accumulator capacitor discharges. The initial air load is represented by an initial charge on the air load capacitor. From this, it was concluded that the magnitude of the initial pressure surge would be approximately the same as would be obtained under a constant air load equivalent to the initial load of the decreasing load configuration, while the bottoming pressure surge would be higher.

### 3.3.7 Return Line Restriction

3.3.7.1 A restriction in the cylinder return line is sometimes used as a piston velocity-limiting device. The effect of this restriction was investigated by studying the pressure waveforms on both sides of the cylinder piston under the following conditions:

- (a) System pressure, 3000 psi.
- (b) Accumulator precharge air pressure, 1000 psi.
- (c) System flow conditions, accumulator in (pump discharge flow rate, 2 gpm), pump discharge flow rates (accumulator out) of 2, 4, and 8 gpm.
- (d) Valve opening rate, 3-30 in<sup>2</sup>-sec<sup>-1</sup>.
- (e) Restrictor flow rates at 3000 psi, 1/4 to 8 gpm.

For these tests, one-way restrictors (Contractor part No. 1V4) of various flow ratings were connected to the return port of the test cylinder such that restriction was offered to the flow from the cylinder. The actual flow rates of the restrictors used were experimentally determined for 3000 psi pressure differential across the orifice. To minimize return line effect, the restrictor was located close to the cylinder and the flow was discharged into a fluid chamber under a constant static pressure. The fluid chamber used was a 200 cu in. piston type accumulator (Contractor part No. 161-58095) with a precharge air pressure of 25 psig. The general procedure for preparing the configuration for test was as follows:

- (a) The desired restrictor was installed in the cylinder return line.
- (b) The accumulator and cylinder were charged with fluid to approximately 60 psi pressure and were bled of entrapped air. Valve "A", Fig. 35, was closed. In this configuration, the fluid and air supplies were opposite to that shown in the schematic diagram.

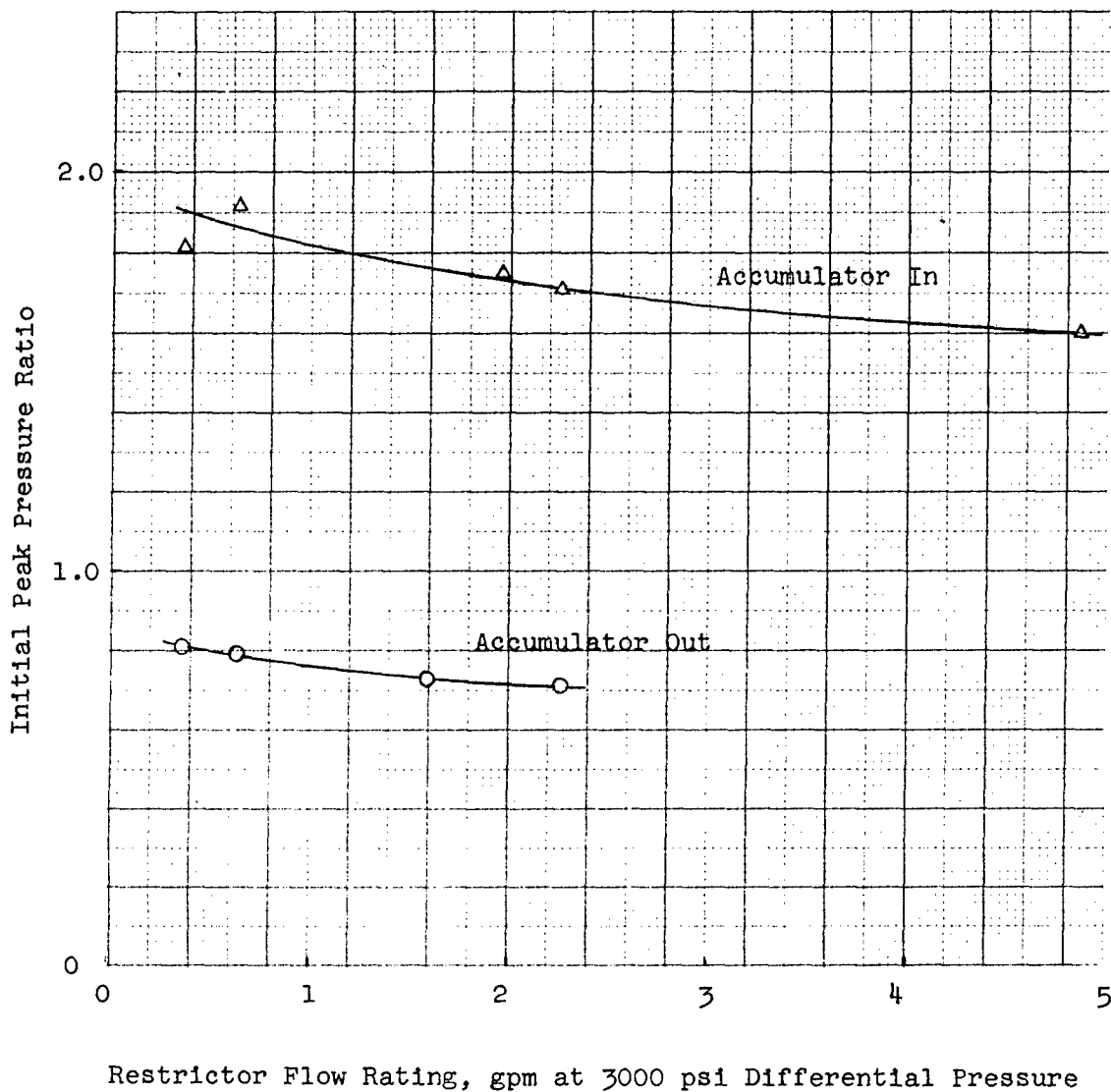
Since the volumetric change due to piston displacement was small, the static pressure in the accumulator remained essentially constant during test runs. There was no mass load, other than the tare weight (10 lb) of the movable parts of the cylinder, applied during these tests.

3.3.7.2 With an accumulator installed in the system, restrictors having small orifices (0.37 - 1.59 gpm, flow rate at 3000 psi pressure differential) gave pressure surges of approximately the same magnitude as were observed in closed-end tube tests with varying valve opening rates on a 96 in. test section (Par. 3.2.2). Increases in the orifice size gave lower peak pressures, as shown in Fig. 55. With the accumulator removed from



Figure 56

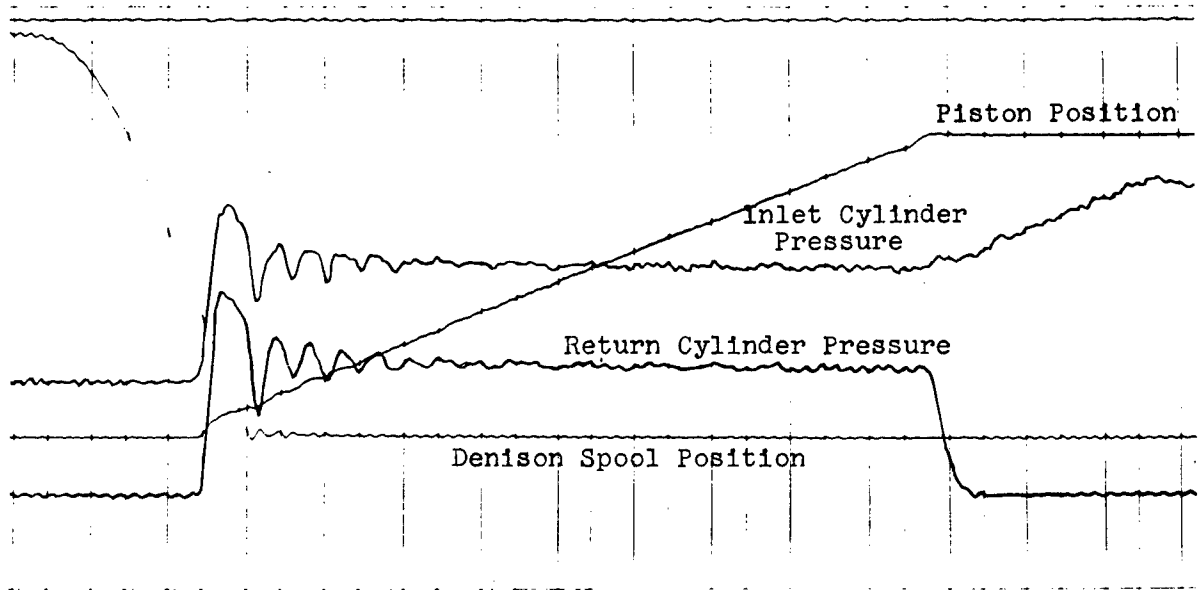
INITIAL PEAK PRESSURE RATIO VS. RESTRICTOR SIZE SHOWING RELATIVE EFFECT ON ACTUATING CYLINDER SYSTEM WITH AND WITHOUT AN ACCUMULATOR



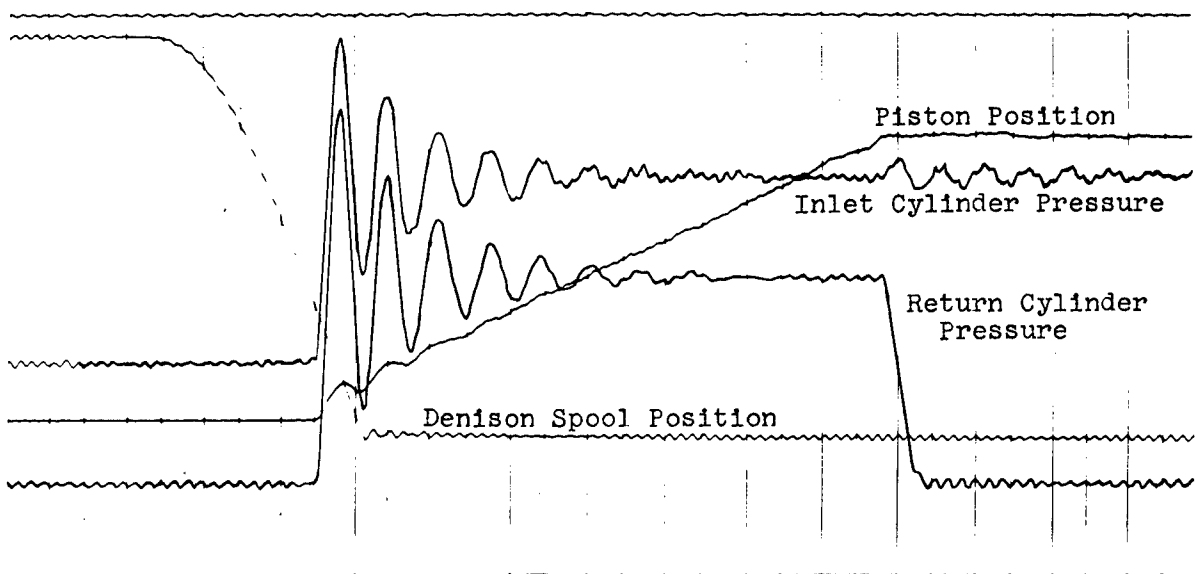
Notes: Valve opening rate,  $28 \pm 2 \text{ in}^2\text{-sec}^{-1}$   
Tare weight, 10.2 lb per unit piston area.

Figure 57

TYPICAL PRESSURE WAVEFORMS SHOWING RELATIONSHIP OF PRESSURES ON OPPOSITE SIDES OF PISTON - ACTUATING CYLINDER SYSTEM WITH A 2 GPM RETURN LINE RESTRICTION



Accumulator Removed from Test System



Accumulator Installed in Test System

the system and the pump discharge flow rate set at 2 gpm, the magnitude of the initial pressure surge was approximately equal to system pressure for all valve opening rates on the 0.37 gpm restrictor. Increases in restrictor size reduced the peak pressure ratio as shown in Fig. 55. Increases in the pump discharge flow rate gave almost linear increases in the initial peak pressure ratio, the ratio increasing from 0.91 at 2 gpm on a 2.27 gpm restrictor to 1.03 at 8 gpm on the same restrictor. For comparative purposes, peak pressure ratios are shown for the initial pressure surges which occurred on the basic test cylinder with no external loads applied. These ratios were determined from analytical work on the data obtained in the mass load and air load tests (Par. 3.3.5 and 3.3.6).

3.3.7.3 A relative effect of restrictor size on a system with and without an accumulator is shown in Fig. 56. The pump discharge flow rate was 2 gpm and the valve opening rate was  $26 \pm 2$  in<sup>2</sup>/sec.

3.3.7.4 Studies of the pressure waveforms in the test cylinder indicated that the magnitude of the initial pressure surge was essentially the same on both sides of the piston. Oscillation of the actuating cylinder piston, shown in the position trace in Fig. 57, was indicative of the acceleration and deceleration which occurs in a fluid system under pressure surge conditions. Although no specific tests were conducted, it is theorized that higher mass loads would increase the magnitude of the pressure surge on the inlet side of the piston, approaching a closed-end tube condition, and decrease the magnitude of the pressure surge on the return side of the piston. Another consideration is the location of the restriction, which might result in dual frequencies reacting upon the piston. Further investigation would be necessary to establish a more exact correlation.

#### 3.4 Accumulators

##### 3.4.1 General Notes

3.4.1.1 The effect of parameters relative to system accumulators was investigated by studying the pressure surges in a closed-end tube when a valve was rapidly opened. The apparatus, except for system accumulator, and general procedure were the same as described in Par. 3.2.1. Unless otherwise noted, the basic test conditions which prevailed were as follows:

- (a) System pressure, 3000 psi.
- (b) Accumulator precharge air pressure, 1000 psi.
- (c) Pump discharge flow rate, 2 gpm
- (d) Fluid temperature,  $38 \pm 5$  C ( $100 \pm 9$  F).
- (e) Test section length, 96 in.
- (f) Valve opening rate, 2-30 in<sup>2</sup>-sec<sup>-1</sup>.

##### 3.4.2 Geometrical Shape and Size

3.4.2.1 The effect of geometrical shape and size of accumulators on the pressure surges in a closed-end tube were studied by tests on the following accumulators:

- (a) Vickers Model No. AA-14307-A, 200 cu in., diaphragm type (Par. 3.2.2).
- (b) Vickers Model No. AA-14305-A, 60 cu in., diaphragm type.
- (c) Bendix Model No. 405554, 200 cu in., diaphragm type.
- (d) Bendix Model No. 405525, 60 cu in., diaphragm type.
- (e) Bendix Model No. 409201, 60 cu in., piston type, 2 in. diam piston.
- (f) Contractor part No. 161-58095, 200 cu in., piston type, 5-1/2 in. diam piston.

- (g) Contractor part No. 161-58042, .60 cu in., piston type, 3 in. diam piston.

3.4.2.2 Results of the tests indicated that the variations in the geometrical shape and size of the accumulators tested produced no significant effects on the magnitude of the surge peak (Fig. 58), on the logarithmic decrement of the underdamped oscillatory wave (Fig. 59), or on the frequency of the fundamental pressure wave (Fig. 60). This was in agreement with the electrical analog theory developed in Appendix I, which indicated that the effect of accumulator capacitance, inductance, and resistance was comparatively small in the majority of cases.

3.4.2.3 Since the variations in the data shown in Fig. 58, 59, and 60 were considered to be within the general limits of experimental accuracy, there was no practical significance in attempting to differentiate and evaluate the effects of the accumulator parameters.

### 3.4.3 Precharge Air Pressure

3.4.3.1 The effect of accumulator precharge air pressure on the pressure surges in a closed-end tube was studied by comparison of the resulting surges for 600, 800, and 1200 psi precharges with data obtained in Par. 3.2.2 on a Vickers accumulator (Model No. AA-14307-A).

3.4.3.2 Test results indicated that accumulator precharge air pressure had no significant effect on the magnitude of the pressure surge (Fig. 61), on the logarithmic decrement of the underdamped oscillatory pressure wave, or on the frequency of the fundamental wave.

### 3.4.4 Piston Mass

3.4.4.1 Various weights were added to the piston of an accumulator (Contractor part No. 161-58095) to determine the effect of piston mass on the pressure surges in a closed-end tube. These weights were added on the oil side of the piston and the accumulator was precharged to 1430 psi air pressure. This precharge was such that the air volume in the accumulator under 3000 psi oil pressure was the same as that of the basic accumulator when precharged to 1000 psi and then charged to 3000 psi oil pressure.

3.4.4.2 The magnitude of the pressure surge was found to be independent of piston mass over the range tested (Fig. 62). Piston masses up to 8.6 times the original design mass were tested.

3.4.4.3 The logarithmic decrement of the underdamped oscillatory pressure wave increased slightly as the piston mass was increased (Fig. 63), but remained relatively constant over the range of valve opening rates. This effect was attributed to increased friction due to eccentric loading on the piston lands.

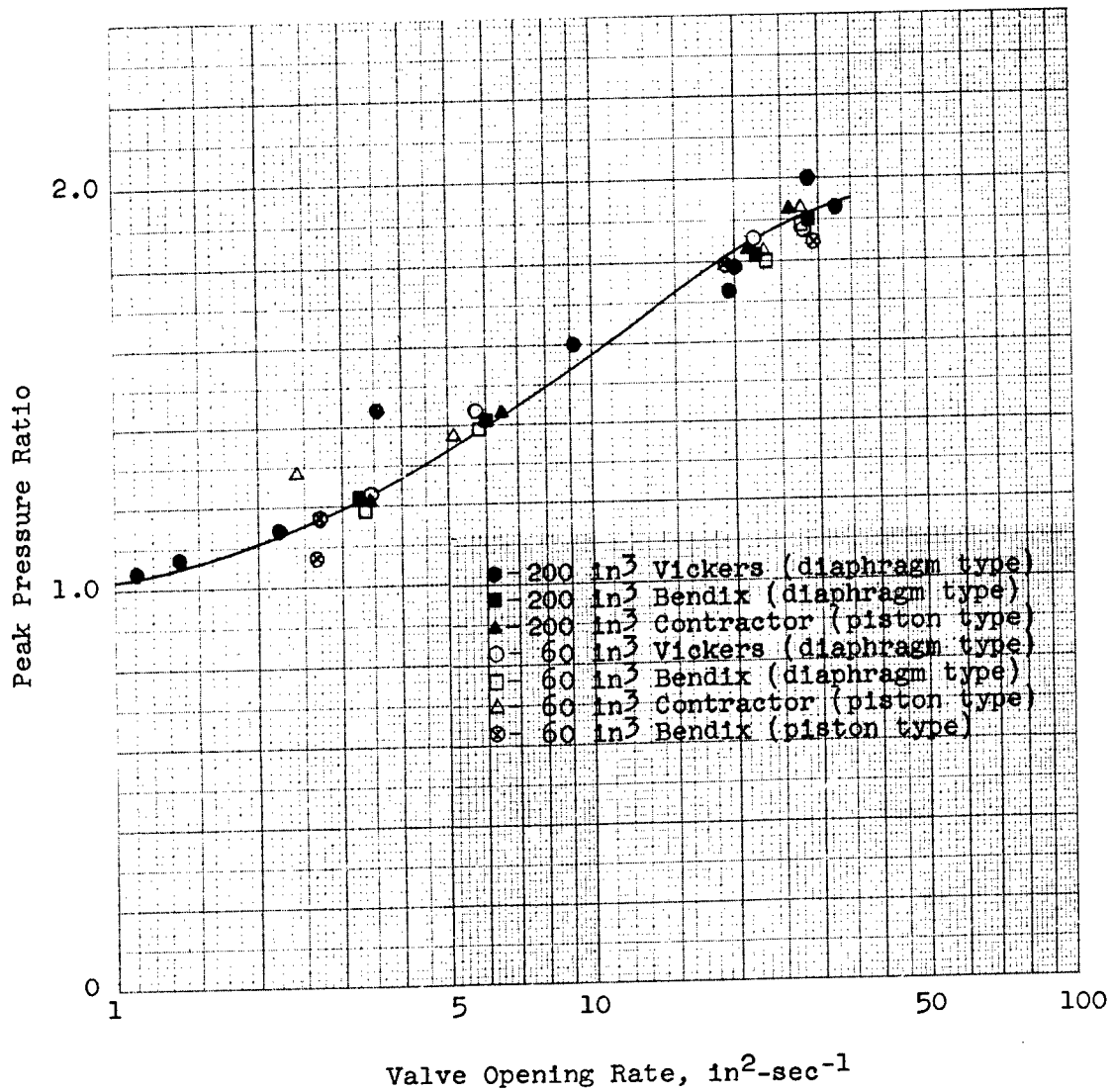
### 3.4.5 Temperature

3.4.5.1 Since it was possible that greater damping due to increased piston friction at low temperature might result in attenuation of the pressure surges, investigation was conducted on a piston type accumulator (Contractor part No. 161-58095) at various temperatures from 71 C (160 F) to -54 C (-65 F). These tests were made in conjunction with the tests described in Par. 3.2.8 which used a spherical diaphragm type accumulator (Vickers Model No. AA-14307-A).

3.4.5.2 Essentially no difference in the magnitude of the pressure surges, logarithmic decrement, or the frequency of the underdamped oscillatory wave was observed between the two different accumulators under identical test conditions. From this it was evident that the change in damping due to piston friction was small and that the relative effect of such damping was of no practical significance.

Figure 58

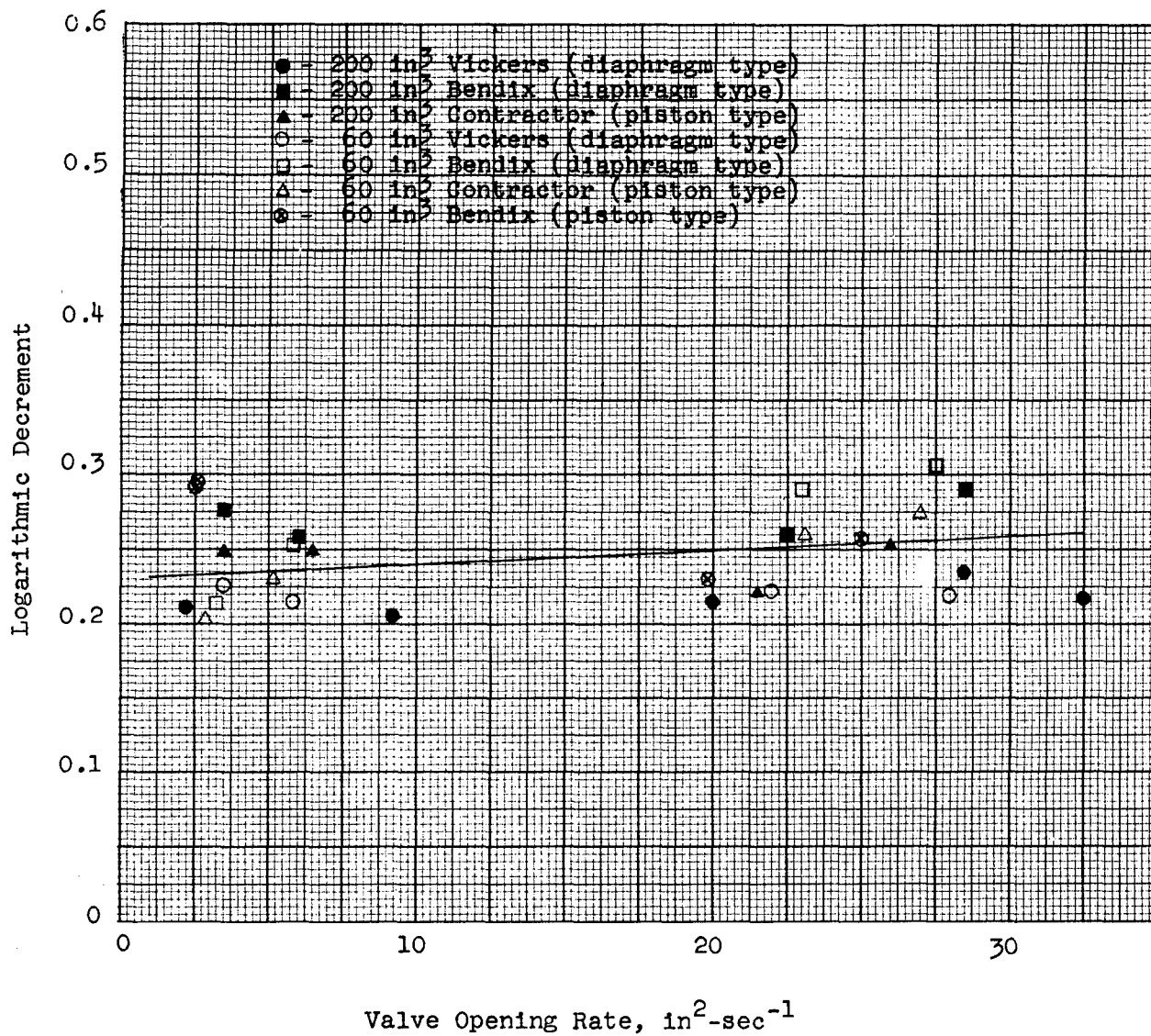
PEAK PRESSURE RATIO VS. VALVE OPENING RATE  
FOR VARIOUS TYPES OF ACCUMULATORS  
IN A CLOSED-END TUBE SYSTEM



Note: 96 in. test section length.

Figure 59

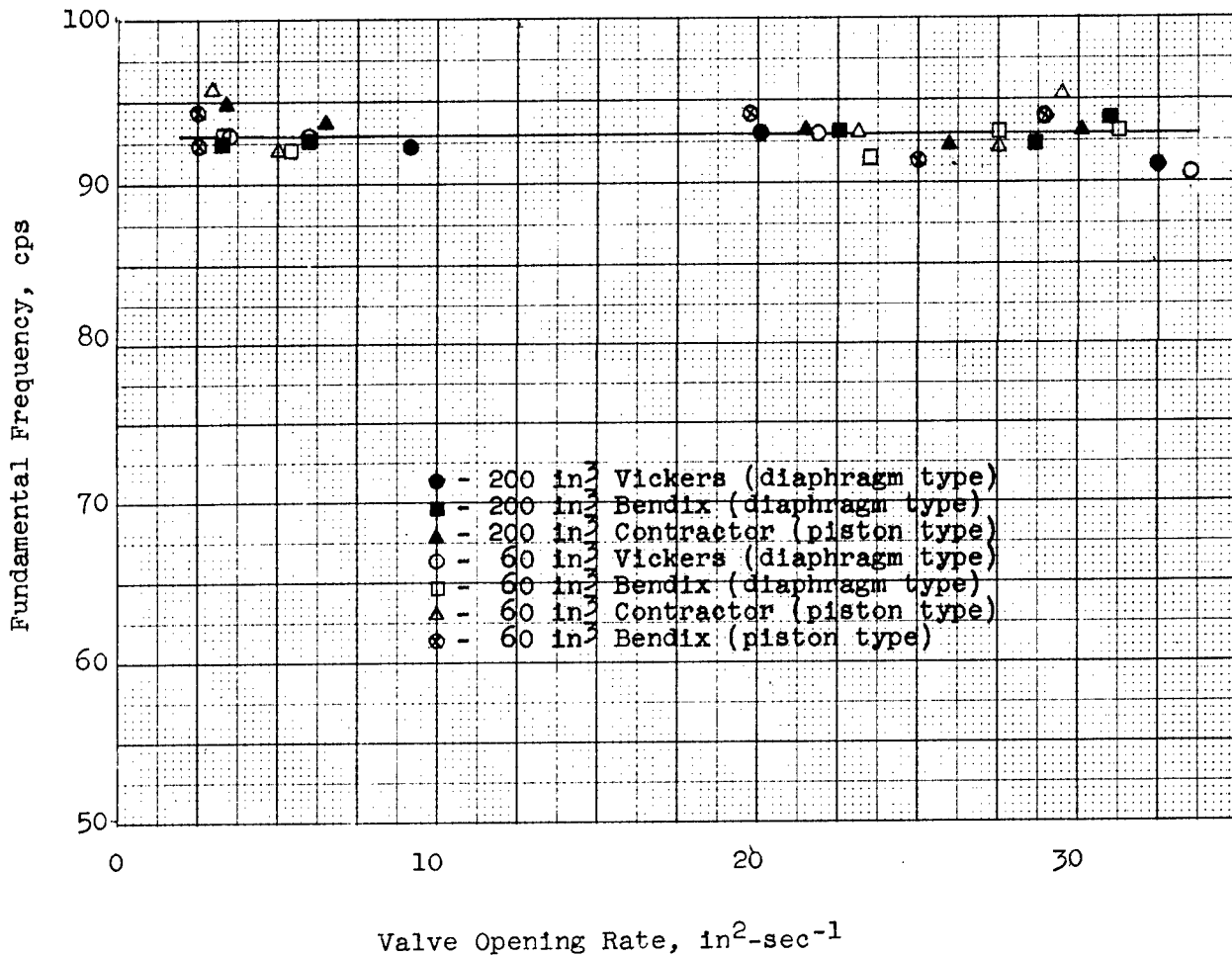
LOGARITHMIC DECREMENT VS. VALVE OPENING RATE  
FOR VARIOUS TYPES OF ACCUMULATORS  
IN A CLOSED-END TUBE SYSTEM



Notes: 96 in. test section length.  
Logarithmic decrement based on first two peaks of pressure oscillation.

Figure 60

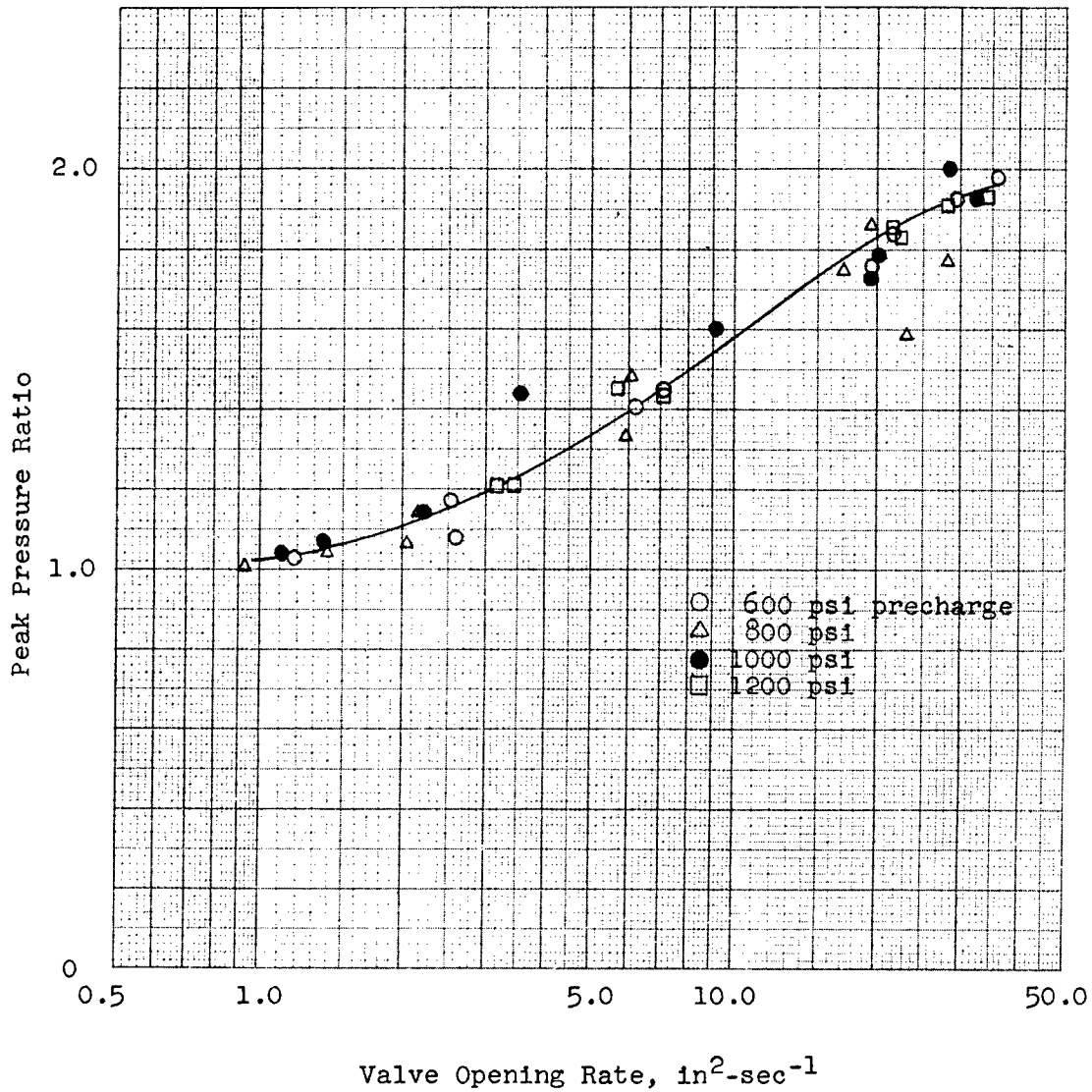
FREQUENCY OF THE FUNDAMENTAL PRESSURE WAVE VS. VALVE OPENING RATE  
 FOR VARIOUS TYPES OF ACCUMULATORS  
 IN A CLOSED-END TUBE SYSTEM



Note: 96 in. test section length

Figure 61

PEAK PRESSURE RATIO VS. VALVE OPENING RATE  
FOR VARIOUS ACCUMULATOR PRECHARGE AIR PRESSURES

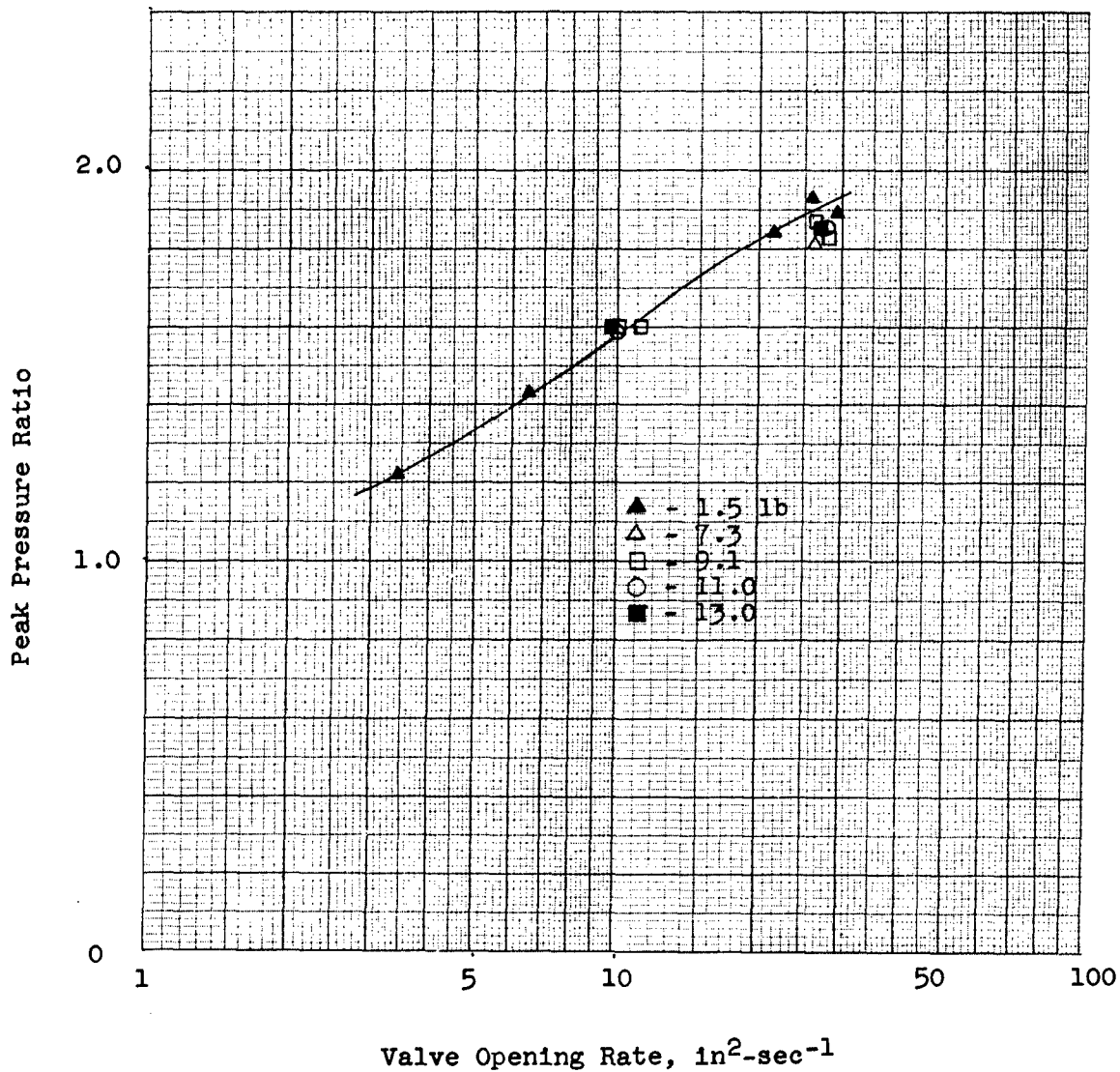


Note: 96 in. test section length.



Figure 62

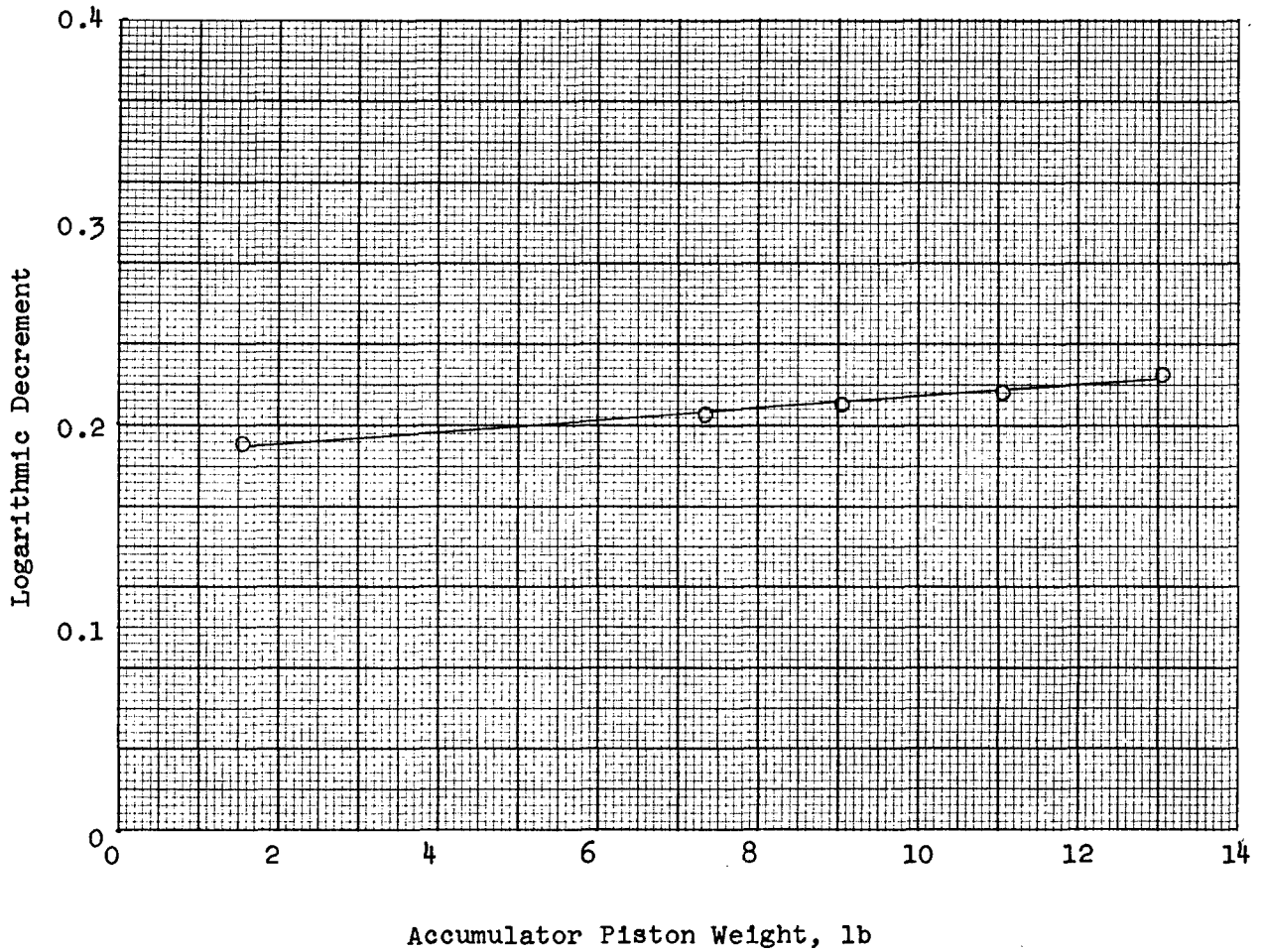
PEAK PRESSURE RATIO VS. VALVE OPENING RATE  
FOR VARIOUS ACCUMULATOR PISTON WEIGHTS



Note: 96 in. test section length.

Figure 63

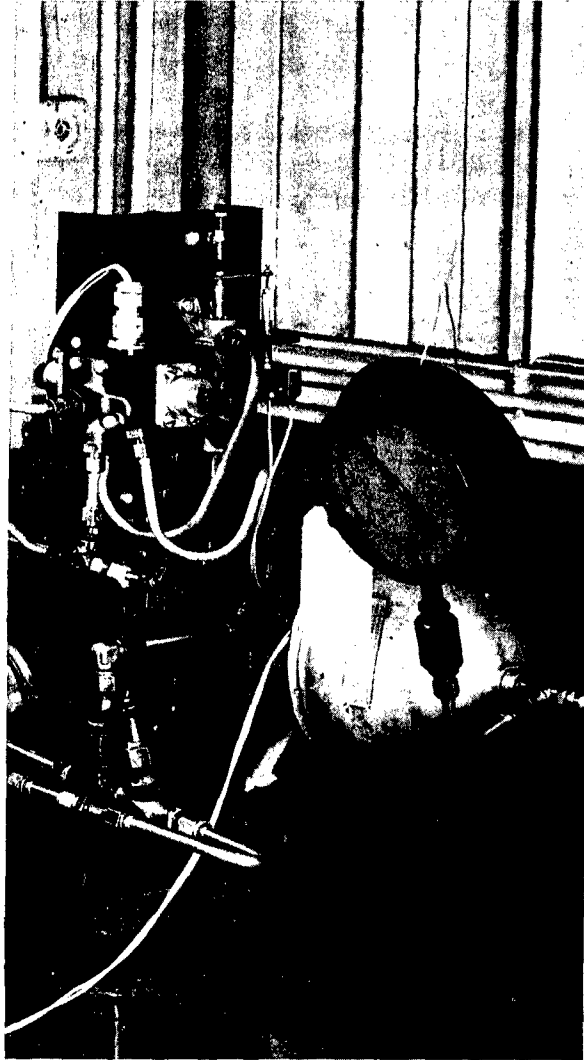
LOGARITHMIC DECREMENT VS. ACCUMULATOR PISTON WEIGHT  
ACCUMULATOR TESTS



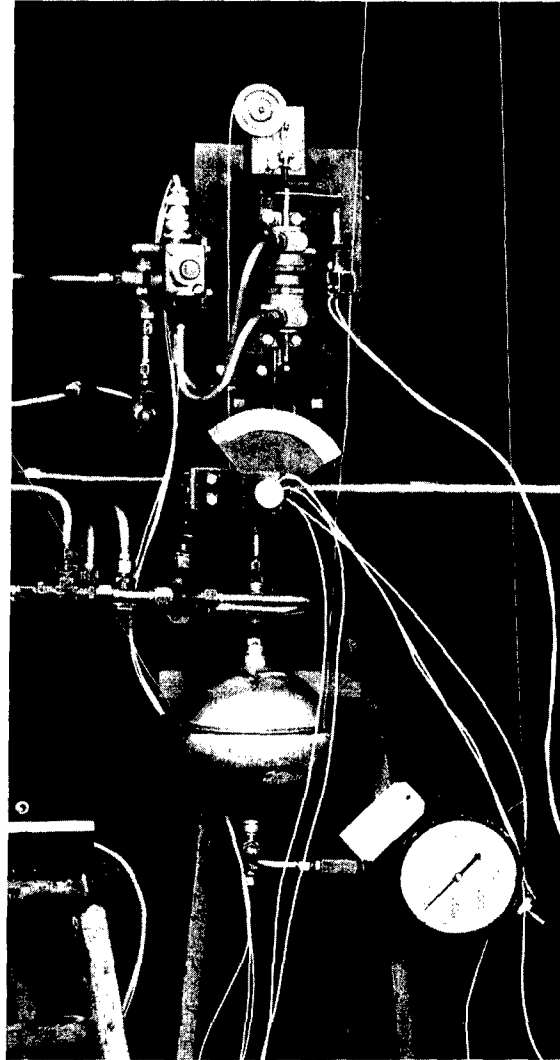
Notes: 96 in. test section length.  
Logarithmic decrement based on first two peaks of pressure oscillation.

Figure 64

MODIFICATIONS IN BASIC TEST APPARATUS TO ACCOMODATE TESTS  
ON DIFFERENT TYPES OF SELECTOR VALVES



Modification for Poppet Type  
Selector Valve  
(Adel part No. 18184-2)



Modification for Shear Seal Type  
Selector Valve  
(Saval part No. 4840-2)

### 3.5 Selector Valves

#### 3.5.1 General Notes

3.5.1.1 The effect of selector valve design was investigated by studying the pressure surges in a closed-end tube when valves of different types were opened in the same basic system configuration (Fig. 1). Specific test conditions which prevailed were as follows:

- (a) System pressure, 3000 psi.
- (b) Accumulator precharge air pressure, 1000 psi
- (c) Pump discharge flow rate, 1 gpm.
- (d) Fluid temperature,  $38 \pm 5$  C ( $100 \pm 9$  F).
- (e) Test section length, 96 in.

The valves tested were a poppet type (Adel part. No. 18184-2) and a shear seal type (Saval part No. 4840-2). These two valves were selected because of the wide difference in their geometry and operating characteristics. Provisions were made such that the valve opening rate could be varied.

3.5.1.2 The instrumentation and general test procedure were essentially the same as described in Par. 3.2.1. The pilot system selector valve was changed to a solenoid operated valve for convenience of operation only.

#### 3.5.2 Adel Valve

3.5.2.1 The Adel valve described in Par. 3.5.1 was modified and mounted on the basic test jig such that the poppet could be externally operated by the basic pilot system actuating cylinder (Fig. 64). With this configuration the valve opening rate could be varied as desired from a maximum rate of  $18 \text{ in}^2 \text{ sec}^{-1}$ . The pressure drop-flow-displacement characteristics were determined for steady-state flow conditions and are shown in Fig. 65. From the valve geometry and actual dimensions, calculation of the area vs. displacement relationship was made. This relationship is also shown in Fig. 65. Valve opening rates were determined from the velocity of the pilot system actuating cylinder piston and the average slope of the area vs. displacement curve.

3.5.2.2 The peak pressure ratio was found to decrease with decreasing valve opening rate in approximately the same manner as was observed on the basic test valve (Fig. 67). Studies of the logarithmic decrement indicated that the damping effective during the oscillatory wave (i.e., following the initial peak) was higher with the Adel valve installed than was observed on the Denison valve. This was attributed to the smaller maximum port area of the Adel valve. With this higher damping it might be expected that slightly lower peak pressure ratios would occur with the Adel valve, but this was not indicated from the test results. From this it was apparent that the relative effect of the valve resistance on the total system damping during the initial pressure rise was of primary importance in valve comparison. The need for further investigation to establish a method for evaluating the effect of valve resistance (which is non-linear in characteristic) on the initial pressure rise was evidenced by this analysis.

3.5.2.3 The average logarithmic decrement based on the first two peaks of the underdamped oscillatory pressure wave was 0.4 for the tests conducted. The frequency of the oscillatory wave was in agreement with the frequency vs. system length curve shown in Fig. 20.

#### 3.5.3 Saval Valve

3.5.3.1 The Saval valve described in Par. 3.5.1 was mounted on the basic test jig such that the shaft on the valve plate could be operated by the basic pilot system actuating cylinder. Operation of the shaft was accomplished through the pulley-cable arrangement shown in Fig. 64. Angular displacement of the valve plate was indicated with a potentiometer type position transducer, the signal being recorded with an Aeroquip Hydrauliscope. The pressure drop-flow-angular displacement characteristics of the

Figure 65

PERTINENT DATA ON THE CHARACTERISTICS OF A POPPET TYPE  
SELECTOR VALVE (ADEL PART NO. 18184-2)

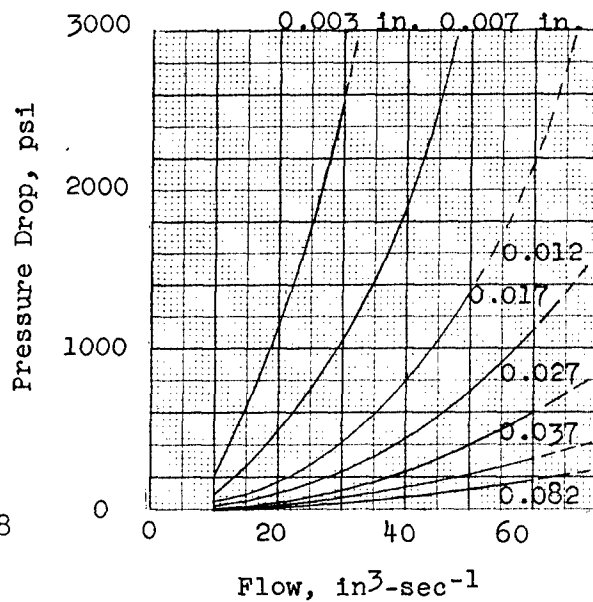
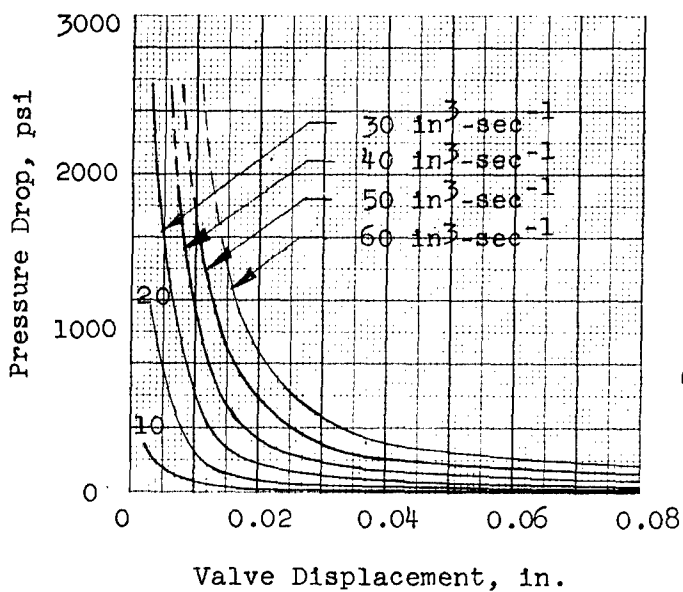
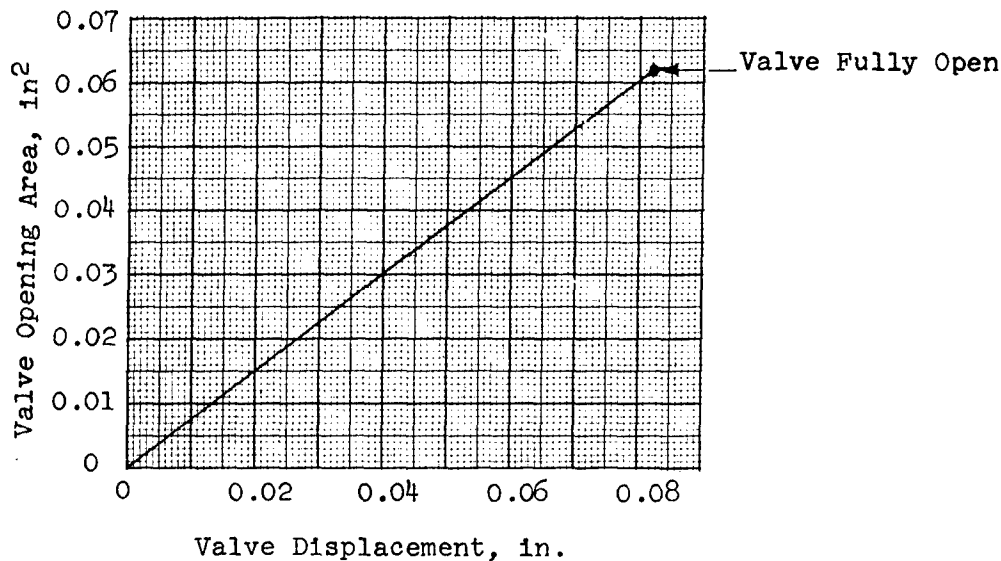


Figure 66

PERTINENT DATA ON CHARACTERISTICS OF A SHEAR SEAL TYPE  
SELECTOR VALVE (SAVAL PART NO. 4840-2)

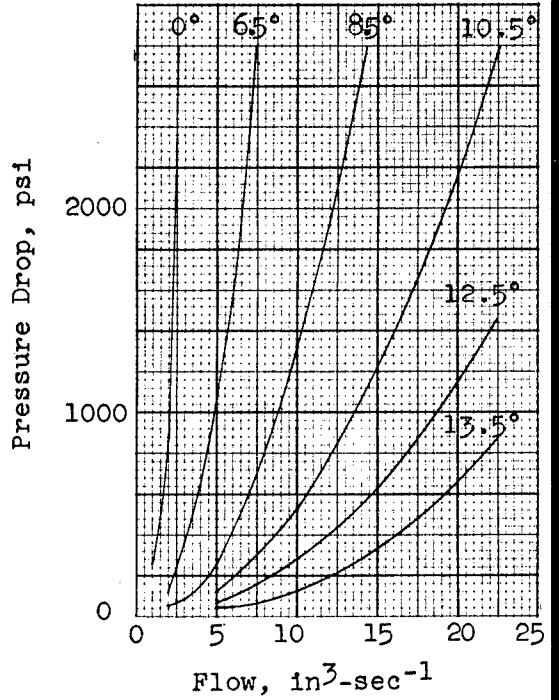
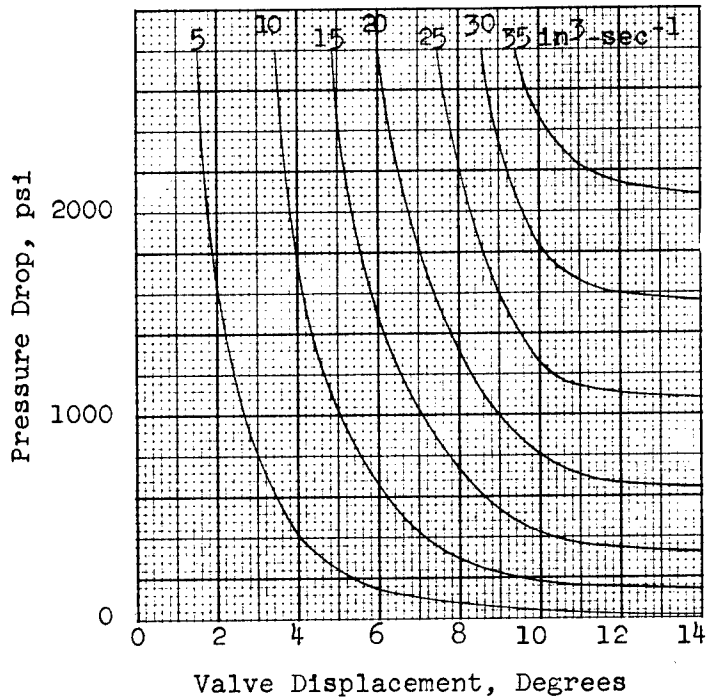
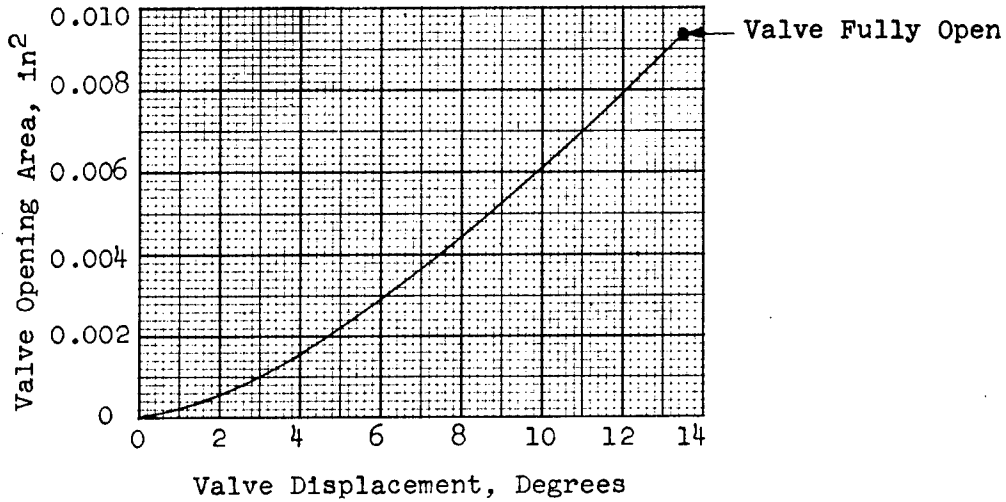
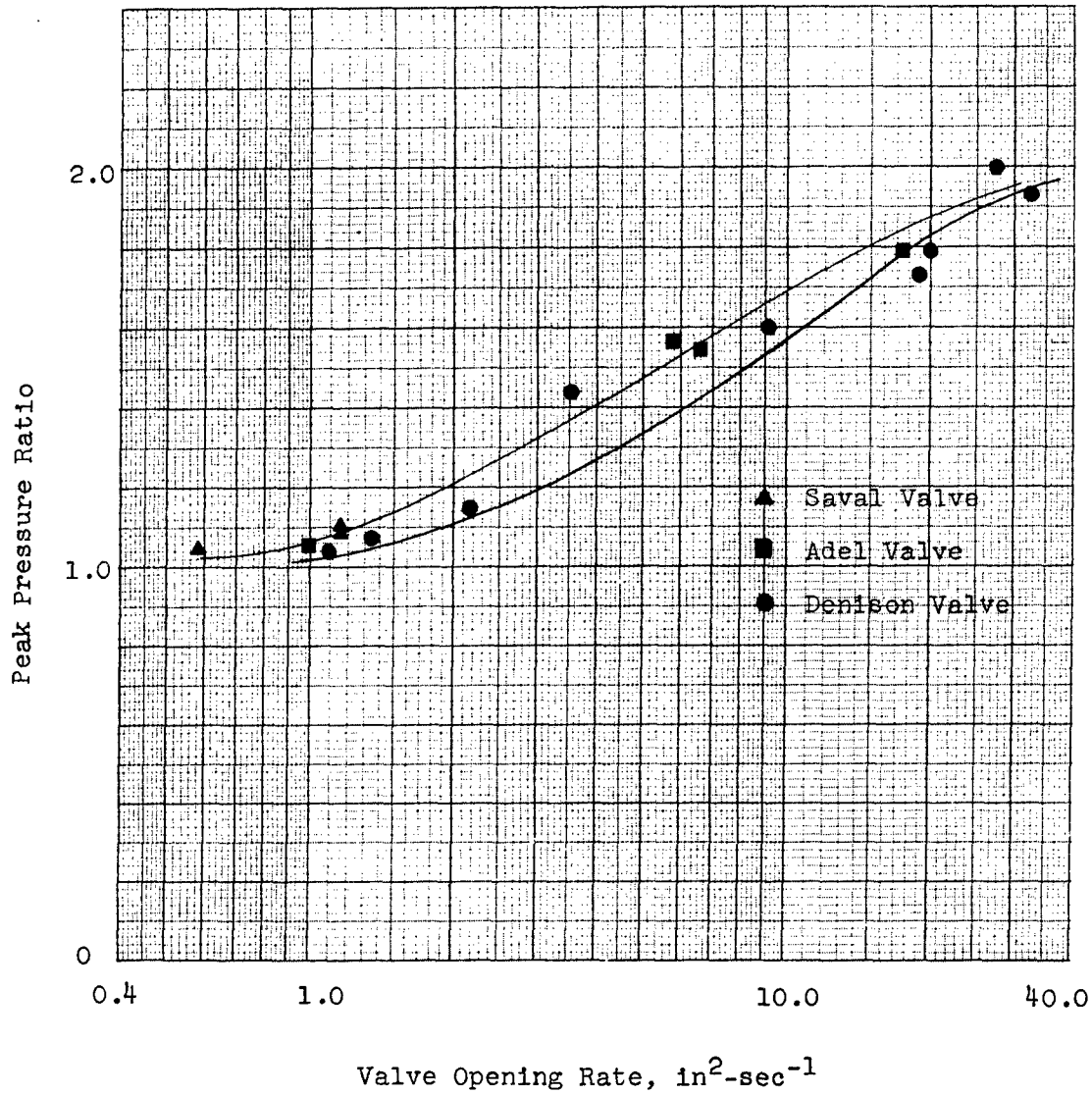


Figure 67

PEAK PRESSURE RATIO VS. VALVE OPENING RATE  
 FOR VARIOUS TYPES OF SELECTOR VALVES  
 IN THE SAME CLOSED-END TUBE SYSTEM



Note: 96 in. test section length.

valve were determined for steady state flow conditions and are shown in Fig. 66. From valve geometry and actual dimensions, the area vs. angular displacement relationship was calculated and this curve is shown on Fig. 66 also.

3.5.3.2 With the test configuration shown in Fig. 64, the angular velocity of the valve plate could be varied as desired from a maximum of 1250 deg per sec. However, due to the small orifice size (0.109 in. diam) in the valve plate, and the valve geometry, the valve opening rates were comparatively low, (0.6-1.2 in<sup>2</sup>-sec<sup>-1</sup>). Valve opening rates were determined from the angular displacement curve (Fig. 66).

3.5.3.3 The peak pressure ratio with the Saval valve in the system was found to be very low compared to those observed for the Denison and Adel valves tested (Fig. 67). This was attributed to the high damping of the small orifice in the Saval valve plate. Similar characteristics were observed in experimental investigation of orifices located near the energy source (Par. 3.2.6). From this, it was evident that even at high valve opening rates, the magnitude of the pressure surge could be controlled if the maximum port area was properly selected for the system configuration.

### 3.6 Pumps

#### 3.6.1 General Notes

3.6.1.1 The pressure surges studied in this part of the investigation were those which occurred when a valve was rapidly closed in the pressure line from a variable volume (or displacement) pump incorporating an unloader device. The basic hydraulic system used for these tests is shown schematically in Fig. 68. The Denison valve was hydraulically actuated as described in Par. 3.2.1.1. The instrumentation and method of recording data were as described in Par. 3.2.1.3. All tests were conducted with fluid at a temperature of  $38 \pm 5^\circ\text{C}$  ( $100 \pm 9^\circ\text{F}$ ).

3.6.1.2 The general procedure followed for a specific test run was as follows:

- (a) With the Denison valve open, the pump speed was adjusted to give the desired free flow discharge rate.
- (b) The pilot system was adjusted to give the desired Denison valve spool velocity.
- (c) The pilot system selector valve was operated at a uniform rapid rate and simultaneous records of pressure and spool position were taken as the Denison valve closed.
- (d) Records were made of the necessary reference traces.

3.6.1.3 The aircraft hydraulic pumps given consideration during these tests were:

- (a) Vickers Model No. AA32507L2, Ser. No. X273683, variable displacement type, unloaded through a compensator valve.
- (b) New York Air Brake part No. 67WA200, Ser. No. A-117, variable volume type, unloaded through a compensator valve.
- (c) Pesco part No. S-2324-B, Ser. No. PEEXD921, variable volume type, unloaded by shifting the primary gears to allow slippage of flow.

The pump performance characteristics were experimentally determined and are presented in Fig. 69.



Figure 68

SCHMATIC DIAGRAM OF BASIC HYDRAULIC SYSTEM  
 FOR INVESTIGATION OF PRESSURE SURGES IN DISCHARGE LINE  
 FROM A VARIABLE VOLUME (OR DISPLACEMENT) PUMP  
 RAPIDLY CLOSING VALVE

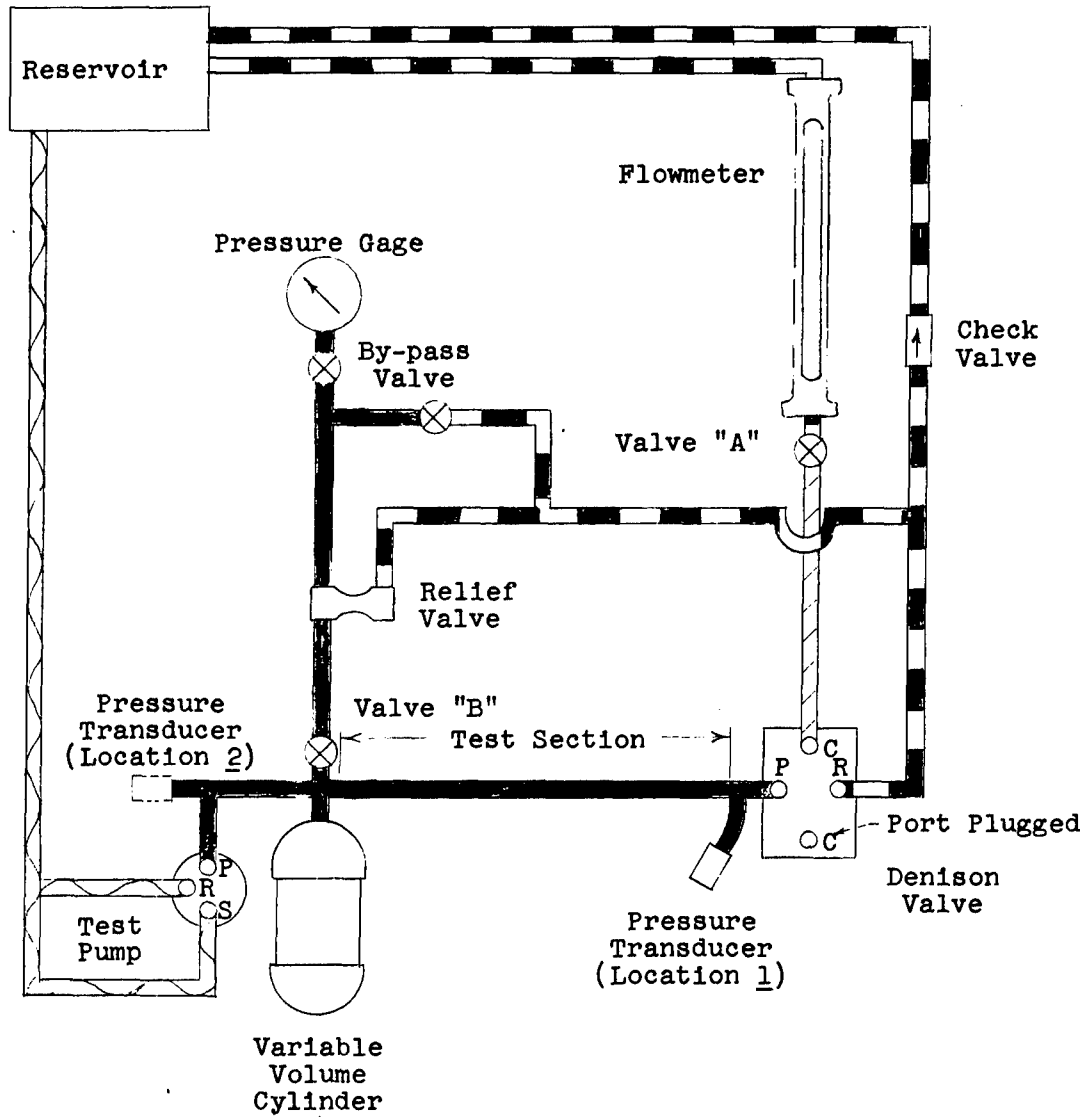


Figure 69

PERFORMANCE CHARACTERISTICS OF THE VARIABLE VOLUME (OR DISPLACEMENT) PUMPS INVESTIGATED

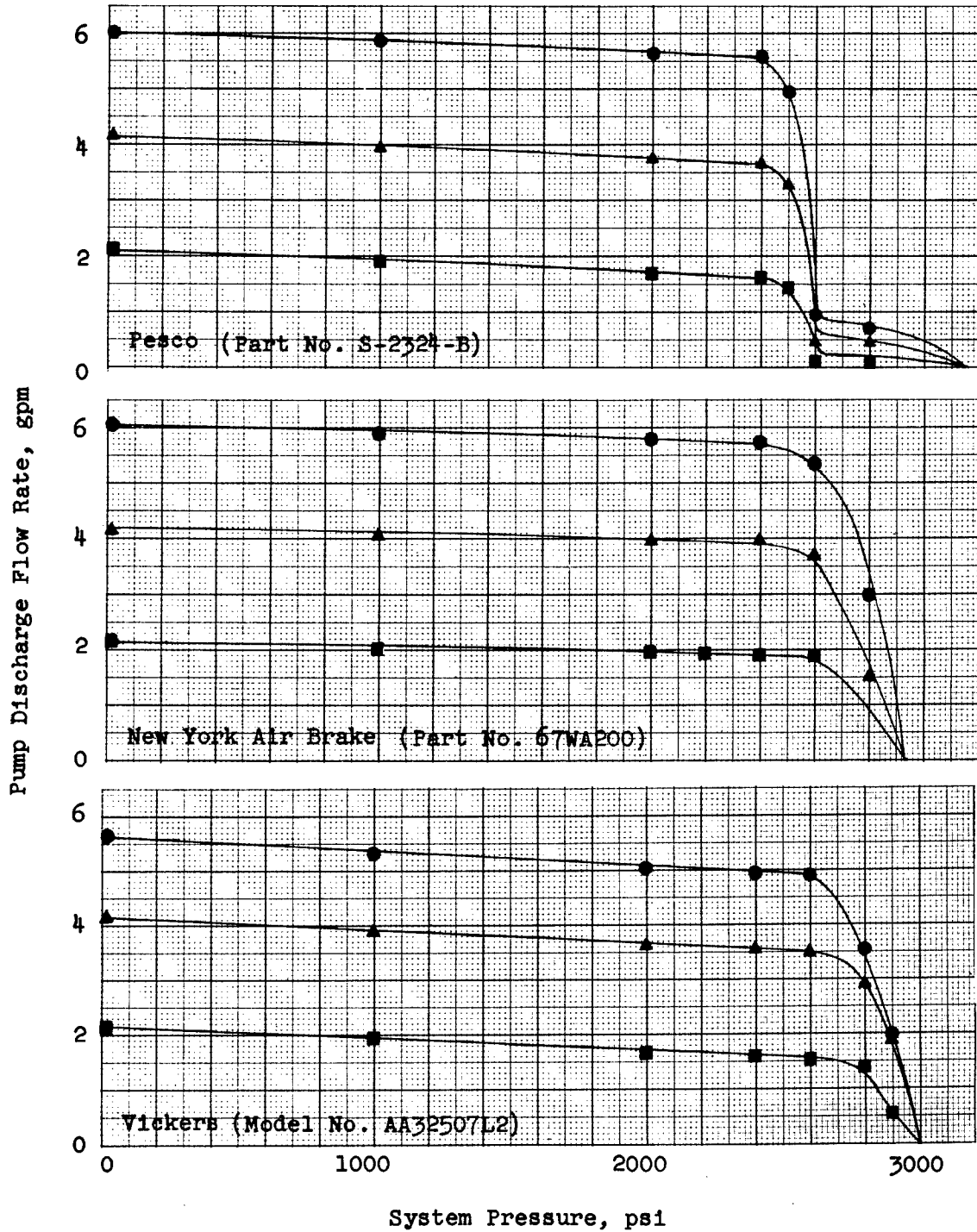
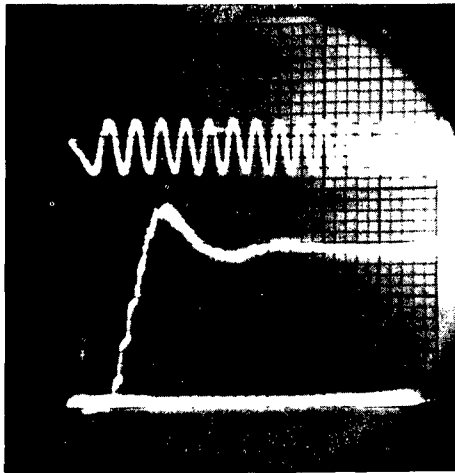
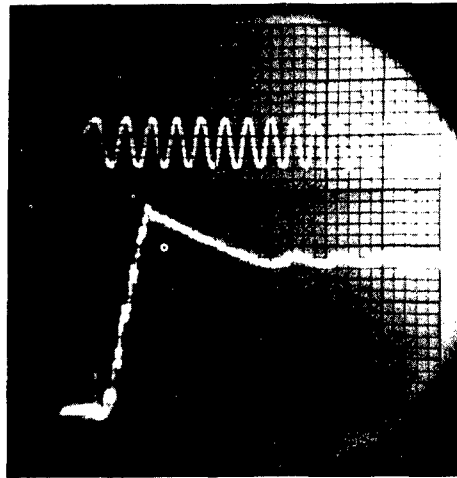


Figure 70

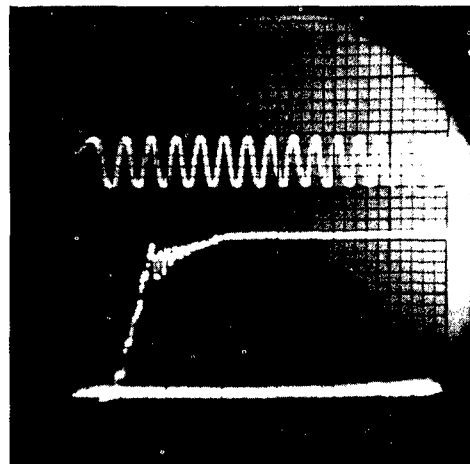
TYPICAL PRESSURE WAVEFORMS RESULTING FROM  
RAPID VALVE CLOSURE IN THE DISCHARGE LINES  
OF VARIOUS TYPES OF VARIABLE VOLUME (OR DISPLACEMENT) PUMPS

New York Air Brake  
Variable Volume Pump  
(Part No. 67WA200)



Vickers  
Variable Displacement Pump  
(Model No. AA-32507L2)

Pesco  
Variable Volume Pump  
(Part No. S-2324-B)



3.6.1.4 In preliminary work, test results indicated that the response characteristics of the system relief valve and the relief valve setting were affecting the pressure characteristics in the pump discharge line. To facilitate theoretical analysis, it was considered advisable to isolate the relief valve by closing valve B, Fig. 68, prior to each test run.

### 3.6.2 Valve Closing Rate

3.6.2.1 The effect of valve closing rate was investigated by studying the pressure waveform in the pump discharge line of the Vickers pump under the following conditions.

- (a) System pressure, 3000 psi (pump unloaded).
- (b) Pump discharge flow rate, 4 gpm (free flow).
- (c) Valve closing rate, 1-30 in<sup>2</sup>-sec<sup>-1</sup>.
- (d) Test section length, 48 in.
- (e) Variable volume cylinder, removed from system.
- (f) Pressure transducer at location 1 (Fig. 68).

Random tests were also conducted on the New York Air Brake and Pesco pumps.

3.6.2.2 The general characteristics of the pressure waveforms resulting when the selector valve was closed are shown in Fig. 70. With the Vickers or New York Air Brake pump installed in the system the waveforms were characterized by a rise to a peak pressure followed by a more gradual decline to the pump unloading pressure. There was little evidence of an underdamped oscillatory pressure wave of the frequency observed in rapid opening valve tests on closed-end tubes of equivalent system length (Par. 3.2.5). Studies of the pressure waveforms and consideration of the operating principles of the pumps seemed to indicate that these pressure surges were due to the response characteristics of the compensators built into the pumps. With the Pesco pump installed in the system, the pressure waveform was characterized by a rise to an intermediate pressure level followed by an underdamped oscillatory wave superimposed on a more gradual rise to the pump unloading pressure. The magnitude of this intermediate pressure was due to the performance characteristics of the Pesco pump (Fig. 69).

3.6.2.3 The peak pressure ratio of the Vickers pump decreased slightly with slower valve closing rates (Fig. 71). The relative effect of valve closing rate on the peak pressure ratios of the New York Air Brake and Pesco pumps was no greater than shown for the Vickers pump.

### 3.6.3 Initial Test Section Pressure

3.6.3.1 The effect of initial test section pressure on the pressure waveform was studied on each of the three pumps under the following conditions:

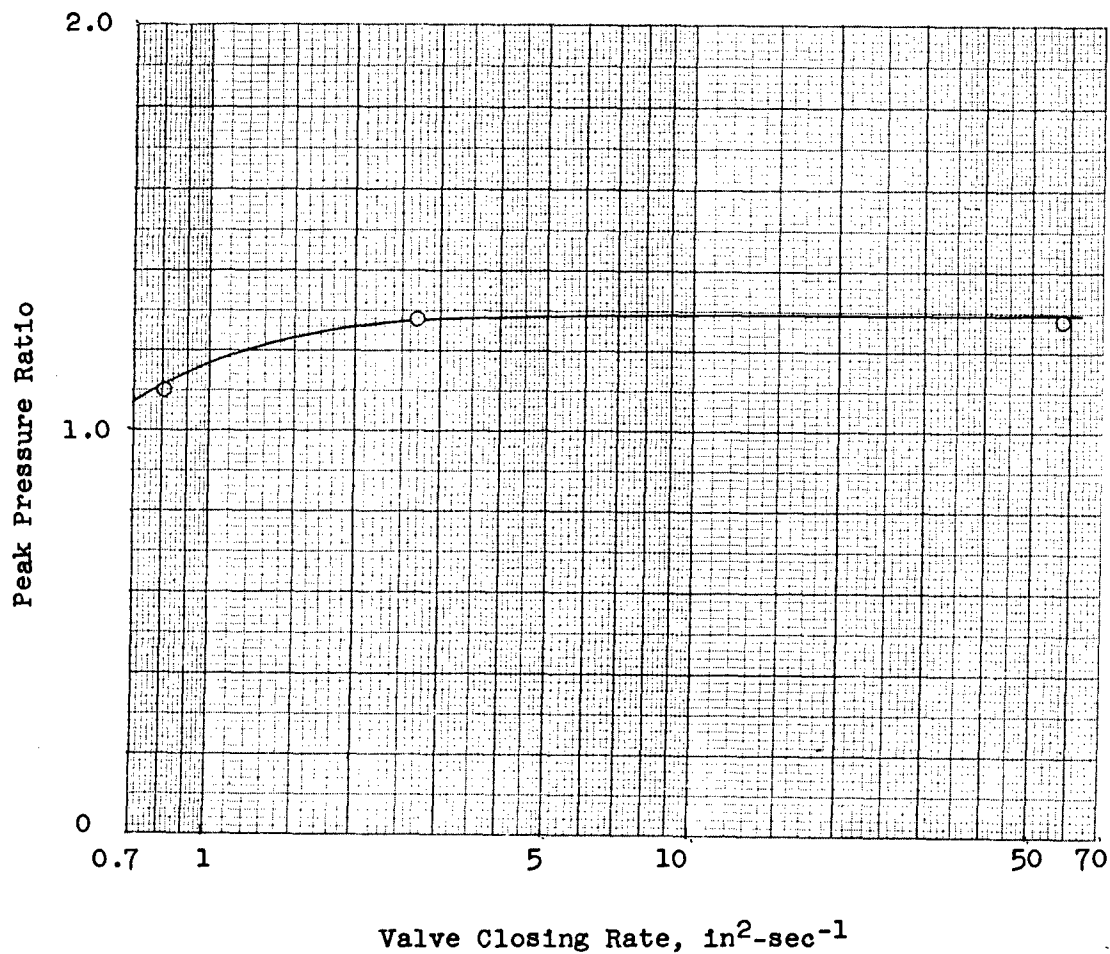
- (a) Initial test section pressure, 0 - 2200 psi.
- (b) System pressure, 3000 psi (pump unloaded).
- (c) Pump discharge flow rate, 4 gpm (free flow).
- (d) Valve closing time, 28 ± 2 in<sup>2</sup>-sec<sup>-1</sup>.
- (e) Test section length, 48 in.
- (f) Variable volume cylinder, removed from system.
- (g) Pressure transducer at Location 1 (Fig. 68).

Initial pressure in the pump discharge line was obtained by throttling the flow at valve A, Fig. 68.

3.6.3.2 Results of the tests (Fig. 72) indicated that the magnitude of the pressure surge was independent of the initial pressure in the pump discharge line, even though this pressure was as much as 70 percent of pump unloaded pressure (3000 psi).

Figure 71

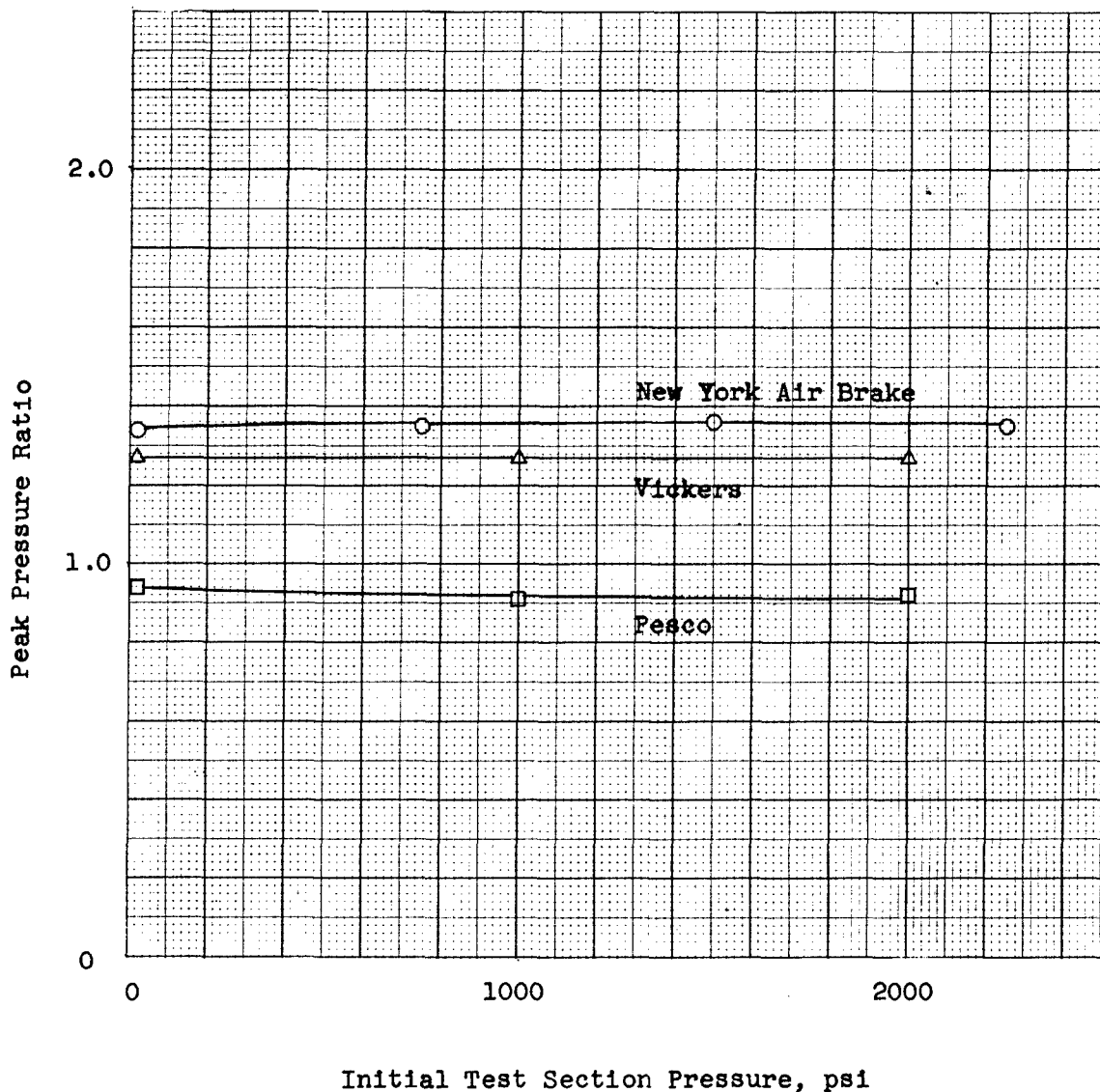
PEAK PRESSURE RATIO VS. VALVE CLOSING RATE  
 FOR A VARIABLE DISPLACEMENT PUMP  
 (VICKERS MODEL NO. AA-32507L2)



Note: 96 in. test section length.

Figure 72

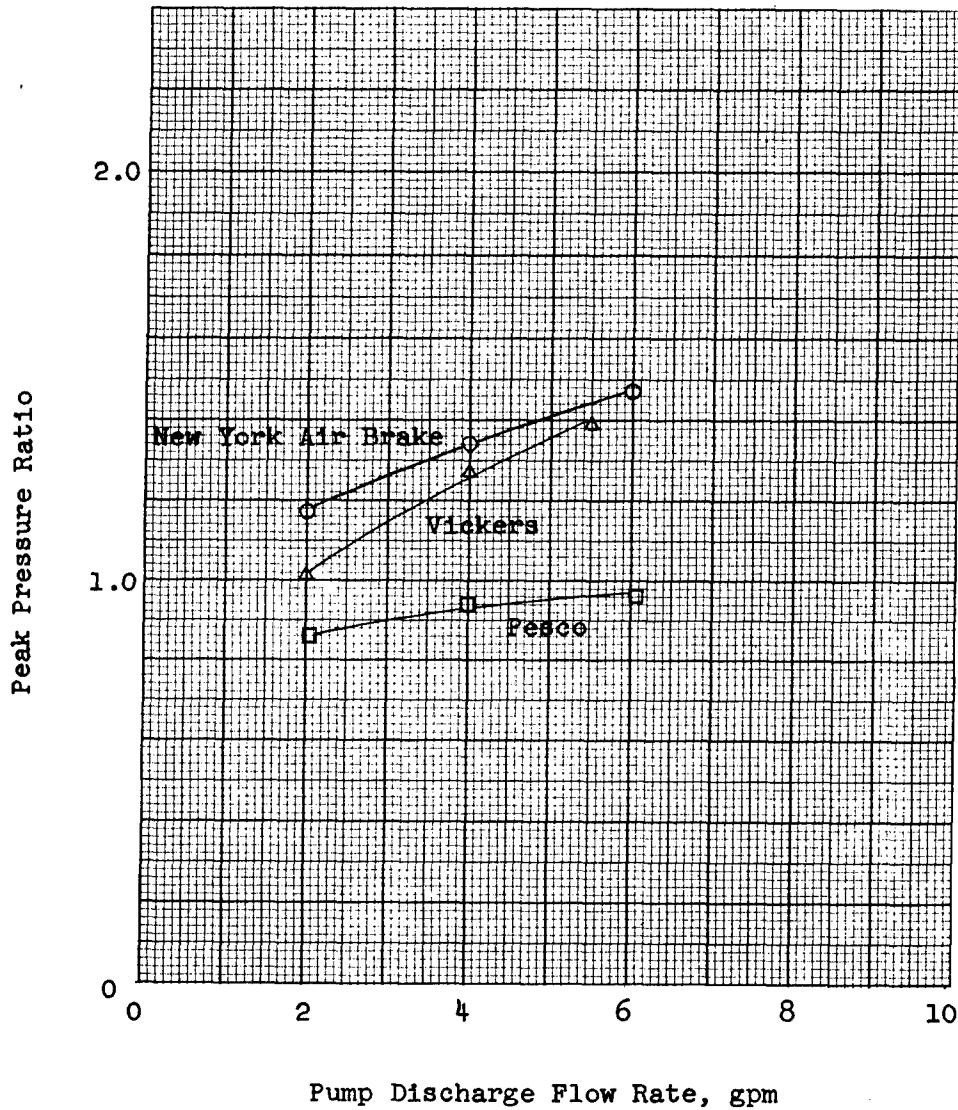
PEAK PRESSURE RATIO VS. INITIAL TEST SECTION PRESSURE  
FOR RAPID CLOSING VALVE  
VARIABLE VOLUME (OR DISPLACEMENT) PUMP TEST



Note: 96 in. test section length.

Figure 73

PEAK PRESSURE RATIO VS. PUMP DISCHARGE FLOW RATE  
 FOR RAPID CLOSING VALVE  
 VARIABLE VOLUME (OR DISPLACEMENT) PUMP TESTS



Note: 96 in. test section length.

3.6.4 Pump Discharge Flow Rate

3.6.4.1 The effect of pump discharge flow rate on the pressure waveform was studied on each of the three pumps under the following conditions:

- (a) System pressure, 3000 psi (pump unloaded).
- (b) Pump discharge flow rate, 2, 4, and 6 gpm (free flow).
- (c) Valve closing rate,  $28 \pm 2 \text{ in}^2\text{-sec}^{-1}$ .
- (d) Test section length, 48 in.
- (e) Variable volume cylinder, removed from system.
- (f) Pressure transducer at Location 1 (Fig. 68).

3.6.4.2 The magnitude of the pressure surge was found to increase almost proportionally with the pump discharge flow rate on all three pumps, the highest peaks being observed on the New York Air Brake pump (Fig. 73).

3.6.4.3 The relationship between the peak pressure ratio and rate of pressure rise for the three pumps tested is shown in Fig. 74. Differences in the curves were attributed to the relative effect that each pump had on the frequency response characteristics of the system.

3.6.5 System Length

3.6.5.1 With the New York Air Brake pump installed in the basic hydraulic system, the effect of system length was investigated by studying the resulting pressure waveforms under the following conditions:

- (a) System pressure, 3000 psi (pump unloaded).
- (b) Pump discharge flow rate, 4 gpm (free flow).
- (c) Valve closing rate,  $28 \pm 2 \text{ in}^2\text{-sec}^{-1}$ .
- (d) Test section length, 48 (Par. 3.6.2), 96, and 144 in.
- (e) Variable volume cylinder, removed from system.
- (f) Pressure transducer at Location 1 (Fig. 68).

3.6.5.2 The magnitude of the pressure surge decreased almost linearly with line length, as indicated by the following data:

<u>Test Section Length, in.</u>	<u>Peak Pressure Ratio</u>
48	1.35
96	1.31
144	1.28

3.6.6 System Volume

3.6.6.1 The effect of system volume was investigated by studying the pressure surge characteristics of each of the three pumps under the following conditions:

- (a) System pressure, 3000 psi (pump unloaded).
- (b) Pump discharge flow rate, 4 gpm (free flow).
- (c) Valve closing rate,  $28 \pm 2 \text{ in}^2\text{-sec}^{-1}$ .
- (d) Test section length, 48 in.
- (e) Nominal cylinder volume, 0, 90, and 180 in<sup>3</sup>.
- (f) Pressure transducer at Location 1 (Fig. 68).

The system volume was varied by means of the variable volume cylinder described in Par. 3.3.1.2. From data obtained in closed-end tube system tests (Par. 3.3.2.1), the system volumes and isothermal compressibilities of the configurations tested were interpolated (or extrapolated) to be as follows:

<u>Nominal Cylinder Volume, in<sup>3</sup></u>	<u>Total System Volume, in<sup>3</sup></u>	<u>Isothermal Compressibility, psi<sup>-1</sup></u>
0	13	$12.4 \times 10^{-6}$
90	99	$6.1 \times 10^{-6}$
180	188	$5.1 \times 10^{-6}$



Figure 74

PEAK PRESSURE RATIO VS. RATE OF INITIAL PRESSURE RISE  
 FOR RAPID CLOSING VALVE  
 VARIABLE VOLUME (OR DISPLACEMENT) PUMP TESTS

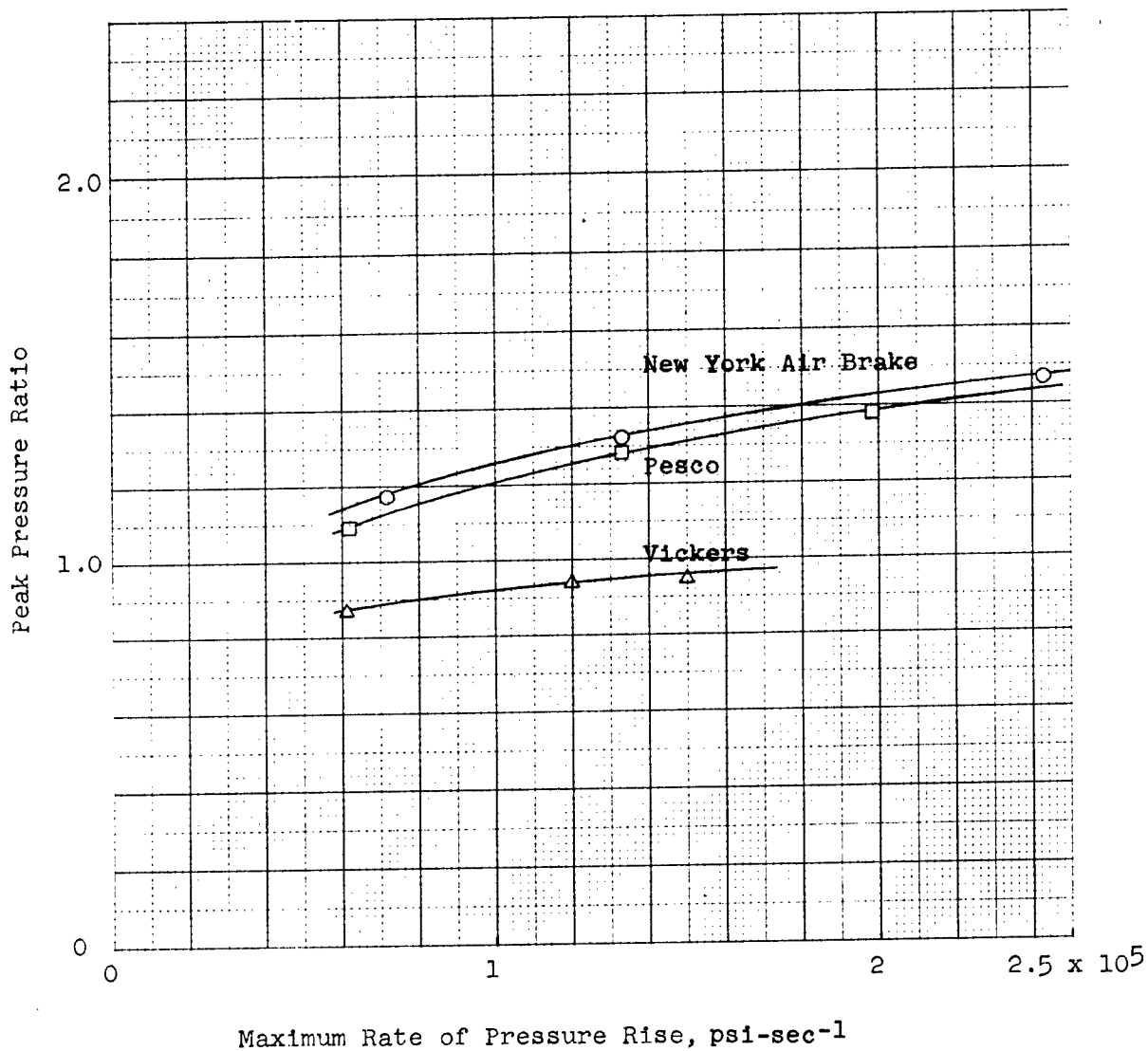


Figure 75

PEAK PRESSURE RATIO VS. SYSTEM VOLUME  
 (BOTTOMED CYLINDER CONFIGURATION)  
 FOR RAPID CLOSING VALVE  
 VARIABLE VOLUME (OR DISPLACEMENT) PUMP TESTS

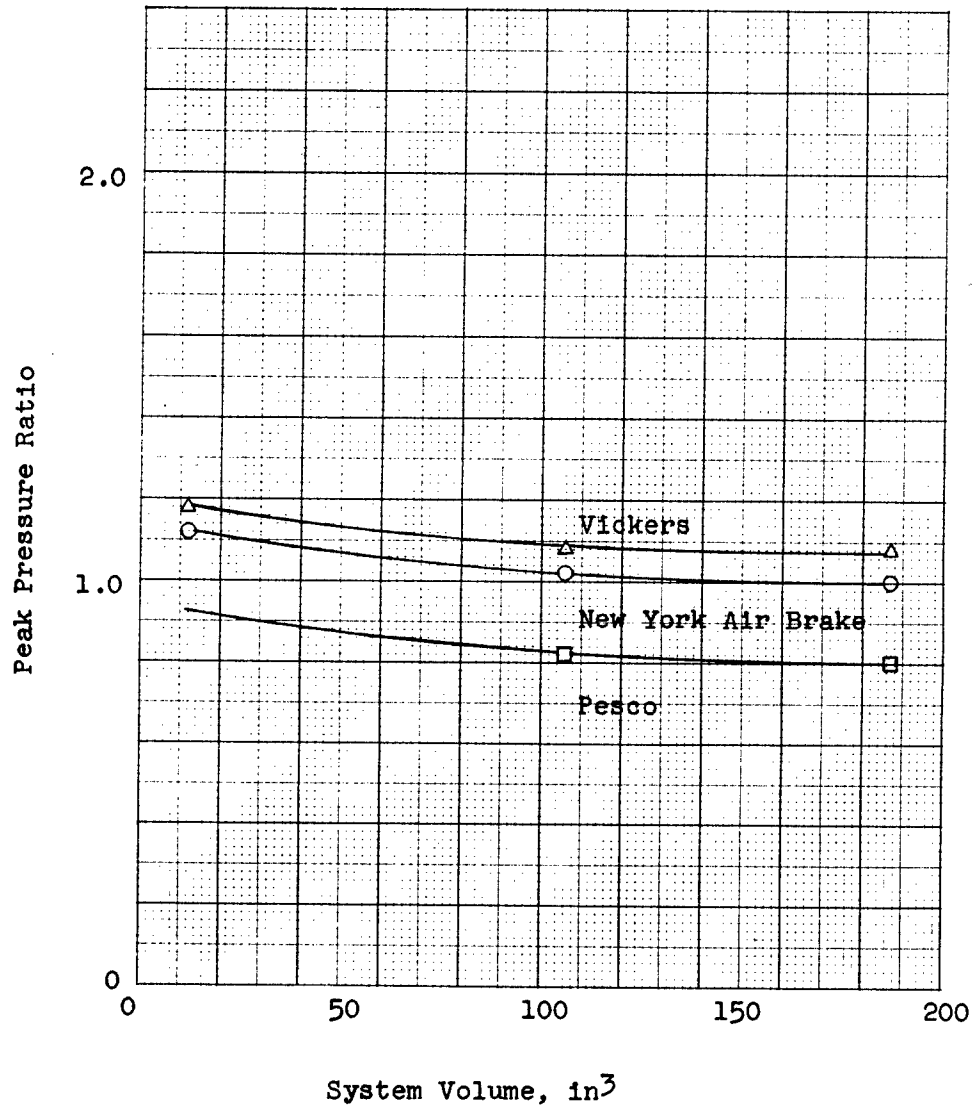
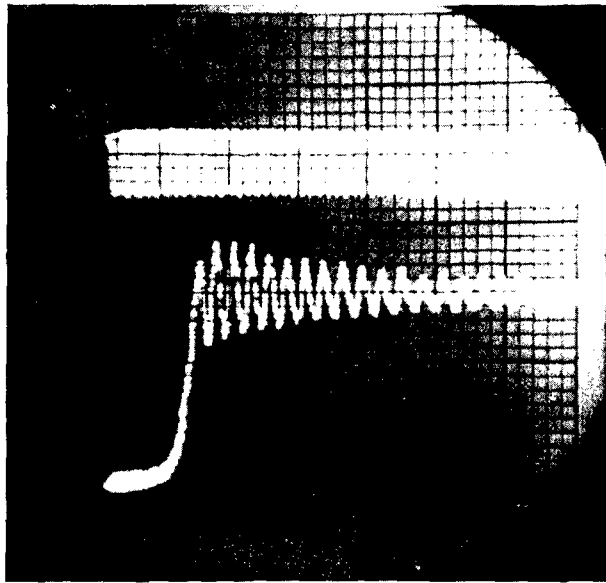
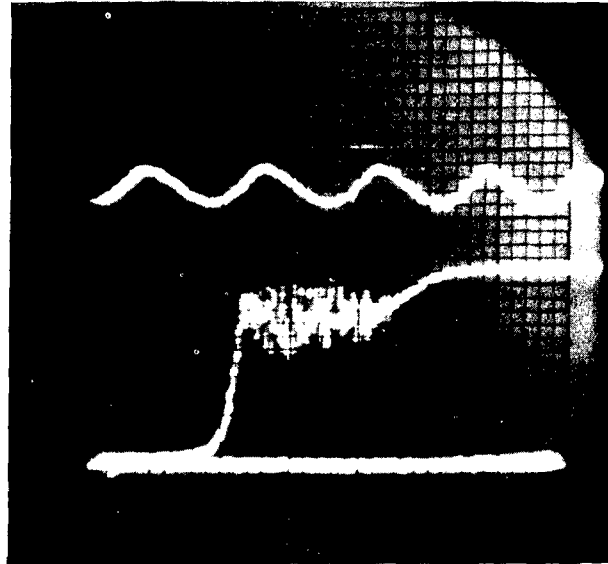


Figure 76

PRESSURE WAVEFORMS SHOWING UNSTABLE PERFORMANCE  
OF NEW YORK AIR BRAKE AND PESCO PUMPS  
DURING VERY SLOW VALVE CLOSURE



New York Air Brake Pump (Part No. 67WA200)



Pesco Pump (Part No. S-2324-B)

Note: Valve closing rate,  $0.2 \text{ in}^2/\text{sec}$ .  
Pump discharge flow rate, 6 gpm (free flow).

3.6.6.2 The magnitude of the pressure surge was found to decrease as the system volume was increased (Fig. 75). A comparison of the test results for the zero-volume cylinder configuration with data obtained on the same system configuration without the cylinder (Par. 3.6.2) indicated a considerably lower peak pressure ratio even though the difference in system volume was only 2.2 cu in. This was attributed to the difference in system compressibility ( $4.7 \times 10^{-6}$  psi<sup>-1</sup> without cylinder and  $12.4 \times 10^{-6}$  psi<sup>-1</sup> with zero-volume cylinder) which changed the response characteristics of the system.

3.6.7 Unstable Pump Performance

3.6.7.1 During the course of the pump tests, unstable performance of the New York Air Brake and Pesco pumps was experienced. At very slow valve closing rates, pressure oscillations (chattering) of varying magnitude and duration were observed (Fig. 76). To investigate the nature of these oscillations, tests were conducted to determine the flow conditions of the unstable performance and studies of the magnitude and frequency of the oscillations were made.

3.6.7.2 With the pump discharge flow rate set at the desired value under free flow conditions, the Denison selector valve (or valve A, Fig. 68) was slowly closed until unstable conditions occurred. The pump discharge flow rate was then measured and the waveform of the oscillations was photographed or observation of the total amplitude of oscillation was made. The basic hydraulic system shown in Fig. 68 was modified such that the combined flow from cylinder port A and the return port of the Denison valve was measured. During these tests, the pressure transducer was located near the pump discharge port (Location 2, Fig. 68) to minimize any attenuation effect of the line.

3.6.7.3 With the New York Air Brake pump set for a free flow discharge rate of 4 gpm and a 48 in. test section installed in the system, a series of tests were made at various conditions of unstable performance. This procedure was repeated with the pump set for a free flow discharge rate of 6 gpm. Results of the tests indicated that the characteristics of the pressure oscillation varied with the discharge conditions as shown in the following table:

Pump Discharge Flow Rate, gpm		Frequency of Oscillation (cps)	Total Amplitude of Oscillation (psi)	Mean Pressure (psi)
Free Flow	Unstable Performance			
4	0.22	--	200	3000
4	0.52	--	500	3050
4	0.60	26.7	1075	2650
4	1.04	--	1000	3000
4	1.41	--	1200	3000
4	1.99	--	0	3000
6	0.22	--	100	2950
6	1.21	--	1100	3050
6	2.22	--	1900	2950
6	2.5	28.9	1350	2625
6	4.2	--	0	3000

With other system configurations (i.e., 96 in. test section, 144 in. test section, or variable volume cylinder installed) the New York Air Brake pump was found stable. Typical oscillations during unstable performance are shown in Fig. 77.

Figure 77

PRESSURE OSCILLATIONS RESULTING FROM UNSTABLE PERFORMANCE  
OF NEW YORK AIR BRAKE PUMP (PART NO. 67WA200)  
UNDER CONSTANT SYSTEM LEAKAGE

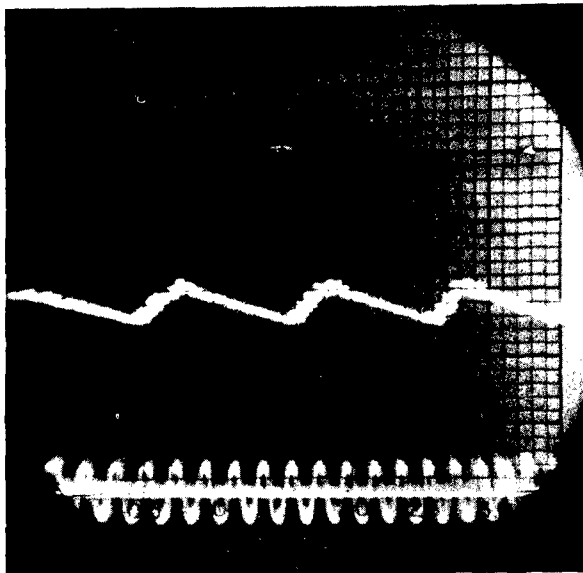
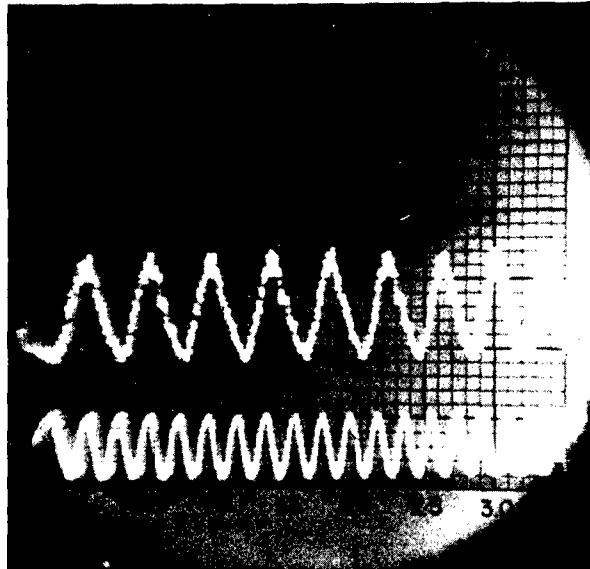
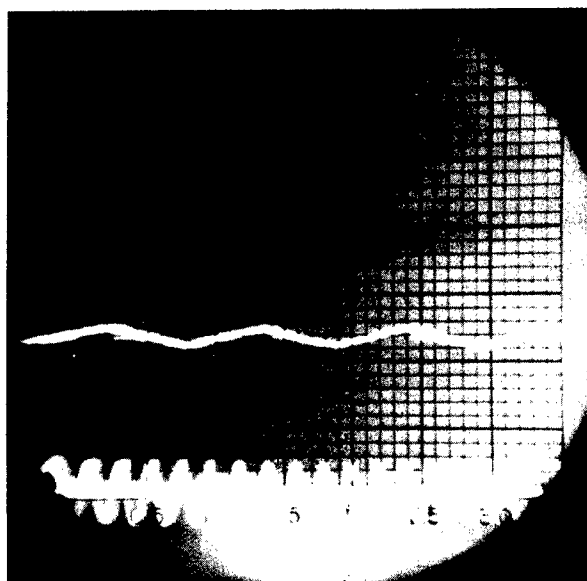
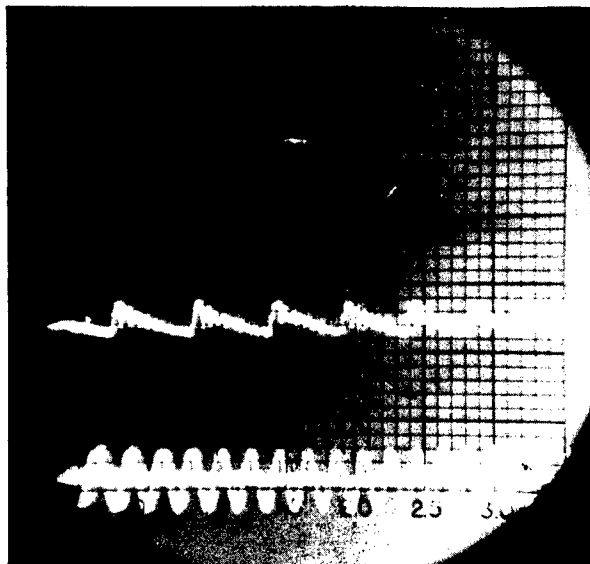


Figure 78

PRESSURE OSCILLATIONS RESULTING FROM UNSTABLE PERFORMANCE  
OF A PESCO PUMP (PART NO. S-2324-B)  
UNDER CONSTANT SYSTEM LEAKAGE



3.6.7.4 With the Pesco pump set for a free flow discharge rate of 4 gpm, a series of tests were made of unstable performance on various system configurations. The Pesco pump did not exhibit the wide range of flow conditions for unstable performance on a given system configuration that the New York Air Brake pump had shown, but the Pesco pump did give unstable performance on all of the system configurations tested. Results of the tests are given in the following table:

System Configuration	Pump Discharge Flow Rate, gpm		Frequency of Oscillation (cps)	Total Amplitude of Oscillation (psi)	Mean Pressure (psi)
	Free Flow	Unstable Performance			
48 in test section	4	0.615	--	400	2400
48 in test section	4	0.671	--	1000	2600
48 in test section	4	0.680	23.7	475	2400
0 in <sup>3</sup> cylinder	4	1.43 to 2.04	14.1	1000	2025
90 in <sup>3</sup> cylinder	4	2.12 to 2.3	12.8	500	2250
180 in <sup>3</sup> cylinder	4	1.73	11.4	250	2325

If it is assumed that the frequency of oscillation under unstable performance conditions is indicative of the frequency response of the system, the effect of system configuration can be seen by comparison of the test results. Typical oscillations during unstable performance are shown in Fig. 78.

3.6.7.5 The Vickers pump was stable for all system configurations and free flow discharge rates tested.

### 3.7 Energy Dissipating Devices

3.7.1 Although no actual experimental work was accomplished on this subject, one significant fact was obtained from another section of the investigation which is considered applicable to energy dissipating devices. From experimental work on orifices (Par. 3.6), it was found that the most effective location of a restriction was near the energy source. Therefore, if restrictors are used for energy dissipating devices, they should be located near the cylinder.

3.7.2 In regard to the use of dashpots as energy dissipating devices, the primary factors which have to be considered are the orifice closing rate and the frequency response characteristics of the system. The use of electric analogs should prove to be an effective means of analyzing the problem by representing the dashpot as a variable resistance in the same manner as a valve. In the case of dashpots, the problem of adequate representation of this variable resistance is one which will require further investigation.

## CHAPTER IV

## THE PRACTICAL SIGNIFICANCE OF PRESSURE SURGE

4.1 General

4.1.1 Pressure surges in aircraft hydraulic systems are primarily of importance because of the stress variations and possible accompanying fatigue damage they produce in system components. Cases have also been known in which component malfunction has occurred without necessarily causing physical damage to the component itself. For the purpose of evaluating the practical significance of these pressure surges, investigation has been made to determine their effect on various hydraulic system components. Information and data were obtained from two sources, namely:

- (a) A survey of existing information and data, portions of which were obtained through correspondence with various aircraft companies and hydraulic system component manufacturers and portions of which were obtained from published reports and literature.
- (b) Experimental investigation to supplement and augment the information and data obtained from the survey.

4.1.2 A lack of actual case histories of component malfunction due to pressure surges, without physical damage, was evidenced by the results of the survey. In general, malfunctions of this nature are rectified without recording specific details as to the case history. Since there was this lack of pertinent information, it was considered impractical to conduct investigations on hypothetical cases. For this reason, the investigation was directed toward the primary concern, i.e., the relationship of pressure surges to component fatigue.

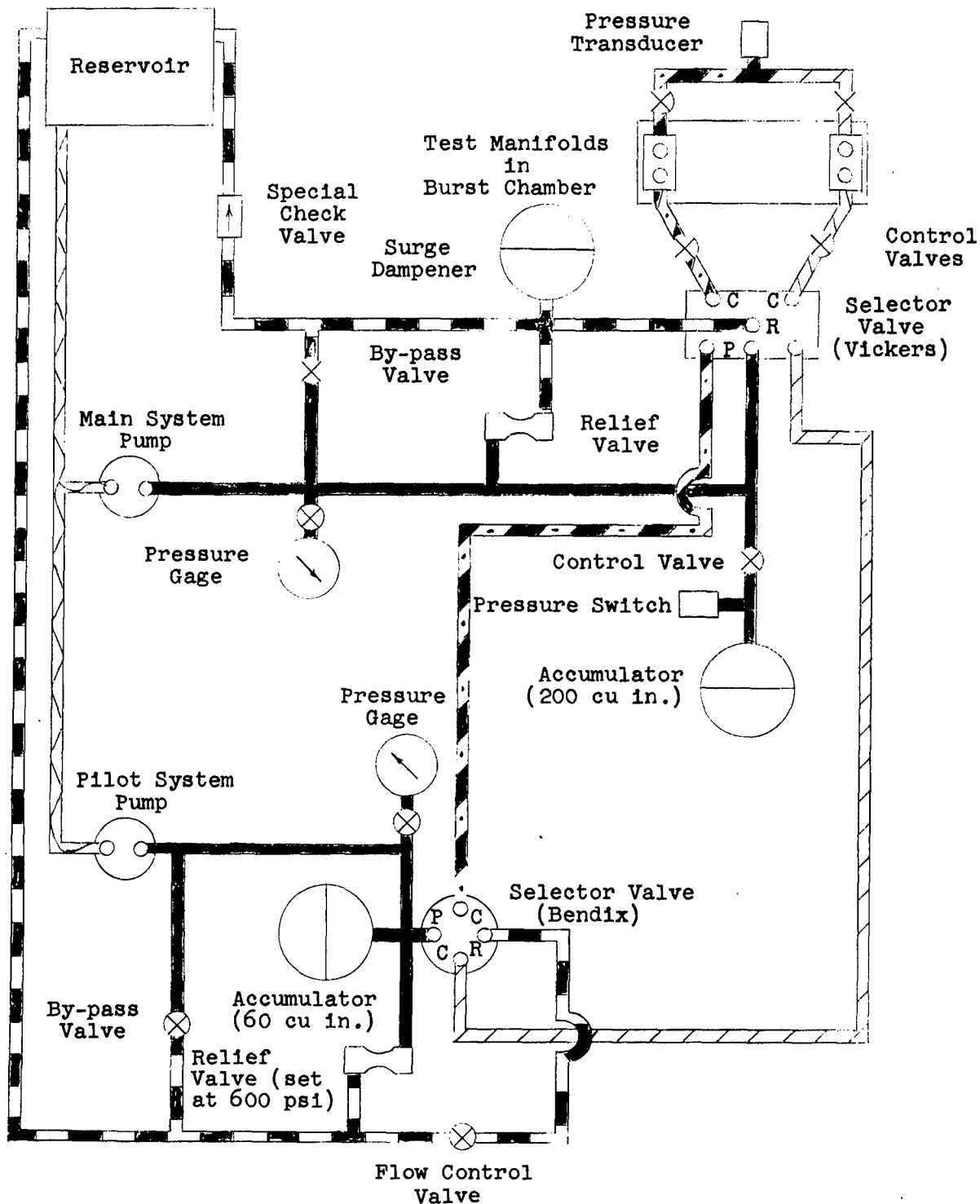
4.1.3 The general apparatus (Fig. 79) used in the experimental investigation was basically the same for all test work and is described as follows:

- (a) The main system selector valve was a closed-center slide type (Vickers No. C2-440) and was hydraulically operated by means of a pilot system. The pilot system selector valve was a closed-center poppet type (Bendix part No. 405883) and was mechanically operated by a controlled variable-speed cycling mechanism. The main system and pilot system pumps were of the fixed displacement type and were driven by a dual-spindle Varidrive unit. A special check valve designed to relieve at 30 psi pressure in the free flow direction was installed in the main system return line. The purpose of this check valve was to minimize secondary high-frequency oscillations of the type described in Par. 3.2.9. Pressure surges in the system return line were damped by means of a 200 cu in. spherical diaphragm accumulator which had a precharge air pressure of one atmosphere (14.7 psia).
- (b) The magnitude of the pressure surges in the test manifolds was controlled primarily by a throttling valve in the pressure line from the main system accumulator. Secondary control was provided by a flow control valve in the return line from the pilot system selector valve. When different peak characteristics were desired in each test manifold, throttling valves were installed between the test manifolds and the main system selector valve.
- (c) A pressure switch in the main system pressure line was connected to a control relay in such a manner that the relay would shut off the motors driving the pumps and the cycling mechanism if the system pressure dropped below a certain predetermined value (i.e., when failure of a component being tested occurred).



Figure 79

SCHMATIC DIAGRAM OF BASIC HYDRAULIC SYSTEM FOR FATIGUE TESTS OF HYDRAULIC SYSTEM COMPONENTS



- (d) The pressure characteristics in the test specimens were determined with an Aeroquip Hydrauliscope (Model No. 10000A) and its associated pressure transducer (Aeroquip part No. 10050). The total cycles of operation were indicated on a mechanical counter connected to the cycling mechanism on the pilot system selector valve.

All tests were conducted at room temperature and the fluid temperature did not exceed 49 C (120 F). The hydraulic fluid used in the system conformed to Spec. MIL-O-5606.

4.2 Tubing

4.2.1 From the survey of existing information and data, a considerable quantity of data were collected on various sizes of aluminum alloy and stainless steel tubing subjected to pressure impulses under a variety of test conditions, as is shown in the following table:

Source of Data	Tubing Description		Specimen Descrip.	Cycling Rate of Test, cpm	Press. Impulse Range psi	Maximum Peak of Surge, psi ± 200	Frequency of Surge, cps
	Nominal Size, in. (OD x Wall)	Material					
Contractor (Data Group I)	1/4 x 0.035	61S-T6 Al. Alloy Commercial Quality Std. Mill Run	90° Bend	40-50	0-3000	4500	120 (450 also present)
	5/16 x 0.035						
	3/8 x 0.049						
	1/2 x 0.065						
	5/8 x 0.065						
Contractor (Data Group II)	1/4 x 0.035	61S-T6 Al. Alloy Spec. WW-T-789, Cond. T6	90° Bend	35	0-3000	4500	75
	5/16 x 0.049						
	3/8 x 0.049						
	1/2 x 0.065						
	5/8 x 0.083						
Douglas Aircraft Co., El Segundo	1/4 x 0.035	61S-T Al. Alloy (Spec. not available)	90° Bend	35-45	0-3000	4500	25
	5/16 x 0.042						
	5/16 x 0.049						
	3/8 x 0.049						
	3/8 x 0.058						
	1/2 x 0.065						
	1/2 x 0.072						
5/8 x 0.083							
Contractor	1/4 x 0.028	24S-T3 Al. Alloy Spec. AMS4086-A	90° Bend	35	0-3000	4500	75
	5/16 x 0.035						
	3/8 x 0.035						
	1/2 x 0.049						
	5/8 x 0.065						
Hughes Aircraft Co.	1/2 x 0.035	24S-T Al. Alloy (Spec. not Available)	90° Bend	35	0-2000	3000	34 Not Available
	1-1/4 x 0.083		Straight	35	0-2000	3000	
Marin and Shelton (Ref. 2)	2.1 x 0.05	24S-T4 Al. Alloy (Spec. Not Available)	Straight	300	Varied	None	None
Douglas Aircraft Co., El Segundo	1/4 x 0.016	Stainless Steel Spec. AMS5566	90° Bend	35-45	0-3000	4500	25
	5/16 x 0.016						
	5/16 x 0.020						
	3/8 x 0.020						
	3/8 x 0.028						
	1/2 x 0.028						
1/2 x 0.035							
Contractor	1/4 x 0.020	Stainless Steel Spec. AMS5566	90° Bend	35	0-3000	4500	75
	5/16 x 0.028						
	3/8 x 0.028						
	1/2 x 0.035						
	5/8 x 0.049						

All tests were conducted on specimens having one end fixed and one end free. In addition to the variations in basic test conditions shown in the above table, variations were found in the following:

- (a) The ratio of the bend radius (to the center line of the tube) to the tubing OD ranged between 3.0 and 4.0 on the majority of the specimens, with a few specimens having a bend ratio of 4.5.
- (b) The bend flatness (i.e., percentage of distortion of the tubing OD) ranged between two and six percent.
- (c) The torques used to tighten the connections ranged with tubing size as follows:

<u>Nominal Tubing OD, in.</u>	<u>Range of Torque Values, in-lb</u>
1/4	50 - 110
5/16	70 - 160
3/8	90 - 200
1/2	200 - 600
5/8	400 - 750

- (d) The types of tubing connectors represented were AN818-AN819 (short type), AN817 (long type), and ER817-ER819 (aircraft Ermeto type).
- (e) Both single-flared (Spec. AND10061) and double-flared (Spec. AND10078) tubing were represented in the 61S-T aluminum alloy tubing data.
- (f) Certain of the specimens were proof-tested to 200 percent of design operating pressure prior to fatigue testing.

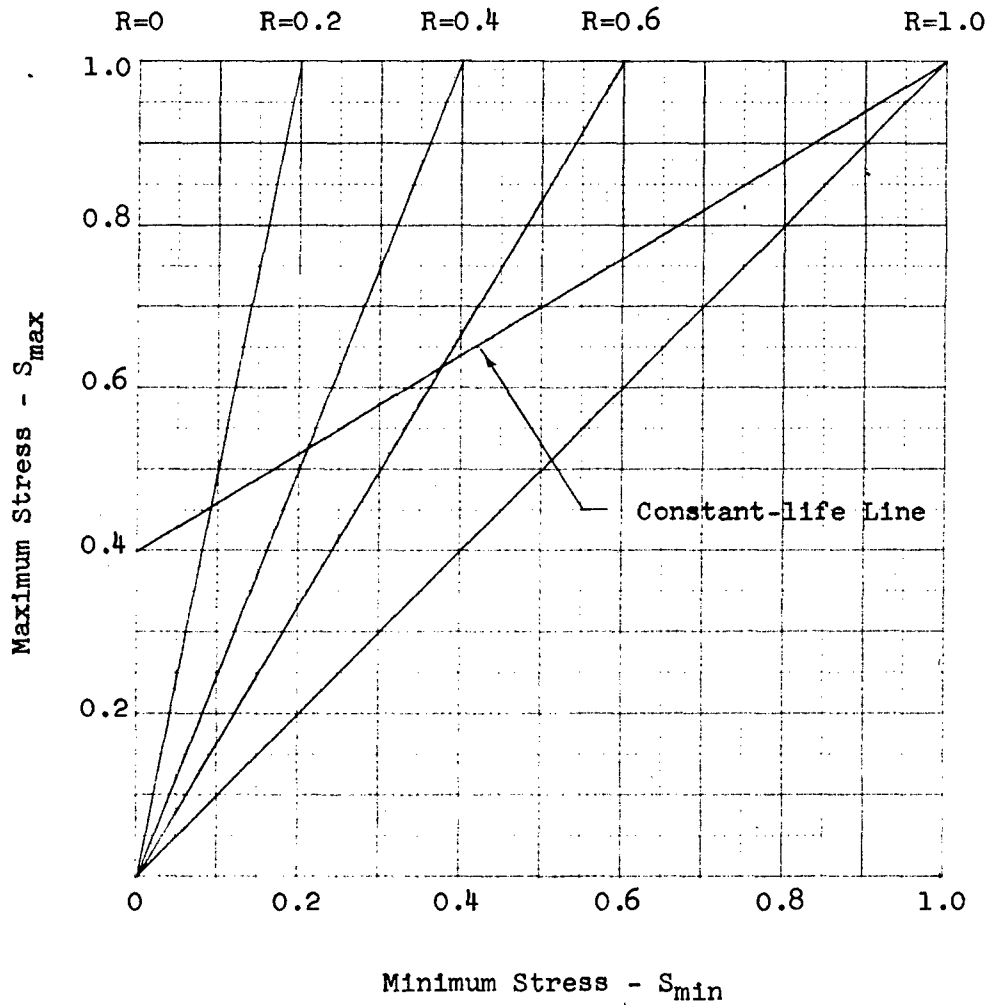
4.2.2 Analytical studies of the data obtained from the survey indicated that the use of multiple-correlation methods of statistical analysis, to evaluate the effect of variations in pressure waveform on the fatigue life of the tubing, was impractical due to the number of significant parameters represented. Comparison of data on individual specimens gave the following information:

- (a) Tubing bends indicated reduced fatigue life, but the effect of variations in bend radii over the range tested gave no significant trend indication.
- (b) Double-flared tubing was more susceptible to failures in the flare than was single-flared tubing. It appeared that higher torques accentuated the number of failures. In some groups of data, the number of double-flare failures was greater than the number of bend failures.
- (c) No significance could be attached to the type of tubing connector other than that mentioned in the case of double-flared tubing using AN connectors.
- (d) Variations in bend flatness over the range observed gave no significant trend indication.
- (e) There was some indication that proof-testing of the tubing prior to fatigue testing increased the fatigue life.
- (f) Considering the effects of the aforementioned parameters, no significant variation in fatigue life could be attributed to the differences in pressure waveform represented in the existing data.

All comparative work was based on the maximum calculated stress in the tubing and a stress ratio (i.e., minimum-maximum stress ratio) of  $R = 0$ . In actual tests, except Ref. 2, the actual stress ratios were +0.01 to +0.03 due to the system return line pressure, but these ratios were low enough to be considered zero. In Ref. 2, the actual stress ratios ranged between +0.1 to +0.25.

Figure 80

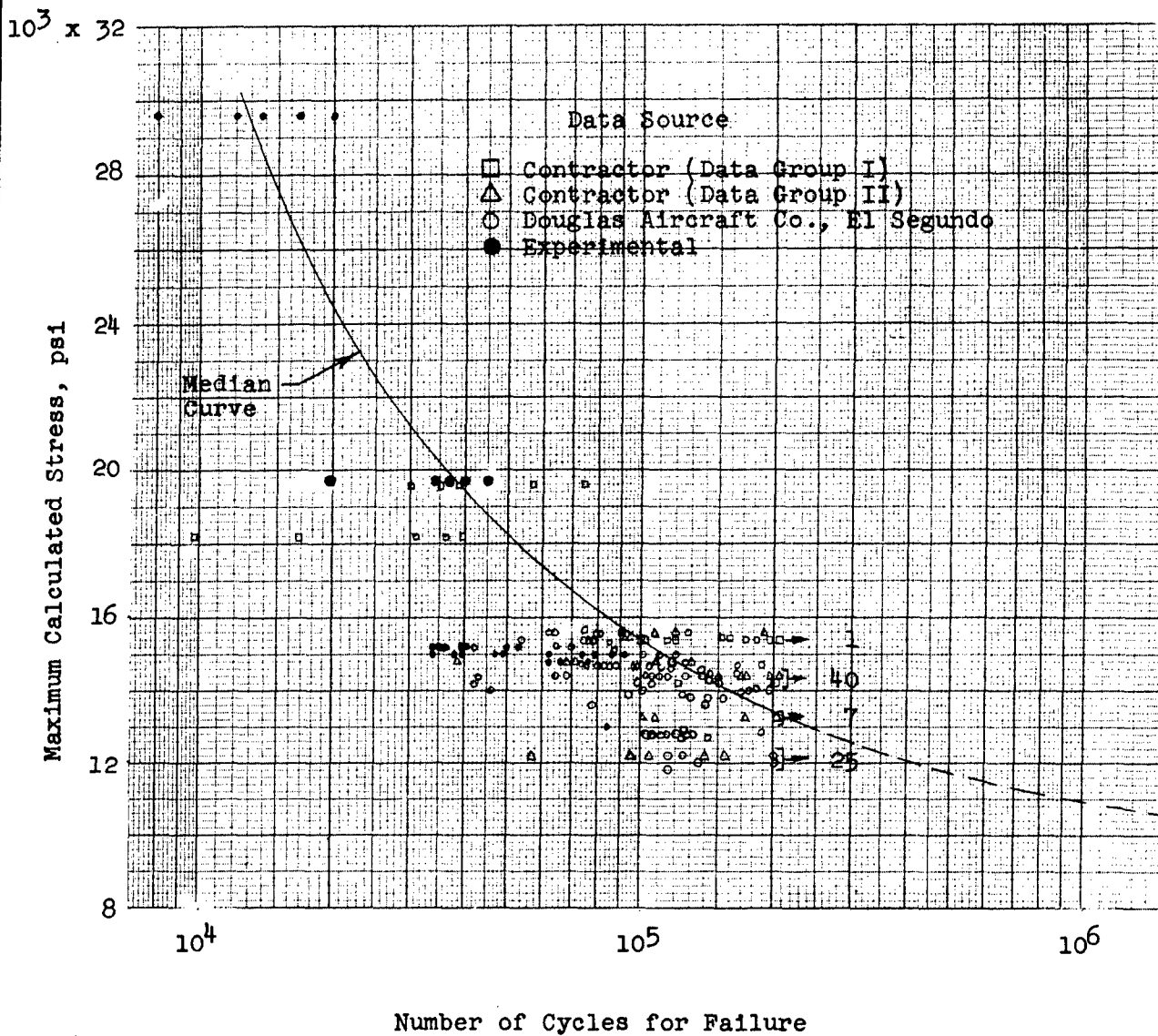
MODIFIED GOODMAN'S DIAGRAM SHOWING APPROXIMATE METHOD FOR ADJUSTING DATA FROM ONE STRESS RATIO TO ANOTHER STRESS RATIO



Notes: Stress Ratio,  $R = S_{min}/S_{max}$   
 Stresses are expressed in fractions of the ultimate tensile strength (48,000 psi).

Figure 81

FATIGUE DATA ON 61S-T ALUMINUM ALLOY TUBING  
WITH 90 DEGREE BENDS  
SUBJECTED TO PRESSURE IMPULSES (STRESS RATIO, R=0)



Notes: All data, except experimental tests at 19,700 psi stress level, were obtained from pressure impulses with surge peaks.

↪ indicate no failure and number of specimens.

These were adjusted to zero by means of the modified Goodman's Diagram shown in Fig. 80. Although actual test data do not conform to straight constant-life lines on the stress diagram (Ref. 3, p. 135), the error in this case was considered small because of the proximity of the actual stress ratios to the desired stress ratio. Maximum calculated stresses in the tubing were based on the Lame' formula for thick-walled cylinders,

$$S = P \left( \frac{D^2 + d^2}{D^2 - d^2} \right) \quad (4-1)$$

where

S = stress, psi  
 P = internal pressure, psi  
 D = outside diameter of cylinder (or tube), in.  
 d = inside diameter of cylinder (or tube), in.

using the peak pressure in the pressure waveform and actual tubing dimensions, or nominal tubing dimensions in a few cases where the actual dimensions were unavailable.

4.2.3 To supplement and extend the data obtained from the survey, additional tests were conducted on 61S-T6 aluminum alloy tubing (Spec. AMS4083) under the following conditions:

Nominal Size OD x Wall, in.	Specimen Description	Cycling Rate of Test, cpm	Pressure Impulse Range, psi	Maximum Peaks of Surge, psi ±200
5/16 x 0.049	90 deg Bend	125	0-3000	4500
5/16 x 0.049	Straight	125	0-3000	4500
3/8 x 0.049	90 deg Bend	80	0-3000	4500
3/8 x 0.049	90 deg Bend	125	0-3000	4500
3/8 x 0.049	Straight	125	0-3000	4500
1/2 x 0.035	90 deg Bend	80	0-3000	None
1/2 x 0.035	90 deg Bend	80	0-3000	4500
1/2 x 0.035	Straight	80	0-3000	None
1/2 x 0.035	Straight	80	0-3000	4500
1/2 x 0.065	90 deg Bend	80	0-3000	4500
5/8 x 0.083	90 deg Bend	60	0-3000	4500
5/8 x 0.083	90 deg Bend	80	0-3000	4500
5/8 x 0.083	90 deg Bend	120	0-3000	4500

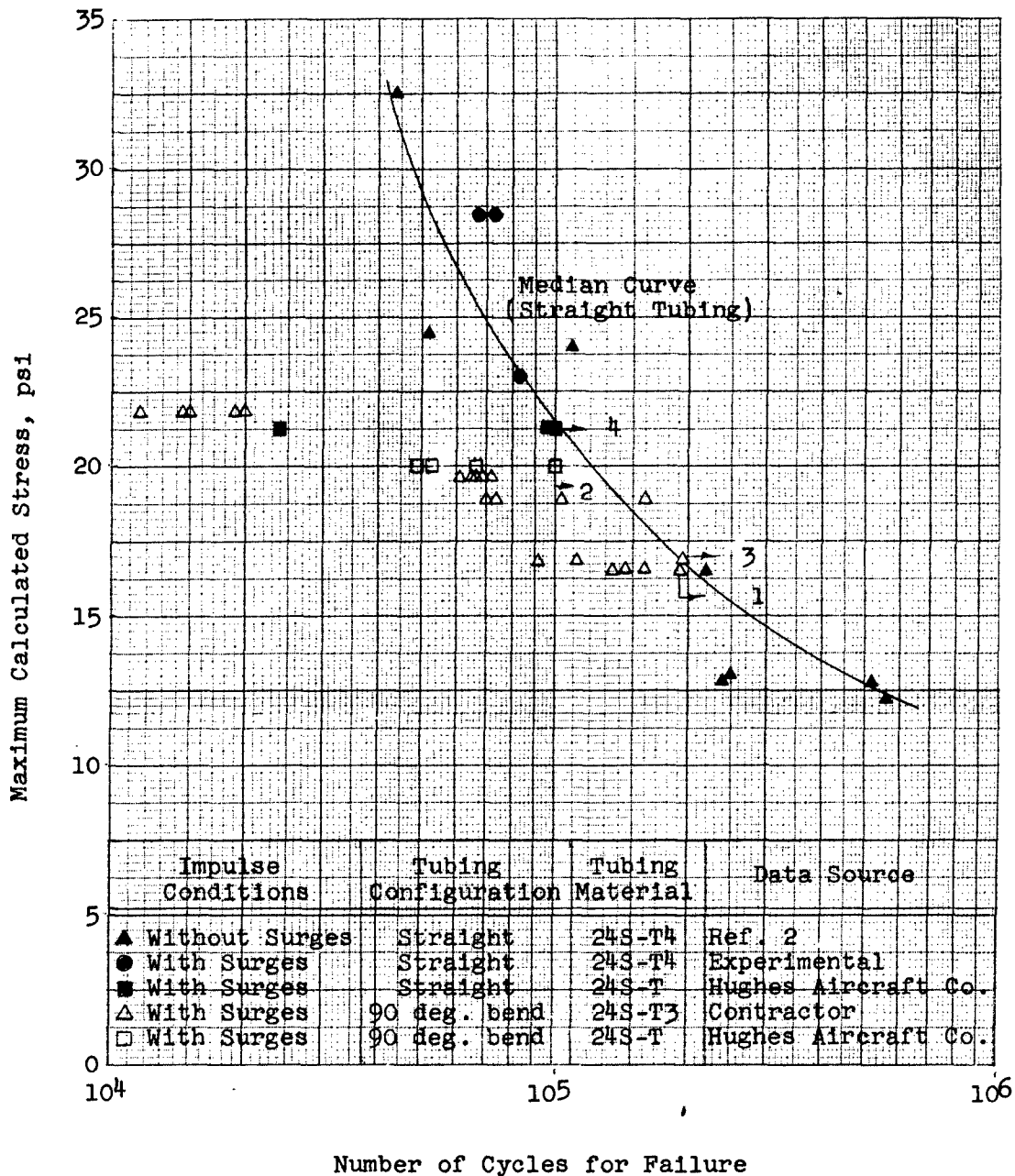
The 5/16 and 3/8 in. OD tubing were double-flared and the remaining sizes were single-flared in accordance with the applicable specifications. The bend radii of the tubing in all cases were the minimum recommended for design, which gave bend ratios between 3.0 and 3.5. The bend flatness in all specimens was less than six percent, the maximum allowable in general production practice. The frequency of the fundamental pressure surge was between 60 and 95 cps in all tests with surge peaks.

4.2.4 Comparison of the results of the experimental tests on 61S-T aluminum alloy tubing, with 90 deg bends, to data collected from the survey is shown in Fig. 81. The major significance in the data was that the data determined by tests without surge peaks fell in line with the data for tests with surge peaks. The S-N curve shown is the median determined from logarithmic probability plots of the data at different stress levels. The experimental tests on 61S-T aluminum alloy tubing without bends gave a similarly smooth S-N curve even though one group of data was determined without surge peaks (Fig. 82). Comparison of the S-N curves in Fig. 81 and 82 indicated that the fatigue life of tubing was definitely lowered by tubing bends, but the scatter bands of the data were overlapping.



Figure 83

FATIGUE DATA ON 24S-T ALUMINUM ALLOY TUBING  
WITH AND WITHOUT BENDS  
SUBJECTED TO PRESSURE IMPULSES (STRESS RATIO, R=0)

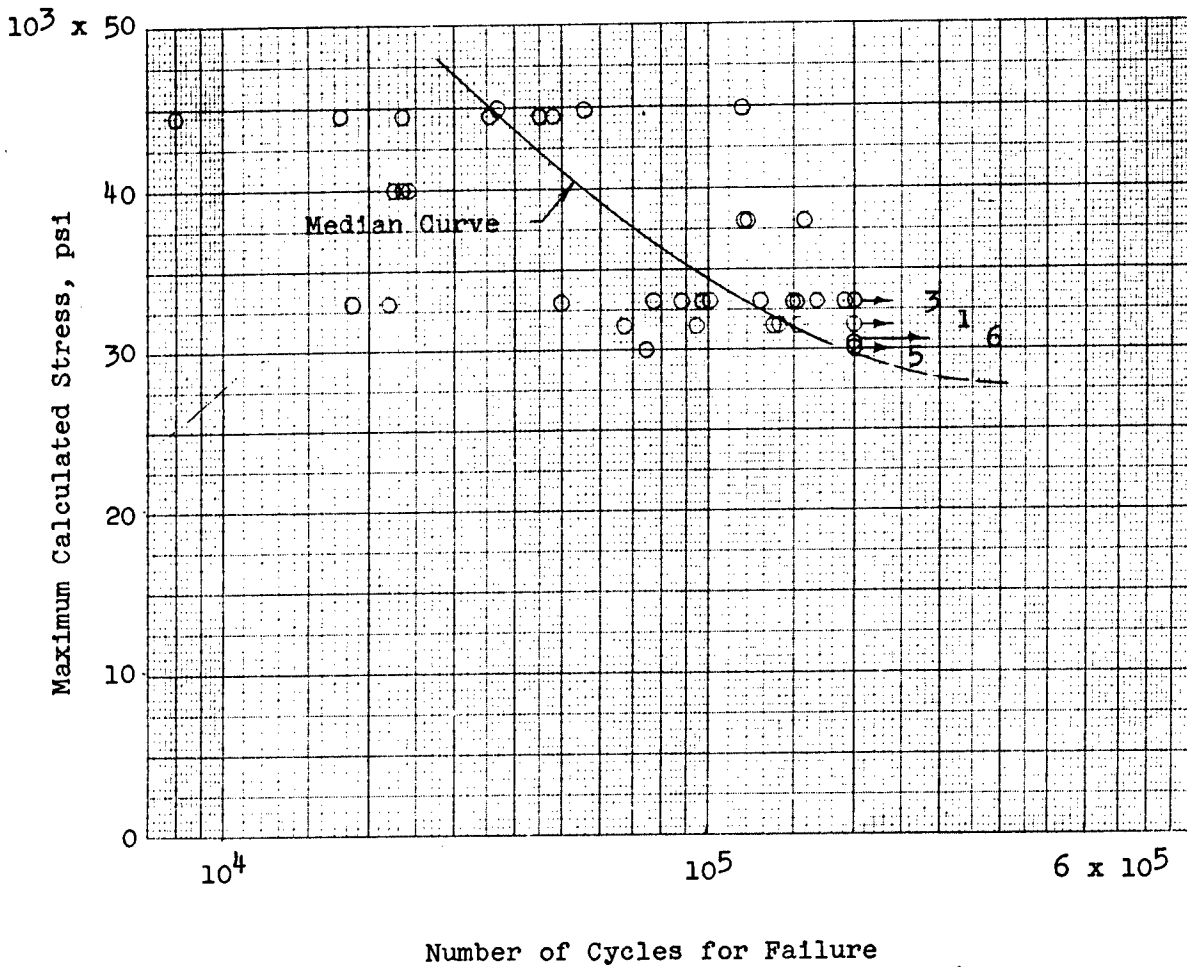


Note: —▶ indicate no failure and number of specimens.



Figure 84

FATIGUE DATA ON STAINLESS STEEL TUBING (SPEC. AMS 5566),  
 WITH 90 DEGREE BENDS,  
 SUBJECTED TO PRESSURE IMPULSES (STRESS RATIO, R=0)



Notes: Data sources - Douglas Aircraft Co., El Segundo and Contractor.  
 → Indicate no failure and number of specimens.

4.2.5 During the experimental tests on the 5/16 and 3/8 in. OD tubing, approximately 25 percent of failures occurred near the base of the double flare and were circumferential in nature. These failures appeared to have originated from a critical stress concentration created when the sleeve had coined the flare surface during assembly. The actual torques used to tighten the fittings were 120 in-lb on the 5/16 in. OD tubing and 180 in-lb on the 3/8 in. OD tubing, which were in accordance with general assembly practice.

4.2.6 During experimental investigation on actuating cylinder assemblies (Par. 4.3), fatigue-strength values were obtained on the cylinder barrels (24S-T4 aluminum alloy tubing) which compared favorably with data obtained from Ref. 2. Here again, it was significantly noted that the data were comparable even though certain of the data were for tests conducted with pressure surges while other of the data were for tests conducted without surge peaks (Fig. 83). Fatigue results on 24S-T aluminum alloy tubing with 90 deg bends are also presented in Fig. 83 for comparison, but insufficient data were available to establish any definite relationship between bent and straight tubing.

4.2.7 The data collected on stainless steel tubing (Spec. AMS5566) with 90 deg bends are presented in Fig. 84 and show greater scatter than did the data on aluminum alloy tubing. From previous investigation by the Contractor it was indicated that nominal sizes of stainless steel tubing being currently used in military aircraft hydraulic systems did not present the fatigue problem of aluminum alloy tubing. This was substantiated by the results of tests by the Glenn L. Martin Company (Par. 4.2.8 and 4.2.9).

4.2.8 The Glenn L. Martin Company submitted data on fatigue failure of 61S-T aluminum alloy tubing (Spec. WW-T-789 and AMS4083) subjected to high-frequency oscillations with a total range from 2100 to 4800 psi pressure (Fig. 85). These oscillations were produced when a constant displacement, piston type, pump was cavitated by reducing the pump inlet pressure to 9.92 in. Hg abs. The pump shaft speed was 3750 rpm and the system relief valve was set at 3000 psi. Analysis of the pressure surge characteristics (Fig. 85) indicated that the frequency of the oscillation was 1420 cps, with two oscillations occurring during each piston stroke. The tests were conducted on 1/2 in. OD x 0.065 in. wall tubing having 90 deg bends and all failures occurred on the neutral axis of the tubing bends. The average fatigue life of 18 specimens was  $6.75 \times 10^6$  cycles (100 min running time) with the life ranging between  $0.81 \times 10^6$  (12 min) and  $18.56 \times 10^6$  (275 min). No noticeable difference between the two types of 61S-T aluminum alloy material was observed.

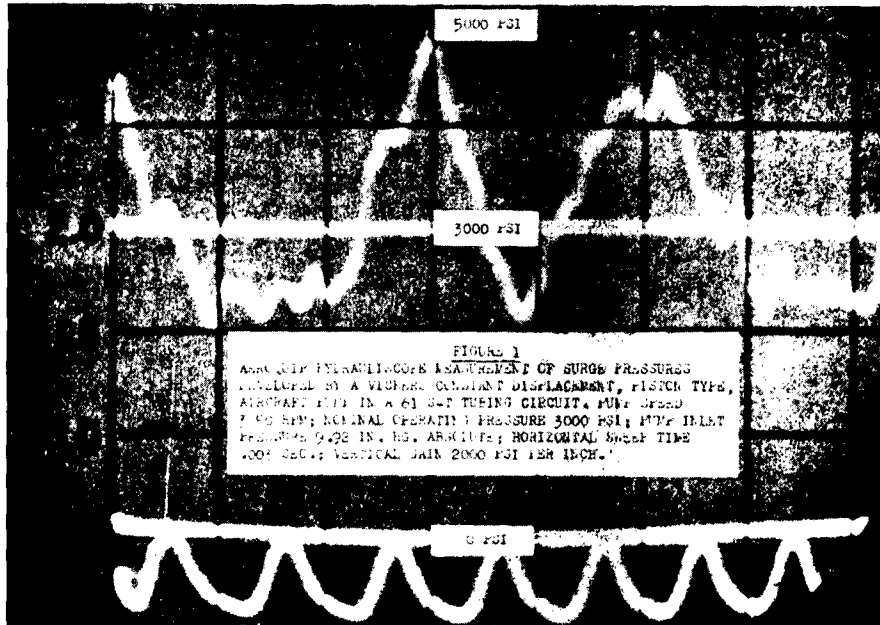
4.2.9 In addition to the fatigue tests on 61S-T aluminum alloy tubing, the Glenn L. Martin Company also subjected stainless steel tubing (Spec. MIL-T-6847) to similar fatigue conditions, except that the total range was 1300 to 4800 psi pressure and the frequency of the oscillation was 1500 cps (Fig. 85). This tubing (1/2 in. OD x 0.035 in. wall) withstood  $113.4 \times 10^6$  cycles (28 hr of running) without failure.

4.2.10 Using the median curve shown in Fig. 81 for a stress ratio of  $R = 0$  and the modified Goodman's Diagram shown in Fig. 80, a family of curves was drawn for various stress ratios (Fig. 86). The mean life obtained from the tests conducted by the Glenn L. Martin Company compared rather favorably with these curves. This seemed to indicate that even high-frequency oscillations did not affect the fatigue strength appreciably. However, the need for further investigation of this parameter seems quite evident.

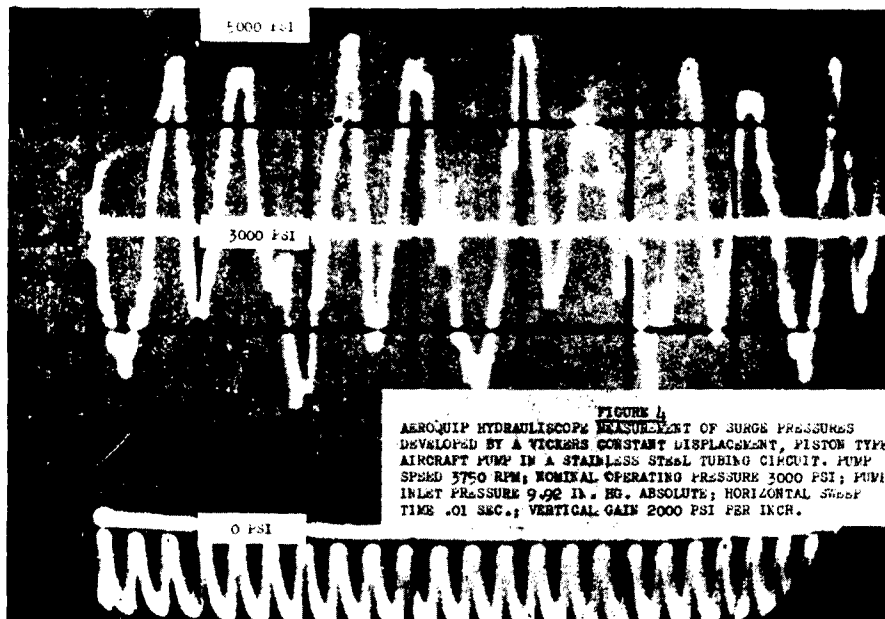
4.2.11 In Ref. 4, Freudenthal has proposed that the distribution characteristics of fatigue data can be represented by logarithmic-normal distribution, which gives a straight line on logarithmic probability graph paper. Plotting of actual test data indicated good correlation with this distribution (Fig. 87). A comparison of the distribution of a single group of data, obtained under a specific set of test conditions, to the distribution of the combined data from various sources (Fig. 87) indicated an appreciable increase in the width of the scatter band of the latter, but this increase seemed reasonable when consideration was given to the relationship between random sample distribution and population distribution shown in general statistical problems. According to

Figure 85

PRESSURE SURGE CHARACTERISTICS OF HIGH-FREQUENCY FATIGUE TESTS  
CONDUCTED ON TUBING AT THE GLENN L. MARTIN COMPANY



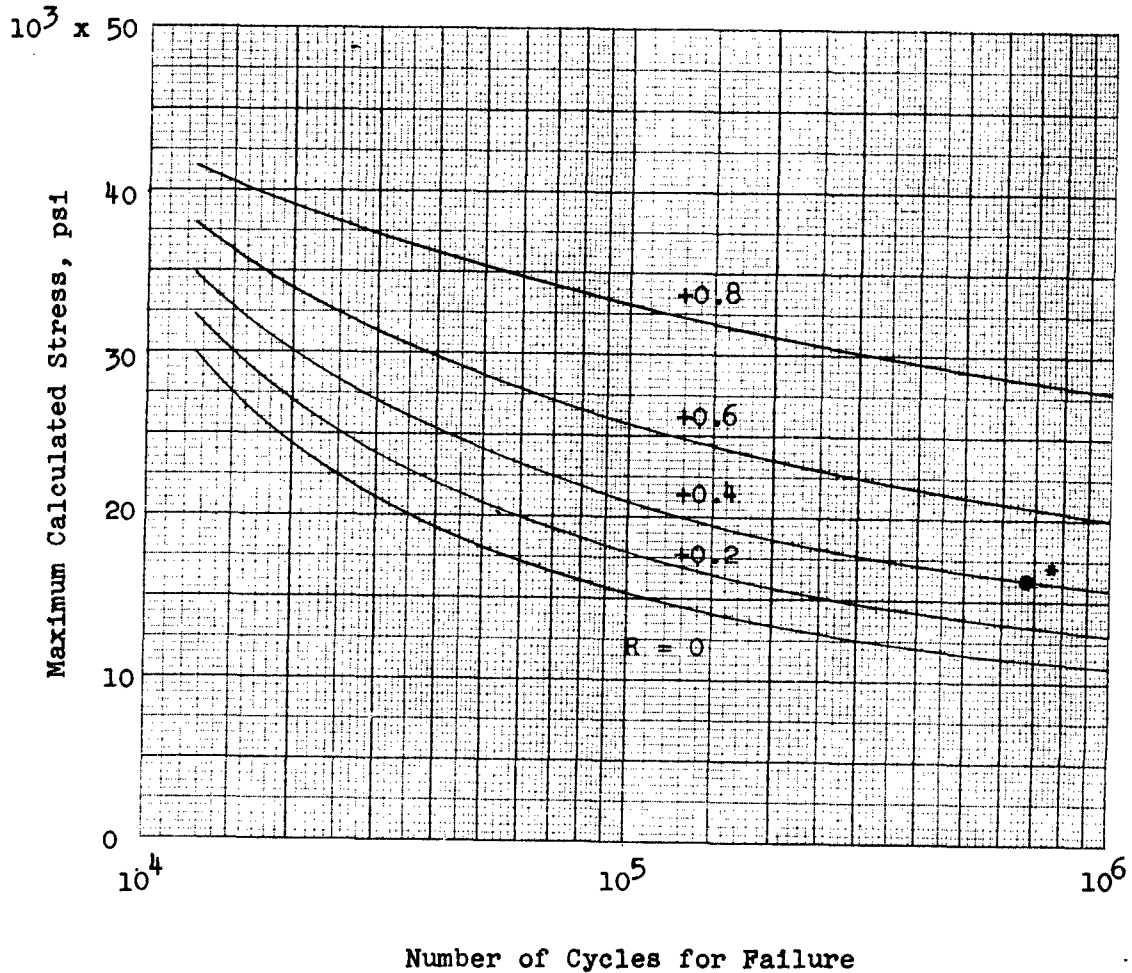
Pressure Characteristics on 61S-T Aluminum Alloy Tubing



Pressure Characteristics on Stainless Steel Tubing

Figure 86

FATIGUE-STRENGTH CURVES ON 61S-T ALUMINUM ALLOY TUBING  
WITH 90 DEGREE BENDS  
AT VARIOUS STRESS RATIOS

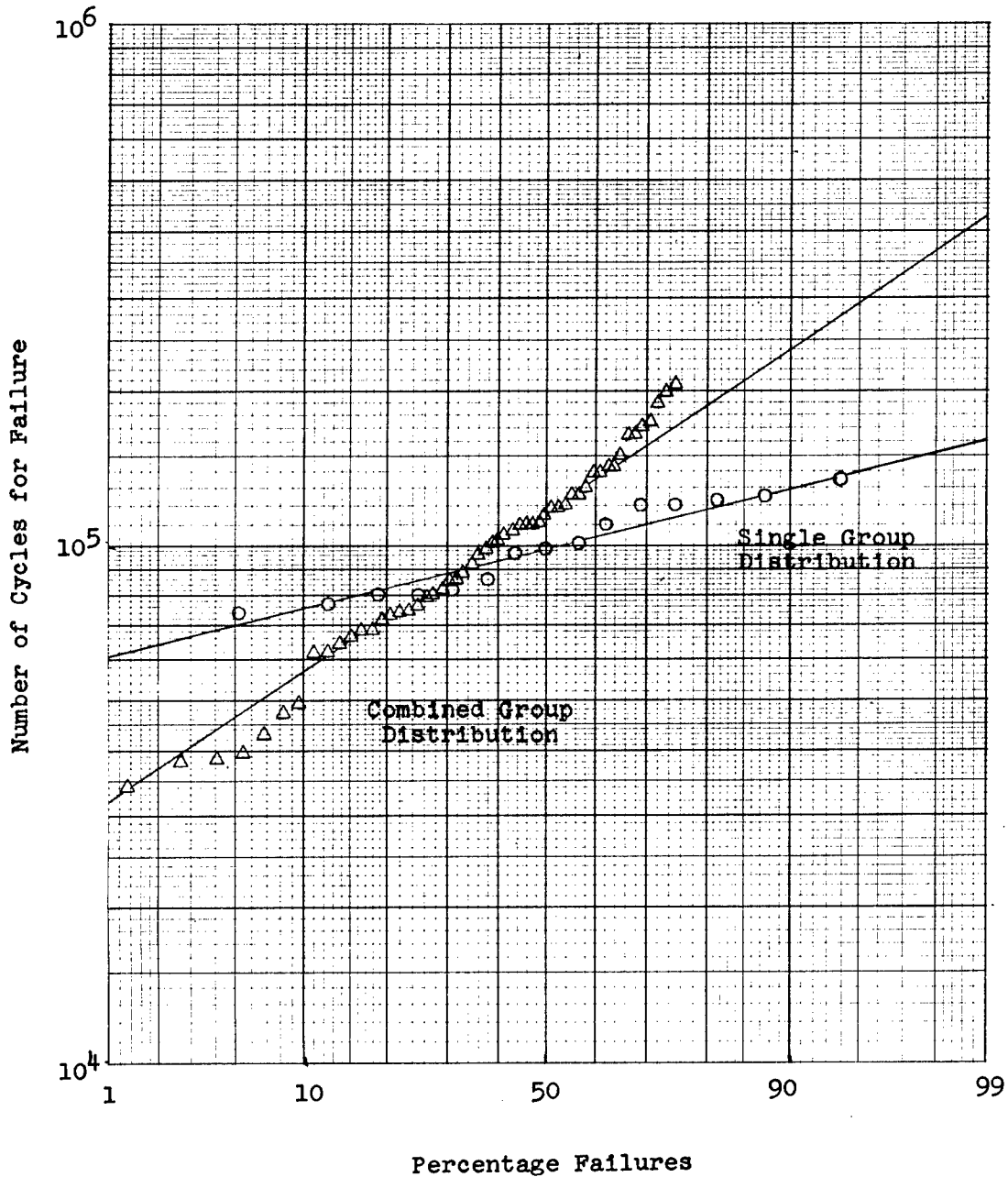


Notes: Median curves, determined from Fig. 80 and 81, for tubing with 90 deg bends.

\*Median of 18 specimens tested by the Glenn L. Martin Co. under test conditions shown in Fig. 85 (upper),  $R = +0.44$ .

Figure 87

LOGARITHMIC PROBABILITY PLOTS OF FATIGUE DATA  
 SHOWING THE DIFFERENCE IN LIFE RANGE BETWEEN  
 SINGLE GROUP DISTRIBUTION AND COMBINED GROUP DISTRIBUTION OF  
 VARIOUS DATA SOURCES



Notes: Data taken from Fig. 81.  
 Straight line represents logarithmic-normal distribution.

Freudenthal, at least six specimens, preferably 8 or 10, should be tested under a given set of conditions to establish the median value of fatigue life. From this it becomes apparent that an extensive investigation would be necessary to determine the relative effects of variations in the pressure surge waveform (i.e., frequency and cumulative damage due to underdamped fundamental oscillations, etc.). For establishment of lower limits for design, Freudenthal has indicated that at least 20 specimens should be tested at a particular stress level.

4.2.12 Studies of the pressure surge waveform indicated that the subsequent oscillations following the initial surge peak might result in cumulative damage which would reduce the fatigue life of the tubing. In Ref. 5, Miner has proposed that fatigue failure from cumulative damage under varying stress conditions can be represented by the following expression,

$$\sum \frac{n}{N} = \frac{n_1}{N_1} + \frac{n_2}{N_2} + \frac{n_3}{N_3} + \dots + \frac{n_n}{N_n} = 1 \quad (4-2)$$

where

$N_1$  = number of stress cycles to failure for stress conditions of  $S_{\max 1}$  and  $S_{\min 1}$ .

$n_1$  = number of stress cycles applied for stress conditions  $S_{\max 1}$  and  $S_{\min 1}$ .

$S_{\max 1}$  = maximum stress in loading cycle.

$S_{\min 1}$  = minimum stress in loading cycle.

For fatigue tests with pressure surges,  $n_1 = n_2 = n_3 = \dots = n_n$ , since there is one cycle applied for each set of stress conditions during each pressure impulse cycle. Therefore, Eq. 4-2 can be written

$$n \left( \frac{1}{N_1} + \frac{1}{N_2} + \frac{1}{N_3} + \dots + \frac{1}{N_n} \right) = 1 \quad (4-3)$$

where

$n$  = number of impulse cycles for failure.

Using actual pressure surge waveforms and the family of curves shown in Fig. 86, analysis of the effect of cumulative damage was made for several groups of data. Results of this analysis indicated that even for the more highly stressed tubes, the reduction in fatigue life due to the subsequent oscillations might not result in more than 10 - 15 percent variation from a fatigue-strength value based on the initial peak only. The hypothesis presented by Miner was used because it seemed the simplest to apply with the data available, and was indicative of the trend. Further studies of the cumulative damage in fatigue can be found in Ref. 6.

4.2.13 From investigation by Marin and Shelton (Ref. 2) on 24S-T aluminum alloy tubing, it was found that uniaxial fatigue-strength values, determined by standard fatigue test methods, could not be used to predict fatigue strength under biaxial stress conditions. The agreement of results obtained in this investigation with results obtained by Marin and Shelton on fatigue tests of tubing subjected to pressure impulses tends to substantiate the preceding conclusion. Comparison of the fatigue-strength values shown in

Fig. 84 for biaxial stress conditions on stainless steel tubing with published data on uniaxial fatigue-strength values of the same type of material seemed to indicate that the above conclusion also holds true for steel. Further investigation would be necessary to establish a more exact conclusion.

#### 4.3 Cylinders

4.3.1 Fatigue tests were conducted on three cylinder assemblies under the following conditions:

Cylinder Assembly No., (Contractor part No.)	Cycling Rate of Test, cpm	Impulse Range, psi	Maximum Peak of Surge, psi $\pm$ 200	Frequency of Surge, cps
157-58027	80	0-3000	4500	29
151-58044-1	60	0-3000	4500	57
151-58044-3	60	0-3000	4500	57

In all cases, the piston was initially in the fully retracted position so that the cylinder end and packing glands on the piston rod side were subjected to the pressure surges. When failure of the cylinder end occurred, it was not a complete failure; consequently, it was possible to fully extend the piston and continue the test until failure of the cylinder barrel was obtained. In event of a packing gland failure, a new gland was installed and the test was continued.

4.3.2 Pertinent data on the cylinders tested were as follows:

- (a) The cylinder ends of the 157-58027 assembly were made of 24S-T42 aluminum alloy bar and the cylinder barrel (2-7/8 in. OD x 0.250 in. wall) was made of 24S-T4 aluminum alloy tube. Hydrostatic burst pressure of the cylinder occurred at 11,000 psi, the barrel splitting longitudinally.
- (b) The cylinder ends of the 151-58044-3 assembly were made of 75S-T6 aluminum alloy bar and the cylinder barrel (2-1/4 in. OD x 0.156 in. wall) was made of 24S-T4 aluminum alloy tube. Hydrostatic burst pressure of the cylinder was 8600 psi, the barrel splitting longitudinally.
- (c) Cylinder assembly 151-58044-1, was essentially the same as the 151-58044-3 assembly, except that the cylinder end on the rod side of the piston was made of 24S-T4 aluminum alloy bar and was designed for greater structural strength.

4.3.3 Results of the fatigue tests gave the following sequence of failures:

<u>Cylinder Assembly No.</u>	<u>Cycles of Impulse</u>	<u>Location of Failure</u>
157-58027	77,565 83,162	Cylinder end (Fig. 88, upper) Cylinder barrel (Fig. 89, upper)
151-58044-1	27,734 71,722 73,624	Packing gland on piston rod (Fig. 90, upper) Cylinder end (Fig. 88, lower) Cylinder barrel (Fig. 89, lower)
151-58044-3	15,225 15,225	Packing gland on piston rod (similar to Fig. 90) Static seal on cylinder end (Fig. 90, lower)

Figure 88

FATIGUE FAILURES OF CYLINDER ENDS SUBJECTED  
TO PRESSURE IMPULSES WITH SURGE PEAKS

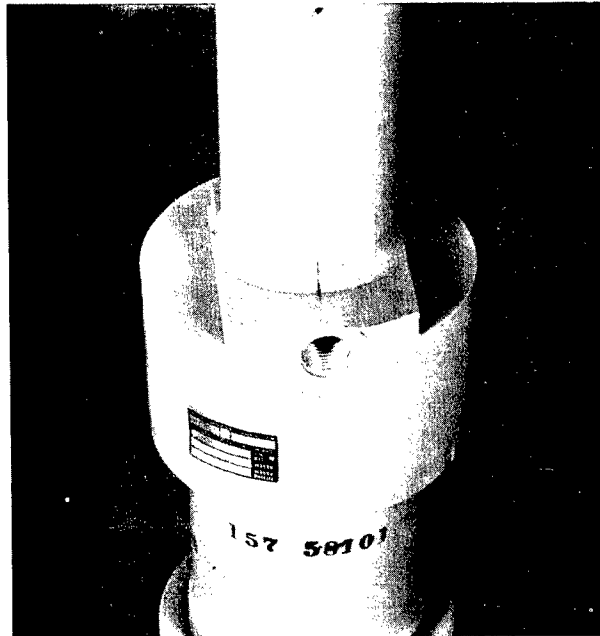




Figure 89

FATIGUE FAILURES OF CYLINDER BARRELS  
SUBJECTED TO PRESSURE IMPULSES WITH SURGE PEAKS

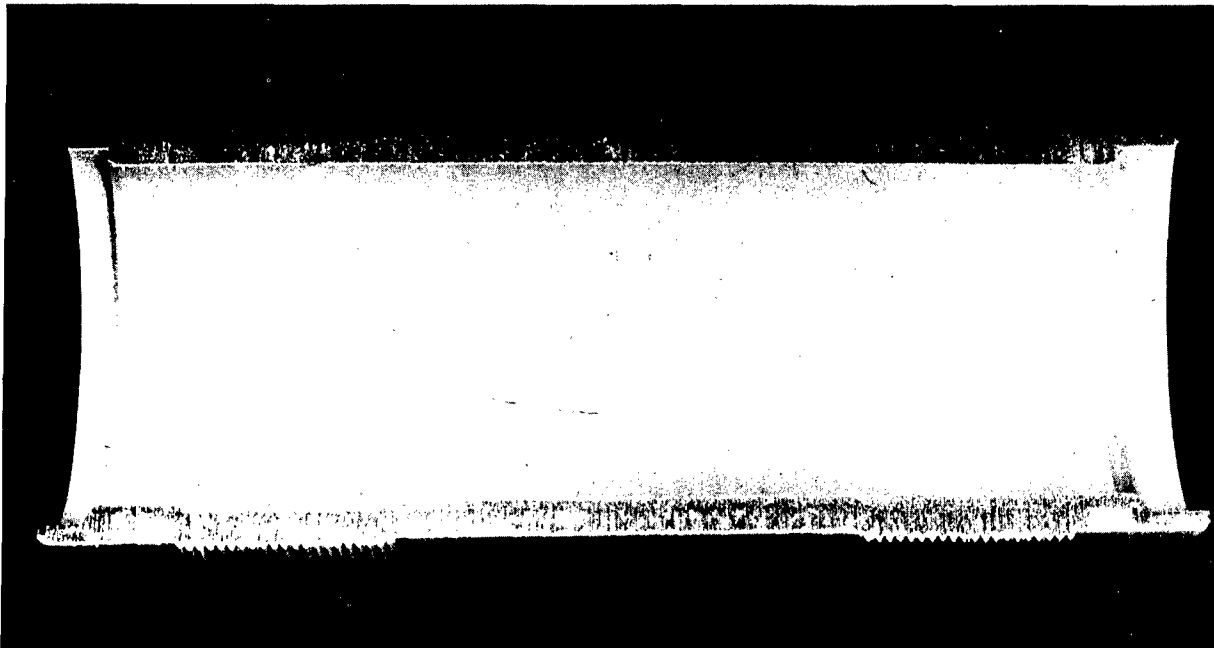


Figure 90

FATIGUE FAILURES OF PACKING GLANDS IN  
ACTUATING CYLINDER ASSEMBLIES SUBJECTED TO  
PRESSURE IMPULSES WITH SURGE PEAKS

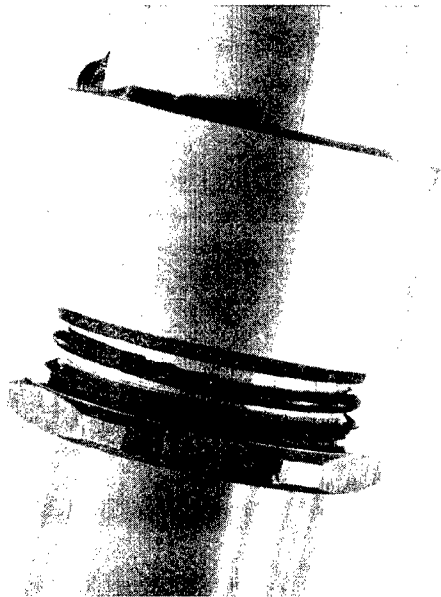
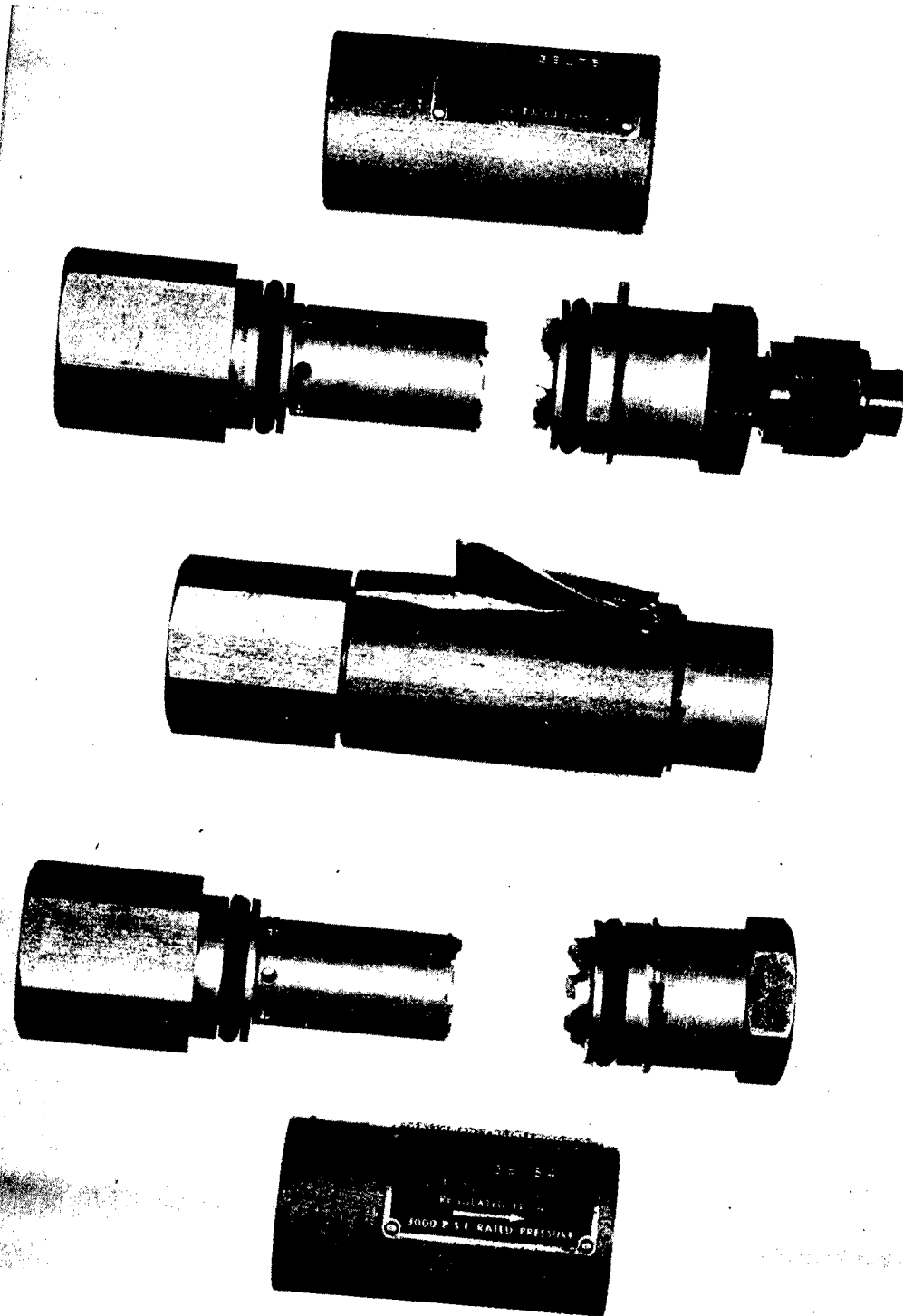


Figure 91  
FATIGUE AND HYDROSTATIC BURST PRESSURE  
FAILURES OF FLOW REGULATORS (WATERMAN NO. 196-8-5.89)



27,735	Second failure of static seal on cylinder end
33,760	Second failure of packing gland on piston rod
46,776	Third failure of static seal on cylinder end
66,837	Cylinder barrel (similar to Fig. 89).

The results of the tests indicated that packing glands and stress concentrations in cylinder end design are of prime importance in determining the fatigue life of a cylinder.

4.3.4 No contributing factor could be established for the prevalence of gland failures on the 151-58044-3 cylinder assembly. Actual dimensions indicated the gland widths on the 151-58044-3 assembly to be less than 0.001 in. greater than on the 151-58044-1 assembly. There might have been a possibility that "breathing" of the cylinder end, due to the difference in design (Par. 4.3.2), could have been a contributing factor. All packing glands in the cylinders tested were in accordance with the applicable specifications and had leather back-up rings. Although no specific tests were conducted to determine the effect of Teflon back-up rings on the fatigue life of packing glands subjected to pressure surges, results of general research by the Contractor have indicated that Teflon back-up rings might increase the life of packing glands. In this general research it has been noted that Teflon back-up rings retain the O-ring better than leather back-up rings. However, more specific research will be required to determine the relative effect under pressure impulse conditions.

4.3.5 The data on the fatigue life of the cylinder barrels were of significant value as was pointed out in Par. 4.2.6.

#### 4.4 Flow Regulators

4.4.1 Fatigue tests on two flow regulators (Waterman No. 196-8-5.89) subjected to pressure impulses (0-3000 psi) with surge peaks (4500 ± 200 psi) resulted in failures, as shown in Fig. 91, after 40,720 and 41,000 cycles, respectively. Cycling rates of the tests were 80 cpm. Metallurgical analysis of the component parts indicated the material in the regulator body and housing to be 14S-T aluminum alloy. A hydrostatic burst test of an identical flow regulator resulted in a split housing failure at 10,300 psi (Fig. 91).

4.4.2 Stress concentration was considered a contributing factor to the relatively short fatigue life of these components. Since the fatigue life was low compared to other system components subjected to the same pressure impulse conditions, these flow regulators might be critical in determining the life of a hydraulic system.

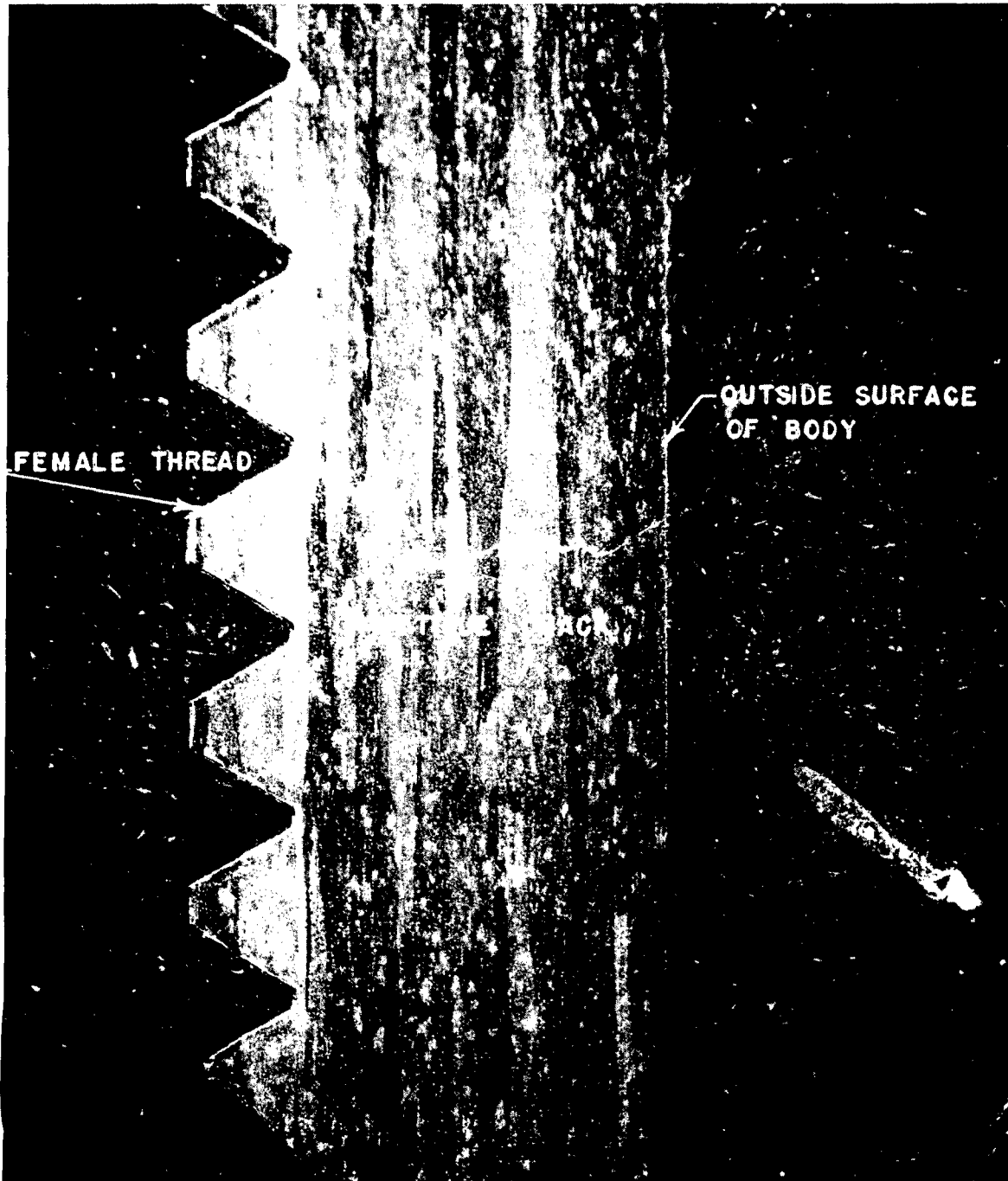
#### 4.5 Valves

4.5.1 Fatigue tests under conditions as described in Par. 4.4.1 were conducted on two types of restrictor valves, Contractor part No. 1V7 (two-way restrictor) and Contractor part No. 1V4 (one-way restrictor). Circumferential failures occurred in the threaded section of the valve assembly as shown in Fig. 92. On the two-way restrictors, the failures occurred in the threaded section where the valve body engaged the orifice fitting. On the one-way restrictors, the failures occurred where the threaded section engaged the external AN fittings. The detail dimensions in the section of the failure were the same in all cases. Consequently, the fatigue life values obtained were considered representative of scatter, the actual values ranging between 240,510 cycles and 612,800 cycles.

4.5.2 Examination of the valve bodies in the vicinity of the failures indicated that the shorter fatigue life values were associated with greater "bell-mouthing" of the valve body, which apparently occurred during assembly. Exact torque values were not available, but it was determined that this "bell-mouthed" condition was indicative of higher assembly torques. No further

Figure 92

FATIGUE FAILURE OF RESTRICTOR VALVE BODY  
SUBJECTED TO PRESSURE IMPULSES WITH SURGE PEAKS  
(X20 MAGNIFICATION)



investigation was deemed necessary, since the fatigue lives of these components were high compared to other components.

#### 4.6 Fittings

4.6.1 No specific tests were conducted on fittings, since the applicable specifications require 200,000 cycles of pressure impulse (0-3000 psi) with surge peaks ( $4500 \pm 200$  psi) for qualification. Although increased torque to prevent leakage could result in reducing the fatigue life to an undesirable value, it appeared from data obtained on tubing (Par. 4.2) that this increase might be more critical in regard to the tubing than to the fitting. There were indications from the survey that the primary complaint concerning fittings was the maintenance problem of preventing leakage.

4.6.2 During the course of general test work by the Contractor, several failures of AN fittings made of aluminum alloy have been observed. No record of the actual test conditions or of the fatigue life were available, but the failures were considered as typical. Male thread fitting failures were circumferential failures at the root of the thread. Failures of AN818 nuts were longitudinal, the nut splitting into halves. One interesting fact in the latter type of failure was that the failure followed the identification stampings on the surface of the nut.

#### 4.7 Hoses

4.7.1 Based on the results of many pressure impulse tests, both with and without pressure surges, the B. F. Goodrich Co. had the following information to offer:

- (a) Variances to 1000 percent in test results might be expected where the stresses are in the range that occurs with 4500 psi surge peaks in hydraulic hose. At present, no physical differences in the reinforcement have been detected which might account for this large variation. Increases of 200 to 500 percent have been observed in the fatigue life of hoses subjected to cycle tests in which the stress in the reinforcement has been reduced by approximately two percent.
- (b) In some cases, particularly in a hose that has only one wire braid reinforcement, pinholing of the rubber inner tube has occurred before failure of the reinforcement.
- (c) The rate of pressure change in pressure impulse tests might account for considerable variation in the fatigue life of the hose. Few exact comparisons were available for substantiating this opinion because of inability to control the rate of pressure change and still maintain the desired surge peaks.

4.7.2 Information and data obtained from tests by the Contractor and by Aeroquip, Inc. indicated variances of 200 percent, and more, in the fatigue life of a given hose from the same manufactured lot. The variance shown in combined data for comparable hoses indicated a much wider scatter, substantiating the information submitted by the B. F. Goodrich Company. Actual test data available indicated that the fatigue life of hose assemblies being presently used in 3000 psi aircraft hydraulic systems might be as low as 40,000 cycles when subjected to pressure impulses (0-3000 psi) with surge peaks ( $4500 \pm 200$  psi). From this, it was evident that hose assemblies could be of primary importance in determining the life of a hydraulic system. The wide variance in fatigue life indicated that quality control was probably the major problem.

4.7.3 Due to the scatter in fatigue results on hoses, no relationship as to the effect of rate of pressure rise could be established from the data available. The importance of the effect of this parameter was considered secondary to the establishment of quality control.

4.8 Pressure Switches

4.8.1 Fatigue tests performed by the Contractor on Bourdon tube type pressure switches (Meletron No. 1512-16-13) provided the following data:

Cycling Rate of Test, cpm	Pressure Impulse Range, psi	Maximum Peak of Surge, psi $\pm$ 200	Fatigue Life, Cycles
35	0 - 3000	None	96,000
35	0 - 3000	4500	15,210

Failures occurred on the major axis of the elliptical cross-section of the Bourdon tube. Design information revealed that the Bourdon tubes of these pressure switches were made of SAE 4130 steel, heat treated to 136,000 - 155,000 psi, ultimate tensile strength. The hydrostatic burst pressure of an identical switch was found to be 12,500 psi, the failure occurring on the major axis of the elliptical cross-section of the Bourdon tube.

4.8.2 These failures indicated the relative reduction in fatigue life due to the presence of pressure surges. Also of significance was the fact that these pressure switches had small orifices (0.0275 in. diam) installed at the inlet of the Bourdon tube, the purpose of which was presumably to damp the pressure surges and protect the Bourdon tube. Supplementary investigation, Par. 4.8.3, indicated that when a pressure surge with a 4500 psi peak was applied to the orifice, the pressure surge in the Bourdon tube was approximately the same.

4.8.3 In this supplementary investigation, the orifice was removed from the pressure switch and was installed in a special fitting. Then, a short length of steel tubing and an Aeroquip pressure transducer, having a combined volume which was the same as the volume of the Bourdon tube, were connected to the orifice fitting. When a pressure surge with a 4500 psi peak was applied to the orifice, the pressure surge in the transducer was observed to have a 4400 psi pressure peak. This was not considered too unexpected since the orifice was near the closed end of the tube and it was found in closed-end tube investigation (Par. 3.6) that the damping offered by an orifice at this location was small.

## BIBLIOGRAPHY

1. Campbell, J. E., "Investigation of the Fundamental Characteristics of High Performance Hydraulic Systems", USAF Report No. 5997, United States Air Force Air Materiel Command, Wright-Patterson Air Force Base, Dayton, June 1950 (Restricted)
2. Marin, Joseph and William Shelton, "Biaxial Fatigue Strength of Aluminum Alloy", NACA Technical Note No. 1889, National Advisory Committee for Aeronautics, Washington, May 1949, work done at Pennsylvania State College
3. "Prevention of the Failure of Metals Under Repeated Stress", a Handbook prepared for the Bureau of Aeronautics, Navy Department, by the Staff of Battelle Memorial Institute, under the auspices of the National Research Council of the National Academy of Sciences, John Wiley and Sons, Inc., New York, 1942
4. Freudenthal, A. M., "Planning and Interpretation of Fatigue Tests", American Society for Testing Materials Preprint for Fifty-fourth Annual Meeting, June 18-22, 1951
5. Miner, M. A., "Cumulative Damage in Fatigue", Journal of Applied Mechanics, Volume 12, No. 3, September 1945, pp. A-159 to A-164.
6. Richart, F. E., Jr. and N. M. Newmark, "An Hypothesis for the Determination of Cumulative Damage in Fatigue", Proceedings of American Society of Testing Materials, Volume 48, February 1949, pp. 767-798
7. Guillemin, E. A., "Communications Networks", Volume II, Fifth Printing, John Wiley and Sons, Inc., New York, 1946
8. Steinmetz, C. P., "The General Equations of the Electric Circuit - III", American Institute of Electrical Engineers, Volume XXXVIII, Part I, 1919, pp. 191-245
9. Campbell, J. E., "An Investigation of Hydraulic Damping", Society of Automotive Engineers Preprint for Annual Meeting, Detroit, January 8-12, 1951
10. Gardner, M. F. and J. L. Barnes, "Transients in Linear Systems", Volume I, Third Printing, John Wiley and Sons, Inc., New York, 1946

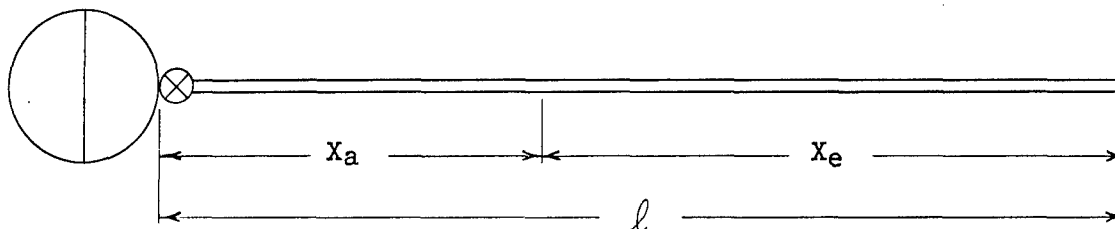


## APPENDIX I

## HYDRAULIC SURGE THEORY

1. Introduction

1.1 The basic hydraulic circuit used through most of the test program to determine the fundamental nature of pressure surges created by an opening valve was a closed-end tube system which contained a tube plugged at one end and affixed to the valve cylinder port at the other end. The valve pressure port was attached to an accumulator as shown below:



Unless otherwise noted, the above hydraulic circuit is the one to which the following development refers.

1.2 The nomenclature used for this development of hydraulic surge theory is as follows:

- $l$  = system length, in.
- $l_e$  = effective system length, in.
- $X$  = distance along tube, in.
- $X_a$  = distance along tube measured from accumulator end, in.
- $X_e$  = distance along tube measured from closed end, in.
- $X_{e1}$  = distance along tube measured from closed end to a particular point in the system, in. ( $i = 1, 2, 3, \dots$ )
- $X_r$  = distance along tube measured from closed end to orifice location, in.
- $x_p$  = instantaneous displacement of piston, in.
- $X_p$  = preload displacement of air load spring, in.
- $A$  = internal cross-sectional area of tube, in<sup>2</sup>
- $A_p$  = effective cross-sectional area of piston, in<sup>2</sup>
- $V$  = volume, in<sup>3</sup>
- $V_a$  = volume of hydraulic fluid in accumulator, in<sup>3</sup>
- $E$  = battery potential
- $e$  = instantaneous electrical potential
- $i$  = instantaneous electrical current

- $p$  = instantaneous pressure, psi  
 $p_e$  = instantaneous pressure at closed-end of system, psi  
 $p_{e_n}$  = instantaneous pressure at closed-end of the "n" branch, psi  
 $p_p$  = instantaneous pressure acting on piston, psi  
 $P_0$  = accumulator pressure = pressure step forcing function, psi  
 $P_w$  = defined in Eq. 76  
 $P_s$  = preload acting on piston, psi  
 $q$  = instantaneous flow rate,  $\text{in}^3\text{-sec}^{-1}$   
 $q_p$  = instantaneous flow rate in cylinder,  $\text{in}^3\text{-sec}^{-1}$   
 $L_e$  = hydraulic inductance per unit system length,  $\text{lb-sec}^2\text{-in}^{-6}$   
 $C_e$  = hydraulic capacitance per unit system length,  $\text{in}^4\text{-lb}^{-1}$   
 $R_e$  = hydraulic resistance per unit system length,  $\text{lb-sec-in}^{-6}$   
 $L_{ea}$  = electric inductance per unit line length  
 $C_{ea}$  = electric capacitance per unit line length  
 $R_{ea}$  = electric resistance per unit line length  
 $L_m$  = hydraulic inductance of mass loaded piston,  $\text{lb-sec}^2\text{-in}^{-5}$   
 $L_0$  = effective hydraulic inductance between accumulator and branch point  
 $L_i$  = effective hydraulic inductance between branch point and closed-end of branch line ( $i = 1, 2, 3, \dots$ )  
 $C_a$  = effective hydraulic accumulator capacitance,  $\text{in}^5\text{-lb}^{-1}$   
 $C_{ae}$  = defined in Eq. 45  
 $C_c$  = effective hydraulic cylinder capacitance,  $\text{in}^5\text{-lb}^{-1}$   
 $C_T$  = defined in Eq. 58  
 $C_{Ta}$  = defined in Eq. 60  
 $C/p = C_{e_l e} + C_c$   
 $C_0$  = effective hydraulic capacitance between accumulator and branch point,  $\text{in}^5\text{-lb}^{-1}$   
 $C_B$  = air load capacitance,  $\text{in}^5\text{-lb}^{-1}$   
 $C_i$  = effective hydraulic capacitance between branch point and closed-end of branch line,  $\text{in-lb}^{-1}$  ( $i = 1, 2, 3, \dots$ )  
 $R_0$  = effective hydraulic resistance between accumulator and branch point,  $\text{lb-sec-in}^{-5}$   
 $R_i$  = effective hydraulic resistance between branch point and closed-end of branch line,  $\text{lb-sec-in}^{-5}$  ( $i = 1, 2, 3, \dots$ )  
 $R_r$  = effective hydraulic orifice resistance,  $\text{lb-sec-in}^{-5}$   
 $R_v$  = effective hydraulic valve resistance,  $\text{lb-sec-in}^{-5}$

- $R_t$  = effective hydraulic tubing resistance per unit system length, lb-sec-in<sup>-6</sup>  
 $R_l$  = effective hydraulic line resistance per unit system length, lb-sec-in<sup>-6</sup>  
 $R_{p1}$  = effective hydraulic point resistance, lb-sec-in<sup>-5</sup> (1 = 1, 2, 3....)  
 $Z_0$  = hydraulic line characteristic impedance, lb-sec-in<sup>-5</sup>  
 $\mu_p$  = velocity of wave propagation, in-sec<sup>-1</sup>  
 $v_p$  = instantaneous piston velocity, in-sec<sup>-1</sup>  
 $t$  = time, sec  
 $f$  = oscillation frequency, cps  
 $f_a$  = actual oscillation frequency, cps  
 $f_p$  = instantaneous force acting on piston rod, lb  
 $\omega$  =  $2\pi f$  = circular oscillation frequency, rad-sec<sup>-1</sup>  
 $\omega_{n1}$  = defined in Eq. 46  
 $\omega_{n2}$  = defined in Eq. 47  
 $m$  = slope of the system logarithmic decrement vs. length characteristic, in<sup>-1</sup>  
 $n$  = number of artificial networks  
 $N$  = number of equal branch lines  
 $W$  = combined weight of piston assembly and mass load, lb  
 $g$  = acceleration of gravity, in-sec<sup>-2</sup>  
 $K_s$  = spring rate of air load, lb-in<sup>-1</sup>  
 $\alpha$  = attenuation factor, sec<sup>-1</sup>  
 $\alpha_1$  = attenuation factor which is a function of frequency, sec<sup>-1</sup> (1 = 1, 2, 3....)  
 $\delta$  =  $\alpha f_a^{-1}$  = logarithmic decrement  
 $\epsilon_z$  = characteristic impedance error  
 $\beta$  = effective compressibility factor, psi<sup>-1</sup>  
 $\rho$  = fluid mass density, lb-sec<sup>2</sup>-in<sup>-4</sup>  
 $s$  = Laplace operator defined by the equation (Ref. 10)

$$F(s) = \int_0^{\infty} f(t)e^{-st}dt$$

$$B = \sum_{i=1}^{\infty} e^{-\alpha_i t}$$

2. General Theory

2.1 Fundamental Wave Equations

2.1.1 In Appendix IX of Ref. 1 an equation is presented which describes the instantaneous pressure response to a pressure step function; that is, an instantaneously opening valve.

$$p(x_e, t) = P_0 \left\{ 1 + \sum_{i=1}^{\infty} (-1)^i \frac{4}{(2i-1)\pi} e^{-\alpha t} \cos \frac{(2i-1)\pi}{2\ell} x_e \left[ \cos \omega t + \frac{\alpha}{\omega} \sin \omega t \right] \right\} \quad (1)$$

where

$$\omega = \sqrt{\frac{(2i-1)^2 \pi^2}{4\ell^2 \beta \rho} - \alpha^2}$$

$$\alpha = \frac{\text{Re}A}{2\rho}$$

$$\text{if } \alpha \ll \frac{(2i-1)\pi}{2\ell \sqrt{\beta \rho}}$$

then Eq. 1 becomes

$$p(x_e, t) = P_0 \left\{ 1 + \sum_{i=1}^{\infty} (-1)^i \frac{4}{(2i-1)\pi} e^{-\alpha t} \cos \frac{(2i-1)\pi}{2\ell} x_e \cos \frac{(2i-1)\pi}{2\ell} \mu_p t \right\} \quad (2)$$

where

$$\mu_p = (\beta \rho)^{-1/2}$$

2.1.2 In Eq. 1 and 2,  $x_e$  is the distance measured along the tube from the closed end back towards the accumulator. For convenience in subsequent analytical procedure, the variable  $x_e$  was replaced by the variable  $x_a$  which is the distance measured along the tube from the accumulator towards the closed end (Par. 1.1 above).

Since  $\ell = x_e + x_a$  or  $x_e = \ell - x_a$

Eq. 2 can be written

$$p(x_a, t) = P_0 \left\{ 1 + \sum_{i=1}^{\infty} (-1)^i \frac{4}{(2i-1)\pi} e^{-\alpha t} \cos \left[ (2i-1) \frac{\pi(\ell - x_a)}{2\ell} \right] \cos \frac{(2i-1)\pi}{2\ell} \mu_p t \right\} \quad (3)$$

or

$$p(x_a, t) = P_0 \left\{ 1 + \sum_{i=1}^{\infty} (-1)^i \frac{4}{(2i-1)\pi} e^{-\alpha t} \cos \frac{(2i-1)\pi}{2\ell} \mu_p t \left[ \cos \frac{(2i-1)\pi}{2} \cos \frac{(2i-1)\pi}{2\ell} x_a + \sin \frac{(2i-1)\pi}{2} \sin \frac{(2i-1)\pi}{2\ell} x_a \right] \right\} \quad (4)$$

Since  $\cos \frac{(2i-1)\pi}{2} = 0$ , and  $\sin \frac{\pi(2i-1)}{2} = -(-1)^i$

the Eq. 4 becomes

$$p(x_a, t) = P_0 \left\{ 1 - \sum_{i=1}^{\infty} \frac{4}{(2i-1)\pi} e^{-\alpha t} \sin \frac{(2i-1)\pi}{2\ell} x_a \cos \frac{(2i-1)\pi}{2\ell} \mu_p t \right\} \quad (5)$$

By incorporating the trigometric identity

$$2 \sin \frac{(2i-1)\pi}{2\ell} x_a \cos \frac{(2i-1)\pi}{2\ell} \mu_p t = \sin \frac{(2i-1)\pi}{2\ell} (x_a - \mu_p t) + \sin \frac{(2i-1)\pi}{2\ell} (x_a + \mu_p t) \quad (6)$$

Eq. 5 becomes

$$p(x_a, t) = P_0 - \sum_{i=1}^{\infty} \frac{2P_0}{(2i-1)\pi} e^{-\alpha t} \left\{ \sin \frac{(2i-1)\pi}{2\ell} (x_a - \mu_p t) + \sin \frac{(2i-1)\pi}{2\ell} (x_a + \mu_p t) \right\} \quad (7)$$

In a similar fashion the instantaneous flow rate in the system can be determined (Ref. 7)

$$q(x_a, t) = - \sum_{i=1}^{\infty} \frac{2P_0}{(2i-1)\pi Z_0} e^{-\alpha t} \left\{ \sin \frac{(2i-1)\pi}{2\ell} (x_a - \mu_p t) - \sin \frac{(2i-1)\pi}{2\ell} (x_a + \mu_p t) \right\} \quad (8)$$

where

$$Z_0 = \frac{1}{A} \sqrt{\frac{\rho}{\beta}} = \text{hydraulic line characteristic impedance.}$$

2.1.3 Before further operations are performed on the pressure wave equation (Eq. 7), a discussion of its physical meaning is desirable. The equation states that after the valve is opened the resultant pressure in the system, if the attenuation factor  $\alpha$  is assumed negligible, is equal to the accumulator pressure ( $P_0$ ) minus the sum of a pair of rectangular waves; each having a wave length equal to  $4\ell$ , an amplitude of  $P_0/2$ , and traveling in opposite directions with a velocity ( $\mu_p$ ). Using the above physical meaning, the non-attenuated pressure wave magnitude at any point in the system can be determined as a function of time. The resultant pressure in the system (Fig. 93) is a constant  $P_0$  at the accumulator end of the tube. At the closed end of the tube, the pressure is zero for the time required for the wavefront to travel from the valve to the closed end ( $\ell/\mu_p$ ), and then the pressure oscillates between  $2P_0$  and zero. At any point between the valve and the closed end of the tube, the pressure varies from zero, to  $P_0$ , to  $2P_0$ , to  $P_0$ , and

Figure 93

GRAPHICAL DESCRIPTION OF THEORETICAL, NON-ATTENUATED  
HYDRAULIC PRESSURE WAVE  
CLOSED-END TUBE SYSTEM

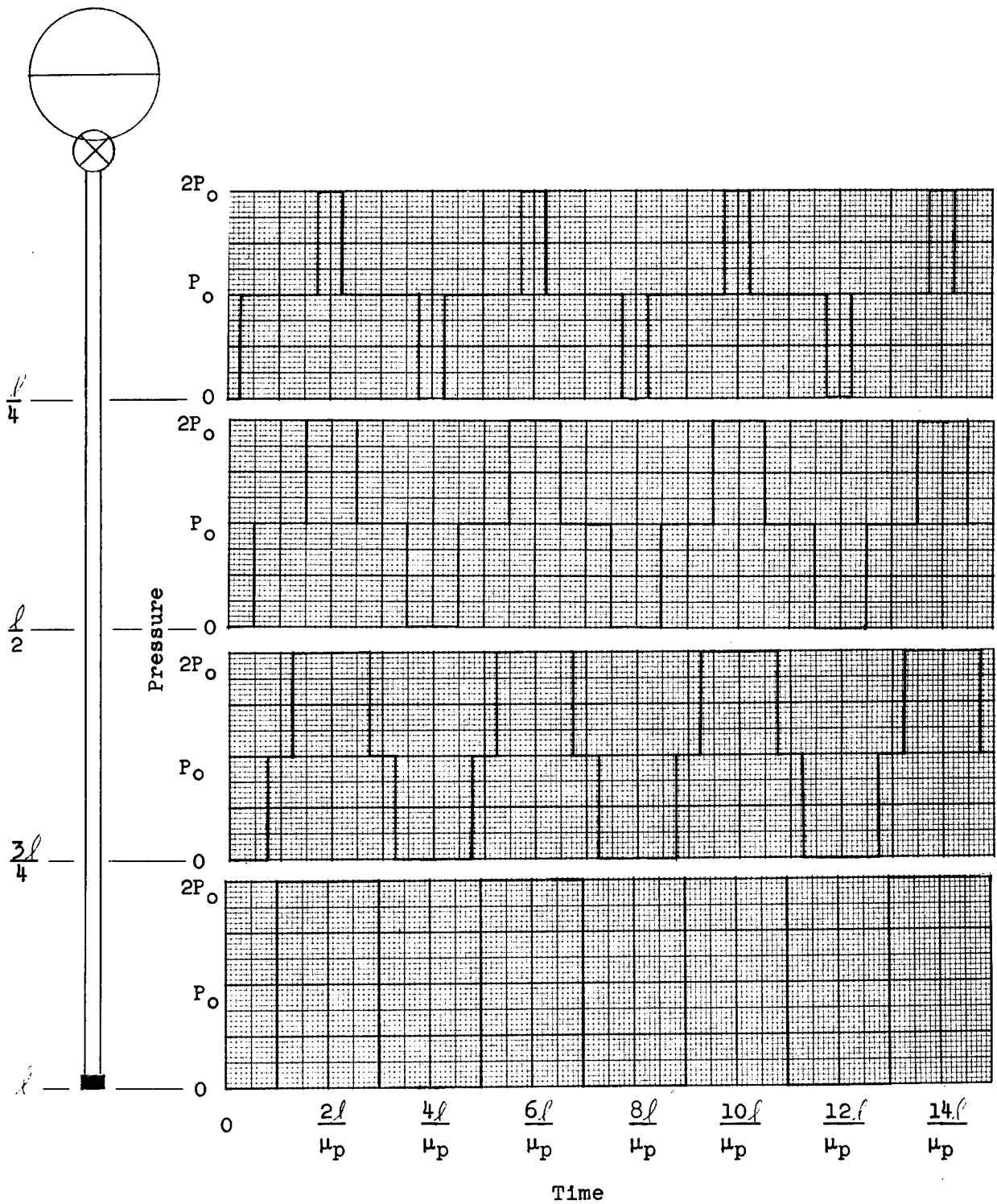


Figure 94

GRAPHICAL DESCRIPTION OF THEORETICAL, ATTENUATED  
HYDRAULIC PRESSURE WAVE  
CLOSED-END TUBE SYSTEM

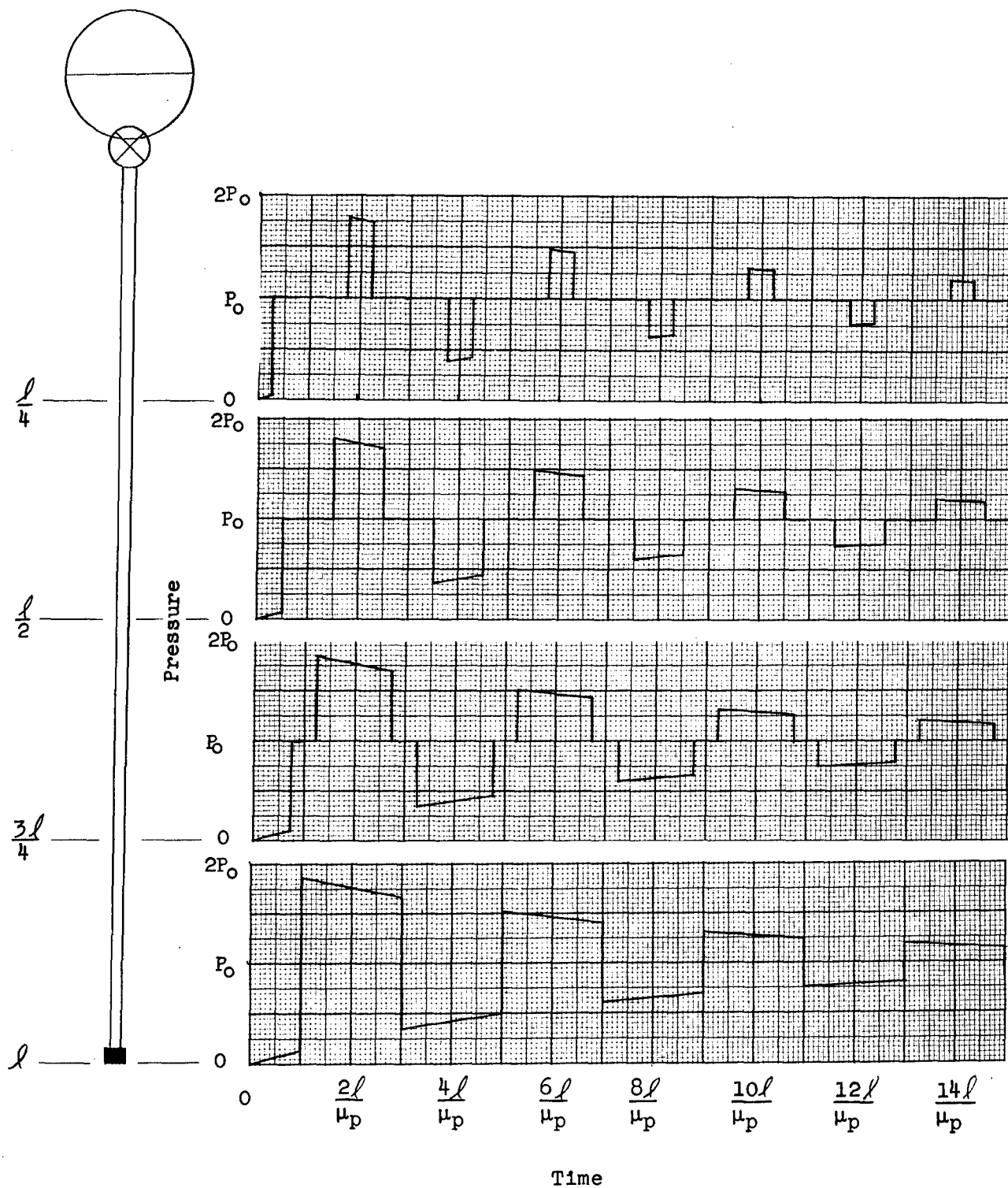
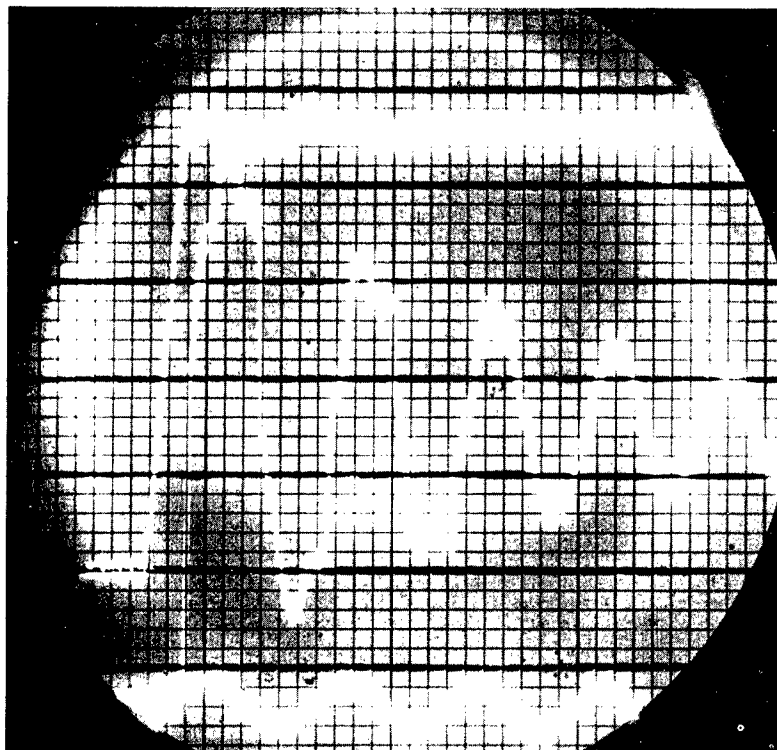


Figure 95

## PRESSURE WAVE DISTORTION - CLOSED-END TUBE SYSTEM



Valve Poppet Position

Pressure Waveform at  
Closed end of  
192 in. Test Section

Timing Wave

Note: Adel Valve with valve opening rate of  $12 \text{ in}^2\text{-sec}^{-1}$ .

back to zero. Including the attenuation factor ( $\alpha$ ), Eq. 7 states that as time increases, the amplitude of the rectangular waves decrease in magnitude which results in pressure oscillation at various points in the system which are similar to those previously described, but which are contained between a pair of envelope curves (Fig. 94) described by

$$p(t) = P_0(1 \pm e^{-\alpha t})$$

## 2.2 Wave Distortion

2.2.1 Oscilloscope pictures indicated that the theoretical wave equations, which include an infinite number frequency components, do not completely describe the pressure waveforms observed. During the first few cycles of oscillation, particularly during the first quarter of the first cycle, the theoretical wave equations describe the physical result, but after the first few cycles the higher harmonics of the equation have been attenuated until finally only the first harmonic remains evident (Fig. 95). Incorporation of this phenomena into the wave equation would necessitate consideration of the accumulated distortion of the original step function wave due to repeated passage through the tube.



2.2.2 In the wave equations stated so far, all the terms, with the exception of  $x$  and  $t$ , are assumed to be constant. Such is not the case. In particular, the circuit resistance is not constant in the turbulent flow range; therefore, the attenuation factor ( $\alpha$ ) should be included in the wave equations as a function of frequency. Rewriting Eq. 5,

$$p(x_a, t) = P_0 - \frac{4}{\pi} P_0 \sum_{i=1}^{\infty} \frac{e^{-\alpha_i t}}{(2i-1)} \sin \frac{(2i-1)\pi}{2l} x_a \cos \frac{(2i-1)\pi}{2l} \mu_p t \quad (9)$$

### 2.3 Initial Slope

2.3.1 The first derivative of Eq. 9 with respect to time is

$$\begin{aligned} \dot{p}(x_a, t) = \frac{4}{\pi} P_0 \sum_{i=1}^{\infty} \frac{e^{-\alpha_i t}}{(2i-1)} \sin \frac{(2i-1)\pi}{2l} x_a \left[ \alpha_i \cos \frac{(2i-1)\pi}{2l} \mu_p t \right. \\ \left. + \frac{(2i-1)\pi}{2l} \mu_p \sin \frac{(2i-1)\pi}{2l} \mu_p t \right] \quad (10) \end{aligned}$$

Employing two trigonometric identities, Eq. 10 becomes

$$\begin{aligned} \dot{p}(x_a, t) = \frac{2}{\pi} P_0 \sum_{i=1}^{\infty} \frac{e^{-\alpha_i t}}{(2i-1)} \left\{ \alpha_i \sin \left[ \frac{(2i-1)\pi}{2l} (x_a + \mu_p t) \right] \right. \\ \left. + \alpha_i \sin \left[ \frac{(2i-1)\pi}{2l} (x_a - \mu_p t) \right] + \frac{(2i-1)\pi}{2l} \mu_p \cos \left[ \frac{(2i-1)\pi}{2l} (x_a - \mu_p t) \right] \right. \\ \left. - \frac{(2i-1)\pi}{2l} \mu_p \cos \left[ \frac{(2i-1)\pi}{2l} (x_a + \mu_p t) \right] \right\} \quad (11) \end{aligned}$$

Since the maximum pressure rise occurs at the wavefront, that is, when  $\mu_p t = x_a$ , Eq. 11 becomes

$$\begin{aligned} \dot{p}_m(x_a, t) = \left( \frac{\mu_p}{l} \right) P_0 \sum_{i=1}^{\infty} e^{-\alpha_i t} - \left( \frac{\mu_p}{l} \right) P_0 \sum_{i=1}^{\infty} e^{-\alpha_i t} \cos \left[ \frac{(2i-1)\pi}{l} x_a \right] \\ + \left( \frac{2}{\pi} \right) P_0 \sum_{i=1}^{\infty} \frac{\alpha_i e^{-\alpha_i t}}{(2i-1)} \sin \left[ \frac{(2i-1)\pi}{l} x_a \right] \quad (12) \end{aligned}$$

However, if  $\alpha_i$  changes slightly with frequency,

$$\sum_{i=1}^{\infty} \cos \frac{(2i-1)\pi}{l} x_a \cong 0 \quad \text{for } 0 < \frac{x_a}{l} < 1$$

and

$$\sum_{i=1}^{\infty} \frac{1}{(2i-1)} \frac{\sin((2i-1)\pi x_a)}{\ell} \approx \frac{\pi}{4} \quad \text{for } 0 < \frac{x_a}{\ell} < 1$$

Except at  $x_a = 0$  and  $x_a = \ell$ , an approximate expression for the maximum rate of rise of the wavefront obtained from Eq. 12 is

$$\dot{p}_m(x_a, t) \approx P_0 \left( \frac{\mu_p}{\ell} \right) \sum_{i=1}^{\infty} e^{-\alpha_i t} + \frac{P_0}{2} \sum_{i=1}^{\infty} \alpha_i e^{-\alpha_i t} \quad (13)$$

Since the first term on the right hand side of Eq. 13 will normally be very much greater than the second term, Eq. 12 reduces further to

$$\dot{p}_m(x_a, t) \approx P_0 \left( \frac{\mu_p}{\ell} \right) B = 4P_0 f B \quad (14)$$

where

$$B = \sum_{i=1}^{\infty} e^{-\alpha_i t}$$

2.3.2 Incorporated in the preceding development is the wavefront theory used by Steinmetz (Ref. 8) in analyzing electrical transients in quarter wave transmission lines which are considered analogous to quarter wave hydraulic transmission lines. In Eq. 14, for a given pressure step function ( $P_0$ ) and system fundamental frequency ( $f$ ), the factor "B" governs the maximum rate of pressure rise. It follows that if the exponents ( $\alpha_i t$ ) in the factor "B" are small, or approach zero, the factor "B" is large, or approaches infinity. Such was the case for a fast opening valve with a relatively large maximum port area. From an actual photograph of the pressure characteristics at the closed end of a single tube circuit (Fig. 95), it can be seen that the shape of the wavefront was essentially that of the step input. This indicated that the wavefront was only slightly attenuated (or distorted) as it traveled down the tube. Studies of other photographs indicated that the wavefront was attenuated considerably by slower valve opening rates, by other than infinite impedance at the receiving end, and by point restrictions located in the tube circuit.

#### 2.4 Development of Electric-Hydraulic Circuit Constants

2.4.1 In the preceding analysis of pressure surges in hydraulic systems, classical mathematical approaches are used in which are incorporated distributed parameter circuit constants. However, the classical approaches become impractical when applied to multi-element hydraulic systems, because of cumbersome mathematics. In order to analyze complex hydraulic systems, a network of lumped parameters is an expedient approach to the problem. Since an electrical analog can be physically constructed with relative ease, an advantage is gained if the lumped parameters of a hydraulic system are determined in terms of electrical lumped parameters.

2.4.2 From Ref. 1, Appendix IX, the basic partial differential equations for a fluid system give

$$\frac{\partial p}{\partial x} = \frac{\rho}{A} \frac{\partial q}{\partial t} + R_{eq} \quad (15)$$

and

$$\beta = \frac{\partial V}{V \partial p} = \frac{\frac{\partial V}{\partial t}}{V \frac{\partial p}{\partial t}} = \frac{q}{A dx \frac{\partial p}{\partial t}} = \frac{\frac{\partial q}{\partial x} dx}{A dx \frac{\partial p}{\partial t}} \quad (16)$$

therefore

$$\frac{\partial p}{\partial t} = \frac{1}{\beta A} \frac{\partial q}{\partial x} \quad (17)$$

By differentiating Eq. 15 with respect to time (t) and Eq. 17 with respect to distance (x), the combined results give

$$\frac{1}{\beta A} \frac{\partial^2 q}{\partial x^2} = \frac{\rho}{A} \frac{\partial^2 q}{\partial t^2} + R_e \frac{\partial q}{\partial t} \quad (18)$$

The partial differential equation for an electric transmission line (Ref. 7) is

$$\frac{1}{C_{ea}} \frac{\partial^2 i}{\partial x^2} = L_{ea} \frac{\partial^2 i}{\partial t^2} + R_{ea} \frac{\partial i}{\partial t} \quad (19)$$

To formulate an analog in which electrical potential and current are analogous to hydraulic pressure and flow rate respectively, Eq. 18 must be mathematically similar to Eq. 19. Therefore,

$$R_{ea} = R_e = \frac{e}{i} = \frac{\Delta p}{q} \text{ (Resistance)} \quad (20)$$

$$C_{ea} = \beta A = C_e \quad \text{(Capacitance)} \quad (21)$$

$$L_{ea} = \frac{\rho}{A} = L_e \quad \text{(Inductance)} \quad (22)$$

Equations 20, 21, and 22 define the hydraulic resistance, capacitance, and inductance for a unit length of a hydraulic transmission line.

**2.4.3** Electrical analog representation of certain basic hydraulic system components is accomplished by establishing the equivalent electrical capacitances, inductances, and resistances.

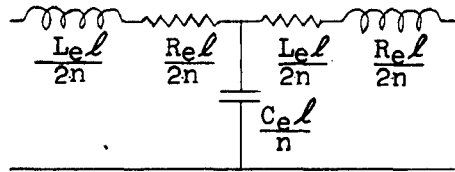
**2.4.3.1** For an accumulator, the electrical analog is a series circuit of capacitance, inductance, and resistance. The capacitance is determined from the accumulator discharge characteristics (i.e., slope of pressure-volume curve) and is represented by the following application of Eq. 16.

$$C_a = \beta V_a = \frac{\partial V_a}{\partial p} \quad (23)$$

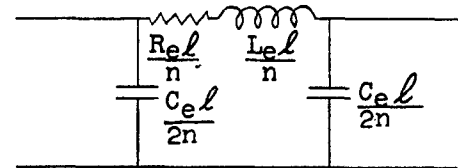
Accumulator inductance is the lumped sum of the incremental inductances defined by Eq. 22. Accumulator resistance is a function of the hydraulic output port restriction.

2.4.3.2 The hydraulic valve is represented by a variable resistance in the same manner as an electronic vacuum tube. An approximate determination of the valve resistance can be made from the steady-state leakage characteristics of the valve. A more useable value of effective valve resistance can be obtained from the use of experimental surge data (Eq. 37).

2.4.4 In electric theory, the lumped constant method of analysis for a mathematical description of energy transmission down a line is in general use. The same approach may be applied to energy transmission down a hydraulic line. Normally, a lumped parameter transmission line is represented either with a series of  $\pi$  networks or T networks or a combination of both types.



T Network



$\pi$  Network

The more networks used to represent a line, the more nearly the artificial line represents a true line. To determine the most economical number of networks to be used in obtaining a desired accuracy of transmission line representation, the following formula was developed (Ref. 7):

$$\epsilon_z = \frac{L_e C_e}{8} \omega^2 \left( \frac{l}{n} \right)^2 \quad (24)$$

This equation defines  $\epsilon_z$  which is the decimal error between the characteristic impedance of a distributed parameter transmission line and that of a lumped parameter line, both being considered to have zero resistance. The decimal error in the propagation function is one-third that of the characteristic impedance error. The characteristic impedance and the propagation function completely describe a transmission line. Substituting  $2\pi f = \omega$  in Eq. 24 and solving for "n",

$$n = \pi f l \sqrt{\frac{L_e C_e}{2 \epsilon_z}} \quad (25)$$

When the highest frequency of interest of the pressure or flow rate oscillations is the fundamental natural frequency of the system, Eq. 25 is modified to

$$n = \frac{\pi}{4 \sqrt{2 \epsilon_z}} \quad (26)$$

Eq. 24, 25, and 26 are of particular interest when an analog computer is employed to simulate a complex hydraulic circuit.

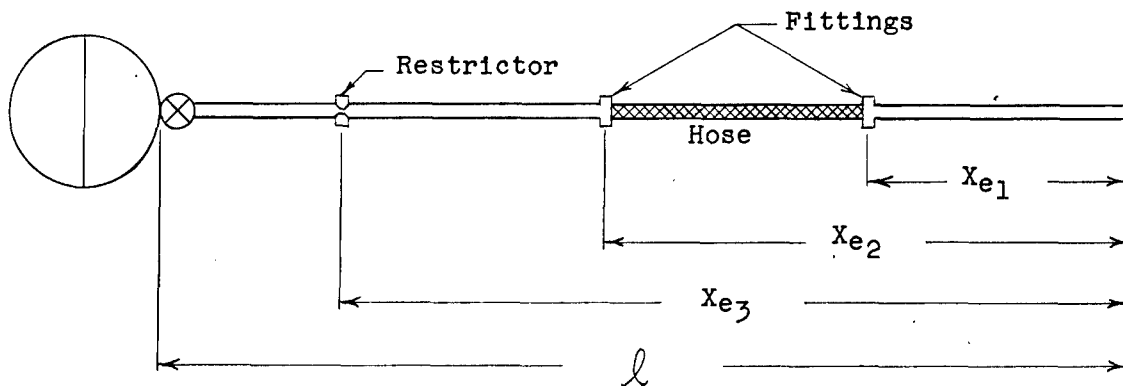
## 2.5 Effective Hydraulic Resistance

2.5.1 In Ref. 9, which presents in electrical analog terminology the pressure surge theory developed in Ref. 1, a method was developed by which the effective circuit resistance can be determined for a series circuit of hydraulic elements. If the effective circuit resistance ( $R_e$ ) is known, along with the hydraulic fluid mass density ( $\rho$ ) and the internal cross-sectional area of the tubing (A), the circuit attenuation constant ( $\alpha$ ) can be evaluated from the equation

$$\alpha = \frac{R_e A}{2\rho} = f_a \tag{27}$$

2.5.2 The essence of the development in Ref. 9 can be stated in a single equation

$$R_e = 2R_{p1} \left( \frac{X_{e1}}{\ell^2} \right) + 2R_{p2} \left( \frac{X_{e2}}{\ell^2} \right) + \dots + R_{\ell 1} \left( \frac{X_{e1}^2 - 0}{\ell^2} \right) + R_{\ell 2} \left( \frac{X_{e2}^2 - X_{e1}^2}{\ell^2} \right) + \dots \tag{28}$$



where

- $R_e$  = effective circuit resistance per unit length of system
- $\ell$  = total length of system
- $X_{e1}, X_{e2}, \dots, X_{en}$  = distances from closed end of the tube to particular points in the system
- $R_{p1}, R_{p2}, \dots, R_{pn}$  = point resistances of localized restrictions, such as valves, restrictors, and fittings
- $R_{\ell 1}, R_{\ell 2}, \dots, R_{\ell n}$  = line resistances of components such as straight tubing bent tubing, straight hose, and bent hose

2.5.3 Equation 28 was developed for an underdamped series hydraulic system agitated by a step forcing function at one end of the system and closed tube at the other end. If the system attenuation constant is very much smaller than the system natural frequency, Eq. 27 applies to a system containing hydraulic lines with a common internal cross-sectional area filled with fluid free of entrained air (i.e., air not in solution). To approximate as closely as possible a true forcing function, the rapidly opening valve should be located at the accumulator discharge port.

### 3. Specific Application

#### 3.1 Hydraulic Resistance

3.1.1 One objective for the development of Eq. 28 was to determine the magnitude of the various circuit restrictions located in the system from experimental surge data. Inversely, after the resistive values are determined, Eq. 28 can be used to evaluate the system effective circuit resistance; thereby, the effective system logarithmic decrement,  $\delta$ , can be evaluated, realizing that

$$\delta = \frac{\alpha}{f_a} = \frac{2\pi\alpha}{\sqrt{\omega_n^2 - \alpha^2}} \tag{29}$$

where  $f_a$  is the actual fundamental frequency of system oscillation and  $\omega_n$  the natural fundamental circular frequency of the system.

3.1.2 In Fig. 17, experimental logarithmic decrements ( $\delta$ ) are given for various lengths of tubing for a closed-end tube test configuration. From these data, an equation can be written which describes the system logarithmic decrement as a function of tube length for the particular valve and accumulator restriction involved.

$$\delta = ml + \delta_0 \quad (30)$$

where

- $\delta$  = system logarithmic decrement
- $l$  = total length of system lines
- $m$  = slope of the  $\delta$  vs.  $l$  characteristics
- $\delta_0$  = the  $\delta$  of the system as  $l$  approaches zero

Assuming that in the experimental test configuration the valve and accumulator are located at the same point and are the only point restrictions in the system, then Eq. 28 becomes

$$R_e = R_t + \frac{2R_v}{l} \quad (31)$$

Substituting Eq. 27 into Eq. 31, the result is

$$\frac{2pf_a}{A} \delta = R_t + \frac{2R_v}{l} \quad (32)$$

For an underdamped system,

$$f_a = \frac{1}{4l\sqrt{\beta\rho}} \quad (33)$$

therefore,

$$\frac{1}{2Al} \sqrt{\frac{\rho}{\beta}} \delta = R_t + \frac{2R_v}{l} \quad (34)$$

Rearranging the terms

$$\delta = \left(2AR_t \sqrt{\frac{\beta}{\rho}}\right)l + \left(4AR_v \sqrt{\frac{\beta}{\rho}}\right) \quad (35)$$

Comparing Eq. 35 with Eq. 30

$$m = 2AR_t \sqrt{\frac{\beta}{\rho}} \quad (36)$$

$$\delta_0 = 4AR_v \sqrt{\frac{\beta}{\rho}} \quad (37)$$

therefore,

$$R_t = \frac{m}{2A} \sqrt{\frac{\rho}{\beta}} \quad (38)$$

$$R_v = \frac{\delta_0}{4A} \sqrt{\frac{\rho}{\beta}} \quad (39)$$

3.1.3 By knowing the magnitude of tubing resistance per unit length and the effective valve resistance, the resistance of a third element placed in the circuit can be determined by surge experiment. For the case of an orifice located in the line, Eq. 28 becomes

$$R_e = R_t + \frac{2R_v}{l} + 2R_r \left( \frac{X_r}{l^2} \right) \quad (40)$$

Rearranging terms

$$R_r = \frac{l}{X_r} \left[ \frac{l}{2} (R_e - R_t) - R_v \right] \quad (41)$$

Since Eq. 36 indicates that

$$R_e = \frac{\delta}{2Al} \sqrt{\frac{\rho}{\beta}} \quad (42)$$

Eq. 41 can be stated in terms of system logarithmic decrement

$$R_r = \frac{l}{X_r} \left[ \frac{l}{2} \left( \frac{\delta}{2Al} \sqrt{\frac{\rho}{\beta}} - R_t \right) - R_v \right]$$

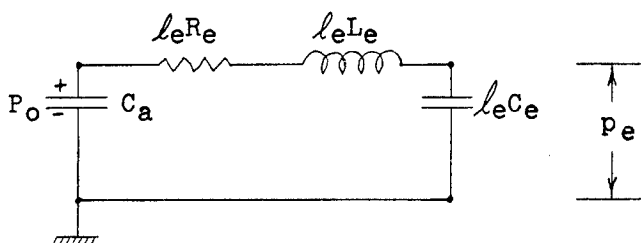
or

$$R_r = \frac{l}{X_r} \left[ \frac{\delta}{4A} \sqrt{\frac{\rho}{\beta}} - \frac{l}{2} R_t - R_v \right] \quad (43)$$

From Eq. 43 the amount of resistance an orifice of a given diameter will offer a traveling pressure surge can be evaluated, but Eq. 40 is more significant from a design point of view. Since the effective system resistance ( $R_e$ ) is directly proportional to system damping, the greater its magnitude, the more damped is the pressure wave which reaches the end of the tube. Noting the third term on the right hand side of Eq. 40, an orifice size with a particular resistance value ( $R_r$ ) will increase the magnitude of the effective system resistance ( $R_e$ ) the greatest amount when  $X_r = l$  (i.e., when the orifice is located at the valve port).

## 3.2 Single L-Network Representation of a Hydraulic Transmission Line

3.2.1 Although a lumped parameter transmission line is normally represented by a series of  $\Pi$  networks or T networks, or a combination thereof (Par. 2.4.4 above), it was considered advisable to use a more simplified circuit to decrease the labor involved in circuit solutions by manual calculation. The circuit developed for the basic accumulator, valve, closed-end tube system is represented thus:



where

- $P_o$  = accumulator pressure
- $C_a$  = accumulator capacitance
- $l_e$  = effective length of tubing in the system
- $R_e$  = the lumped effective resistance of the system per unit length of tubing
- $L_e$  = the lumped effective inductance of the system per unit length of tubing
- $C_e$  = the lumped effective capacitance of the system per unit length of tubing

Using the Laplace operator "s" (Ref. 10), the pressure oscillation,  $p_e(s)$ , at the closed end of the hydraulic line for a pressure step function applied by the accumulator can be represented by the equation

$$p_e(s) = \frac{\frac{P_o}{l_e^2 C_e L_e}}{s \left\{ \left( s + \frac{l_e R_e}{2 l_e L_e} \right)^2 + \left( \frac{1}{C_{ae} l_e L_e} - \left[ \frac{l_e R_e}{2 l_e L_e} \right]^2 \right) \right\}} \quad (44)$$

where

$$C_{ae}^{-1} = C_a^{-1} + (C_e l_e)^{-1} \quad (45)$$

Letting

$$\omega_{n1}^2 = (l_e^2 C_e L_e)^{-1} \quad (46)$$

$$\omega_{n2}^2 = (C_{ae} l_e L_e)^{-1} \quad (47)$$

$$\alpha = \frac{l_e R_e}{2 l_e L_e} = \frac{R_e}{2 L_e} \quad (48)$$

the solution becomes

$$\frac{p_e(s)}{P_o} = \frac{\omega_{n1}^2}{s \left[ (s + \alpha)^2 + (\omega_{n2}^2 - \alpha^2) \right]} \quad (49)$$



The inverse Laplace transform of Eq. 49 is

$$\frac{P_e(t)}{P_o} = \left[ \frac{\omega_{n1}}{\omega_{n2}} \right]^2 + \frac{\omega_{n1}^2 e^{-\alpha t}}{\omega_{n2} \sqrt{\omega_{n2}^2 - \alpha^2}} \sin \left[ t \sqrt{\omega_{n2}^2 - \alpha^2} - \tan^{-1} \sqrt{\frac{\omega_{n2}^2}{\alpha^2} - 1} \right] \quad (50)$$

If  $C_a \gg l e^{C_e}$ , which is normally the case, then

$$\omega_{n1}^2 = \omega_{n2}^2 = \omega_n^2$$

and Eq. 50 becomes

$$\frac{P_e(t)}{P_o} = 1 + \frac{e^{-\alpha t}}{\sqrt{1 - \left(\frac{\alpha}{\omega_n}\right)^2}} \sin \left[ t \sqrt{\omega_n^2 - \alpha^2} - \tan^{-1} \sqrt{\left(\frac{\omega_n}{\alpha}\right)^2 - 1} \right] \quad (51)$$

If  $\alpha \ll \omega_n$ , then Eq. 51 can be reduced to

$$\frac{P_e(t)}{P_o} = 1 - e^{-\alpha t} \cos \omega_n t \quad (52)$$

The frequency of oscillation in Eq. 52 is

$$f = \frac{\omega_n}{2\pi} = \frac{1}{2\pi l_e \sqrt{C_e L_e}} \quad (53)$$

Since

$$C_e = \beta A \quad (\text{Eq. 21})$$

$$L_e = \frac{\rho}{A} \quad (\text{Eq. 22})$$

Eq. 53 becomes

$$f = \frac{1}{2\pi l_e \sqrt{\beta \rho}} \quad (54)$$

3.2.2 The evaluation of the effective value of tube length, which is used in the determination of the magnitude of the circuit constants, may be accomplished by equating Eq. 33 (frequency equation for a distributed parameter circuit) and Eq. 54 (frequency for a lumped parameter circuit).

$$\frac{1}{4l \sqrt{\beta \rho}} = \frac{1}{2\pi l_e \sqrt{\beta \rho}} \quad (55)$$

Therefore

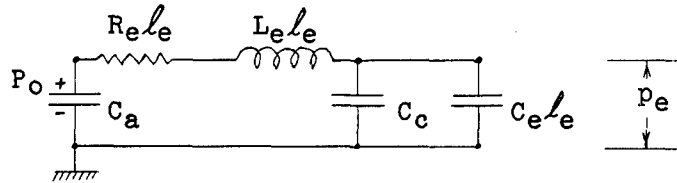
$$l_e = \frac{2}{\pi} l \tag{56}$$

3.2.3 An investigation of the attenuation factor ( $\alpha$ ) indicates that the distributed parameter (Eq. 27) and simplified lumped parameter (Eq. 48) methods of analysis give the same final result, that is

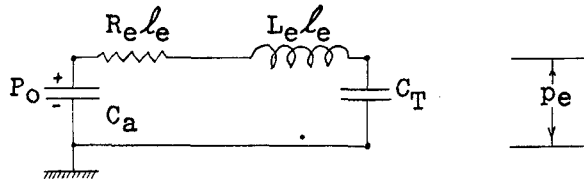
$$\alpha = \frac{ReA}{2p} = \frac{Re}{2L_e} \quad \text{and} \quad \alpha = \frac{Re}{2L_e} \tag{57}$$

### 3.3 Bottomed Cylinder Configuration

3.3.1 The electrical analog for the bottomed cylinder test configuration (Fig. 35) is represented thus:



The above circuit can be simplified thus:



where

$$C_T = C_c + C_e l_e \tag{58}$$

Replacing  $C_e l_e$  by  $C_T$  in the formulae developed in Par. 3.2 above, it can be shown that the attenuation factor does not change, but the natural frequency of the system becomes

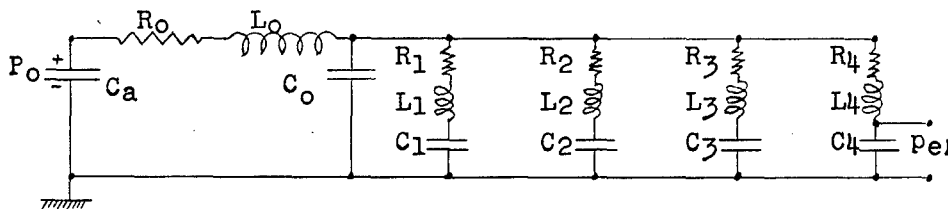
$$f = \frac{1}{2\pi \sqrt{C_{Ta} L_e l_e}} \tag{59}$$

where

$$C_{Ta}^{-1} = C_T^{-1} + C_a^{-1} \tag{60}$$

### 3.4 Branch Line Configuration

3.4.1 For the branch line test configuration the simplified electrical analog is a grouping of five L-networks when considering four branch lines.



where

$R_0 - L_0 - C_0$  network represents the system between the accumulator and branch line manifold.

$R_1 - L_1 - C_1$  networks represent various branch lines.

Using the Laplace operator "s", the solution to a step forcing function of the above circuit for  $pe_4(s)$  is

$$\frac{pe_4(s)}{P_0} = \frac{1}{C_4 s (L_0 s + R_0) (L_4 s^2 + R_4 s + C_4^{-1}) (C_0 s + Y_0 + Y_1 + Y_2 + Y_3 + Y_4)} \quad (61)$$

where

$C_0$  is assumed to be very large

$$\begin{aligned} Y_0 &= (L_0 s + R_0)^{-1} \\ Y_1 &= (L_1 s + R_1 + C_1^{-1} s^{-1})^{-1} \\ Y_2 &= (L_2 s + R_2 + C_2^{-1} s^{-1})^{-1} \\ Y_3 &= (L_3 s + R_3 + C_3^{-1} s^{-1})^{-1} \\ Y_4 &= (L_4 s + R_4 + C_4^{-1} s^{-1})^{-1} \end{aligned}$$

In order to determine the natural frequency of the Eq. 61, the operator "j $\omega$ " is substituted for "s" and the denominator is set equal to zero.

$$\frac{C_4}{Y_0 Y_4} (j\omega C_0 + Y_0 + Y_1 + Y_2 + Y_3 + Y_4) = 0 \quad (62)$$

If four equal branch lines are used, Eq. 62 reduces to

$$\frac{C_1}{Y_0 Y_1} (j\omega C_0 + Y_0 + N Y_1) = 0 \quad (63)$$

where  $N = 4$

Letting the circuit resistance approach zero, Eq. 63 becomes

$$j\omega L_0 C_1 \left( j\omega L_1 + \frac{1}{j\omega C_1} \right) \left( j\omega C_0 + \frac{1}{j\omega L_0} + \frac{N}{j\omega L_1 + \frac{1}{j\omega C_1}} \right) = 0 \quad (64)$$

Equation 64 reduces to

$$\omega^4 L_0 C_0 L_1 C_1 - \omega^2 (L_0 C_0 + L_1 C_1 + N L_0 C_1) + 1 = 0 \quad (65)$$

Solving for the smaller circular frequency

$$2L_0 C_0 L_1 C_1 \omega^2 = (L_0 C_0 + L_1 C_1 + N L_0 C_1) - \sqrt{(L_0 C_0 + L_1 C_1 + N L_0 C_1)^2 - 4L_0 C_0 L_1 C_1} \quad (66)$$

Realizing that  $L = \frac{\rho}{A} l_e = \frac{\rho}{A} \frac{2}{\pi} l$

$$C = \beta A l_e = \beta A \frac{2}{\pi} l$$

then

$$\omega^2 = \frac{1}{2\left(\frac{2}{\pi}\right)^2 \beta \rho l_0^2 l_1^2} \left[ (l_0^2 + l_1^2 + N l_0 l_1) - \sqrt{(l_0^2 + l_1^2 + N l_0 l_1)^2 - 4 l_0^2 l_1^2} \right] \quad (67)$$

$$f^2 = \frac{(l_0^2 + l_1^2 + N l_0 l_1) - \sqrt{(l_0^2 + l_1^2 + N l_0 l_1)^2 - 4 l_0^2 l_1^2}}{32 \beta \rho l_0^2 l_1^2} \quad (68)$$

3.4.2 Although Eq. 68 was derived for a four branch line network in which all branches have the same impedance, the equation gives a reasonable answer when N (number equal branch lines) is equal to a number other than 4.

3.4.3 Because of the assumptions made in deriving the branch line frequency equation, the calculated frequency for a single 96 in. test section branch line is 9.5 percent higher than that calculated by the distributed parameter equation (Eq. 33). In order to increase the accuracy of the branch line frequency equation further, mathematic manipulations are necessary. Replacing the factor 32 by a constant D, then letting N = 1 and f equal to Eq. 33, Eq. 68 becomes

$$\left[ \frac{1}{4(l_0 + l_1) \sqrt{\beta \rho}} \right]^2 = \frac{(l_0^2 + l_1^2 + l_0 l_1) - \sqrt{(l_0^2 + l_1^2 + l_0 l_1)^2 - 4 l_0^2 l_1^2}}{D \beta l_0^2 l_1^2} \quad (69)$$

Solving for D

$$D = \frac{16(l_0 + l_1)^2 \left[ (l_0^2 + l_1^2 + l_0 l_1) - \sqrt{(l_0^2 + l_1^2 + l_0 l_1)^2 - 4 l_0^2 l_1^2} \right]}{l_0^2 l_1^2} \quad (70)$$

therefore,

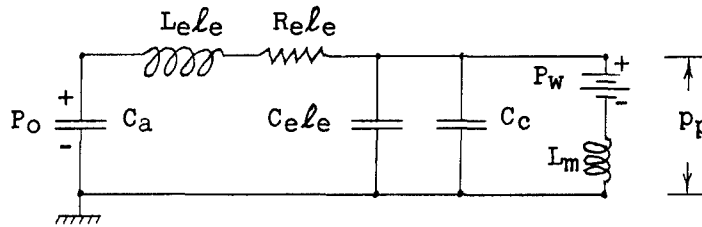
$$f^2 = \frac{1}{16 \beta \rho (l_0 + l_1)^2} \left[ \frac{(l_0^2 + l_1^2 + N l_0 l_1) - \sqrt{(l_0^2 + l_1^2 + N l_0 l_1)^2 - 4 l_0^2 l_1^2}}{(l_0^2 + l_1^2 + l_0 l_1) - \sqrt{(l_0^2 + l_1^2 + l_0 l_1)^2 - 4 l_0^2 l_1^2}} \right] \quad (71)$$

From Eq. 71, it can be seen that the natural frequency of a multi-branch line network is decreased from that of a single branch network by the factor

$$\frac{(l_0^2 + l_1^2 + N l_0 l_1) - \sqrt{(l_0^2 + l_1^2 + N l_0 l_1)^2 - 4 l_0^2 l_1^2}}{(l_0^2 + l_1^2 + l_0 l_1) - \sqrt{(l_0^2 + l_1^2 + l_0 l_1)^2 - 4 l_0^2 l_1^2}} \quad (72)$$

3.5 Mass Loaded Cylinder Configuration

3.5.1 The simplified electrical analog for the mass loaded cylinder configuration (Fig. 35) is .



The impedances  $L_e l_e$ ,  $R_e l_e$ , and  $C_e l_e$  form an L-network to represent the hydraulic transmission line between the accumulator and the cylinder. The impedance  $C_c$  is the hydraulic cylinder capacitance while  $P_w$  and  $L_m$  represent the effect of the mass load on the system. Assuming friction to be negligible, the magnitudes of  $P_w$  and  $L_m$  are evaluated by writing the differential equation of the forces acting on the mass.

$$f_p = W + \frac{W}{g} \frac{dv_p}{dt} \tag{73}$$

where

- $f_p$  = instantaneous force acting on piston = instantaneous force acting on the weight
- $W$  = weight of the mass load
- $g$  = acceleration of gravity
- $v_p$  = instantaneous piston velocity = instantaneous mass velocity

Since

$$q_p = A_p v_p$$

$$p_p = \frac{f_p}{A_p}$$

where

- $q_p$  = instantaneous flow rate to cylinder piston
- $p_p$  = instantaneous pressure acting on piston
- $A_p$  = effective piston area

Eq. 73 becomes

$$p_p = \frac{W}{A_p} + \frac{W}{g} \frac{1}{A_p^2} \frac{dq_p}{dt} \tag{74}$$

The mathematical equation for the potential drop across a series circuit containing a battery and an inductance is

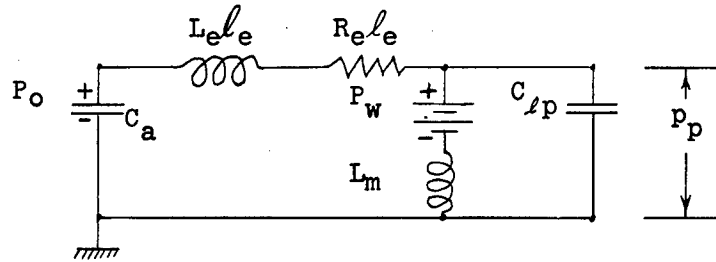
$$e = E + L \frac{di}{dt} \tag{75}$$

where both circuit elements are opposing the flow of electricity from the main electrical source. Comparing Eq. 74 with Eq. 75, and introducing the symbolism employed in the hydraulic circuit above, it can be seen that

$$P_w = \frac{W}{A_p} \tag{76}$$

$$L_m = \frac{W}{gA_p^2} = \frac{M}{A_p^2} \tag{77}$$

3.5.2 The above circuit for the mass loaded cylinder configuration is simplified into a two loop network



where

$$C_{lp} = C_e l_e + C_c$$

The solution to an applied step forcing function of the above circuit for the cylinder pressure ( $p_p$ ), in terms of the Laplace operator "s", is

$$p_p(s) = \frac{\frac{1}{L_e l_e C_{lp}} \left[ (P_o + \frac{L_e l_e}{L_m} P_w) s + \frac{R_e l_e}{L_m} P_w \right]}{s \left[ s^3 + \frac{R_e}{L_e} s^2 + \frac{1}{C_{lp}} \left( \frac{1}{L_m} + \frac{1}{L_e l_e} \right) s + \frac{R_e}{L_m L_e C_{lp}} \right]} \tag{78}$$

where the accumulator capacitance ( $C_a$ ) is assumed large in comparison to the capacitance of the rest of the system. To determine the natural frequency of the system, the circuit resistance is set equal to zero,  $j\omega$  is substituted for "s", and the characteristic equation is set equal to zero.

$$(j\omega)^3 + \frac{1}{C_{lp}} \left( \frac{1}{L_m} + \frac{1}{L_e l_e} \right) (j\omega) = 0 \tag{79}$$

Simplifying and solving for the circular frequency of oscillation ( $\omega$ )

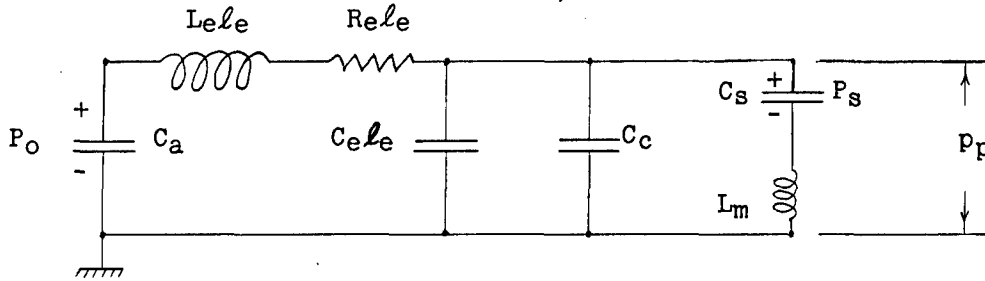
$$\omega = \sqrt{\frac{1}{C_{lp}} \left( \frac{1}{L_m} + \frac{1}{L_e l_e} \right)} \tag{80}$$

Rearranging terms and substituting Eq. 77, the natural frequency of the system is

$$f = \frac{1}{2\pi} \sqrt{\frac{1}{C_{lp}} \left( \frac{A_p^2}{M} + \frac{1}{L_e l_e} \right)} \tag{81}$$

3.6 Air Loaded Cylinder Configuration

3.6.1 The simplified electrical analog for the air loaded cylinder configuration (Fig. 35) is



The impedances  $L_{ele}$ ,  $R_{ele}$ , and  $C_{ele}$  form an L-network to represent the hydraulic transmission line between the accumulator and the cylinder. The impedance  $C_c$  is the hydraulic cylinder capacitance while  $C_s$ ,  $L_m$ , and  $P_s$  represent, respectively, the air load capacitance, piston "tare" weight, and the piston preload. Assuming friction to be negligible, the magnitudes of  $C_s$ ,  $L_m$ , and  $P_s$  are evaluated by writing the differential equation of the forces acting on the piston.

$$f_p = K_s x_p + \frac{W}{g} \frac{dv_p}{dt} + K_s x_p \tag{82}$$

where

- $f_p$  = instantaneous force acting on piston rod
- $W$  = weight of mass load = weight of piston assembly
- $g$  = acceleration of gravity
- $v_p$  = instantaneous piston velocity
- $x_p$  = instantaneous displacement of piston
- $X_p$  = preload displacement of air load spring
- $K_s$  = spring rate of air load
- $A_p$  = effective piston area

Since

$$q_p = A_p v_p = A_p \frac{dx_p}{dt}$$

$$p_p = \frac{f_p}{A_p}$$

Eq. 82 becomes

$$p_p = \frac{K_s}{A_p^2} \int q_p dt + \frac{W}{g A_p^2} \frac{dq_p}{dt} + \frac{K_s X_p}{A_p} \tag{83}$$

The mathematical equation for the potential drop across a series circuit containing a capacitance, inductance, and a potential charge on the condenser is

$$e = \frac{1}{C} \int i dt + L \frac{di}{dt} + E \tag{84}$$

**UNCLASSIFIED**

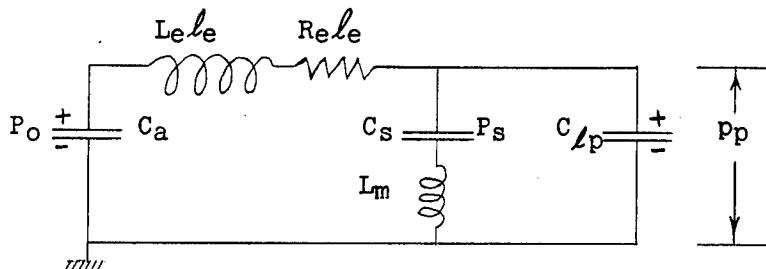
where the circuit elements are opposing the flow of electricity from the main electrical source. Comparing Eq. 83 with Eq. 84, and introducing the symbolism employed in the hydraulic circuit above, it can be seen that

$$C_s = \frac{A_p^2}{K_s}$$

$$L_m = \frac{W}{gA_p^2}$$

$$P_s = \frac{K_s X_p}{A_p}$$

3.6.2 The above circuit for the air loaded cylinder configuration is simplified into a two loop network



where

$$C_{lp} = C_{ele} - C_c$$

The solution of the above circuit for cylinder pressure ( $p_p$ ), in terms of the Laplace operator "s", when a step forcing function is applied to the circuit by the accumulator ( $C_a$ ), is

$$p_p(s) = \frac{\frac{1}{L_e l_e C_{lp}} \left[ \left( P_o + \frac{L_e l_e}{L_m} P_s \right) s^2 + \left( \frac{R_e l_e}{L_m} P_s \right) s + \frac{P_o}{L_m C_s} \right]}{s \left\{ s^4 + \frac{R_e}{L_e} s^3 + \left[ \frac{1}{C_{lp}} \left( \frac{1}{L_m} + \frac{1}{L_e l_e} \right) + \frac{1}{L_m C_s} \right] s^2 + \frac{R_e}{L_m L_e} \left( \frac{1}{C_s} + \frac{1}{C_{lp}} \right) s + \frac{1}{L_m L_e l_e C_s C_{lp}} \right\}} \quad (85)$$

where the accumulator capacitance ( $C_a$ ) is assumed large in comparison to the capacitance of the rest of the system. Using the method previously employed, the natural frequency of Eq. 85 is

$$f^2 = \frac{1}{8\pi^2} \left\{ \left[ \frac{1}{C_{lp}} \left( \frac{1}{L_m} + \frac{1}{L_e l_e} \right) + \frac{1}{L_m C_s} \right] - \sqrt{\left[ \frac{1}{C_{lp}} \left( \frac{1}{L_m} + \frac{1}{L_e l_e} \right) + \frac{1}{L_m C_s} \right]^2 - \frac{4}{L_m L_e l_e C_s C_{lp}}} \right\} \quad (86)$$

**UNCLASSIFIED**



If the piston mass is assumed small (i.e.,  $L_m \cong 0$ ), Eq. 85 can be further simplified and the natural frequency becomes

$$f = \frac{1}{2\pi} \sqrt{\frac{1}{L_e l_e (C_s + C_{lp})}} \quad (87)$$

3.6.3 The types of air load configurations considered in the investigation were as follows:

1. Constant air load
2. Air load force increasing with piston displacement
3. Air load force decreasing with piston displacement

All three types of air loads are represented in Eq. 85.

3.6.3.1 For a constant air load, the capacitance  $C_s$  becomes infinite (i.e., a battery) and Eq. 85 can be written

$$p_p(s) = \frac{\frac{1}{L_e l_e C_{lp}} \left[ \left( P_0 + \frac{L_e l_e P_s}{L_m} \right) s + \frac{R_e l_e P_s}{L_m} \right]}{s \left[ s^3 + \frac{R_e}{L_e} s^2 + \frac{1}{C_{lp}} \left( \frac{1}{L_m} + \frac{1}{L_e l_e} \right) s + \frac{R_e}{L_m L_e C_{lp}} \right]} \quad (88)$$

The natural frequency becomes

$$f = \frac{1}{2\pi} \sqrt{\frac{1}{C_{lp}} \left( \frac{1}{L_m} + \frac{1}{L_e l_e} \right)} \quad (89)$$

When  $L_m$  (or piston mass) is very small, Eq. 88 reduces to

$$p_p(s) = \frac{P_s}{s} \quad (90)$$

The inverse Laplace transform of Eq. 90 is

$$p_p(t) = P_s = \text{constant air load pressure} \quad (91)$$

3.6.3.2 When air load force increases directly as the piston is displaced, Eq. 85, 86 and 87 do not change as  $C_s$  has a finite value.

3.6.3.3 When air load force decreases as the piston is displaced,  $C_s$  can be represented by a negative value capacitor or by an arbitrary function device.